Replacement of animal models of cardiac arrest and resuscitation strategies using a computer simulation

Clara Daudré-Vignier, Meng 20205015

Supervisors:

Dr. Marianna Laviola

Prof. Jonathan G. Hardman

Anaesthesia & Critical Care, Academic Unit 3 (Injury, Inflammation and Recovery Sciences), School of Medicine, University of Nottingham

This work leading to submission of this thesis was funded by the National Centre for the Replacement, Reduction and Refinement of Animals in Research (NC3Rs, NC/S001328/1)

Table of Contents

Table of Tables

Table of Figures

Table of Equations

Abstract

This doctoral thesis explores cardiac arrest (CA) and cardiopulmonary resuscitation (CPR) from a multidisciplinary perspective, with a focus on three main objectives: enhancing the Interdisciplinary Collaboration in Systems Medicine (ICSM) simulation suite, investigating the pathophysiology of CA, and proposing an alternative to animal models in CA and CPR research.

The ICSM simulation suite was significantly improved, with additions such as a thoracic model for chest compressions, multiple organ tissue compartments, a vasculature equation accounting for resistance changes, circulatory transport delays, retrograded blood flow during CPR, and respiratory and cardiovascular control mechanisms.

Utilizing the enhanced ICSM simulation suite, a series of studies were conducted to examine various aspects of CPR strategies, all with the aim of improving resuscitation outcomes. These studies encompassed investigations into the impact of positive end-expiratory pressure (PEEP) on cardiac output during CPR, the effects of chest compression rate, depth, and duty cycle, the influence of the precipitating aetiology on CPR strategy optimization, and the comparison of personalized CPR strategies to current guidelines. The research also quantitatively identified the effect of CPR parameters on cardiac output, with end compression force and positive end expiratory pressure emerging as significant contributors. The validation of the ICSM simulation suite thoracic model using individual haemodynamic recordings of a patient undergoing CPR demonstrated its capacity to simulate individualized patient data for retrospective identification of optimized CPR protocols. These outcomes collectively emphasize the potential of computational models, particularly the ICSM simulation suite, to revolutionize CA and CPR research by providing humane, informative, and personalized alternatives to traditional animal models.

The findings of this research suggest that the ICSM simulation suite offers a valuable alternative to animal models in the study of CA and CPR. This computational model allows for the simulation and investigation of personalized CPR strategies, which can be tailored to individual patients' needs.

Acknowledgments and COVID-19 Statement

I want to express my heartfelt appreciation to Dr. Marianna Laviola, whose unwavering support has been a guiding light throughout my doctoral thesis journey. Her remarkable assistance and inspiration have played an instrumental role in the successful completion of this work. Dr. Laviola's availability and collaborative spirit have not only made this endeavour possible but also enriched it with valuable insights. I am particularly grateful for the amazing opportunities she provided, including co-leading student projects and guiding me through the grant application process.

In addition, my sincere thanks extend to Prof. Jonathan Hardman, whose guidance has been pivotal in shaping the trajectory of my research. His expertise and encouragement helped me focus my work in the necessary direction, transforming it into compelling and relevant topics. Prof. Hardman's passion for the subject matter has been contagious, and I am truly grateful for his mentorship.

As I reflect on this academic journey, I am acutely aware of the extraordinary circumstances under which most of my thesis was carried out—the challenging times of the COVID-19 pandemic. The Research Office being situated in Queen’s Medical Centre meant that much of the thesis work had to be conducted remotely. Despite the disruptions caused by the global health crisis, the support and adaptability of both Dr. Laviola and Prof. Hardman were unwavering.

These acknowledgments would not be complete without recognizing the support and encouragement from others who have contributed to this academic journey. Their collective influence has made a lasting impact on my research and personal growth, especially during these unprecedented times.

Chapter 1. Introduction and literature review on cardiac arrest

1.1 Aim of the literature review

The aims of this literature review are to:

a) cover the current knowledge of the physiological processes of cardiac arrest and cardiopulmonary resuscitation (CPR);

b) identify the gaps in knowledge and recognise what is urgent to investigate;

c) identify the use of animal model and different alternatives research approaches to investigate cardiac arrest and CPR.

The databases used to retrieve the information are PubMed, Embase, MEDLINE, Web of Science Core Collection and Google Scholar.

1.2 Cardiac Arrest (CA)

From 2008 and 2018, the leading cause of death in the UK was ischemic heart disease accounting for 10.3% of all deaths [1]. Worldwide, it remains a leading cause of mortality and is responsible for approximately half of all deaths from cardiovascular disease [2]. It is a global public health burden which has considerable economic and societal impacts (loss of productive years and neurologic injuries and disabilities) [3].

1.2.1 History

The sudden collapse and death caused by a cardiac arrest has intrigued the medical community for centuries. The first historical reference made of a sudden cardiac death dates back to the 4th century BC, by the founder of modern medicine, Hippocrates. He defined it as “those who are subject to frequent and severe fainting attacks without obvious cause die suddenly”.[4]

Cardiac arrest became a major public health concern after the Second World War. Indeed, the incidence of cardiac arrests started to dramatically increase in the twentieth century, and by 1940 coronary artery disease (CAD) induced cardiac arrest was the leading cause of death in the USA and in the UK [5, 6]. This increase can be explained by the considerable lifestyle changes that took place at the beginning of the century with the increased of life expectancy, inactivity, tobacco smoking and obesity.

1.2.2 Definition

Cardiac arrest or sudden cardiac arrest (SCA) is defined by American Heart Association (AHA) and the American College of Cardiology, as the sudden cessation of cardiac activity so that the victim becomes unresponsive, with no normal breathing resulting in the absence of circulation of blood [7]. The word sudden emphasizes the rapidity at which the cardiac arrest occurs after the onset of the first symptoms (less than an hour). During cardiac arrest the cessation or reduction of circulation stops blood from flowing to vital organs, causing global ischaemia, depriving the tissues of oxygen (phenomena known as hypoxia).

Hypoxia

Hypoxia is defined as a state of inadequate oxygen delivery to the tissue cells. It can be categorised into four main types: hypoxemic hypoxia, ischemic or stagnant hypoxia, anaemic hypoxia and histotoxic hypoxia. The variation from normoxia for each type of hypoxia as reported in [7] is resumed in the Table 1.1.

During cardiac arrest the disruption of cardiac activity will result in ischaemia, followed by local hypoxaemia and hypercapnia in the tissue capillary blood due to the stagnation of blood.

Table 1.1 Type of hypoxia.

Type of Hypoxia	**Definition**	**CaO_2 ($ml.L^{-1}$)**	**CvO_2 ($ml.L^{-1}$)**	**CO ($L.min^{-1}$)**	**VO_2 ($ml.min^{-1}$)**
Normoxia	Normal level of O_2 in blood, perfusion and O_2 usage	20	15	5	250
Ischemic	Hypoperfusion causing limited O_2 delivery	Normal	↓	↓↓	Normal
Hypoxemic	Decrease in arterial blood oxygenation	↓↓	↓	↑	Normal
Anaemic	Decrease in arterial blood O_2 due to low haemoglobin content in the blood	↓↓	↓	Normal or ↑	Normal
Histotoxic	Reduction in ATP production by the Mitochondria due to a defect in the cellular usage of O_2	Normal	↑	Normal	↓↓

CaO_2: arterial oxygen concentration; CvO_2: venous oxygen concentration; CO: cardiac output; VO_2: oxygen consumption rate.

However, other types of hypoxias can be present in cardiac arrest depending on the aetiology of the arrest. During carbon monoxide (CO) poisoning, anaemic hypoxia occurs because of the high affinity between CO and the haemoglobin, therefore limiting the transport of oxygen bounded to haemoglobin. Similarly, in cyanide poisoning, a form of histotoxic hypoxia, the inhibition of a mitochondrial enzyme renders impossible the production of ATP from oxygen. [8]

1.2.3 Physiological Mechanisms

Cardiac arrest may manifest in two distinct ways: the first, known as sudden cardiac arrest (SCA), is typically triggered by abrupt malignant rhythms (such as VF/pVT) and occurs without any preceding 'shock.' The second form is a more gradual process, unfolding in three stages: the initial development of an underlying cause, the onset of shock, and eventually, cardiac arrest. Once the cardiac arrest is initiated the physiological mechanisms of the cardiac arrest is similar for all. Cardiac arrest is characterised by four main physiologic disturbances: the loss of respiratory functions (no ventilation), rhythm disturbances, circulatory disturbances and metabolic disturbances.

Shock

Shock is defined as a critical condition that is triggered by a sudden drop in blood pressure (BP) and inadequate tissue perfusion [9]. The cardiac output is greatly reduced, dramatically restricting the delivery of oxygen to the tissues. If left untreated the tissue can start being necrotic leading to multiple organ failure. There are four main types of shock related to the system failing: hypovolemic, distributive, cardiogenic and obstructive defined in the Table 1.2.

Shock usually progresses in various stages; there is first a compensatory mechanism to adapt to the low perfusion and hypotension, next there is decline and finally, there is a refractory component that will lead to cardiac arrest.

Table 1.2 Types of shock.

Type of shock	Mechanism	Possible cause
Hypovolemic	Intravascular volume loss	trauma, severe dehydra
Distributive	Hypovolemia resulting from pathological redistribution of the absolute intravascular volume	sepsis, anaphylaxis
Cardiogenic	Inadequate function/pumping of the heart	cardiomyopathy, MI
Obstructive	Hypoperfusion due to elevated resistance	pulmonary embolism

Ventilation disruption

During untreated out of hospital cardiac arrest (OHCA) there is a cessation of ventilation of the patient. If the cardiac arrest is not witnessed and CPR is initiated, the subject will be undergoing apnoea. Additionally, soon after onset of cardiac arrest, there can be various physiological changes that affect the airway, potentially leading to airway obstruction or narrowing. The Loss of muscle tone can result in the tongue or other airway soft tissues partially blocking the airway.

Additionally, during CA the loss of rib cage muscle tone, lung compliance and CC cause a reduction in lung volume. Lung volume reduction and CC can promote lung injury, progressive atelectasis and pulmonary congestion which can be exacerbated with a lack of ventilation [10]. Furthermore, the loss of muscle tone can result in the tongue or other airway soft tissues partially blocking the airway, potentially leading to airway obstruction or narrowing.

Lungs volume below the functional residual capacity (FRC) will cause a negative intrathoracic pressure, which causes a reduction of oxygen partial pressure and an increase of CO_2 partial pressure [11].

Rhythms disturbance

The normal active state heart rate ranges from 60 to 100 beats per minute. However, during episodes of bradycardia (low heart rate) or tachycardia (high heart rate) associated with heart failure, there is a decrease in cardiac output. When the electrical activity of the heart is altered the synchronous ability of the heart is lost. There are four primary arrhythmias associated with cardiac arrest: ventricular fibrillation (VF), pulseless ventricular tachycardia (pVT), pulseless electrical activity (PEA), and asystole. These arrhythmias are usually divided into two categories: “shockable” arrhythmias (i.e., VF and pVT) that responds to defibrillation, and “non-shockable” arrhythmias (i.e. PEA and Asystole) that do not respond to defibrillation [3]. Table 1.3 describes the four types of primary cardiac arrest arrhythmias.

Ventricular fibrillation (VF) and ventricular tachycardia (VT) were initially thought to be the most common causes of out-of-hospital cardiac arrest. More recent studies show pulseless electrical activity (PEA) and asystole as more frequent [12]. Approximately 42.4% of patients initially have asystole, and 17.1% have PEA as the first identifiable rhythm while 20.6% have a shockable rhythm (VF or pVT).

Table 1.3 The types and characteristics of primary cardiac arrest arrhythmias [2]

	Ventricular Fibrillation	**Pulseless Ventricular Tachycardia**	**Pulseless Electrical Activity**	**Asystole**
Definition	Uncoordinated electrical activation of heart, resulting in loss of organized contraction of the ventricles	Organized electrical activation of heart, with absent or ineffective contraction of the ventricles, due to rate or extent of disease	The heart's electrical activity is present, often slow and/or irregular, but the signal fails to initiate a mechanical response in the cells, resulting in insufficient ventricle contraction	Absence of electrical activity of the heart; no signal to initiate contraction of the ventricles
ECG appearance	Grossly irregular electrical pattern on ECG, without identifiable QRS complexes	Regular QRS complexes, usually wide and fast	Usually wide QRS complexes, often slow and irregular; sometimes narrow QRS complexes	No electrical activity
Electrical activity	Yes	Yes	Yes	No
Palpable pulse	No	No	No	No
Responds to shock	Yes (usually)	Yes (usually)	No	No

Circulatory disruption

Generally, in the late phase of shock, the extreme hypotension leads to a peripheral vasoconstriction. However, in some cases, such as septic shock, vasodilation occurs worsening the hypotension. During cardiac arrest, the arrhythmia leads to a decrease in the left ventricular pressure further decreasing the systemic pressure and worsening hypotension. The lack of contractions causes the loss of blood pressure gradient throughout the entire vascular system, leading to a global mean systemic filling pressure (MSFP) of around 10-20 mmHg [13]. MSFP refers to the pressure in the entire circulation at zero blood flow, following pressure equilibration throughout the systemic vasculature, excluding the heart chambers and the lungs. It serves as an indicator of the elastic recoil of the entire vasculature, influenced by the total blood volume and the overall vascular compliance.

Global ischaemia leads to hypoxaemia. The cardiovascular system is regulated by control mechanisms such as the baroreflex and chemoreflex. Decreased arterial pressure induces a decrease of the firing of arterial baroreceptors (i.e. carotid sinus and aortic arch receptor) leading to an increased chronotropy, inotropy of the heart and vasoconstriction. Similarly, hypoxaemia, hypercapnia or acidosis triggers chemoreceptor firing, enhancing sympathetic and respiratory activity [13]. Additionally, other autonomic reflexes affect the cerebral and myocardial perfusion. High levels of $PaCO_2$ lead to a vasodilation of the cerebral vasculature promoting cerebral blood flow (CBF), while low levels of $PaCO_2$ decrease CBF.

Global ischemia prompts a complex cellular response, shifting cells to anaerobic metabolism and producing lactate. Beyond a mere indicator of oxygen debt, lactate is a dynamic player in cellular homeostasis, participating in the lactate shuttle where it serves as an energy substrate. However, during global ischemia and reduced ATP levels, lactate equilibrium is disrupted, causing an acidic environment and intracellular pH decrease. This disrupts ion transport mechanisms, leading to profound consequences such as intracellular electrolyte imbalance, loss of membrane integrity, cell swelling, and, ultimately, cell death [14]. The accumulation of cellular injury leads to oedema formation, which is particularly harmful in the brain (because of the lack of space for expansion). Cerebral oedema also restricts the

cerebral perfusion during CPR, further damaging the neural cells. A significant portion of resuscitated patients suffer hypoxic ischemic brain injuries (HIBI) and many of those surviving to hospital discharge will face long term cerebral damage. In fact about 80% of survivors are functionally independent although about 50% of all survivors will have some cognitive deficits [15].

Additionally, global ischaemia promotes free radical formation and oxidant injury in organs. This damage and the metabolic cascade trigger the release of inflammatory mediators (i.e. interleukins, tumour necrosis factor) which exacerbates injury to the brain and myocardium [16].

Some researchers [17] have discussed the possibility that the lack of blood flow or the presence of inflammatory mediators lead to microvascular thrombosis during CPR and up to 48 h after return of spontaneous circulation (ROSC). However, in randomised, controlled trials where antithrombotic therapy was delivered during CPR [18], no improvement in outcomes compared to placebo was detected and antithrombotic therapy was associated with more intracranial haemorrhage.

Metabolic disruption

The main metabolic disturbances present during cardiac arrest are acidaemia with serum arterial pH<7.20, hyperlactatemia (lactate levels > 2 mmol.L^{-1}), hyperglycaemia and general electrolyte disturbances (hypokalaemia, hypocalcaemia and hypomagnesaemia). The metabolic and electrolyte disturbances are proportional to the extent of ischaemia [19].

Oxygen stores in the brain are depleted within 20 s, and glucose and ATP within 5 min of complete anoxia. This leads to a loss of membrane resting potential, influx of calcium and release of excitatory neurotransmitters (e.g., glutamate activates a specific calcium channel, worsening intracellular calcium overload), which further exacerbates neuronal injury due to tissue hypoxia. [20]

1.2.4 Epidemiology

In hospital cardiac arrest (IHCA) versus out of hospital cardiac arrest (OHCA)

Return of spontaneous circulation (ROSC) and survival to discharge following out of hospital cardiac arrest (OHCA) and in hospital cardiac arrest (IHCA) vary substantially. Multiple factors can explain these disparities, including the aetiologies, the population affected (age, comorbidities, etc), and the response time from the onset of cardiac arrest [3]. The main differences between OHCA and IHCA are summarised in the Table 1.4.

Table 1.4 Comparison of OHCA and IHCA in the UK.

	OHCA	**IHCA**
Incidence in the UK	60,000 persons/year [12]	30,000 persons /year [21]
ROSC	25.8%	45%
Survival to hospital discharge	7.9%	25%
Presenting rhythm	Primarily non-shockable (asystole/PEA) for 59.5% and shockable (VT/VF) for 20.6%	Primarily non-shockable (asystole/PEA) for 72.3% and shockable (VF/VT) for 16.9%
Predominant aetiology	Cardiogenic (60.9%)	Primarily cardiogenic and respiratory
ALS response time	14 minutes	Often instantaneously [22]

Resuscitation attempted	29,000 (48.3%) **	100% *

* DNACPR are excluded** The vast majority of OHCA happening at home (60.8%), Advance life support (ALS).

Incidence

There is a wide variation in incidence and outcomes after cardiac arrest between regions in the world [2]. Cardiac arrest is a major health problem in Western countries accounting for 20% of all natural deaths and is expected to further increase [23, 24]. In the UK, approximately 60,000 people sustain an out-of-hospital cardiac (OHCA) each year resulting in an incidence of 53 per 100,000 person per year [12].

The incidence for OHCA increases exponentially with age, and men (60%) are more at risk than women (40%), the median age being 65 years [12]. Coronary artery disease is regarded as the most prevalent disease in Occidental countries and the leading risk factors of cardiac arrest [25]. Other risk factors associated with cardiac arrest are heart failure, family history of sudden death, diabetes mellitus, hypertension, obesity, cigarette smoking, air pollution, low vital capacity, increased resting heart rate and sepsis [26].

Aetiology of cardiac arrest

Historically, the aetiologies of cardiac arrest have been dichotomized as cardiac or noncardiac. Now, the Utstein template [27] assigns cardiac arrest aetiologies into two main categories: medical (previously known as presumed cardiac) and no-medical (non-cardiac). Knowing the precipitating aetiology is crucial for the correct management and treatment of patients as well as for prevention. Because patients can present multiple aetiologies and patients with no obvious cause are generally classified as cardiac, and because discrepancies often exist between clinical and post-mortem diagnoses, the causes of cardiac arrest are often uncertain [22]. Cardiogenic arrests are estimated to account for 60% of OHCA and around 30% of IHCA with CAD being the predominant one [28]. However, cardiac arrest appears to be the first manifestation of heart disease for 40%-60% of all

patients, making prevention difficult to implement [26]. Respiratory failure is the leading aetiology of IHCA and the second one in OHCA [28].

Considerable regional differences in the incidence of aetiologies exist. In the USA, the incidence of drug overdose induced cardiac arrest is three times higher than in the UK [29].

The main precipitating aetiologies are cardiovascular disease (acute myocardial infarction, acute coronary syndrome, cardiomyopathy), respiratory failure (COPD, asthma), central nervous disease (cerebrovascular accident), thromboembolic disease (pulmonary embolism), toxicologic (overdose, poisoning) and infection (sepsis, pneumonia) [28].

1.3 Cardiopulmonary Resuscitation (CPR)

Since the development of CPR with the combination of artificial respiration and circulation in the 1960s, the treatment of cardiac arrest has remained a challenge and continues to evolve. The primary goals of CPR are to maintain adequate organ perfusion and restore spontaneous circulation.

Today, the advanced life support (ALS) guidelines advise a ratio of 30 chest compressions for 2 rescue breaths and administration of algorithmic vasopressor (and other drugs) dosing [30]. The compressions should be delivered on the lower half of the sternum, compression depth should be of 5-6 cm and the rate should be of 100-120 compression per minute (i.e. the tempo of "*Stayin' alive*" by the Bee Gees).The recommended resuscitation remains uniform across all cardiac arrest patients [31].

1.3.1 Chest compression

Artificial circulation emerged in the 1870, with the first mention of cardiac compression being done on patients to counter chloroform-induced cardiac arrest [32]. Since then, efforts have been made to optimize manual cardiac massage and mechanical CPR devices have been developed to optimise circulation.

The generation of cardiac output during CPR is mainly based on two complementary theories: the theory of the thoracic pump and the theory of the cardiac pump [33]. The sternal recoil during the decompression phase decreases intrathoracic pressure, and this is crucial to maintaining venous return and therefore cardiac output [31].

The mechanisms by which closed chest cardiac massage produces and maintains blood flow during cardiopulmonary resuscitation are still debated. Figure 1.1 by Cipani *et al.* [34] summarises the main theories of blood flow maintenance during CPR. To date, two main theories exist: the ‘‘cardiac pump’’, which assumes that blood flow is driven by direct cardiac compression and the ‘‘thoracic pump’’, which hypothesizes that blood flow is caused by changes in intrathoracic pressure. Newer hypotheses including the ‘‘atrial pump’’, the ‘‘lung pump’’, and the ‘‘respiratory pump’’ were also proposed. On the basis of current evidence, a single theory is probably not sufficient to explain how cardiac massage produces blood flow. This suggests that different simultaneous mechanisms might be involved. The relative importance of these mechanisms depends on several factors, including delay from collapse to starting of resuscitation, compression force and rate, body habitus, airway pressure, and presenting electrocardiogram. [34]

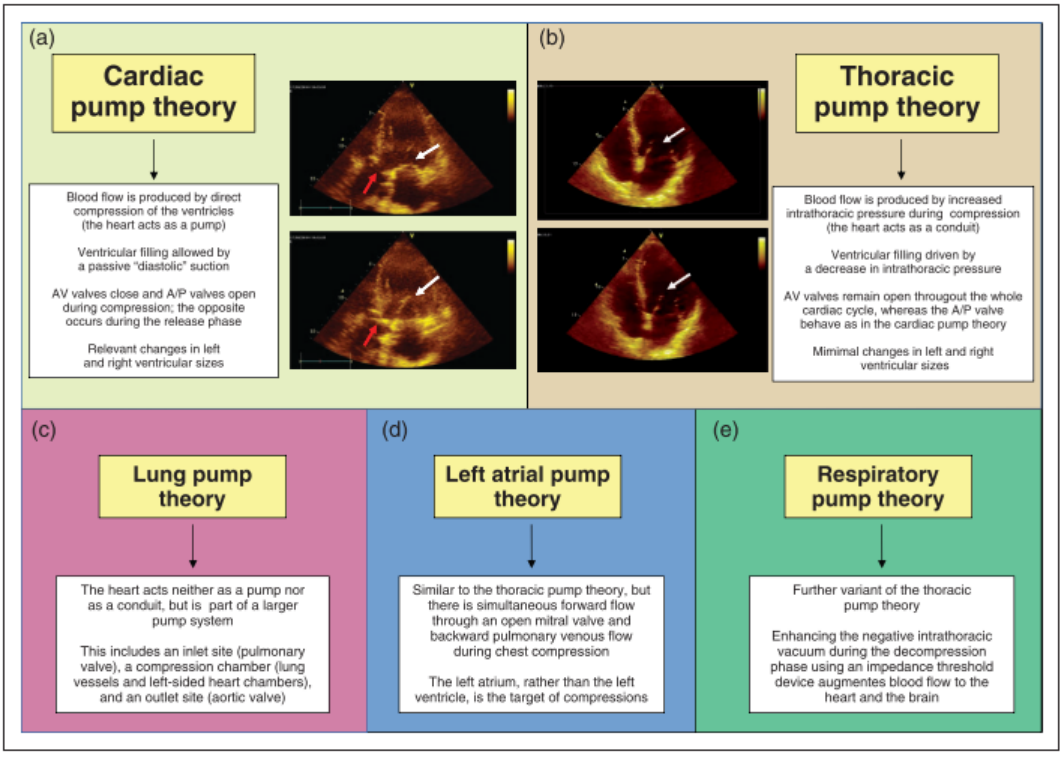

Figure 1.1 Main theories on blood flow production and maintenance during cardiac massage. (a) In the cardiac pump theory, during compression, the mitral valve closes (white arrows), whereas the aortic valve opens (red arrows) when the intraventricular pressure exceeds aortic diastolic pressure. During release, the aortic valve closes, and the mitral valve opens, allowing ''diastolic'' filling. Similar changes can be seen in right-sided cardiac valves. (b) In the thoracic pump theory, during compression the intrathoracic pressure increases and forces blood from the thoracic vessels into the systemic circulation, with the heart acting as a conduit and not as a pump. Thus, a venous-arterial pressure gradient develops, leading to antegrade blood flow through the atrioventricular valves and the aortic and pulmonary valves during compression. This theory requires the mitral valve to be open throughout the whole cardiac cycle (white arrows) and implies minimal changes in ventricular volumes. (c–e) Main principles of newer theories, based on the heart as part of a larger pumping system (lung theory), or on pathophysiological variants of the thoracic pump (left atrial and respiratory theories).[34]

Chest compression components

When performing chest compression three main components can be varied: rate, depth and chest wall recoil [35].

In a systematic review and meta-analysis by Considine *et al.* [35], thirteen studies involving 15,164 patients (14,610 adults and 554 children) reported outcomes associated with chest compression (CC) rate. Overall, the majority of the studies did not find any associations between the CC rate and outcomes (survival with good neurological outcomes, survival to hospital discharge and ROSC) in OHCA. Only two studies found otherwise: Idris *et al.* [36] found an association between CC rate and ROSC with the rate of ROSC peaking at 125 CC per minute, and Idris *et al.* [37] found that CC rates between 100 and 120 per minute were associated with greatest survival to hospital discharge. Additionally, in a review and meta-analysis by Ashoor *et al.* [38] it was demonstrated that for adults CPR a ratio of 30:2 is associated with better survival and favourable neurological outcomes when compared to CPR 15:2.

Similarly, for CC depth, contradictory evidence exists. In Vadeboncoeur *et al.* [39] CC depth during CPR was measured using real-time audiovisual feedback (RTAVF) for CC quality metrics whilst Stiell *et al.* [40] and Stiell *et al.* [41] used an accelerometer interface between the

rescuer and the patient's chest using commercially available defibrillators. In a prospective analysis by Vadeboncoeur *et al.* [39] and an observational study by Stiell *et al.* [40] each 5 mm increase in CC depth was associated with increased survival to hospital discharge for both studies and increased survival with favourable neurological outcome in Vadeboncoeur *et al.* [39] study. However, in another observational study by Stiell *et al.* [41] CC depth increase was not associated with increased survival to hospital discharge. Additionally, compared to a CC depth of >51 mm, survival to hospital discharge decreased when CC depth was <38 mm [40]. Specific CC depth were not associated with survival with favourable neurological outcome [42] apart for Vadeboncoeur *et al.* [39] study. In a study by Babbs *et al.* [43] for shocks delivered after 5 min of CC, a CC depth >5 cm compared with CC depth <5 cm was associated with higher transient ROSC. None of the other studies reported a statistically significant relationship between ROSC and different CC depths [40-42].

Two studies reported conflicting results on the association with chest compression release velocity (CCRV) and outcomes. One study by Cheskes *et al.* [44] found that compared to slow CCRV (<300 $mm.s^{-1}$), fast CCRV (>400 $mm.s^{-1}$) was associated with an increase in survival with favourable neurological outcome and in survival to hospital discharge. While the second study by Kovacs *et al.* [45] did not find any significant association between CCRV and any outcomes. [35]

CPR alternatives

Passive leg raising CPR (PLR-CPR) is a simple manoeuvre which involves the elevation of the lower limbs from the horizontal plane (HP). The effect of PLR is to shift blood from the lower extremities towards the intrathoracic compartment and increase venous return. However, in a study by Holmen *et al.* [46] PLR-CPR was not associated with improved survival to 30 days.

Interposed abdominal compression CPR (IAC-CPR) is a simple manoeuvre which consists in compressing the abdomen in a similar manner to the CC (depth and rate) during the relaxation phase of CC. It is believed that IAC-CPR can increase diastolic aortic pressure,

coronary perfusion, and venous return and can improve blood flow to other vital organs. However, in a study by Movahedi *et al.* [47], while the end-tidal CO_2 ($EtCO_2$) was increased during IAC-CPR compared to standard CPR, there was no increase in ROSC or survival.

CPR Devices

Mechanical CPR (mCPR) devices were introduced with the hope that this would be better than manual CPR as there is a predictable level and rate of chest compressions and this also frees up the rescuer to perform other critical resuscitation activities.[48] There are two main types of mCPR devices currently in use are: the pneumatic piston devices (e.g. Michigan® and Lucas®), and the load-distributing band devices (e.g. Zoll AutoPulse®). Although these mCPR devices present advantage to manual CPR (such as human error and inconsistency or rescuer fatigue), major studies such as (CIRC, LINC, and ParaMeDiC [49]) and review [50], have not found mCPR devices to be superior to conventional manual compressions and prospective multicentre study in Japan (SOS-KANTO) found that mCPR in the emergency department was associated with decreased likelihoods of good clinical outcomes [51].

Extracorporeal CPR (ECPR) or Extracorporeal Life Support (ECLS) refers to placement of veno-arterial Extracorporeal Membrane Oxygenation (ECMO) device in patients with refractory cardiac arrest [48]. ECPR has been associated with improved survival and better neurological outcomes compared to conventional CPR [52]. In a recent systematic review and meta-analysis of randomized clinical trials (RCTs) Gomes et al. [53] found that ECPR was not associated with a significant improvement in survival with favourable neurologic outcomes in refractory OHCA patients compared to standard CPR.

Active compression-decompression cardiopulmonary resuscitation (ACD CPR) employs a handheld suction device or is frequently integrated directly into mechanical CPR devices, like LUCAS. This method involves mid-sternum application for chest compression, followed by active chest decompression after each compression [54]. The Cochrane intervention review found that ACDR CPR was not associated with any clear benefit. [54]

The impedance threshold device (ITD) is designed to enhance venous return and cardiac output during CPR by increasing the degree of negative intrathoracic pressure by preventing respiratory gases from entering the lungs during the chest compression decompression phase. In the Resuscitation Outcomes Consortium (ROC) PRIMED cardiac arrest trial, there was no significant improvement in survival with favourable functional outcomes among patients with out-of-hospital cardiac arrest receiving standard CPR [55]. However, a post-hoc analysis of the ROC PRIMED database [56] showed an improved survival after witnessed cardiac arrest when ITD was combined with adequate-quality conventional CPR.

An animal study found that the use of ITD during ACD-CPR improved hemodynamic parameters, increased 48 h survival and decreased the degree of post-cardiac arrest acute kidney injury in the resuscitated animals [57].

Blood circulation monitoring

Intensive monitoring is highly recommended by the American heart association (AHA) during CPR to guide and improve CC quality. The use of real-time audio-visual (AV) feedback during CPR in a study [58] improved compliance with CPR depth and rate targets. Similarly, in a prospective observational study [59] clinician-reported that, the use of either end tidal carbon dioxide ($ETCO_2$) or diastolic blood pressure (DBP) to monitor CPR quality, was associated with improved ROSC. An $ETCO_2$ >10 mmHg during CPR was associated with a higher rate of survival compared to events with $ETCO_2$ ≤10 mmHg. In a porcine model of CPR [60], the DBP failing to reach 34 mmHg during CPR was found to be highly predictive of non-survival.

Coronary perfusion pressure (CPP) is defined as the difference between the aortic diastolic pressure minus the right atria diastolic pressure. CPP gives an indication of the myocardial blood flow during CPR. In an animal study by Naim *et al.* [61], targeting a systolic blood pressure of 100 mmHg and CPP>20 mmHg improved survival compared to guidelines.

Cerebral oximetry has emerged as a real-time indicator of regional haemoglobin oxygen saturation in the brain (rSO_2) which could be used to optimise cerebral oxygenation during

CPR. However, although higher rSO_2 is associated with higher rates of ROSC, the association between rSO_2 during CPR and ROSC or early neurological outcome is not completely clear. Similarly, although rSO_2 is positively correlated with cerebral perfusion the exact relation is not yet know [62].

1.3.2 Ventilation

Artificial ventilation was first mentioned in the second century B.C. by Galen, who insufflated air in a dead animal's lung. Since then, artificial ventilation has evolved from mouth-to-mouth, positive pressure ventilation techniques of the 18th and 19th century and development of mechanical ventilation equipment [32] . Today, the emergency medical services (EMS), can use non-invasive ventilation device like bag-and-mask or invasive techniques, such as intubation to ventilate patients' lungs. The European Resuscitation Council (ERC) 2015 guidelines recommend a tidal volume of 6-7 $ml.kg^{-1}$ at a rate of 10.min^{-1} during CPR [63].

During cardiac arrest, the essential process of ventilation involves supplying air or a gas mixture to the lungs, facilitating the exchange of oxygen and carbon dioxide in the blood. In Advanced Life Support (ALS), positive-pressure ventilation with pure oxygen is widely considered the standard practice. However, there is a lack of clarity regarding the overall effectiveness of this method. Furthermore, uncertainties persist regarding the hemodynamic effects of positive end-expiratory pressure (PEEP) and the optimal role of high oxygen concentration during cardiopulmonary resuscitation (CPR). These questions underscore the need for further research to better understand and refine ventilation practices in the context of cardiac arrest [64].

<u>The need of ventilation during CPR</u>

In two studies, Aufderheide *et al.* [65, 66] showed the detrimental effects of hyperventilation during CPR. In a clinical observational study, they showed that when minute ventilation during CPR reaches 30 L minute, patients are very likely not to survive. Consistently, animals ventilated at high respiratory rates have worse hemodynamic profile (i.e. lower

coronary perfusion pressure) and higher mortality than animals receiving less ventilation per minute [67]. Additionally, hyperventilation could also cause hyperinflation of the lungs during CPR acting like cardiac tamponade. Berg *et al.* [68] suggested that chest compression interruptions are an additional harmful effect of hyperventilation. They demonstrated with an animal study that chest compression interruption for positive pressure ventilation reduce cerebral and coronary blood flow and perfusion pressure. Moreover, hyperventilation leads to hypocapnia which causes vasoconstriction of the cerebral vasculature and reduces cerebral blood flow jeopardizing neurological outcome.

In non-asphyxia CA, ventilation becomes crucial only as CO_2 clearance becomes necessary during prolonged CPR, while at the beginning ensuring blood circulation is key. Some researchers have suggested that the chest compression could possibly generate some tidal ventilation. However, in a clinical observation study, passive tidal volume produced by chest compression alone was found to be systematically low and far less than the average anatomical deadspace, thereby impeding alveolar ventilation [69]. Additionally, in animal models, absence of ventilation during CPR have resulted in worse 24 h neurological outcomes and decreased coronary blood flow likely as a consequence of prolonged exposure to hypoxaemia, hypercapnia and acidosis [70]. In addition to the peripheral vasodilation and reduced cardiac inotropism [71], these metabolic derangements increase pulmonary vascular resistance limiting pulmonary gas exchange and further decreasing CPR efficacy.

Recently, a proposed explanation behind the absence/presence of passive tidal ventilation from CC decompression was the concept of intrathoracic airway closure (IAC). IAC occurs when the end-expiratory lung volume falls below the closing capacity, which is the sum of residual and closing volume. In a cadaver study, Charbonney *et al.* [72] demonstrated that when IAC occurs during CPR, the negative pressure produced by chest decompression in the alveoli cannot be transmitted at the airway opening impeding any inspiratory flow despite a significant pressure gradient. Consistently, Grieco *et al.* [73] demonstrated that a small amount of PEEP (between 5-10 cmH2O) prevents IAC, increase airway opening index and the amount of CC passive ventilation.

Influence of positive pressure on circulation

The effect of positive end-expiratory pressure (PEEP) during intermittent positive pressure ventilation (IPPV) in patients undergoing cardiopulmonary resuscitation (CPR) on outcome is unknown. Positive pressure in the airways increase intrathoracic pressure proportionally to lung compliance and chest wall elastance. The impact of intrathoracic pressure on circulation is controversial. Some researchers have hypothesised the high intrathoracic pressure during decompression could prevent venous return and therefore stroke volume and organ perfusion. While others have speculated that high intrathoracic pressure could enhance CC by further ejecting blood out of the left ventricle.

In a small human study by Duchatelet *et al.* [74], OHCA patients treated with 5 cmH2O PEEP had increased likelihood of ROSC compared to patients without PEEP. Similarly, in an animal study by Voelckel *et al.* [75], pigs were randomly treated with different level of PEEP or without PEEP in addition to ACD-CPR with ITV. PEEP administration improved arterial partial pressure of oxygen and static lung compliance, whereas airway pressure was shown to decrease far below atmospheric pressure during decompression even with PEEP of 10 cmH2O. Additionally, in an asphyxia animal model of CA, McCaul *et al.* [76] found that continuous application of PEEP (5 cmH2O) during CPR increased survival without adverse cardiovascular effects.

In an animal study, Hevesi *et al.* [77] evaluated the use of continuous positive airway pressure (CPAP) compared to IPPV. The study found significant increased arterial partial pressure and decrease in CO_2 partial pressure; however, the haemodynamic profile was similar. In two human study by Saissy *et al.* [78] and Bertrand et al. [79], constant flow insufflation of oxygen (CFIO) with a flow rate of 15 $L.min^{-1}$ was also evaluated against IPPV. In both studies, the outcomes were not statistically significant; however, in Saissy *et al.* study [78] increased oxygen partial pressure and CO_2 clearance was observed with CFIO. However, in an animal study by Moore *et al.* [80], CFIO was evaluated against standard CPR and ACD-CPR with ITV. At no point in time did CFIO generate negative intrathoracic

pressures during CPR suggesting that CFIO does not enhance CPR but can potential have haemodynamic detrimental effect.

There are few data available regarding the best ventilation pattern when using positive-pressure ventilation.

Airway intervention

There are a variety of approaches to airway management during CPR; the ALS guidelines recommend a stepwise approach based on patient factors and the skills of the rescuer [30]. Identifying the most adequate ventilation technique remains a challenge. In the pre-hospital setting, no statistically significant difference in survival or neurological outcome has been identified between different airway interventions.

In a prospective RCT (AIRWAY-2) by Benger *et al.* [81] and a systematic review and meta-analysis by White *et al.*[82], no significant outcome differences were found in pre-hospital use of supraglottic airway versus. tracheal intubation; however, in a 21 multicentre RCT (PART) by Wang *et al.* [83], initial use of supraglottic airways (laryngeal tube) by prehospital personnel in CA patients was associated with higher survival rates at 72 h. The latter finding may be partly explained by the decrease in multiple attempts at endotracheal intubation, tube misplacement, and interruption of CPR when using a supraglottic airway. In an RCT (CAAM) by Jabre *et al.* [84], assessing the noninferiority of bag mask ventilation (BMV) against endotracheal intubation (ETI), no statistical difference in survival to 28 days between the groups was found. Emergency physicians supervised airway intervention and performed ETI. Nonetheless, a twofold increase of aspiration in the BVM group compared to the ETI group was reported, suggesting an important adverse risk in using BVM compared to ETI during initial airway management. [85]

1.3.3 Vasopressors and inotropes (pharmacologic treatments)

Antiarrhythmic drugs, vasopressors and inotropes are commonly used during resuscitation of cardiac arrest. Overall, there is limited evidence supporting the use of these medications. The rationale for the use of (vasopressors) adrenaline in CA is to increase diastolic

pressure, coronary blood flow and myocardial perfusion during CPR [86]. In a systematic review and meta-analysis by Kempton *et al.* [87] the use of epinephrine was associated with improved ROSC and survival to hospital admission. However, the use of epinephrine was not associated with a significant difference in survival to hospital discharge, neurological outcomes, or survival to 3 months.

In contrast, the PARAMEDICS trial, a randomized, double-blind study conducted by Perkins et al. [88], demonstrated that the administration of adrenaline to adults experiencing out-of-hospital cardiac arrest (OHCA) led to a significantly increased rate of 30-day survival compared to the use of a placebo. However, despite this survival benefit, there was no statistically significant difference between the two groups regarding favourable neurological outcomes [88]. In a retrospective study by Hubble *et al.* [89] early vasopressors administration was associated with improved neurological outcomes. Among adult, witnessed, non-traumatic arrests, the odds of hospital discharge with CPC 1 or 2 declined by 10% for every one-minute delay between public safety answering point call-receipt and vasopressor administration. However, the PARAMEDIC-2 study [90] found that while the duration of cardiac arrest is a significant factor influencing the likelihood of ROSC the time to drug administration is a vital determinant for survival. Although the risk ratio for adrenaline versus placebo may increase with time, this should not overshadow the crucial impact of timely drug administration on overall outcomes. Another analysis derived from a risk-adjusted sub-analysis of the PARAMEDIC-2 data [91] showed no significant difference in outcomes between drugs administered by the intraosseous route or by the intravenous route. Furthermore, while vasopressors (adrenaline) increase the chances of ROSC, repeated doses of adrenaline are associated with decreasing odds of survival [92]. In a systematic review and meta-analysis Yan et al. [93] failed to demonstrate increased benefit from vasopressin with or without adrenaline compared with the standard of care. However, vasopressin, steroids and adrenaline were associated with the improvement of ROSC in patients with IHCA.

In CA with shock-refractory ventricular fibrillation/pulseless ventricular tachycardia (VF/pVT), antiarrhythmics (amiodarone or lidocaine) are recommended to improve the chances of successful defibrillation [86]. In a randomized, double-blind trial, controlled trial (ALPS) significant association between lidocaine and ROSC was reported while survival to hospital discharge did not differ between group [94].

1.4 Post-cardiac arrest management

Following ROSC, only a minority of patients survive to hospital discharge. This high mortality following resuscitation is caused by a multitude of pathologies caused by the global ischaemia along with the precipitating aetiology. The conjunction of these pathologies is called ‘post-cardiac arrest syndrome’ (PCAS).

1.4.1 Post-cardiac arrest syndrome

Most patients that achieved a ROSC do not survive to hospital discharge because of the hypoxic-ischaemic injury caused by the CA [95]. The post-cardiac arrest pathologies syndrome are:

1. post-cardiac arrest brain injury, or hypoxic brain injury (HIBI)
2. post-cardiac arrest myocardial dysfunction
3. systemic ischaemia/reperfusion response, or multi organ failure (MOF)
4. persistent precipitating pathology

After CA a large release of cytokine mediates the reperfusion injury and other PCAS and cause systemic inflammation. High levels of inflammatory cytokines have been associated with mortality and/or poor neurological outcomes. [16]

Hypoxic ischemic brain injury (HIBI) is a leading cause of mortality and long-term neurologic disability in CA survivors. The pathophysiology of HIBI can be expressed in a “two hit model”. The primary injury is caused by the immediate cessation of cerebral perfusion. While the secondary injury is caused by combination of factors that may include reperfusion injury, microcirculatory dysfunction, impaired cerebral autoregulation, hypoxaemia, hyperoxia,

hyperthermia, fluctuations in arterial carbon dioxide, cerebral oedema, and concomitant anaemia [95].

Myocardial dysfunction is characterised by a low cardiac output and ventricular systolic and diastolic dysfunction. Most patients experience a reduced LVEF (>50%), due to the overlapping pathologies: ischaemia, reperfusion injury, toxic levels of inflammatory cytokines and other factors. [96]

The effects of whole-body ischaemia followed by reperfusion activate a systemic inflammatory response via immunological and coagulation pathways. Activating coagulation pathways without activating endogenous fibrinolysis will lead to microvascular thrombosis and multi organ failure. [97]

1.4.2 Post cardiac arrest treatments

Post cardiac arrest treatment is primarily directed to reverse the precipitating aetiology and minimise the effects of prolonged global ischaemia. The following areas need to be addressed simultaneously: adequate ventilation and oxygenation, haemodynamic optimization, cardiovascular stabilization, management of metabolic derangement, precipitating aetiology tackling and neurological assessment [98]. CAD is a common cause of precipitating aetiology; early coronary angiography has been associated with better outcomes [99]. Other post cardiac arrest syndrome has been addressed with different treatments: targeted temperature management (TTM), targeted mean arterial pressure (TMAP), targeted PaO_2 and $PaCO_2$ and anticoagulant therapy.

The current Advanced Life Support (ALS) guidelines recommend the administration of 100% oxygen during cardiopulmonary resuscitation (CPR) upon the return of spontaneous circulation (ROSC) and often for an extended period, sometimes hours, in the emergency department [100]. However, many studies and systematic reviews have found that hyperoxia (PaO_2>300 mmHg) is associated with increased mortality and neurological injury [101-104]. The pilot study COMACARE [105, 106] studied the effect of high-normal versus low-normal targets of arterial oxygen (10-15 kPa vs. 20-25 kPa), carbon dioxide (4.5-4.7 kPa

vs. 5.8-6.0 kPa). The study showed significantly improved regional brain oxygenation (rSO_2) with targeting high-normal PaO_2 and $PaCO_2$; however, this did not result in any decrease in markers for HIBI (NSE). The NEUROPROTECT trial [107] studied the effect of early goal directed haemodynamic optimization (targeting MAP between 85 mmHg and 100 mmHg and SVO_2 between 65%, and 75%) versus a MAP 65 mmHg strategy. The NEUROPROTECT study showed an improvement of brain oxygenation with hemodynamic optimisation but without any difference in neurological injury assessed with magnetic resonance imaging.

In another study of COMACARE, targeting low-normal (65-75 mmHg) or high-normal (80-100 mmHg) MAP after cardiac arrest was not found to have any statistical difference in HIBI marker [105].

TTM is a temperature control therapy with the goal of reducing ischaemia and reperfusion neurological injury. Conflicting evidence on the effectiveness of this therapy exists [108, 109]. Two recent publications by Duez *et al.* [110] and Lopez-de-Sa *et al.* [111] did not find significant statistical association between the duration of TTM and prognostic performance or the use different temperature in the range of [32ºC-34ºC] and neurological outcomes respectively.

After the return of spontaneous circulation (ROSC), various metabolic imbalances may manifest, including common ones such as hyperglycaemia and hyperlactatemia, as well as less frequent occurrences like hypoglycaemia. Hyperglycaemia is detrimental and impairs neurological recovery. Thus, moderate glycaemic control (7.992-9.99 $mmol.L^{-1}$) is preferred to strict control and insulin therapy should be targeted to this goal [112].

1.4.3 Outcomes evaluation & prognostic

Considerable research has been undertaken to discern both predictors and associations with outcomes in the realm of cardiac arrest studies. It's crucial to distinguish between predictors and associations when examining various indicators. There are generally three main outcomes highlighted in cardiac arrest studies: the return of spontaneous circulation

(ROSC), survival until hospital discharge, and neurological outcomes assessed through the modified Rankin Scale (mRS).

Predictors of increased survival rates and positive neurological outcomes after out-of-hospital cardiac arrest (OHCA) encompass factors such as an initial shockable rhythm, a witnessed arrest, the administration of bystander CPR, and a short duration from collapse to CPR [113]. These factors are identified as key predictors, implying a more direct influence on the outcomes.

On the other hand, associations with ROSC include high end-tidal CO2 (ETCO2) [114], elevated regional cerebral oxygen saturation (rSO2) [115, 116], increased myocardial contractility assessed with point-of-care ultrasound (PoCUS) [117], and hyperoxia [103]. Indicators associated with survival until hospital discharge involve lactate concentration [118-121], higher mean arterial pressure (MAP) [119], early angiography, and a greater difference between systolic and diastolic pressures. Indicators associated with good neurological outcome encompass factors such as low lactate levels (though not clearance) [118, 120, 121], mild hypercapnia [122], normoxia, and specific biomarkers.

Chapter 2. Aims of the thesis

2.1 The literature gaps and the limitations of standard approaches

Cardiac arrest remains a leading cause of death in many countries. Despite the many years of research on CPR and attempts to improve outcomes, survival to hospital discharge remains consistently low. Many human trials have attempted to identify the optimal CPR strategy, however the ethical constraints, time scale, the presence of confounding variables, the heterogeneity of the population and sample size present major obstacle. Similarly, many animal models fail to summarize the severity of human clinical cardiac arrest due to interspecies physiological discrepancies and lack of methodical rigour.

The hemodynamic effect of ventilation during CPR remains poorly understood. While a general consensus exists on the mechanism of cardiac pump during resuscitation, there is no consensus for the effect of the respiratory pump on CPR quality. Some researchers have argued that high intrathoracic pressure during decompression could prevent venous return and therefore stroke volume and organ perfusion. While others have speculated that high intrathoracic pressure could enhance chest compression by further ejecting blood out of the left ventricle. Therefore, it is urgent to investigate the impact of different airway strategy, ventilation techniques, positive end expiratory pressure (PEEP) and oxygenation (FiO_2) on CPR quality [123]. Furthermore, it is crucial to investigate the impacts vasopressors and inotropes on CPR quality and identifying the optimal dose and dose interval.

2.2 Aims of the thesis

The aims of the PhD thesis are to:

a) reduce the usage of animals in the CA and CPR field of research;
b) better understand the pathophysiology of CA;
c) investigate optimal and personalised CPR strategies.

To do so, a narrative review providing an overview of the current animal models of CA and CPR and the current computational tools applied in Systems in Medicine in the CA and CPR field was performed (Chapter 3).

In all the investigations included in this PhD thesis, the Interdisciplinary Collaboration Systems in Medicine (ICSM) simulation suite, the computational modelling developed by the supervisors at the University of Nottingham and our major collaborators at the University of Warwick, has been further developed, in the cardiac and cardiovascular models (described in section 4.1). In order to better understand the pathophysiology of CA and to investigate the effectiveness of personalised and optimal resuscitation strategies a series of new modules have been developed and integrated into the current ICSM suite (Section 4.2).

The gaps in knowledge related to resuscitation strategies are addressed in the next chapters (Chapters 5 to 11). The computer model, used and further developed, enabled the testing of different CPR strategies on the exact same cohort, allowing a clear comparison. The impact on CPR quality of the following strategies were investigated:

- Various ventilation strategies during CPR
- The impact of PEEP on CO during CPR
- The effect of chest compression rate, depth, and duty cycle
- The effect of the precipitating aetiology on CPR strategy optimization
- Personalised CPR strategies versus CPR following current guidelines

Chapter 3. Animal and computer models for improving CPR outcomes: a scoping review

Background: Cardiac arrest (CA) remains a leading cause of death in many countries. Despite the many years of research on CPR and attempts to improve outcomes, survival to hospital discharge remains consistently low. Innovative approaches to increase the understanding of the underpinnings of CA and CPR promise to enhance CA risk assessment, prevention, prognostic and might pave the way to tailored CPR strategies and post CA therapies.

Conclusion: In this scoping review, I provide an overview of the current animal models of CA and CPR and the current computational tools applied in systems medicine in the cardiac arrest and cardiopulmonary resuscitation field. I will discuss the status and challenges in implementing interdisciplinary systems medicine approaches in cardiac arrest research. [124]

3.1 Introduction

Cardiac arrest (CA) remains a leading cause of death in many countries. Despite the many years of research on CPR and attempts to improve outcomes, survival to hospital discharge remains consistently low. Innovative approaches to increase the understanding of the underpinnings of CA and CPR promise to enhance CA risk assessment, prevention, prognostic and might pave the way to tailored CPR strategies and post CA therapies.

In the first half of the present work, I provide a review of the current animal models of CA and CPR and assess the advantages and limitations of these models. In the second half, I focus on the current computational tools applied to investigate CA and CPR and discuss the status and challenges in implementing interdisciplinary systems medicine approaches in this research field.

3.2 Contemporary animal models of cardiac arrest

3.2.1 Definitions and inclusion/exclusion criteria

In this scoping review a cardiac arrest animal model was defined as intentional induction of cardiac arrest with subsequent cardiopulmonary resuscitation including manual/mechanical chest compressions or extracorporeal cardiopulmonary resuscitation. Studies of all types (diagnostic, prognostic, interventional, or pathophysiological) were included.

Only in vivo studies performed in mammals were included. Since this review focuses on contemporary animal models, I only included studies from the last year. The search was restricted to English studies. Letters, commentaries, editorials, case reports, reviews and solitary abstracts were excluded.

3.2.2 Search strategies and data extraction

I searched PubMed from March 1st 2020 to March 1st 2021. This one-year search window provides a recent snapshot of animal usage within the field of cardiac arrest research. The first part of the search strategy contained keywords relevant to cardiac arrest, while the second part of the search strategy included all relevant types of animals utilizing the search strategy suggested by Hooijmans et al. [125] and shown in Appendix 7.

I first screened titles and abstracts for relevant articles. Following initial screening, I then reviewed full text articles and, if deemed appropriate for inclusion, data were extracted. I only included data that were presented in the paper itself, i.e. I did not consider data provided in References.

3.2.3 Articles included and animal characteristics

I assessed 754 unique titles and abstracts; this yielded full review of 169 articles of which 112 full articles were included, see Figure 3.1. A full list of the 112 studies is provided in the Supplemental material. The 112 articles were published in 70 different journals. Journals publishing the highest number of cardiac arrest animal studies included Resuscitation (10

articles [9%]), Journal of the American Heart Association (7 articles [6%]), and Scientific Reports (6 articles [5%]). Most of the studies were conducted Asia (49 studies [44%]) followed by America (29 studies [26%]), Internationally (18 studies [16%]) and Europe (16 studies [14%]). China and United states of America accounted for most studies (respectively 40 studies [36%] and 28 studies [25%]).

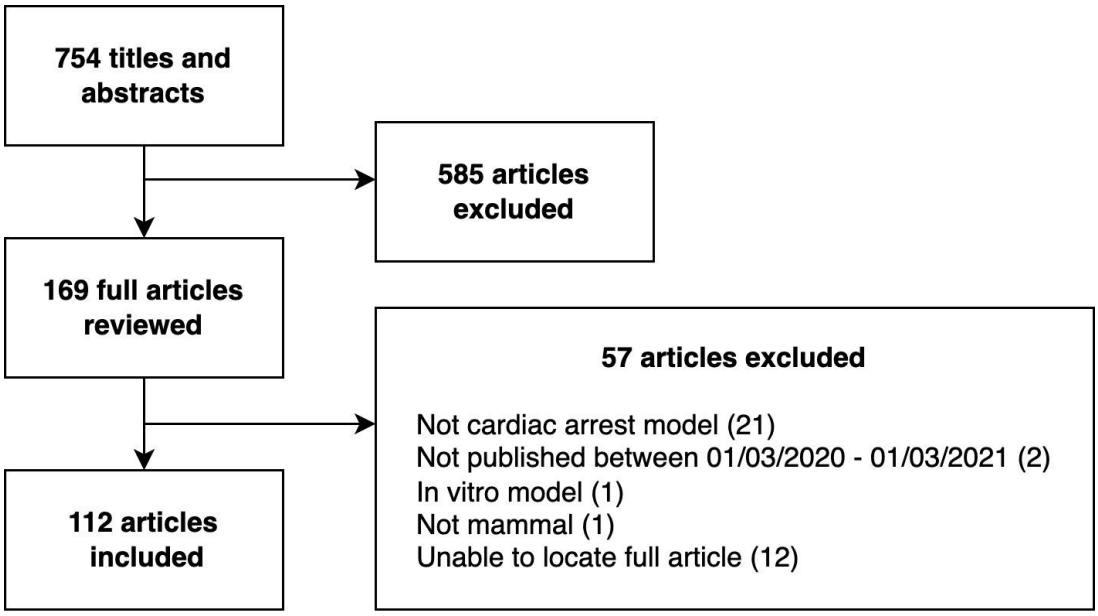

Figure 3.1 Article selection flow chart

The majority of studies investigated post CA interventions (47 [42%]) or CPR strategies (27 [24%]). The remaining studies focused on post CA brain injury (13 [12%]), CPR monitoring (11 [10%]), or other (14 [12%]).

Characteristics of the animals included in the studies are provided in Table 3.1. The most common animal type used was rat followed by pig, mouse, and rabbit. Male animals were used four times more often than female animals. Less than 10% of the studies used both female and male animals. The vast majority of the studies used adult animals that were otherwise healthy.

Table 3.1 Animals' characteristics.

Variable	Studies (n = 112)
Type of animal – n (%)	
Rat	51 (46%)
Pig	48 (43%)
Mouse	8 (7%)
Rabbit	3 (3%)
Sheep	2 (2%)
Age – n (%)	
Adult	86 (77%)
Paediatric	26 (23%)
Aged	0 (0%)
Morbidity – n (%)	
Healthy	112 (100%)
Genetically modified	0 (0%)
Co-morbidity condition	0 (0%)
Sex – n (%)	
Male	72 (64%)
Female	17 (15%)
Both	9 (8%)
Not reported	14 (13%)

Almost all the studies reported anaesthetizing and mechanically ventilating the animals prior to the induction of cardiac arrest. To induce cardiac arrest, most studies employed asphyxia induced cardiac arrest followed by ventricular fibrillation (induced by electric shock/pacing), potassium induced arrest or Haemorrhage induced cardiac arrest.

3.2.4 Animal models limitations

Cardiac arrest animal models still play an essential role in the advancement of our knowledge regarding the complex pathophysiology of cardiac arrest and the development of new treatments. However, many animal models fail to capture the severity of human cardiac arrest pathophysiology. Firstly, most animal studies of cardiac arrest use healthy young (or even new-born) animals and involve the asphyxia, electrocution, injection of potassium chloride or sudden occlusion of coronary arteries. This considerably differs from the

progressive development of human cardiovascular disease in patients who are older and have multiple co-morbidities [126, 127]. Co-morbidities may strongly influence the cardiac arrest pathophysiology and modify the effect of treatment [127]. Additionally, important anatomical and functional differences between humans and animals exists. Indeed, small mammals (rats, mice, guinea pigs, etc) can decrease their energy expenditure when facing lower oxygen availability (hypoxic hypometabolism) making them “oxyconformers”. Humans on the other hand are “oxyregulators”, compensating oxygen debt with anaerobic ATP production. The lack of metabolic rate regulation under hypoxic conditions constitutes a considerable physiological difference between humans and small animal models when studying cardiac arrest and CPR [128]. Similarly, the coronary circulation of pigs, animals that more closely resemble humans (due to the high percentage of genetic conservation and similar body/heart weight), has no anastomoses between branches [126]. Moreover, their thorax geometry and differences with humans, such as collateral ventilation explain the difficulty to extrapolate the effects of ventilation and compression during CPR [129]. Additionally, some of these studies [130-135] investigated the effect of targeted temperature management or hypothermia to improve neurological outcomes using rat, rabbit, and pig models. However, the thermoregulation of these animals is not comparable to the that of humans [136].

Furthermore, insufficient reporting and methodical rigour has been reported in animal models of cardiac arrest [137]. In a 2018 review by Bjorn *et al.*, methodology was not reported or was insufficient in 60% and 68% of the studies, respectively. The study identified major issues with randomisation, report of baseline characteristics, blinding, sample size calculation and specification of the primary outcome [137]. The poor development of methodology poses a considerable risk of bias and consequently a considerable prevalence of irreproducibility of these existing studies [138].

3.3 Computational tools for systems medicine in cardiac arrest and CPR

The objectives of any biomedical model and computer simulation are to advance knowledge in the medical field and provide a quantitative tool for clinicians. Researchers can use mathematical models to conduct virtual experiments and predict the effects of new treatments or manoeuvres. These models can also be used for diagnostic, outcome prediction, training, education, and decision making, and can also help clinicians interpret clinical data near real time and inform their decisions [139].

The following section reviews all the current computational tools used in the field of cardiac arrest and cardiopulmonary resuscitation. Five main computational tools have been identified to be commonly used in the field of CA and CPR: mathematical models of the cardiovascular system, machine learning, virtual and augmented reality, mathematical and finite element method models of the cardiac electrophysiology and computational fluid dynamics.

3.3.1 Mathematical model of the cardiovascular system

The pioneers of cardiovascular and pulmonary models were: Otto Frank [140] who developed Windkessel models (vessels) in 1899 (Figure 3.2) and Guyton *et al.* [141] who developed circulation regulation models in 1972. It is in the 1980s that the first mathematical cardiovascular models were developed to study CPR. In these mathematical models, the cardiovascular system is modelled as an electrical network system where the heart and vessels are modelled as resistive-capacitive networks; pressures in the vascular compartments as voltages; blood flow as electric current; blood inertia as inductance; and the cardiac and venous valves as diodes [142] (Figure 3.2).

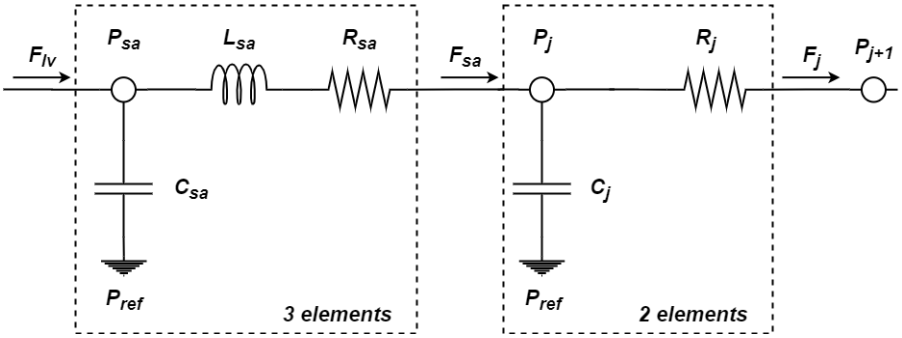

Figure 3.2 Two compartments Windkessel models representing vessels. Where F represents the flow, P the pressure, C the capacitance, L the impedance and R the resistance.

During the literature review, multiple papers investigating different CPR strategies were identified. The earliest mathematical model used to investigate CPR strategies can be traced back to 1984, in which Babbs et al. investigated alternative mechanisms generating artificial circulation during cardiopulmonary resuscitation (CPR) [142]. Since then, the following CPR strategies have been investigated by multiple cardiovascular models: interposed abdominal compression [143, 144], combined chest and abdominal compression and decompression [145-147], impedance valve [148, 149], passive leg raise [150, 151], periodic z-axis acceleration (pGz)-CPR [152], and the ratio of chest compressions to ventilations [153, 154].

The effect of tidal volume of gas exchange during rescue ventilation was investigated by Fitz-Clarke [155].

In another study, Boe et al. investigated the effect of substrate stiffness on chest compression in CPR and found that the effectiveness of chest compression during standard CPR may be seriously degraded on soft supporting surfaces such as hospital beds [156].

Other studies have tried to identify the optimal chest compression and decompression in terms of blood flow. Jung et al. applied optimal control to identify the chest compression and decompression frequency and duty cycle that maximized the coronary perfusion pressure (CPP) [157] and maximized the blood flow as measured by the pressure difference between the thoracic aorta and the right atrium [158]. John et al. also investigated the optimal chest compression pressure and rate to maximize cardiac output and found them to be similar to the ones recommended by the European Resuscitation Council (ERC) and American Heart

Association (AHA) guidelines [159]. Similarly, Babbs et al. investigated the optimal chest compression frequency for different sized people from neonate to adult [160].

Other studies have used mathematical cardiovascular models to offers insights into fundamental aspects of circulation during CPR. Mathematical models offer quantitative results for flows, pressures and volumes under clearly defined conditions, chosen by the experimenters [161]. Noordergraaf et al. investigated the importance of cardiac valves during CPR [161].

More recently, Shin et al. have developed a lumped parameter model of CPR that can more accurately reflect the current CPR physiology. By adding compartments of the superior and inferior vena cava of the thoracic cavity to the existing CPR model, the “hybrid pump” mechanism was applied to simulate CPR [162].

3.3.2 Other cardiac arrest and CPR computational tools

Machine learning

Machine learning (ML) and Artificial intelligence (AI) systems are increasingly being used in healthcare, thanks to the high level of performance that these systems have proven to deliver. So far, clinical applications have focused on diagnosis and on prediction of outcomes. [163]

Multiple machine learning models have been used to predict cardiac arrest in different settings with different clinical data. Two studies use machine learning models for the early prediction of cardiac arrest in in a paediatric intensive care unit [164] [165]. Similarly, machine learning models have been used for early prediction of: cardiac arrest and respiratory failure using simple trajectories of patient data [166], the prediction of SCD in heart failure (hf) patients with low LVEF [167], in-hospital cardiac arrest using value of laboratory results in addition to vital signs [168], hf patients at risk of cardiac arrest in emergency departments. [169], rearrest [170], prognostic model for risk of SCA using clinical, genetic and metabolic data [171], for detecting clinical deterioration on the wards in a large, multicentre database [172], acute clinical deterioration triggered by hypotension,

ventricular fibrillation, and an undiagnosed multiple disease condition using biological signals, such as heart rate, RR interval, and blood pressure [173].

Machine learning is also used for the prediction of multiple arrhythmias [174-177]. This prediction of arrhythmias is crucial for improving resuscitation. In one study, a machine learning is used to produce reliable shock/no-shock decisions during CPR [178]. Machine learning has also been used for the recognition of abnormal chest compression depth [179], for studying correlations between the performance and outcome of resuscitation efforts in real-world clinical settings using data recorded by automatic devices, such as automatic external defibrillators, and to explore effects of shock timing and chest compression depth in the field [43], the optimizing timing of defibrillation [180], and the detection of shockable and non-shockable rhythms [181].

Finally, ML has also been used for early prediction of long-term outcomes. One study used ML to predict functional outcome based on 19-channel-EEG recorded from 267 adult comatose patients during targeted temperature management after CA [182]. Another study created an early prediction of outcome model and use this model to investigate intervention effects on classes of illness severity in cardiac arrest patients treated with targeted temperature management (TTM) [183]. Another study developed a ML algorithm to accurately predict a culprit coronary artery disease lesion in patients with OHCA [184].

Virtual and augmented reality

Computer tools and software have been around for decades to help train and educate the medical and non-medical staff for basic life support (BLS). In 1991, Tanner et al. used “Code Red” software to simulate diverse cardiac emergency [185]. The software displayed rhythm and vital signs change based on actions of the user or to simulate an improving or worsening emergency.

Today, virtual and augmented reality along with complex manikins allows for more complex and “real life scenario” training opportunities for medical staff. Multiple studies have assessed whether virtual and augmented reality could be used to train medical and non-medical staff for basic life support (BLS) [186-189].

Mathematical and finite element method (FEM) models of the cardiac electrophysiology

Starting in the 1960s, a large number of mathematical models of cardiomyocyte electrophysiology have been developed; the complexity of these models has increased progressively since then as more and more experimental data have become available. [190]

These models are used to investigate the pathophysiology of ventricular arrhythmias. [191] [192], predict ablation targets for ventricular tachycardia [193, 194] and predict drug-induced arrhythmogenic risk [195].

Computational fluid dynamics

One study investigated whether the stretch-recoil capability of veins, at least in part accounts for the slower response to simulated cardiac arrest. The effects of stretch-recoil zones of venous vessels with different diameters and velocities on blood velocity and dynamic pressure analysed using computational fluid dynamics (CFD) modelling. [196]

3.4 Future perspectives

I have presented an overview of the recent progress in the field of computational modelling and simulations, highlighting their potential as tools for future clinical translation. Nevertheless, significant obstacles remain before widespread adoption of this methodology in the clinic is feasible [197].

Chapter 4. Methods

4.1 The Interdisciplinary Collaboration in Systems Medicine (ICSM) simulation suite

All of the studies presented in this thesis utilised the Interdisciplinary Collaboration in Systems Medicine (ICSM) suite of physiological simulations, an integrated set of multi-compartmental models that has been developed over the past 20+ years, which has been extensively validated in multiple studies [11, 198-205] by the supervisors, Prof Jonathan Hardman and Dr Marianna Laviola and their research group. The ICSM simulation suite is built in a MATLAB (MathWorks, Natick, MA) superstructure. The model was initially developed as a respiratory model composed of several components: mouth or ventilator compartment, series deadspace (SD) and alveolar compartments, used to investigate novel mechanical ventilation strategies. Later a cardiovascular model was added with pulmonary and systemic vasculatures, cardiac chambers and peripheral tissue compartments [206]. Each component is described as several mass-conserving functions and solved as algebraic equations, obtained or approximated from the published literature, experimental data and clinical observations. These equations are solved in series in an iterative manner, so that solving one equation at current time instant (*tk*) determines the values of the input variables in the next equation. At the end of the iteration, the results of the solution of the final equations determine the input variables of the first equation for the next iteration.[207]

The equations describing the cardiovascular system, shown in Figure 4.1, have been obtained by enforcing conservation of mass and balance of forces for each vascular compartment. The cardiovascular model consists of 19 compartments, each described with a pressure P_x, volume V_x, and flow F_x leaving the compartment, updated at each iteration. Additionally, each compartment is defined by fixed parameters: a linear resistance R_x, an elastance coefficient λ_x, an unstressed volume $V_{x,u}$ and a coefficient $P_{x,c}$ depicting the pressure in the compartment when $V_x = V_{x,u}$.

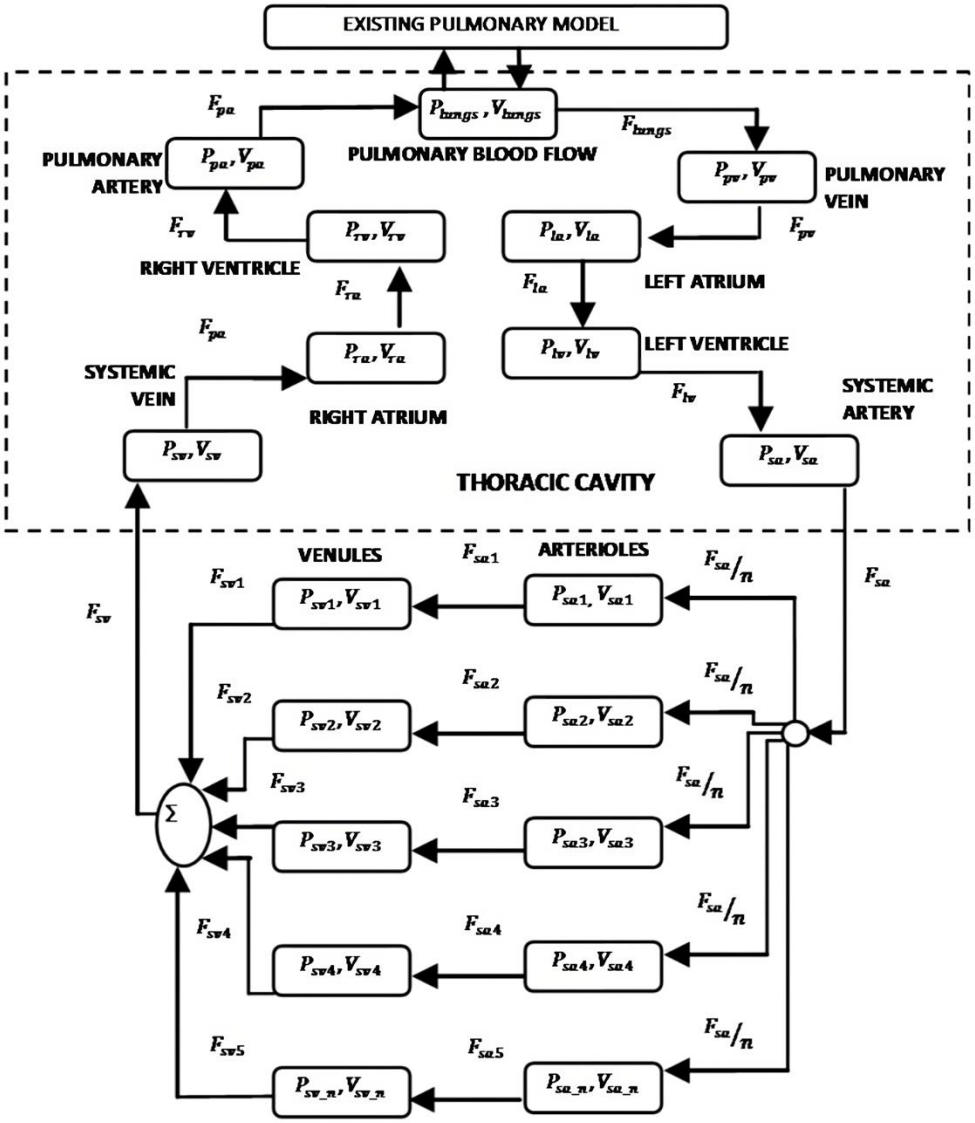

Figure 4.1 Schematic of the cardiovascular system added to the existing pulmonary model [206].

For all the vascular and atrial compartments, vascular elastance is assumed to be nonlinear and to have an exponential relationship governed by the following equation,

Equation 4.1

$$P_x = P_{x,c} e^{\frac{\lambda_x (V_x - V_{x,u})}{(V_x + V_{x,u})}}$$

where the subscript x represents the compartment number and the $\lambda_x, P_{x,c}, V_{x,u}$ are constants that give flexibility in matching specific shapes and peaks of pressure waveforms that could be observed from clinical data [206].

The ventricles are modelled as having time varying elastances over the duration of a cardiac cycle using different exponential functions to describe the filling and emptying of the ventricles. The shift from the systolic to diastolic relationship is governed by a pulsating activation function φ with period T. The pressure in the ventricles is governed by the following equation,

Equation 4.2

$$P_v = \varphi P_{v,sys,c} e^{\frac{\boldsymbol{\lambda_{v.sys}}(V_v - V_{v,sys,u})}{(V_v + V_{v,sys,u})}} + (1-\varphi) P_{v,dys,c} e^{\frac{\boldsymbol{\lambda_{v.dys}}(V_v - V_{v,dys,u})}{(V_v + V_{v,dys,u})}}$$

where the subscript v represents the ventricles, $P_{lv,sys,c}$ is the constant of systolic pressure, $P_{lv,dys,c}$ is the constant of diastolic pressure, $\boldsymbol{\lambda_{lv.sys}}$ is the constant of elastance during systole, $\boldsymbol{\lambda_{lv.dys}}$ is the constant of elastance during diastole, $V_{lv,dys,u}$ is the constant end diastolic volume, $V_{lv,sys,u}$ is the end systolic volume. The activation function φ t is defined as:

Equation 4.3

$$\varphi = \begin{cases} \left(sin\left(\pi \boldsymbol{T} \frac{u}{T_{sys}}\right)\right)^2 & if\ u \geq 0\ and\ u \leq \frac{T_{sys}}{2} \\ 0, & if\ u > \frac{T_{sys}}{2}\ and\ u \leq 1 \end{cases}$$

where T is the period of the heart rate and T_{sys} is the systolic period. u is a real number ranging between 0 and 1 and it models the fraction of the cardiac cycle. $u = 0$ at the end of systole and $u = 1$ at the end of diastole. The blood flow between compartments is determined by the pressure gradient between compartments across a linear time invariant resistance R_x.

Equation 4.4

$$F_x = \frac{\eta_x (P_x - P_y)}{R_x}$$

Equation 4.5

$$\eta_x = \begin{cases} 0, & if\ P_x < P_y \\ 1, & if\ P_x \geq P_y \end{cases}$$

The parameter η_x allows the blood to flow in one direction but can be altered to investigate flow backwards into a compartment, such as during aortic regurgitation. The volume of the blood in each compartment is computed by applying conservation of mass as follows:

Equation 4.6

$$V_x = V_{x,0}\left(F_y - F_x\right)\Delta t$$

While Equation 4.6 accurately captures the conservation of mass in the model by relating the change in blood volume V_x within a compartment to the difference between inflow F_y and outflow F_x rates over the sampling period Δt, it's important to note that this simplified lumped parameter model does not explicitly account for the conservation of momentum. The model assumes instantaneous propagation of changes in flow and pressure throughout the compartment, neglecting the detailed fluid dynamics and interactions that would be described by more complex equations, such as the Navier-Stokes equations, which specifically address the conservation of momentum in fluid flow.

The pulmonary model includes a series deadspace (SD) and 100 independently configurable alveolar compartments. The SD is modelled as series of stacked, rigid laminae ($N_{lam} = 50$) of equal volume and its static total volume is set to 130 ml. The volume is composed of oxygen (O_2), nitrogen, carbon dioxide (CO_2), water vapour and a 5th gas used to model additives. The gases shift up or down the stacked laminae, driven by the pressure gradient between the alveoli and the environment.

The pressure of each alveolar compartment is described by a cubic function,

Equation 4.7

$$p_i = ((10 \cdot v_i - 300)^3/6600) - P_{ext,i} \qquad v_i > 0 \qquad for\ i = 0, \ldots, N_{alv}$$

$$p_i = 0 \qquad otherwise$$

where p_i is the alveolar pressure for the i^{th} of N_{alv} alveolar compartments for the given volume of alveolar compartment, v_i. $P_{ext,i}$ (per alveolar unit, in cmH_2O) represents the effective net pressure generated by the sum of the effects of factors outside each alveolus.

Finally, the model simulations ran with MATLAB version R2019a.v4 (MathWorks Inc., Natick, MA, USA).

4.2 New modules development

While advancing the computational investigations, enhancements were made to the existing ICSM simulator by incorporating several novel cardiac and cardiovascular modules utilizing MATLAB (R2019b Update 7). The newly integrated modules, detailed in the respective chapters denoted in brackets, draw upon equations and input parameters sourced from other research groups. It is noteworthy that the assimilation of these mathematical formulations into the ICSM required model modifications and meticulous calibration for seamless integration and accurate simulation.

- Multiple tissue compartments (Chapter 5)
- Capillary blood compartment (Chapter 5)
- Atrial contraction (Chapter 6)
- Collapsible vasculature (Chapter 6)
- Pleural pressure (Chapter 6)
- Addition of vascular impedance (Chapter 6)
- Compensation mechanism occurring during MI and HS (Chapter 7)
- Circulatory transport delays (Chapter 8)
- Thoracic vein (Chapter 8)
- Thoracic model (Chapter 8)
- Retrograded blood flow model (Chapter 8)
- Cardiovascular and respiratory control mechanism (Chapter 12)

Chapter 5. Gas exchange in the capillary bed during cardiac arrest

5.1 Introduction

The aim of this chapter is to present the development of the ICSM computational model of multi organs tissue and multi within tissue capillary blood compartments in order to investigate the blood flow and gas exchange in the capillary bed during CA and CPR. Modelling multiple organ tissues and their associated capillaries is paramount to understand the different state of hypoxia and hypercapnia in the different organ tissue during CA. Additionally, modelling these will help to evaluate the optimal CPR strategy. These new compartments can help us identify the optimal chest compression strategy to optimize the blood flow to the vital organs, but also guide the ventilation strategy to achieve normal oxygen level without reaching excessive oxygen exposure during CPR which has been associated with cerebral oxidative injury [208]. Finally, modelling the different organ tissue will help us more accurately model the effect of vasopressors which affect each organ tissue differently.

5.2 Methods

For the purpose of this study, I developed two new modules:

- Module 1: representing five organ tissue compartments, i.e. heart, brain, kidney, splanchnic organs and rest of the body (Figure 5.1), implemented to investigate the effect of CA on different vital organs;

- Module 2: consisting in five within tissue capillary blood compartments modelled to investigate the evolution of gas content in the capillary blood during ischaemia (Figure 5.2)

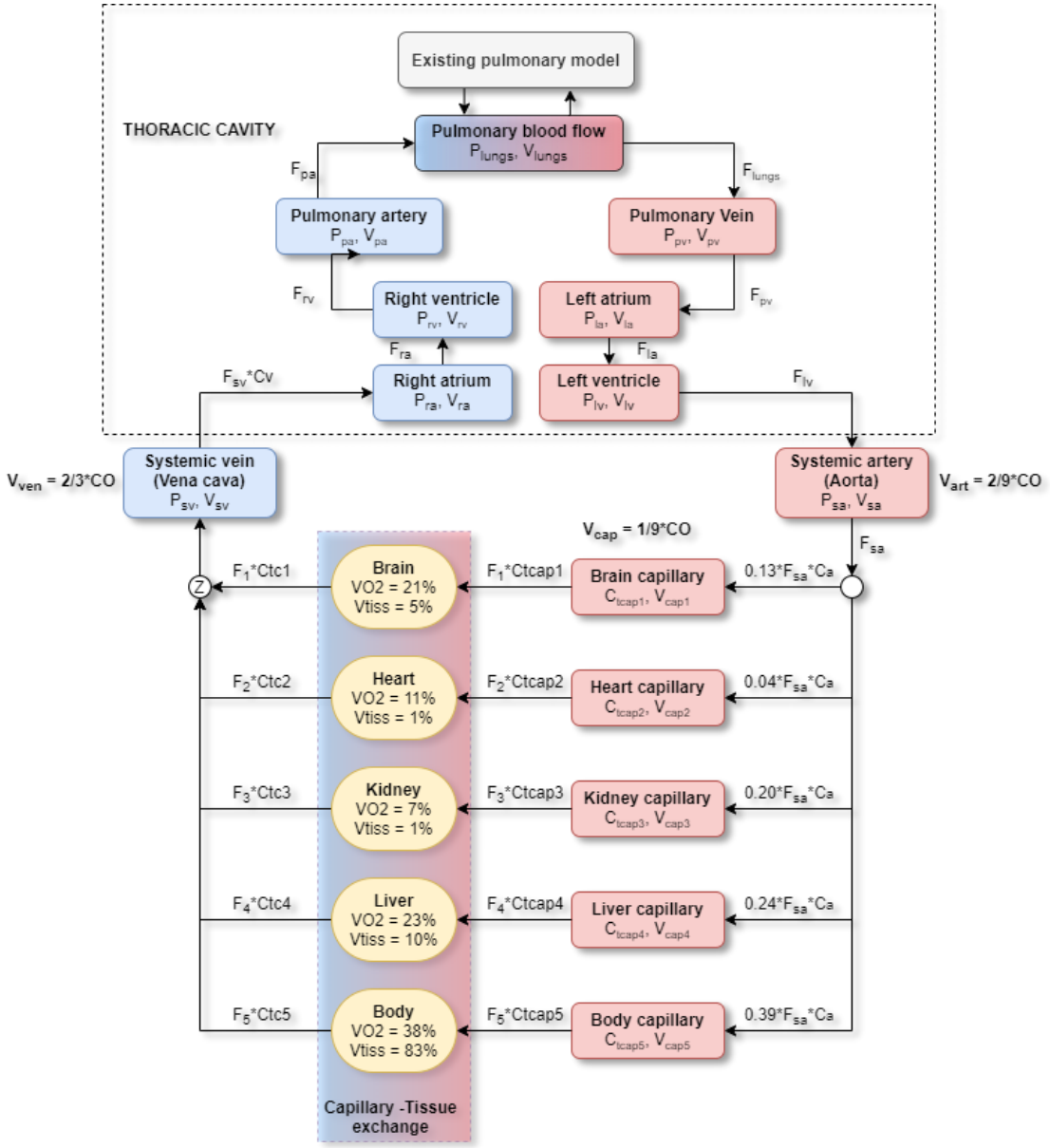

Figure 5.1 Schematic diagram of the multiple organs tissue and capillary compartments.

In module 1, the organ tissue compartments were defined by their oxygen consumption per minute (VO_2), volume (Vtiss) and perfusion (Flow) (Figure 5.1). The total volume of organ tissue was defined as 0.66 of the body weight (set to 70 kg) and the volume of each of the five compartments (Vtiss) was based on the organ weight [13]. The perfusion (Flow) was defined as percentage of the cardiac output ([CO] set to 5 L) to obtain the physiological blood flow specific to the organ tissue compartment [13]. In module 2, the total capillary blood was set to 0.11 of CO and each of the five capillary compartments volume (Vcap) was

based on the organ weight (Table 5.1). During CA, gas exchange between the new capillary blood compartments and tissue capillary will be maintain (Figure 5.2) allowing the capillary blood compartments to act as a reservoir of oxygen.

Table 5.1 Organ tissue and capillary compartments parameters setting.

	VO_2 (%)	Vtiss (%)	Flow (%)	Vcap (%)
Brain	21%	5%	14%	5%
Heart	11%	1%	5%	1%
Kidney	7%	1%	20%	1%
Splanchnic organs	23%	10%	23%	10%
Body	38%	83%	38%	83%

VO_2, oxygen consumption; Vtiss, tissue volume; Flow, perfusion of the organ; Vcap, capillary blood. Each parameter is presented as percentage of its total.

Protocol

A virtual healthy subject was configured as in our previous study [209]. After 5 minutes of spontaneous ventilation (SPV), CA was modelled by setting the heart rate to 0 and activating the apnoea with obstructed upper airway. The oxygen (O_2) and carbon dioxide (CO_2) contents were recorded every 5 ms.

.

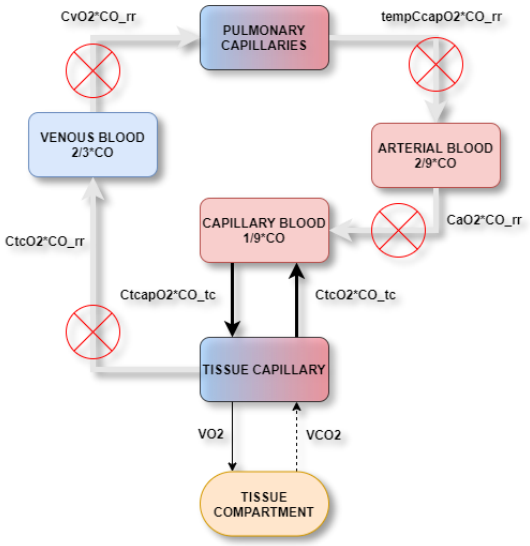

Figure 5.2 Schematic diagram of the exchanges during cardiac arrest.

5.3 Results & Findings

The time course of O_2 content in the tissue capillary for the five organs tissue compartments, during ischaemia is shown in Figure 5.3. the kidney exhibits the swiftest desaturation (40 seconds), succeeded by the heart (50 seconds), the brain (80 seconds), and the liver (100 seconds). The compartment representing the remaining tissues not listed before desaturates in 14 minutes, which is considerably longer than the brain, heart kidney and liver. This sequencing aligns with previous findings underscoring the distinct vulnerability of each organ to severe hypoxia. For instance, acute severe hypoxia can induce loss of consciousness within 10 to 20 seconds and result in permanent brain damage within 3 minutes [210].

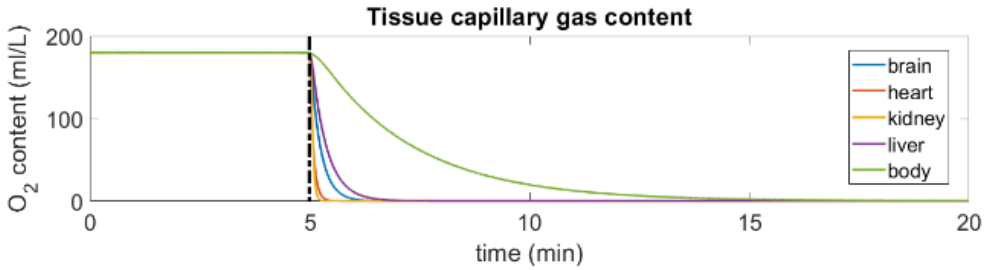

Figure 5.3 Time course of oxygen content in the tissue capillary during SV and ischaemia. The vertical black line represents the beginning of CA.

Using and further developing the ISCM computational modelling, it has been possible to obtain the quantitative evolution of O_2 concentration in multiple capillary blood tissues during untreated cardiac arrest. This study only included oxidative metabolic processes; the addition of anaerobic glycolysis has not been in the modelling of ischaemia.

The split of single tissue compartment into five system specific tissues has been done to assist understanding of the pathophysiology of cardiac arrest. However, the number and partitioning of tissue compartments can be modified to model as many tissue compartments as necessary.

Similar splitting can be found in Albanese *et al.*[211], where the whole body is partitioned into five tissue compartments (extra splanchnic, splanchnic, muscle, brain and heart).

However, their model does not differentiate between arterial and capillary blood compartments.

Chapter 6. Atrial contraction & cardiovascular equations

6.1 Introduction

The aim of this chapter is to present the integration of a new model of cardiac contraction, including atrial contraction, a new model of vasculature (new pressure, volume, and flow equations), a new collapsible systemic vein model (with non-linear and collapsible compliance), and new model of pleural pressure (affecting the intrathoracic pressure). These modules were integrated because of their effects on the modelling of CA and CPR. Indeed, during untreated CA all the system cardio vasculature reaches mean systemic filling pressure, therefore, the vasculature equations need to be updated to be stable during CA. Additionally, during CPR the chest cause a significant increase in intrathoracic pressure which can lead to the collapse of intrathoracic veins. Similarly, during CPR the ventilation can cause an increase in alveolar pressure further increasing the intrathoracic pressure through the pleural pressure.

6.2 Methods

Solving ordinary differential equations (ODE)

The upcoming modules, introducing a new vascular model and a cardiovascular control mechanism, entail the resolution of a set of interconnected ordinary differential equations (ODEs). The 4th order Runge-Kutta method was deliberately chosen due to its accuracy achieved through intermediate steps, stability, efficient convergence, and implementation simplicity in tackling these ODEs. This method ensures a precise and robust numerical solution, aligning seamlessly with the complex dynamics of the physiological systems under consideration.

Equation 6.1

$$\frac{d}{d\mathrm{t}}x = f(t, x)$$

$$k_1 = f(t_n, x_n)$$

$$k_2 = f\left(t_n + \frac{h}{2}, x_t + \frac{h}{2} \cdot k_1\right)$$

$$k_3 = f\left(t_n + \frac{h}{2}, x_t + \frac{h}{2} \cdot k_2\right)$$

$$k_4 = f(t_n + h, x_t + h \cdot k_3)$$

$$x_{t+1} = x_t + \frac{h}{6}(k_1 + 2 \cdot k_2 + 2 \cdot k_3 + k_4)$$

where x is the parameter to solve, and h is the time step, varying from 0.005 s and 1e-04 s. In order to solve the ODE a cardiovascular "while" loop was created to allow a smaller time step (h2 = 1e-04 s). The cardiac "while" loop enhances the precision of the cardiovascular model by focusing on a smaller time step, capturing rapid changes and fluctuations. Within this loop, the pressures, flows and volumes of the cardiovascular compartments are calculated along with the cardiovascular control mechanism parameters.

New cardiac chamber contraction model

The new model of cardiac chambers (atrial and ventricles) contraction is adapted from Bozkurt work [212], specifically referencing Equations 6.2 to 6.6. The ventricles are modelled as having time varying elastances over the duration of a cardiac cycle using different exponential functions to describe the filling and emptying of the ventricles. The shift from the systolic to diastolic relationship is governed by a pulsating activation function $f_{ventricle}(t)$ with period T. The pressure in the ventricles is governed by the following equation:

Equation 6.2

$$P_{lv}(t) = E_{s,lv}[V_{lv} - V_{lv0}]f_{ventricle}(t) + \big(1 - f_{ventricle}(t)\big)[P_{lv0}e^{(B_{lv}V_{lv})} - 1]$$

where the subscript lv represents the left ventricles, P_{lv0} is a constant of the diastolic pressure, B_{lv} is the, $E_{s,lv}$ is the ventricular elastance during systole, V_{lv0} is the unstressed ventricular volume, V_{lv} is the left ventricle volume. The activation function $f_{ventricle}(t)$ is defined as:

Equation 6.3

$$f_{ventricle}(t) = \begin{cases} \dfrac{1 - cos\left(\pi \dfrac{u}{T_1}\right)}{2} & 0 \le u < T_1 \\ \dfrac{1 + cos\left(\pi \dfrac{u - T_1}{T_2 - T_1}\right)}{2} & T_1 \le u < T_2 \\ 0 & T_2 \le u < T \end{cases}$$

where, u is the time over a cardiac cycle, T_1, T_2 and T are the times at the end systole, end of ventricular relaxation and cardiac period.

Similarly, the atria are modelled as having time-varying elastances over the duration of a cardiac cycle. The shift from the systolic to diastolic relationship is governed by a pulsating activation function $f_{atria}(t)$ with period T_a. The pressure in the atria is governed by the following equation,

Equation 6.4

$$P_{la}(t) = E_{la}(t)[V_{la} - V_{la0}]$$

where V_{la} is the instantaneous volume in the atria, V_{la0} is the atrial unstressed diastolic volume and $E_{la}(t)$ is the time varying atrial elastance. The atrial elastance is defined as,

Equation 6.5

$$E_{la}(t) = E_{min,la} + 0.5\big(E_{max,la} - E_{min,la}\big) f_{atria}(u - D)$$

where $E_{min,la}$ and $E_{max,la}$ are the diastolic and systolic elastance and D is the delay. The atrial activation function $f_{atria}(t)$ is defined as,

Equation 6.6

$$f_{atria}(t) = \begin{cases} 0 & 0 \le u \le T_a \\ 1 - cos\left(2\pi \dfrac{u - T_a}{T - T_a}\right) & T_a \le u \le T \end{cases}$$

where T_a is the atrial relaxation period.

Table 6.1 presents the values of cardiac chambers parameters for a healthy subject which were obtain from Bozkurt [212].

Table 6.1 Healthy subject cardiac chambers parameter values obtained from Bozkurt [212]

	Left ventricle	**Right ventricle**	**Left Atrium**	**Right Atrium**
V_0 (ml)	10	40	5	5
E_S (mmHg.ml^{-1})	2.5	1	-	-
P_0	1	1	-	-
B_v	0.02	0.02	-	-
E_{max} (mmHg.ml^{-1})	-	-	0.3	0.3
E_{min} (mmHg.ml^{-1})	-	-	0.2	0.2
T_1 (s)	0.33.T	0.33.T	-	-
T_2 (s)	0.45.T	0.45.T	-	-
T_a (s)	-	-	0.8.T	0.8.T
T (s)	HR/60	HR/60	HR/60	HR/60
D (s)	-	-	0.04	0.04

V_0: zero pressure volume values of the heart chambers; E_s: left and right ventricular end-systolic elastance P_0 constant of the diastolic pressure, B_v: coefficients in the passive component of the ventricular pressure signals; E_{max}: atrial maximal elastance; E_{min}: atrial minimum elastance; T_1, T_2, T_a, T and D: parameters describing the onset of the ventricular and atrial contraction and relaxation times.

New vasculature pressure module

The vascular pressure equations are based on Albanese *et al.* work [211], specifically referencing Equations 6.7 to 6.13. All the vascular compartments are modelled as a two element Windkessel system (Figure 6.1) with a resistance (*R*) that accounts for energy losses, and capacitance (*C*) to determine the blood volume in each compartment. In the systemic artery (representing the aorta) and the pulmonary artery where the inertial forces in blood are relevant an additional impedance (*I*) is added, therefore being a three element Windkessel system (see Figure 6.1).The Windkessel system allow to model the vascular compartments as elastic reservoir. [213]

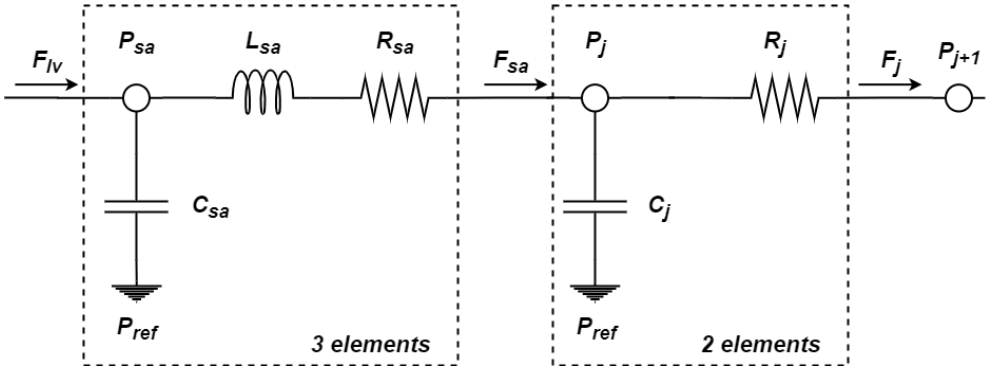

Figure 6.1 Two compartments Windkessel models. Where *F* represents the flow, *P* the pressure, *C* the capacitance, *L* the impedance and *R* the resistance.

The vascular pressures are computed as,

Equation 6.7

$$P_j = \frac{\left(F_{j-1} - F_j\right)}{C_j}$$

where P_j is the vascular compartment pressure, V_j is the volume, $V_{u,j}$ is the unstressed volume and C_j is the capacitance. The flow F_j between compartments is calculated as,

Equation 6.8

$$F_j = \frac{P_j - P_{j+1}}{R_j}$$

where P_{j+1} is the pressure of the compartment receiving flow F_j and R_j is compartment's j vascular resistance. The flow leaving the systemic artery and pulmonary artery are calculated as,

Equation 6.9

$$F_{sa} = \frac{P_{sa} - P_{sa1}}{R_{sa}} - \frac{L_{sa}}{R_{sa}}\frac{dF_{sa}}{dt}$$

Equation 6.10

$$F_{pa} = \frac{P_{pa} - P_{lungs}}{R_{pa}} - \frac{L_{pa}}{R_{pa}}\frac{dF_{pa}}{dt}$$

where L_{sa} and L_{pa} are the systemic and pulmonary arteries inductances. The table 6.2 below presents the values of parameters for a healthy subject directly obtained from Albanese work [211]. Posteriorly a range of values will be identified for healthy subjects.

Table 6.2 Parameters of the vascular system in basal condition for a healthy subject obtained from Albanese [211]

Compartment	Compliance (ml.mmHg^{-1})	Unstressed Volume (ml)	Resistance (mmHg·s·ml^{-1})	Inertance (mmHg s^2·ml^{-1})
sa	0.280	0.000	0.050	2.2 10^{-4}
sa1	0.186	31.800	11.424	–
sa2	0.037	6.360	32.000	–
sa3	0.037	6.360	8.000	–
sa4	0.373	63.600	7.120	–
sa5	3.087	527.000	4.208	–
sv1	1.456	55.650	0.357	–
sv2	0.291	11.130	1.000	–
sv3	0.291	11.130	0.250	–
sv4	2.912	111.300	0.223	–
sv5	24.171	923.790	0.132	–
sv	20	1969.500	0.05	–
pa	0.760	0.000	0.023	1.8 10^{-4}
lungs	5.800	65.500	0.089	–
pv	25.370	272.700	0.006	–

1: splanchnic tissue; 2: extra-splanchnic; 3: muscle tissue; 4: myocardial tissue, 5: cerebral tissue; sa: systemic artery; sv: systemic vein; pa: pulmonary artery; pv: pulmonary vein.

The parameters values have been adapted from Albanese *et al.* [211] to fit the ICSM simulator.

Collapsible Thoracic vein

The thoracic vein (systemic vein) is modelled as a collapsible vein (see Figure 6.2).

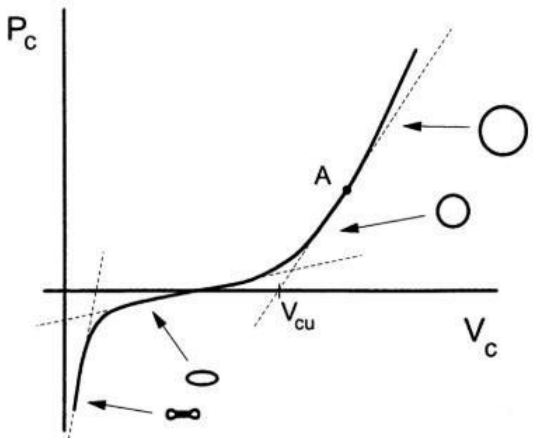

Figure 6.2 Typical Pressure–Volume (PV) relationship of a blood vessel.

The nonlinear PV relationship of the thoracic veins compartment has been derived as,

Equation 6.11

$$P_{sv} = P_{tv} + P_{pl}$$

$$P_{tv} = \begin{cases} D_1 + K_1 \cdot \left(V_{sv} - V_{u,sv}\right) - \psi & V_{sv} \geq V_{u,sv} \\ D_2 + K_2 \cdot e^{\frac{V_{sv}}{K_{xv}}} - \psi & V_{sv} < V_{u,sv} \end{cases}$$

$$\psi = \frac{K_{xp}}{e^{\frac{V_{sv}}{K_{xv}}} - 1}$$

Where P_{tv} and V_{sv} are the transmural pressure and volume of the thoracic veins compartment, respectively.

To account for the fact that when the vessel collapses, the blood flow toward that compartment is extremely reduced, the resistance of the thoracic veins compartment varies as a function of the volume,

Equation 6.12

$$R_{sv} = K_R \cdot \left(\frac{V_{sv,max}}{V_{sv}}\right)^2 + R_{sv,0}$$

Table 6.3 Parameters of the thoracic vein from Albanese [211].

Variable	Value
D_1 (mmHg)	0.3855
K_1 (mmHg.ml^{-1})	0.15
V_{usv} (ml)	130
D_2 (mmHg)	-5
K_2 (mmHg.ml^{-1})	0.4
$V_{sv,min}$ (ml)	50
K_{xp} (mmHg)	2
K_{xv} (mmHg)	8
K_R (mmHg.s.ml^{-1})	0.001
$V_{sv,max}$ (ml)	350
$R_{sv,0}$ (mmHg.s.ml^{-1})	0.025

D_1: scaling factor; K_1: scaling factor; V_{usv}: unstressed volume; D_2: scaling factor; K_2: scaling factor; $V_{sv,min}$: minimum volume; K_{xp}: scaling factor; K_{xv}: scaling factor; K_R: scaling factor; $V_{sv,max}$: maximum volume; $R_{sv,0}$: offset parameter.

Pleural pressure

The plural pressure Ppl is calculated as a function of the lungs pressure and volume:

Equation 6.13

$$Ppl = P_{alv} - \frac{V_{alv} - V_{u,alv}}{C_{alv}}$$

where V_{alv} is the alveolar volume, P_{alv} is the alveolar pressure, C_{alv} is the alveolar compliance, and $V_{u,alv}$ is the alveolar unstressed volume.

Protocol

The cardiovascular pressures and volumes were recorded every 5 ms for 10 minutes of spontaneous breathing.

6.3 Results & Findings

The following paragraph presents the results of the updated model where the cardiac and vascular pressure equations have been updated.

The Figure 6.3 shows the ventricular, atrial, aortic and pulmonary artery pressures in a healthy subject, for the original ICSM (a,b) and the updated ICSM (c,d) models.

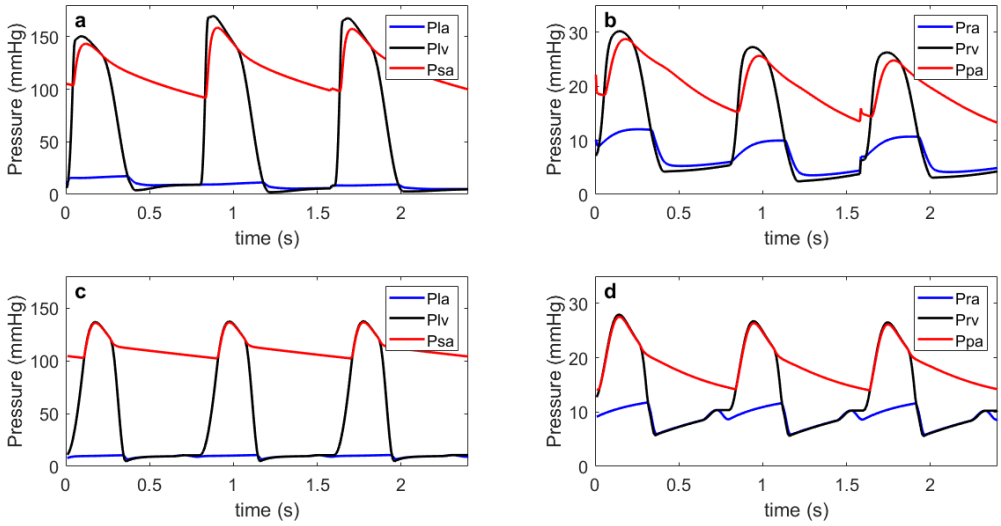

Figure 6.3 a) Pressure in the left ventricle, aorta and left atrium; b) pressure in the right ventricle, pulmonary artery and right atrium; c) pressure in the left ventricle, aorta and left atrium, d) pressure in the right ventricle, pulmonary artery and right atrium. Panels a) and b) refer to the original version of the ICSM simulation suit and panels c) and d) to the updated one.

The updated model pressures are matching the physiological values for a healthy subject. The left ventricular and aortic systolic pressures are around 120 mmHg, while the right ventricular and pulmonary artery systolic pressures are around 20 mmHg.

The Figure 6.4 shows the ventricular and atrial volumes and the pressure-volume loops in a healthy subject for the original ICSM (a,b) and the updated ICSM (c,d) models. The addition of the atrial contraction can be clearly observed in the evolution of volume (Figure 6.4 c). The atrial contraction accounts for around 10% of the ventricular EDV which agrees with the physiological values. The updated ICSM model pressure-volume loop (Figure 6.4 d) is also

matches the physiological values for a healthy subject while the original model left ventricular pressure volume loop is shifted to the left and the right ventricular one is shifted to the left.

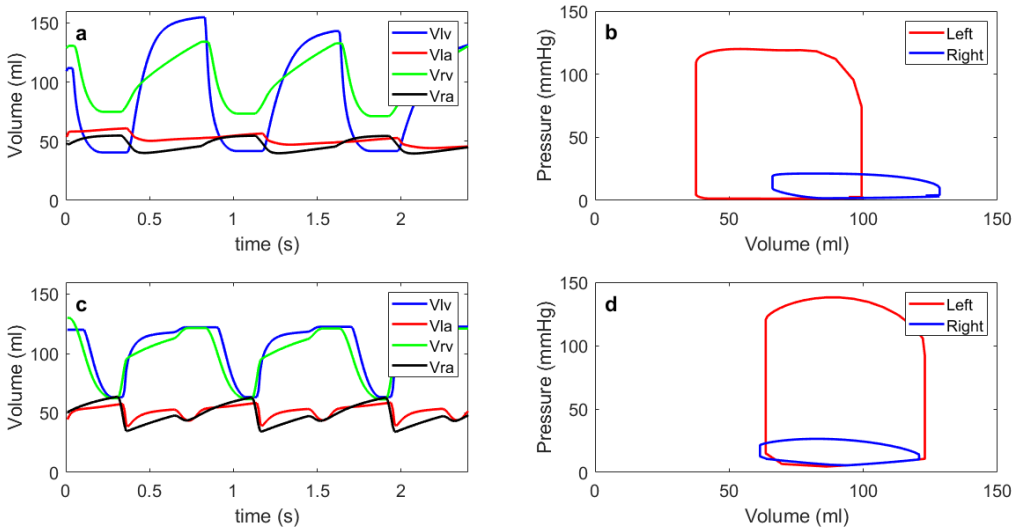

Figure 6.4 a) volume in the left and right ventricles and atria; b) pressure-volume loop in the left and right ventricles; c) volume in the left and right ventricles and atria; d) pressure-volume loop in the left and right ventricles. Panels a) and b) refer to the original version of the ICSM simulation suite and panels c) and d) to the updated one.

Table 6.4 presents the physiological haemodynamic parameters used to evaluate a healthy subject.

Table 6.4 Hemodynamic parameters used to evaluate a healthy subject.

	Healthy subject	**Updated ICSM**
EF (%)	[55 – 70]	45
LVEDV (ml)	[110 – 130]	124
MAP (mmHg)	[70 – 100]	112
CO (ml.min^{-1})	[5000 – 6000]	4448

EF: ejection fraction; LVEDV: left ventricle end diastolic volume; MAP: mean arterial pressure; CO: cardiac output

The hemodynamic values of the updated ICSM model are presented in Table 6.3. While the LVEDV is within a healthy subject physiological range, the EF and CO are lower than the physiological range and the MAP is higher than the physiological range. This is due to incorrect input parameters assignation which will be adjusted to match expected physiological ranges. Notably, the integration of modules from Albanese *et al*. [211] and Bozkurt [212] involved employing the same input parameters. However, as the ICSM simulation suite differs from the base cardiovascular models used by these researchers, a tuning process, using a global optimization algorithm, is needed to achieve the targeted physiological ranges for healthy subjects.

6.4 Conclusions

In this chapter, I have described the integration of a new model of cardiac contraction, including atrial contraction, a new model of vasculature (new pressure, volume, and flow equations), a new thoracic vein model (with non-linear and collapsible compliance), and new model of pleural pressure (affecting the intrathoracic pressure).

These new modules have been added to accurately model and predict the effect of fast-changing pressure in the cardio vasculature during CA and CPR.

Chapter 7. Simulation of myocardial infarction and hypovolaemic shock

This chapter describes the project that was performed as part of the Animal Free Research UK Summer Studentship 2021. I co-supervised the student, Fiona Dang with Dr Marianna Laviola.

My contribution to this work is:

- Coding the new modules
- Running the computational simulations
- Providing guidance in the analysis of the results (understanding the findings and making the figures and tables)
- Revising the student's report

7.1 Introduction

Cardiogenic arrests are estimated to account for 60% of out of hospital cardiac arrest (OHCA) with coronary artery disease being the predominant one [28]. However, OHCA can also by causes unrelated to the heart (extrinsic causes), such as severe haemorrhage, known as hypovolemic shock, due to trauma, hypoxia (severe drop in oxygen level), electrocution and drug overdose. [214]

Reversing the pathology that caused the cardiac arrest is one of the crucial aspects of successful cardiopulmonary resuscitation (CPR). Therefore, modelling different precipitating pathologies is key to determine successful CPR strategies.

In this study, I used and further developed the ICSM simulation suite to investigate two different pathologies leading to cardiac arrest in a virtual healthy subject: myocardial infarction (MI) and haemorrhagic shock (HS).

For the purpose of this work, multiple newly developed compensation mechanisms have been integrated to the current model, to produce high-fidelity models of myocardial infarction and haemorrhagic shock and to study the evolution of haemodynamic, and metabolic parameters and gas exchanges in these pathologies.

For the MI, I simulated coronary blood flow reduction by increasing the arterial myocardial resistance. Three compensation mechanisms were implemented when the coronary blood flow was reduced: 1) reduced left ventricular contractility, 2) concomitant ventricular dilatation and 3) reduced myocardial oxygen demand, as a consequence of the decreased contractility.

Then, I modelled HS in four stages: I) controlled phase (baseline), II) haemorrhage I: 30% of blood volume loss, III) prolonged hypovolemic shock (no further bleeding), and IV) haemorrhage II: further bleeding until the mean arterial pressure was equal to 20 mmHg. The compensation mechanisms occurring during HS were modelled with the baroreflex resulting in increasing heart rate and contractility and peripheral vasoconstriction.

Relevance —The resulting computational model can aid in understanding the underlying pathophysiology of MI and HS and facilitate the development of more effective CPR strategies specific to the precipitating aetiology, without sacrificing animals or conducting clinical trials, difficult in these kind of crisis scenarios.

7.2 Methods

7.2.1 Simulation of cardiac arrest due to myocardial infarction.

To simulate CA due to myocardial infarction, two stages of coronary blood flow reduction were modelled, as in a previous animal study, conducted by Vognsen *et al.* [127].

To simulate myocardial infarction (MI), I used a recently developed module of coronary (myocardial) perfusion and multiple organ tissue compartments (i.e. brain, splanchnic, extra-splanchnic and muscles) in a healthy virtual subject of 70 kg. After 10 minutes of spontaneous ventilation (SPV) to obtain baseline values, myocardial infarction was

simulated for 10 minutes by changing the myocardial resistance, effectively reducing the blood flow to the myocardium. During the MI the subject was spontaneously ventilated and no modifications to the breathing rate or tidal volume was made.

In particular, the coronary blood flow was reduced significantly, between 10% and 50%, by increasing the myocardial arterial resistance, from 17.2 to 31.5 mmHg s.mL^{-1}, thus depriving the myocardial tissue compartment of gas exchange (oxygen and carbon dioxide). Three compensation mechanisms were implemented, when the coronary blood flow was reduced: 1) reduced left ventricular contractility, 2) concomitant ventricular dilatation and 3) reduced myocardial oxygen demand, as a consequence of the decreased contractility. The haemodynamic and metabolic parameters have been evaluated against a previous study [215] in which the authors evaluated the hemodynamic and metabolic parameters during graded reduction in coronary blood flow in dogs. Additionally, the cardiac remodelling resulting from the MI was evaluated, in terms of left ventricle (LV) end-diastolic volume (LVEDV), LV end-systolic volume (LVESV), stroke volume (SV) and ejection fraction (EF).

Compensation mechanisms

Reduced left ventricular contractility and concomitant ventricular dilatation

To model the reduced left ventricular contractility and the concomitant ventricular dilatation during reduced coronary blood flow two parameters from the code are modified: the left ventricular elastance ($Elvsysc$), that represents the left ventricular contractility, and the baseline diastolic pressure ($P_{lv,c}$).

Decreasing the left ventricular elastance ($Elvsysc$) will reduce the left ventricular contractility and increase the left ventricular end diastolic volume causing dilation. However, decreasing the left ventricular elastance ($Elvsysc$) will also cause the decrease of the left ventricular systolic pressure (LVSP), mean arterial pressure (MAP) and stroke volume (SV) and the increase of the left ventricular end diastolic pressure (LVEDP). Therefore, to maintain LVSP, MAP, SV and LVEDP when the coronary blood flow is reduced between 0%-20%, the baseline diastolic pressure ($P_{lv,c}$) will be decreased. When the coronary blood flow is further

reduced (>20%) the baseline diastolic pressure ($P_{lv,c}$) will be increased to model the decrease of the LVSP, MAP, SV and increase of the LVEDP.

Finally, the left ventricular elastance ($Elvsysc$) and the baseline diastolic pressure ($P_{lv,c}$) were both calculated from the myocardial oxygen (O_2) venous concentration that gives an indication of the state of hypoxia. The left ventricular elastance ($Elvsysc$) is given by the equation below:

Equation 7.1

$$Elvsysc = \begin{cases} 3 & CvO2_{heart} > 125 \\ Elv_0 + K_{Elv}(CvO2_{heart} - CvO2_{heart,n})^2 & 125 \geq CvO2_{heart} \geq 110 \\ Elv_0 & 110 > CvO2_{heart} \end{cases}$$

where, Elv_0 is the minimum left ventricular elastance, K_{Elv} is a coefficient, $CvO2_{heart}$ is the myocardial O_2 venous concentration and $CvO2_{heart,n}$is the baseline myocardial O_2 venous concentration.

The left ventricular baseline diastolic pressure ($P_{lv,c}$) is given by the equation below:

Equation 7.2

$$P_{lv,c} = \begin{cases} 1 & CvO2_{heart} > 125 \\ P_{lv,min} + K_{Plv1}(CvO2_{heart} - CvO2_{heart,n})^2 & 125 \geq CvO2_{heart} \geq 110 \\ P_{lv,min} + K_{Plv2}(CvO2_{heart} - CvO2_{heart,n})^2 & 110 > CvO2_{heart} \end{cases}$$

where, $P_{lv,min}$ is the minimum left ventricular baseline diastolic pressure, K_{Plv1} and K_{Plv2} are coefficients.

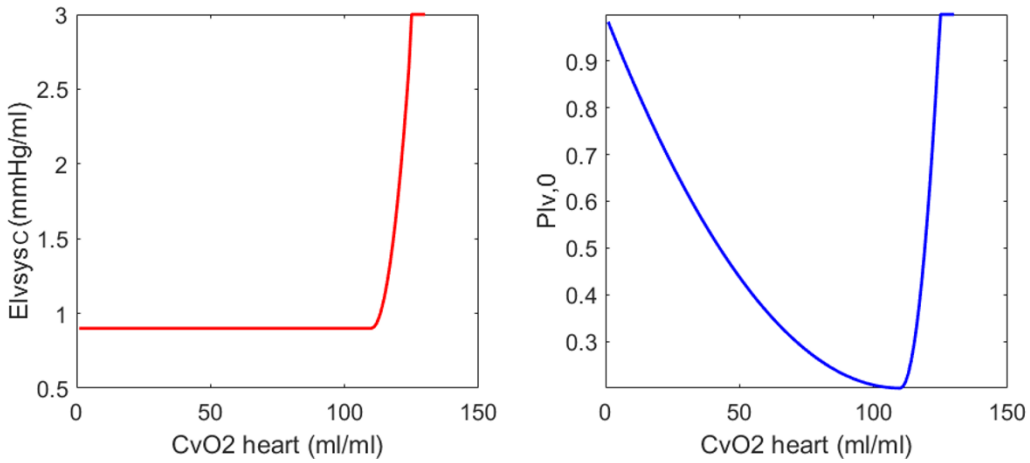

Figure 7.1 Evolution of left ventricular contractility and baseline diastolic pressure as a function of myocardial venous O_2 concentration.

The figure 7.1 shows the evolution of the left ventricular elastance ($Elvsysc$) and the baseline diastolic pressure ($P_{lv,c}$) as a function of the myocardial oxygen (O_2) venous concentration ($CvO2_{heart}$). When the myocardial oxygen (O_2) venous concentration is higher than 125 ml.ml^{-1} both parameters are at their highest respectively, 3 (mmHg.ml^{-1}) and 1 (-). From 125 ml.ml^{-1} to 110 ml.ml^{-1} both parameters exponentially decrease to reach a minimum at 110 (which corresponds to a coronary blood flow reduction of 20%) respectively 0.9 (mmHg.ml^{-1}) and 0.2 (-). Finally, whilst the left ventricular elastance ($Elvsysc$) remains constant when the myocardial oxygen (O_2) venous concentration ($CvO2_{heart}$) further decreases, the baseline diastolic pressure ($P_{lv,c}$) increases.

Reduced myocardial oxygen demand

To model the reduced myocardial oxygen demand, as a consequence of the decreased contractility one parameter from the code is modified: the O_2 consumption rate in the heart ($VO2_h$). The equations and parameters values used to modify the O_2 consumption rate in the heart ($VO2_h$) are obtained from Ursino *et al.* paper [216], specifically referencing Equations 7.3 to 7.5. Briefly, the average power of the cardiac pump (W_h) is calculated from the left and right ventricular pressures and volumes and this computed cardiac pump power is used to calculate the O_2 consumption rate in the heart ($VO2_h$) such as:

Equation 7.3

$$VO2_h = \frac{W_h}{W_{h,n}} \cdot VO2_{h,n}$$

Where $VO2_{h,n} = 0{,}4\ ml.s^{-1}$ is the baseline O_2 consumption rate in the heart and $W_{h,n} = 12{,}660\ mmHg.ml.s^{-1}$ is the baseline average power of the cardiac pump. The average W_h is computed by low-passing filtering the instantaneous power produced by the left and right ventricle (ω_h):

Equation 7.4

$$\omega_h = -P_{lv} \cdot \frac{dV_{lv}}{dt} - P_{rv} \cdot \frac{dV_{rv}}{dt}$$

Equation 7.5

$$\frac{dW_h}{dt} = \frac{1}{\tau_\omega} \cdot (\omega_h - W_h)$$

Where P_{lv} and P_{rv} are respectively the left and right ventricle pressures, $\frac{dV_{lv}}{dt}$ and $\frac{dV_{rv}}{dt}$ are respectively the left and right volume changes and $\tau_\omega = 5\ s$ is the time constant of the filter.

7.2.2 Simulation of cardiac arrest due to hypovolemic shock

To simulate CA due to hypovolaemic (haemorrhagic) shock four phases were modelled, as in a previous animal study, conducted by Watts et al. [217].

First, a control phase was simulated for 5 minutes to obtain the baseline model outputs. Then, an injury phase (haemorrhage I) was simulated by removing 30% of blood volume until the mean arterial blood pressure (MAP) reached 40 mmHg. After that, a prolonged haemorrhagic shock was simulated for 30 minutes without any additional blood loss. Finally, a second haemorrhage (haemorrhage II) was simulated by removing an additional blood volume until the MAP dropped to 20 mmHg. Similarly, to myocardial infarction, compensation mechanisms were implemented.

The compensation mechanisms occurring during HS was modelled with the baroreflex resulting in increasing heart rate, contractility and peripheral vasoconstriction. These compensation mechanisms are presented in more details in the following section.

Compensation mechanisms.

Baroreflex regulation

During haemorrhage, the body compensates for volume loss by increasing heart rate and contractility, followed by baroreceptor activation resulting in sympathetic nervous system activation and peripheral vasoconstriction. It's worth noting that another aspect of this intricate response involves autotransfusion from the spleen. The spleen serves as a reservoir for red blood cells, releasing them into circulation during periods of acute blood loss to augment circulating blood volume. This additional facet of autotransfusion contributes to the overall adaptive response aimed at maintaining vital organ perfusion during haemorrhagic events, however, for simplicity, the modelling did not incorporate the specific effects of autotransfusion from the spleen. To model the increased heart rate, contractility, and peripheral vasoconstriction the following parameter from the code are modified: heart period (T) (which is the inverse of the heart rate: $T = \frac{1}{HR}$), the left and right ventricular contractility ($Elvmax$, $Ervmax$) and the peripheral resistances (R_{sa1}, R_{sa2}, R_{sa3}) and vascular unstressed volume (V_{usv1}, V_{usv2}, V_{usv3}) of the splanchnic, extra-splanchnic and muscle tissue organs. The equations and parameters used to modify these parameters are based upon Ursino *et al.* paper [216], specifically referencing Equations 7.6 to 7.8. The baroreflex takes as an input the aortic pressure (P_{sa}) and calculates the frequency of spikes in the afferent fibres (f_{ab}).

Equation 7.6

$$\frac{d\tilde{P}}{dt} = P_{sa} + \tau_{z,b} \cdot \frac{dP_{sa}}{dt} - \frac{\tilde{P}}{\tau_{p,b}}$$

Equation 7.7

$$f_{ab} = \frac{f_{ab,min} + f_{ab,max} \cdot e^{\left(\frac{\tilde{P}-P_n}{k_{ab}}\right)}}{1 + e^{\left(\frac{\tilde{P}-P_n}{k_{ab}}\right)}}$$

Where $\tau_{pb} = 2.076\ s$ and $\tau_{zb} = 6.37\ s$ are the time constants for the real pole and the real zero in the linear dynamic block, P_{sa} is the aortic pressure, $\tilde{P}$ is the output variable of the

linear dynamic block, f_{ab} is the frequency spikes in the afferent fibres, $f_{ab,max} = 47.78\ spikes.s^{-1}$ and $f_{ab,min} = 2.52\ spikes.s^{-1}$ are the upper and lower saturation of the frequency discharge, $P_n = 92\ mmHg$ is the value of baroreceptor pressure at the central point of the sigmoid function, and $k_{ab} = 11.76\ mmHg$ is a parameter, with the dimension of pressure, related to the slope of the static function at the central point [216].

The effect of the baroreflex directed to the heart rate, heart contractility and peripheral circulation (f_{ab}) is calculated below where θ denotes the heart period (T), the left and right ventricular contractility ($Elvmax$, $Ervmax$) and the peripheral resistances (R_{sa1}, R_{sa2}, R_{sa3}) and vascular unstressed volume (V_{usv1}, V_{usv2}, V_{usv3}):

Equation 7.8

$$\sigma_\theta = \begin{cases} G_\theta \cdot \ln\left(f_{ab} - f_{ab,min} + 1\right) & f_{ab} \geq f_{ab,min} \\ 0 & f_{ab} < f_{ab,min} \end{cases}$$

$$\Delta\theta = \sigma_\theta - \tau_\theta \cdot \frac{d\Delta\theta}{dt}$$

$$\theta = \Delta\theta + \theta_0$$

Where σ_θ is the output of the static characteristic, τ_θ is the time constant of the mechanism, and $\Delta\theta$ is the parameter change caused by the baroreflex. Finally, G_θ is a constant gain factor positive for the parameters for mechanism working on the left and right ventricular contractility ($Elvmax$, $Ervmax$) and the peripheral resistances (R_{sa1}, R_{sa2}, R_{sa3}), and negative for the parameters for mechanism working on the heart period (T), and vascular unstressed volume (V_{usv1}, V_{usv2}, V_{usv3}).

Table 7.1 Basal values of parameters for compensation mechanisms obtained from Ursino [216]

G_T=0.13 $s.v^{-1}$	τ_T=2 s	T_0=0.58 s
G_{Elvsys}=-0.475 $mmHg.ml^{-1}.v^{-1}$	τ_{Elvsys}=8 s	$E_{lvsys,0}$=2.5 $mmHg.ml^{-1}$
G_{Ervsys}=-0.282 $mmHg.ml^{-1}.v^{-1}$	τ_{Ervsys}=8 s	$E_{rvsys,0}$=1 $mmHg.ml^{-1}$
G_{Rsa1}=0.695 $mmHg.ml^{-1}.v^{-1}$	τ_{Rsa3}=6 s	$R_{sa1,0}$=2.49 $mmHg.s.ml^{-1}$
G_{Rsa2}=1.94 $mmHg.ml^{-1}.v^{-1}$	τ_{Rsa2}=6 s	$R_{sa2,0}$=1.655 $mmHg.s.ml^{-1}$
G_{Rsa3}=2.47 $mmHg.ml^{-1}.v^{-1}$	τ_{Rsa3}=6 s	$R_{sa3,0}$=2.106 $mmHg.s.ml^{-1}$
G_{Vusv1}=265.4 $ml.v^{-1}$	τ_{Vusv1}=20 s	$V_{usv1,0}$=865ml
G_{Vusv2}=74.21 $ml.v^{-1}$	τ_{Vusv2}=20 s	$V_{usv2,0}$=481 ml
G_{Vusv3}=58.29 $ml.v^{-1}$	τ_{Vusv3}=20 s	$V_{usv3,0}$=378 ml

Explanation about the signs can be found in (211)

The figure 7.2 shows the behaviour of the heart rate (HR), the left and right contractility ($Elvmax$, $Ervmax$) and the peripheral resistances (R_{sa1}, R_{sa2}, R_{sa3}) and vascular unstressed volume (V_{usv1}, V_{usv2}, V_{usv3}) parameters when the aortic pressure Psa decreases due to haemorrhage. As expected, the heart rate (HR), the left and right contractility ($Elvmax$, $Ervmax$) increase to compensate the blood volume loss and maintain the stroke volume. The peripheral resistances (R_{sa1}, R_{sa2}, R_{sa3}) and vascular unstressed volume (V_{usv1}, V_{usv2}, V_{usv3}) of the splanchnic, extra-splanchnic and muscle tissue organs respectively increase and decrease therefore causing vasoconstriction of the nonvital organs (heart and brain).

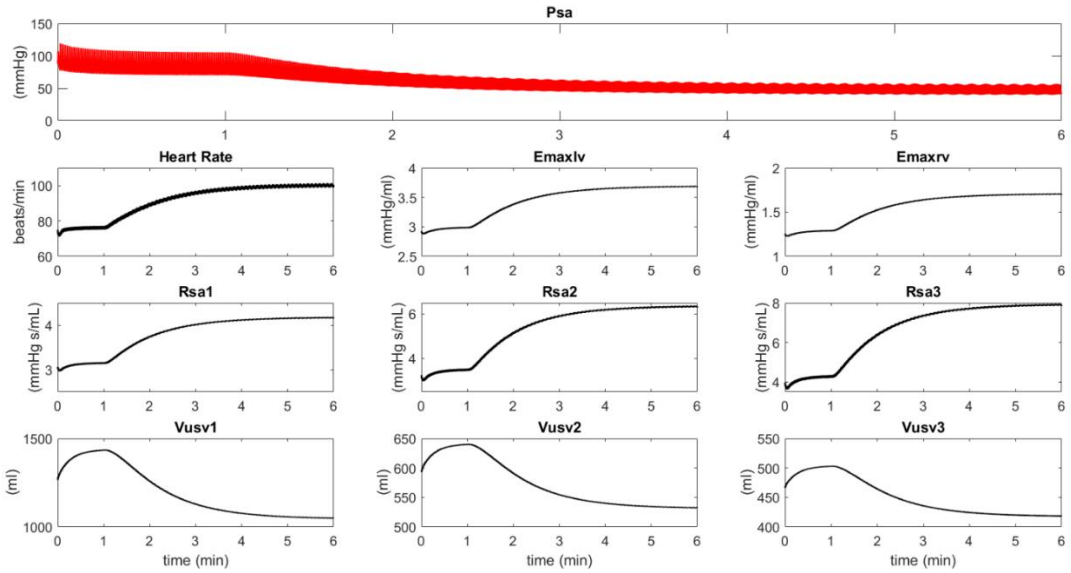

Figure 7.2 Behaviour of the modified parameters during a decrease in aortic blood pressure. Where HR is the heart rate, $Elvmax$ and $Ervmax$ are the left and right contractility, R_{sa1}, R_{sa2}, R_{sa3} are the splanchnic, extra-splanchnic and muscle arterial resistance and V_{usv1}, V_{usv2}, V_{usv3} are the splanchnic, extra-splanchnic and muscle venous unstressed volumes.

7.3 Result & Findings

7.3.1 Simulation of cardiac arrest due to myocardial infarction.

Table 7.2 shows the haemodynamic, metabolic and gas exchanges model parameters for different degrees of myocardial infarction from 10% to 50% coronary blood flow reduction. As expected, when the coronary artery resistance (R_h) is increased the coronary blood flow decreases. Similarly, when the CF decreases the left ventricular elastance ($Elvsysc$) and the baseline diastolic pressure ($P_{lv,c}$) decrease and after 20% of blood flow reduction the left ventricular elastance ($Elvsysc$) remains constant and the baseline diastolic pressure ($P_{lv,c}$) slowly increases. The stroke volume is maintained constant up to 10% of blood flow reduction and then decreases by up to 11% when the coronary blood flow is halved. Finally, it can be observed that left ventricular end diastolic and end systolic volume constantly increases showing a ventricular dilatation which is confirmed by a reducing ejection fraction.

Table 7.2 Haemodynamic, metabolic and gas exchanges model parameters for different degrees of myocardial infarction.

		Coronary blood flow reduction				
	baseline	**10%**	**20%**	**30%**	**40%**	**50%**
Model parameters						
R_h (mmHg s.ml^{-1})	17.2	18.9	20.5	23.5	26.8	31.5
E_{lvsysc}(mmHg.ml^{-1})	2.4	1.30	1.00	0.90	0.90	0.90
Plv_0	0.8	0.40	0.20	0.20	0.20	0.30
Haemodynamic model outputs						
SV (ml.beat^{-1})	65.1	65.0	62.4	61.1	60.2	58.2
CPP (mmHg)	74.6	73.6	71.2	70.5	69.8	67.8
CF (ml.beat^{-1})	3.2	2.9	2.6	2.2	1.9	1.6
LVSP (mmHg)	120	118	113	112	110	107
LVEDP (mmHg)	4.8	5	5.3	5.7	6	8
LVEDV (ml)	124	161	190	197	194	189
LVESV (ml)	58	96	128	136	134	131
EF (%)	40%	30%	20%	20%	20%	20%
LV work (mmHg.ml.s^{-1})	9383	9130	8499	8271	8000	7427

HR (beats.min^{-1})	75	75	75	75	75	75
Metabolic parameters						
$VO2_h$ (ml.min^{-1})	21.1	20.6	19.3	18.9	18.4	17.3
$VtissO2_h$ (ml)	0.40	0.30	0.30	0.30	0.30	0.20
Gas exchange parameters						
$CvO2_h$ (ml.ml^{-1})	124	118	113	102	90	75
PaO_2(kPa)	12.5	12.7	12.7	12.6	12.6	12.7
$PaCO_2$(kPa)	5.5	5.5	5.5	5.5	5.5	5.5

* R_h: coronary artery resistance; Elvsysc: left ventricular elastance; Plv0: baseline diastolic pressure; SV: stroke volume; CPP: coronary perfusion pressure; CF: coronary flow; LVSP: left ventricular systolic pressure; LVEDP: left ventricular end diastolic pressure; LVEDV: left ventricular end diastolic volume; LVESV: left ventricular end systolic volume; EF: ejection fraction; LV work: left ventricular work; HR: heart rate; $VO2_h$: myocardial oxygen consumption rate; $VtissO2_h$: myocardial tissue oxygen volume; $CvO2_h$: myocardial oxygen venous concentration; PaO_2: arterial oxygen partial pressure; $PaCO_2$: arterial carbon dioxide partial pressure.

7.3.2 Simulation of cardiac arrest due to hypovolemic shock

Table 7.3 Model parameters for different stages of haemorrhagic shock shows the haemodynamic and gas exchange model parameters during the four stages of haemorrhagic shock. Through the four stages of the haemorrhagic shock, the heart rate, left ventricular contractility and the systemic vascular resistance increase in accordance with the literature. Similarly, the mean arterial pressure, stroke volume, cardiac output, and coronary perfusion pressure decrease. However, the gas exchange parameters, PaO_2, $PaCO_2$, SaO_2 and pH remain unchanged. The absence of pH change is attributed to the lack of modelling of lactate production and anaerobic respiration in the current ICSM simulation suite.

Table 7.3 Model parameters for different stages of haemorrhagic shock

	Control	Haemorrhage I	Shock phase	Haemorrhage
Haemodynamic model outputs				
Blood volume (ml)	5279	3707	3707	3232
MAP (mmHg)	82	43	44	21
SV ($ml.beats^{-1}$)	58	19	20	8
HR ($beats.min^{-1}$)	78	101	101	115
CO$(ml.min^{-1})$	4526	1880	2050	885
CPP (mmHg)	71	43	43	23
Elvsys ($mmHg.ml^{-1}$)	3.00	3.70	3.70	3.90
SVR ($mmHg\ s.ml^{-1}$)	1.10	1.50	1.50	1.60
Gas exchange parameters				
PaO_2(kPa)	12.4	12.1	11.9	12.3
$PaCO_2$(kPa)	5.5	5.3	5.5	5
SaO_2(%)	1.0	1.0	1.0	1.0
pH	7.4	7.4	7.4	7.4

*MAP: mean arterial pressure; SV: stroke volume; HR: heart rate; CO: cardiac output; CPP: coronary perfusion pressure; Elvsys: left ventricular contractility; SVR: systemic vascular resistance; PaO_2: arterial oxygen partial pressure; $PaCO_2$: arterial carbon dioxide partial pressure; SaO_2: arterial oxygen saturation

7.4 Conclusion

In this study, using and further developing the ICSM simulation suite computational model of pulmonary and cardiovascular systems I simulated myocardial infarction and haemorrhagic shock, as causes of cardiac arrest. I was able to simulate both the pathologies and the occurring compensation mechanisms. The resulting haemodynamic (cardiac output, heart rate, stroke volume, mean arterial pressure), metabolic (tissue oxygen consumption) and gas exchange (arterial oxygen and carbon dioxide partial pressure) model outputs were in line with a previous animal study [127, 217] but within physiological human ranges. This new

development of the simulation suite allows us to develop more effective cardiopulmonary resuscitation strategies specific to the precipitating aetiology, without sacrificing animals and without conducting clinical trials.

Chapter 8. Evaluating Current Guidelines for Cardiopulmonary Resuscitation using an Integrated Computational Model of the Cardiopulmonary System

Part of this chapter has been published in IEEE Engineering in Medicine and Biology Society conference proceeding 2021:

C. Daudre-Vignier, M. Laviola, A. Das, D.G. Bates and J.G. Hardman, "Identification of an optimal CPR chest compression protocol". Proceedings of the 43rd Annual International Conference of the IEEE Engineering in Medicine and Biology Society, 2021.

My contribution to the work is:

- Conception and design of the study
- Running simulations
- Analysis and interpretation of data
- Drafting the article and revising it critically for important intellectual content
- Final approval for all aspects of the work
- Final approval of the version to be submitted and agreement to be accountable for all aspects of the work.

The methods (gas exchange model, cardiopulmonary interactions, genetic algorithm for subject configuration and the protocol), results and the discussion presented in this chapter have been published in the Resuscitation journal as original article:

Clara Daudre-Vignier, Declan G. Bates, Timothy E. Scott, Jonathan G Hardman, Marianna Laviola, "Evaluating Current Guidelines for Cardiopulmonary Resuscitation using an Integrated Computational Model of the Cardiopulmonary System"

Both the papers can be found in the Appendix 3 and Appendix 4.

My contribution to the work is:

- Conception and design of the study
- Running simulations
- Analysis and interpretation of data
- Drafting the article and revising it critically for important intellectual content
- Final approval for all aspects of the work
- Final approval of the version to be submitted and agreement to be accountable for all aspects of the work.

In this chapter, I use the pronoun “I” because I am writing the PhD thesis, however, the work has been done with my supervisors and collaborators.

8.1 Introduction

Some clinical trials in humans have attempted to identify optimal CPR strategies [36, 37, 39, 45]. However, ethical and practical constraints, short time scales, the presence of confounding variables, and heterogeneity of the patient population present major obstacles to performing clinical research in this area. Animal models often fail to represent the severity of human CA accurately, due to interspecies physiological differences and lack of methodical rigor [127, 137]. Computer simulation is a novel and promising alternative to animal and clinical trials that is free of most ethical and practical constraints, allows complete reproducibility of methods and results, and offers mechanistic insight into the effectiveness of treatment strategies.

When performing chest compression (CC), three main components are typically considered: depth, rate, and compression ratio. While the European Resuscitation Council (ERC) advanced life support guideline [63] advises a compression depth of 5-6 cm, a rate of 100-120 compressions min^{-1}, and a compression ratio (i.e. the proportion of compression time during the compression / decompression cycle) of 50%, the majority of studies have failed to find an association between these parameters and outcomes. A recent systematic review and meta-analysis by Considine *et al.* [35], which included more than 15,000 subjects, reported outcomes associated with CC rate. Overall, the majority of the studies did not find any associations between the CC rate and outcomes (survival with good neurological

outcome, survival to hospital discharge and return of spontaneous circulation [ROSC]) in out-of-hospital cardiac arrest). Only two studies found otherwise; Idris *et al.* [36] found an association between CC rate and ROSC with the rate of ROSC peaking at 125 compressions min^{-1}, and Idris *et al.* [37] found that CC rates between 100 and 120 compressions min^{-1} were associated with greatest survival to hospital discharge.

The evidence regarding the effect of CC depth on ROSC and survival is more consistent. In the study of Babbs *et al.* [43], for shocks delivered after 5 min of CA, a CC depth >5 cm compared with CC depth <5 cm was associated with a greater chance of transient ROSC. Similarly, Stiell *et al.* [41] found a strong association between survival outcomes and increased compression depth, and that maximal survival was in the depth interval of 4.03-5.53 cm [40], suggesting that the target depth in the AHA guidelines may be too great. The effect of the CC compression ratio on ROSC and long-term outcome has not been investigated in any clinical studies. However, in a study by Johnson *et al.* [218] the median compression ratio was 38.8% and a relatively shorter compression phase (lower compression ratio) was associated with a greater chance of survival.

The haemodynamic effects of pulmonary ventilation during CPR also remain unclear. Some researchers [67] have argued that whilst modest PEEP could help mitigate alveolar collapse, high intrathoracic pressure during decompression could prevent venous return and thus reduce stroke volume and organ perfusion, while others [70] have speculated that high intrathoracic pressure could enhance CC-generated CO by further ejecting blood out of the left ventricle. There is therefore an urgent need for further research into the combined impact of different airway strategies, ventilation techniques, positive end expiratory pressures (PEEP) and inhaled oxygen (FiO_2) on CPR effectiveness [123].

8.2 Methods

8.2.1 Cardiopulmonary computational model

In this study, I used the ICSM simulation suite presented in the previous Chapter 4. Compared to the previous iteration of the model the cardiovascular model consists of 20

compartments instead of 19 (Figure 8.1). The vena cava was divided into two compartments to account for the section in the thorax (thoracic vein) and the extra-thoracic section (systemic vein).

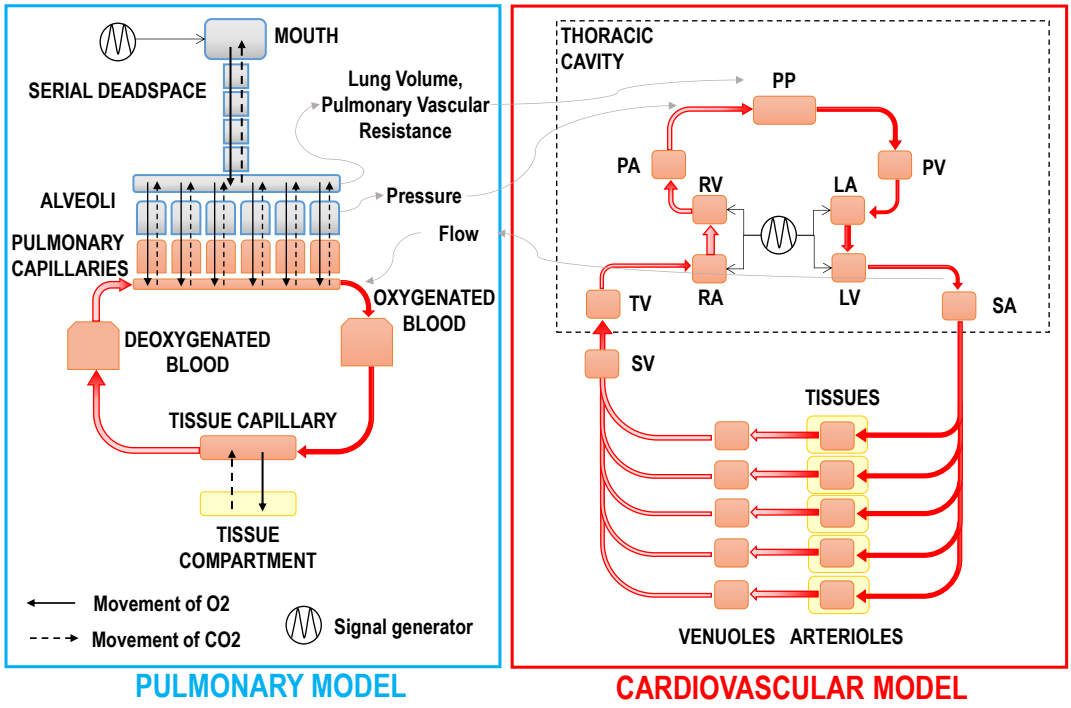

Figure 8.1 Schematic of pulmonary and cardiovascular model. The cardiovascular abbreviations are SV, systemic vein; TV, thoracic vein; RA, right atria; RV, right ventricle; PA, pulmonary artery; PP, pulmonary perfusion; PV, pulmonary vein; LA, left atrium; LV, left ventricle; and SA, systemic artery.

Each vascular compartment i was modelled as a two elements Windkessel system with a resistance (R_i), and capacitance (C_i). In the systemic artery and the pulmonary artery an additional impedance (L_i) was added (Figure 8.2). Additionally, a similar partitioning of the tissues was made, i.e., splanchnic, extra-splanchnic, muscle, brain, and heart.

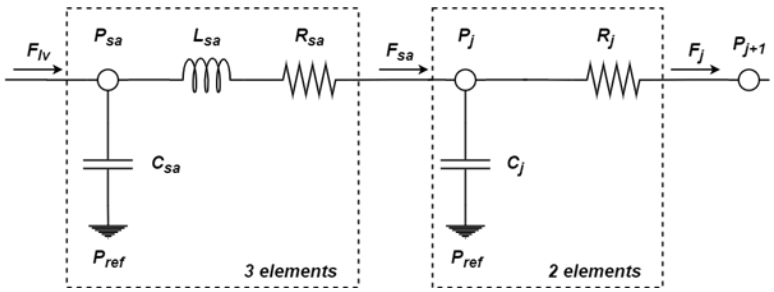

Figure 8.2 Two compartments Windkessel models, where F characterizes the flow, P the pressure, C the capacitance, L the impedance and R the resistance.

Similarly, to the systemic vein (sv), a new thoracic vein (tv) compartment was modelled to enable its collapse when the extra-vascular pressure exceeded the intra-vascular pressure. Additionally, the compartment resistances and compliances were modified to account for the compartment volume, according to:

Equation 8.1

$$R_i = \frac{R_{ic} {V_{ic}}^2}{{V_i}^2}$$

Equation 8.2

$$L_i = \frac{L_{ic} V_{ic}}{V_i}$$

where R_i is the compartment resistance, V_i is the compartment volume and the subscript c defines the unstressed value of the parameter. This modification was crucial to avoid any negative volumes in the compartments and to account for the sharp increase in resistance as the volume decreased.

8.2.2 Gas exchange model

Two new circulatory transport delays were included in the model to account for the time that it takes for blood to transport gases from the lungs to the systemic tissues and from the systemic vein back to the pulmonary capillaries (T_{LT} = 18s, T_{VL} = 10s, respectively) (Figure 8.3) [211].

The tissue compartments were defined by their oxygen consumption rate ($V\dot{O}_2$), carbon dioxide production rate ($V\dot{C}O_2$), blood flow ($Flow$) and volume ($Vtiss$) (Table 8.1). The total volume of organ tissue was defined as 0.66 of the body weight (set to 70 kg). The volume of each of the five compartments was based on the organ weight, the total oxygen consumption rate was set to 250 ml.min^{-1} and the total carbon dioxide production rate was set to 175 ml.min^{-1}.

Table 8.1 Organ tissue and capillary compartments parameters setting obtained from Albanese [211].

Organ tissue compartment	VO_2 (%)	Flow (%)	Vtiss (%)
Splanchnic tissue	44	29	8
Extra-splanchnic tissue	6	28	1
Muscle tissue	21	23	87
Heart tissue	10	5	1
Brain tissue	19	15	3

VO_2, oxygen consumption; Flow, percentage of blood flow received, oxygen consumption;

The updated cardiovascular and gas exchange models described above were integrated so that the tissue and pulmonary capillary blood flows, needed to calculate the blood gas concentration, were defined as the blood flow leaving the systemic arterioles and the blood flow leaving the pulmonary artery, respectively (Figure 8.3).

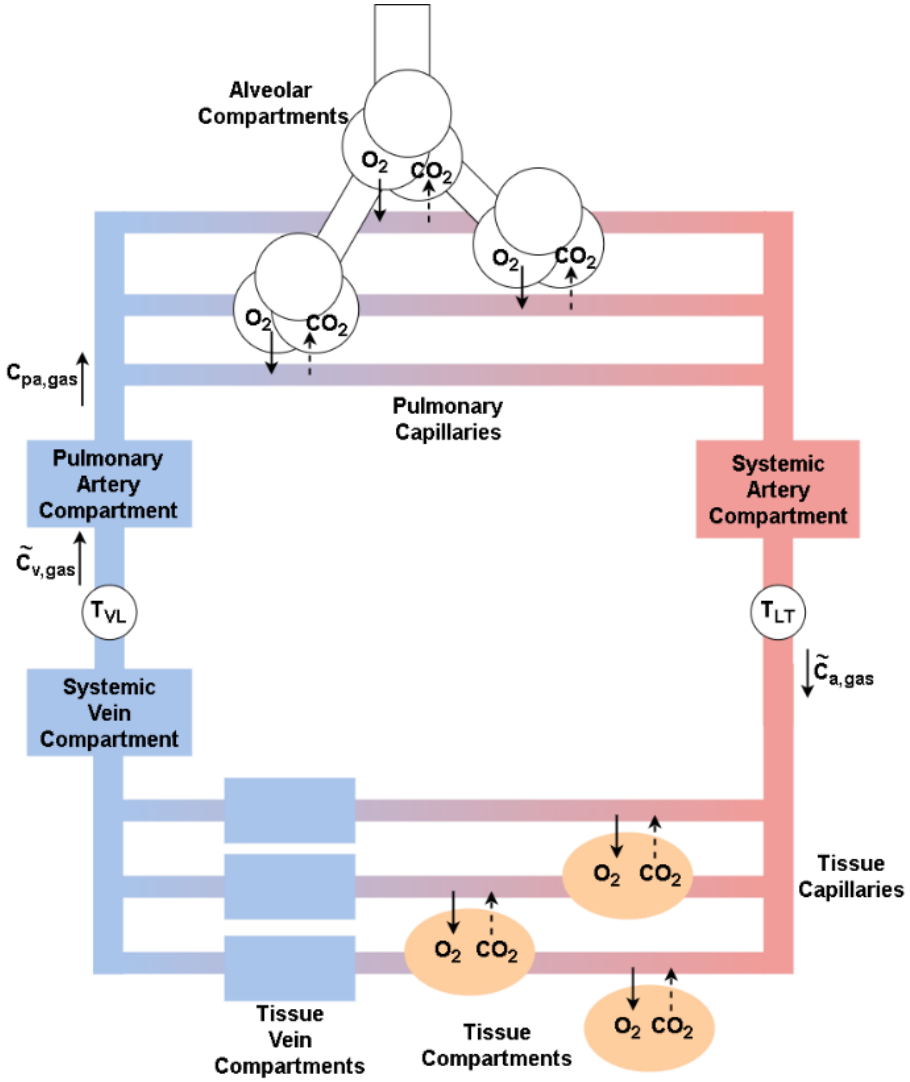

Figure 8.3 Schematic diagram of the gas exchange and transport model highlighting the alveolar and tissue components, and the blood transport delays. $\tilde{C}_{a,gas}$, delayed arterial blood gas concentrations; $\tilde{C}_{v,gas}$, delayed mixed venous blood gas concentrations; $C_{pa,gas}$, the pulmonary artery gas concentration; T_{LT}, transport delay from lungs to systemic tissues; and T_{VL}, transport delay from thoracic veins to lungs.

Additionally, to account for the effect of retrograded blood flow in the lungs, the blood gas concentrations were calculated at the pulmonary artery level. The gas concentrations were calculated as follows:

Equation 8.3

$$\frac{dC_{pa,gas}}{dt} = \begin{cases} \dfrac{C_{pa,gas}(V_{pa} - F_{pa}) + \tilde{C}_{v,gas} \cdot F_{rv}}{V_{pa}} & F_{pa} > 0 \\ \dfrac{C_{pa,gas}(V_{pa}) - F_{pa} \cdot C_{a,gas} + \tilde{C}_{v,gas} \cdot F_{rv}}{V_{pa}} & F_{pa} < 0 \end{cases}$$

where $C_{pa,gas}$ is the arterial pulmonary gas concentration, V_{pa} is the pulmonary artery volume, F_{pa} is the blood flow leaving the pulmonary artery, $F_{rv}$is the blood flow leaving the right ventricle, $\tilde{C}_{v,gas}$ delayed mixed venous blood gas concentrations, and $C_{a,gas}$ is the arterial gas concentration.

To account for gas exchange during CA, when the tissue volume of oxygen is depleted, passive exchange between the arterial and the capillary blood was allowed to provide further oxygen.

Finally, to avoid overproduction of CO_2 when all the available O_2 was utilized, the consumption of oxygen and the production of CO_2 were linked by the following equation:

Equation 8.4

$$\dot{VCO}_2 = \dot{VO}_{2,extracted} \cdot RQ$$

where $\dot{VO}_{2,extracted}$ is the extracted VO_2 and RQ = 0.7 is the respiratory quotient.

8.2.3 Cardiopulmonary interactions

The model includes the effect of pulmonary vasoconstriction which results in a 'U' shape change in pulmonary vascular resistance (PVR) at around the functional residual capacitance (FRC). The effect of hypoxic vasoconstriction was also modelled by increasing the PVR in response to hypoxia caused by alveolar collapse.

During simulated spontaneous breathing the pleural pressure was on average negative (-5 to -8 cmH_2O)). However, during CA and CPR the pleural pressure becomes positive. The variation of the pleural pressure was considered in the following equation obtained from Albanese *et al*. [211]:

Equation 8.5

$$Ppl = (P_{lungs} - P_{atm}) - \frac{V_{lungs} - V_{u,lungs}}{C_{lungs}}$$

where P_{lungs} is the alveolar pressure, V_{lungs} is the alveolar volume, $C_{lungs} = 0.2\ L/cmH_2O$ is the alveolar compliance, $V_{u,lungs} = 1.263\ L$ is the alveolar unstressed volume, and $P_{atm} = 101.3\ kPa$ is the atmospheric pressure.

8.2.4 Thoracic model

For this study I developed and integrated a new thoracic model (Figure 8.4). This thoracic model is adapted from Babbs chest wall model [147] and has been extensively described in our previous publication [219]. Equations 8.6 to 8.10 and 8.12 were directly obtained from Babbs chest wall model [147].

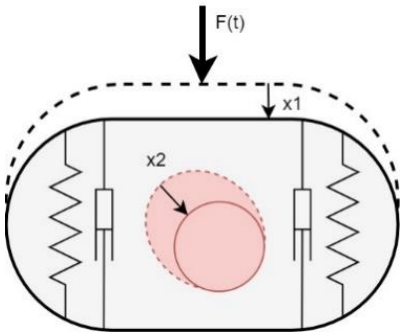

Figure 8.4. Schematic of the thoracic model. The paired spring and damper represent the elastic behaviour of the chest wall under the compression force F(t), including hysteresis. x_1 and x_2 represent the displacements of the sternum and the cardiac chambers under the compression force F(t), respectively. The red and grey area represents the mediastinal tissue.

The external CC force $F(t)$, applied at the sternum, was expressed as a function of the end compression force (F_{max}) a surrogate for the maximal sternal displacement, compression rate (CC_{rate}) and the compression ratio (i.e., the proportion of time under compression during compression and decompression cycle), (C_R) such as:

Equation 8.6

$$F(t) = \begin{cases} F_{max}\dfrac{1-cos\left(\pi(t-T1)\right)}{2} & 0 \le t < T2 \\ 0 & T2 \le t < T \end{cases}$$

where T is the CC and decompression period, $T2$ is the period of compression $T2 = T \cdot C_R$ and $T1$ is the half compression period ($T1 = \frac{T2}{2}$).

To relate the external chest compression force $F(t)$ and the sternum displacement (x_1), the thorax is modelled as a simple mechanical spring-damper system (Figure 8.4). The displacement of the sternum in response to the compression force is given by the following equation:

Equation 8.7

$$F(t) - kx_1 - \mu\dot{x}_1 = 0$$

where x_1 is sternal displacement, $\dot{x}_1$ is the velocity of sternal displacement, k is the spring constant, and μ is the damping constant. To relate the sternal displacement (x_1) to the intrathoracic tissue (mediastinum) pressure (P_M), the mediastinum is modelled as an elastic material of Young's modulus of elasticity E.

The rate of change of the cardiac chambers diameters ($\dot{x}_2$) due to the changes in internal blood volume are considered and defined as follows:

Equation 8.8

$$\dot{x}_2 = \frac{F_{in} - F_{out}}{A_c}$$

where F_{in} and F_{out} are respectively the flows entering and leaving the cardiac chambers, and A_c is the cross-sectional area of cardiac chambers. However, the changes in diameters in the intrathoracic vascular compartments are negligeable ($\dot{x}_2 = 0$). Therefore, the relationship between the mediastinum pressure (P_M), the velocity of sternal displacement ($\dot{x}_1$) and rate of change of the compartment diameters ($\dot{x}_2$) is given by:

Equation 8.9

$$\frac{P_M}{dt} = \alpha \frac{E(\dot{x}_1 + \dot{x}_2)}{d_0}$$

Where α is a scalar, and d_0 is the combined mediastinal tissues width. The effect of chest compression on the alveolar pressure is also modelled. The resulting pressure on the alveoli (P_{CC}) is related to the sternal displacement (x_1) by the following equation:

Equation 8.10

$$P_{CC} = \frac{x_1 A_{lungs}}{C_{lungs}}$$

where, A_{lungs} is the cross-section of lung squeezed by sternal compression and C_{lungs} is the combined lung-chest wall compliance. The pressure in each alveolus (pi) is then updated as:

Equation 8.11

$$pi = \begin{cases} \frac{Si(10 \cdot vi - 300)^3}{6600} - P_{ext,i} - P_{CC} \ , vi > 0 \\ 0 \ , otherwise \end{cases}$$

$$for\ i = 1, \dots, Ncomp$$

where Si is a scalar that determines the intra-alveolar pressure for a given volume, vi is the volume of the ith alveolar compartment, and $P_{ext,i}$ is the effective net pressure generated by the sum of the effects of factors outside each alveolus that act to distend that alveolus. The updated alveolar pressure affects the pleural pressure (Ppl) (Equation 8.5).

In this model, all the cardiovascular compartments enclosed in the thoracic cavity (Figure 8.1) experienced a combination of pleural (Ppl) and mediastinal pressure (P_M), such that:

Equation 8.12

$$\frac{dP_i}{dt} = \frac{F_{in} - F_{out}}{C_i} + \frac{dPpl}{dt} + f_{tpi} \cdot \frac{dP_M}{dt}$$

where, P_i is the intrathoracic compartment pressure, f_{tpi} is the thoracic pump factor which determines the degree to which the ‘‘thoracic pump’’ mechanism of CPR is working which varies between 0 and 1.

In a human study, Kim *et al.* [220] observed moderate retrograded blood flow from the left ventricle into the left atrium and no aortic regurgitation. Therefore, retrograde blood flow was

allowed between all the compartments except from the aorta to the left ventricle and the pulmonary artery to the right ventricle. The flow between compartments was therefore defined as:

Equation 8.13

$$F_i = \begin{cases} \dfrac{P_i - P_{i+1}}{R_i} & P_i > P_{i+1} \\ Retro_i\left(\dfrac{P_i - P_{i+1}}{R_{i+1}}\right) & P_i < P_{i+1} \end{cases}$$

where $Retro_i$ is the retrograde flow factor which determines the degree of retrograded flow which varies between 0 and 1.

Finally, to better simulate the observed behaviour of the rapid rise of the aortic pressure over the first few compressions [221], a factor of ($1\text{-}e^{-t}$) was applied to the CC force upon initiation of the CC [222]. The resulting simulated aortic pressure waveform after initiation of CPR is shown in the Figure 8.5.

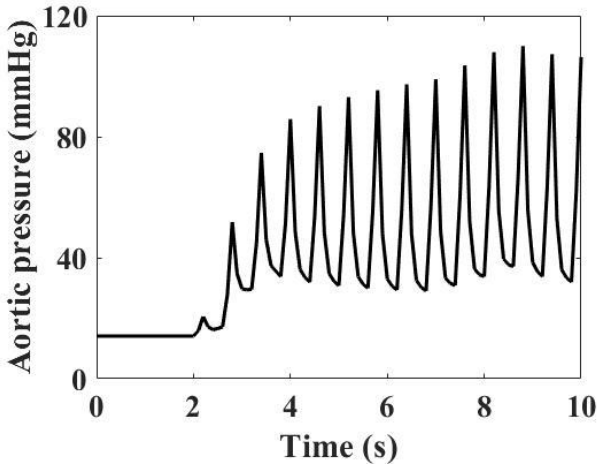

Figure 8.5 The aortic pressures generated upon initiation of CPR.

8.2.5 Genetic algorithm (GA) for subject configuration

In this paper, I used a GA method to solve the optimization problem. Briefly, the algorithm: 1) creates a random initial population from the parameter space defined by the boundaries of the input parameters; 2) calculates the individual scores of each member of this population, by running the simulation and deriving the cost (8); 3) generates members of the next

population through the selecting best individuals of the existing population (elitism), combining the characteristics of two different members (crossover), and making changes to randomly selected individuals (mutation) 4) repeats steps 2)-3) until an optimal solution is found that satisfies a pre-defined criteria, in this case the improvement in cost function between consecutive generations is below 10^{-3} or the number of generations exceed 100.

I used the hemodynamic and gas exchange human data from three different sources to validate our model; the end-compression and end-decompression pressures from Kim *et al.* work [220], which describes the mechanisms of forward blood flow generation during CPR in ten patients with non-traumatic CA; the end-compression and end-decompression left ventricular volume from Redberg *et al.* [223] which used transoesophageal echocardiography in 18 patients to evaluate end-compression and end-decompression left ventricular volume; the end tidal CO_2 ranges from Sheak *et al.* [224] which evaluated the $ETCO_2$ during CPR of 583 in- and out-of-hospital CAs. All the model outputs shown in Table 8.2 are within the physiological ranges observed in human during CPR.

I used the genetic algorithm (GA) to fine-tune a set of 58 cardiovascular parameters crucial for capturing the intricate dynamics of hemodynamic and gas exchange responses during cardiac arrest (CA) and cardiopulmonary resuscitation (CPR). To build a bank of 10 virtual subjects, I utilized a standard 5-minute period of spontaneous ventilation (SPV) from a healthy subject. The chosen parameters, covering resistances, capacitances, inductances, and elastances, were specifically targeted for tuning because of their crucial role in simulating compensatory mechanisms like baroreflex and chemoreflex during CA and CPR.

The process of selecting these parameters involved setting upper and lower limits to ensure physiological relevance. Subsequently, I defined an expected range of model outputs based on literature data [220, 223, 224] (Table 8.2), considering the inherent variability in these physiological responses. The genetic algorithm was subsequently employed to identify sets of cardiovascular parameters, ensuring that the model outputs met the predefined range. The simulation itself consisted of a 5-minute period of CA followed by 1 minute of CPR.

The GA iterations continued until 10 distinct sets of cardiovascular parameters were identified, ensuring that the corresponding model outputs aligned closely with the anticipated range of desired outputs. This comprehensive approach aimed to capture the complexities of the cardiovascular system's response during CA and CPR, accounting for individual variability. The list of the 58 cardiovascular parameters tuned for the thoracic model validation are presented in Appendix 1. The cost function ($Cost_{Val}$) was defined as:

Equation 8.14

$$\begin{aligned} Cost_{Val} = {} & w\,|PeakLV_m - PeakLV_d| + w\,|EDLVP_m - EDLVP_d| + w\,|PeakSA_m - PeakSA_d| \\ & + w\,|EDSAP_m - EDSAP_d| + w\,|PeakRA_m - PeakRA_d| \\ & + w\,|EDRAP_m - EDRAP_d| + w\,|CPP_m - CPP_d| + w\,|SV_m - SV_d| \\ & + w\,|EF_m - EF_d| + w\,|EDVLV_m - EDVLV_d| + w\,|ESVLV_m - ESVLV_d| \\ & + w\,|ETCO2_m - ETCO2_d| \end{aligned}$$

where, $PeakLV$ is the peak left ventricular pressure, $EDLVP$ is the left ventricular end compression pressure, $PeakSA$ is the peak aortic pressure, $EDSAP$ is the aortic end compression pressure, $PeakRA$ is the peak right atrial pressure, $EDRAP$ is the right atrial end compression pressure, CPP is the coronary perfusion pressure, SV is the stroke volume, EF is the ejection fraction, $EDVLV$ is the end diastolic left ventricular volume, $ESVLV$ is the end systolic left ventricular volume and $ETCO2$ id the end tidal CO_2. The subscript ‘m defines the simulation output parameters, the subscript ‘d defines the desired value of these output parameters and $w = \frac{1}{12}$ is the weight assigned to each objective. The desired value of all the parameters were defined as the hemodynamic and gas exchange data in Table 8.2.

8.2.6 Genetic algorithm for the optimal personalised CPR parameters

The aim of the GA was to find the sets of CPR parameters that minimize the cost function ($Cost_{Opt}$) defined as:

Equation 8.15

$$\begin{aligned} Cost_{Opt} = {} & w\left|\frac{CPP_m - CPP_d}{CPP_d}\right| + w\left|\frac{CO_m - CO_d}{CO_d}\right| + w\left|\frac{brainO2_m - brainO2_d}{brainO2_d}\right| \\ & + w\left|\frac{heartO2_m - heartO2_d}{heartO2_d}\right| \end{aligned}$$

where, CPP is the coronary perfusion pressure, CO is the cardiac output, brainO_2 is the cerebral tissue oxygen volume, heartO_2 is the myocardial tissue oxygen volume, the subscript ‘m defines the simulation output parameters, and the subscript ‘d defines the desired value of these output parameters. The weighting factor, $w = \frac{1}{4}$, evenly distributes the weight across each objective. The desired value of CPP, CO, brainO_2 and heartO_2 during CPR were defined as those during spontaneous ventilation (Table 8.2).

I selected these outcome parameters (CPP, CO, brainO_2 and heartO_2) because of their association with return of spontaneous circulation. Indeed, CPP is defined as the difference between the aortic diastolic pressure minus the right atria diastolic pressure and gives an indication of the myocardial blood flow during CPR. In an animal study by Naim et al. [61], targeting a systolic blood pressure of 100 mmHg and CPP>20 mmHg improved survival compared to the guidelines. The CO is the amount of blood flow restored during CPR, therefore crucial to achieve return of spontaneous circulation. Finally, the brain and the heart are the two vital organs that need to be oxygenated to preserve life. Therefore, optimizing their oxygen volume will increase the chances of return of spontaneous circulation.

Additionally, I added constraints related to the safety and practicality of the CC. The end compression force (F_{max}) was ranged between 0 and 500 N, the CC rate (CC_{rate}) between 60 and 150 compressions per minute (cpm), the compression ratio (C_R) between 20% and 80%, tidal volume (V_T) between 100 and 1000 ml, the ventilatory frequency (V_f) between 0 and 20 breaths per minute, the positive end expiratory pressure (PEEP) between 0 and 15 cmH_2O and the fraction of inspired oxygen (FiO_2) between 21% and 100%. Finally, I constrained the step increase of each parameter to have relevant values.

8.2.7 Virtual subjects and protocol

For the thoracic model validation, a bank of ten virtual healthy subjects were configured by matching the model outputs to the literature data [220, 223, 224]. Whilst the ten virtual subjects were identical during spontaneous ventilation (SPV), during CA and CPR their cardiovascular input parameters were different to allow a variation in model outputs during

CPR (Table 8.3). The 58 cardiovascular parameters that define each subject can be found in the Appendix 1.

After 5 minutes of SPV, CA was simulated for 5 minutes by setting the heart rate to 0, effectively forcing the heart to be in constant diastole. Additionally, the apnoea module was activated with obstructed upper airway. During CPR, the subjects were no longer apnoeic, and the airway were no longer obstructed. The CPR strategy followed as closely as possible the one used in Kim's work [220] which in turn followed the American Heart Association (AHA) guidelines: CC rate 100 compressions.min^{-1}, compression ratio 50%, CC depth 5 cm, tidal volume 650 mls, ventilation rate 12 breaths.min^{-1} and fraction of oxygen 100%. However, the effect of epinephrine administration every 3 minutes was not modelled since the simulation lasted 5 minutes.

To simulate CA and CPR more accurately, the GA cardiovascular input parameters were changed gradually over a minute during CA. This enabled any sudden changes in volumes, flow, or pressure that may be unrealistic. Additionally, the distribution of organ perfusion during CPR was not well documented in humans. Therefore, whilst the systemic vascular resistance was changed by the GA, the relative distribution of organ perfusion was maintained to avoid unrealistic results.

For the optimal personalised CPR identification, the ten virtual healthy subjects were configured as described above. When running the GA, CPR was simulated for 5 minutes, and the cardiovascular parameters were tuned according to the results from the previous GA (Appendix A).

I then simulated CPR using the median values of the optimized compression depths, rates, compression ratio, and ventilation found for the entire cohort, to determine whether a modified CPR protocol could offer advantages over current guidelines.

The GA and model simulations used MATLAB version R2019b.v9 (MathWorks Inc., Natick, MA, USA).

8.3 Results

8.3.1 Model validation

Table 8.2 compares the simulated cardiovascular model outputs when CPR was performed following the AHA guidelines *versus* the haemodynamic and gas exchange data during CPR from the literature described above [220, 223, 224]. All the model outputs are within the physiological ranges observed during standard CPR in humans (see also the online supplementary material).

Table 8.2 Literature human data [220,223,224] versus model outputs during CPR.

Variable	**Unit**	**Literature human data**	**Model outputs**
EC LV pressure	mmHg	112 ± 37 [1]	111 ± 13
EC aorta pressure	mmHg	105 ± 41 [1]	110 ± 13
EC RA pressure	mmHg	89 ± 27 [1]	88 ± 9
ED LV pressure	mmHg	8 ± 11 [1]	11 ± 7
ED aorta pressure	mmHg	33 ± 10 [1]	36 ± 4
ED RA pressure	mmHg	8 ± 6 [1]	6 ± 3
CPP	mmHg	25 ± 9 [1]	30 ± 7
Stroke volume	ml	19 ± 6 [2]	19 ± 1
EC LV volume	ml	50 ± 7 [2]	72 ± 6
ED LV Volume	ml	70 ± 10 [2]	70 ± 7
Ejection fraction	%	34 ± 16 [1]	50 ± 8
$ETCO_2$	mmHg	30± 5 [3]	26 ± 1

EC, end compression; ED, end diastolic; LV, left ventricle; RA, right atria; CPP, coronary perfusion pressure; $ETCO_2$, end tidal CO_2; 1: Kim *et al.* [220]; 2: Redberg *et al.* [223]; 3: Sheak *et al.* [224].

After the onset of CA, the aortic pressure exponentially decreased and reached mean systemic filling pressure (MSFP) of 10 mmHg after 4 minutes of CA (Figure 8.6).

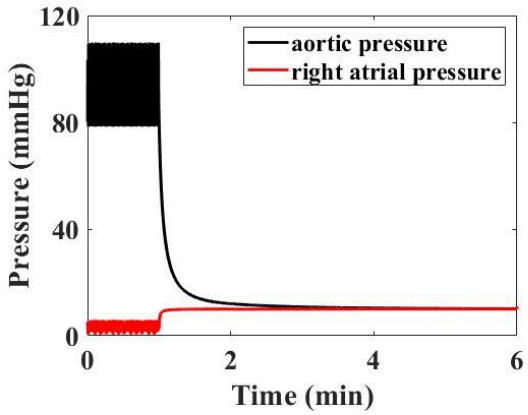

Figure 8.6 Aortic and right atrial pressure during 1 minute of spontaneous ventilation and after the onset of CA

Figure 8.7 shows the resultant pleural pressure during standard CPR following the AHA guidelines. The pleural pressure oscillated between -4 and 10 cmH_2O due to the mechanical ventilation, but further oscillations of about 1 cmH_2O of amplitude can also be observed. These smaller oscillations are due to the CC.

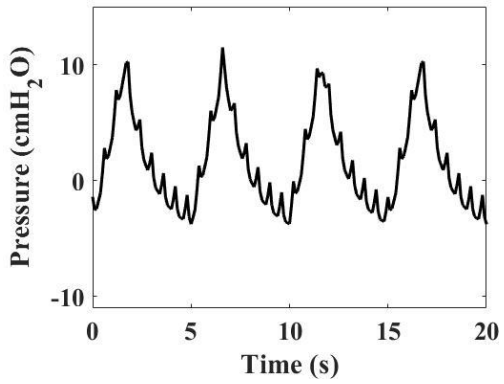

Figure 8.7 Pleural pressure during standard CPR.

8.3.2 Optimal median & personalised CPR parameters

Table 8.3 shows the optimal personalised CPR parameters for each subject identified by the GA, as well as the median optimized values over the cohort. The CC rate and compression ratio are the two parameters with the largest ranges over the cohort, from 62-104 compressions min^{-1} and 41-58%, respectively. The PEEP, CC force and its associated maximal sternal displacement are the two parameters that remain relatively constant at 0

cmH_2O and 495 N (5-6 cm of displacement), respectively. Similarly, all the ventilatory parameters varied with a mean tidal volume of 250 ml, ventilatory frequency of 6 breaths min^{-1} and a fraction of inspired oxygen of 80%. Overall, the optimal median optimal minute ventilation was 1500 ml min^{-1}.

Table 8.3 Optimal CPR parameters for 10 subjects

Parameter	CC rate	Max Force	CC depth	C_R	V_T	V_f	PEEP	FiO_2
Subject 1	66	495	6.1056	41	550	2	0	70
Subject 2	62	500	6.3431	50	200	9	0	70
Subject 3	80	494	6.0817	49	250	8	0	50
Subject 4	104	494	6.0023	58	250	6	0	70
Subject 5	65	498	6.2379	46	300	5	0	100
Subject 6	60	493	6.2813	51	200	8	0	90
Subject 7	67	500	6.3807	58	300	2	0	90
Subject 8	65	499	6.3365	53	300	5	0	100
Subject 9	87	497	6.0989	52	200	6	0	90
Subject 10	93	499	6.0654	52	250	6	0	80

CC rate, chest compression rate (compressions min^{-1}); Max Force, maximal chest compression force (N); CC depth, maximal sternal displacement (cm); C_R, compression ratio (%); V_T, tidal volume (ml); V_f, ventilatory frequency (breaths min^{-1}); PEEP, positive end expiratory pressure (cmH2O); FiO_2, fraction of inspired oxygen (%).

Table 8.4 Model outputs using the standard CPR protocol (AHA-CPR), the optimized CPR protocol (OPT-CPR) and personalised CPR (PERS-CPR).

	AHA-CPR				**OPT-CPR**				**PERS-CPR**			
	CPP	CO	$brainO_2$	$heartO_2$	CPP	CO	$brainO_2$	$heartO_2$	CPP	CO	$brainO_2$	$heartO_2$
	mmHg	ml min^{-1}	ml	Ml	mmHg	ml min^{-1}	ml	Ml	mmHg	ml min^{-1}	ml	ml
Median		1853 ±	0.80 ±	0.061 ±		2822	1.73	0.326		2830 ±	1.68 ±	0.320 ±
±SD	30 ± 7	100	0.7	0.05	39 ± 7	±143	±0.06	±0.05	38 ± 8	300	0.1	0.02
Subject1	30	1806	0.75	0.002	38	2946	1.74	0.327	35	2891	1.71	0.331
Subject2	34	2014	0.88	0.048	45	3105	1.80	0.324	46	3151	1.78	0.325
Subject3	32	1912	0.89	0.121	39	3001	1.82	0.379	38	2920	1.68	0.339
Subject4	20	1759	0.79	0.166	25	2778	1.77	0.450	22	2404	1.5	0.323
Subject5	27	1761	0.74	0.002	34	2700	1.68	0.291	35	2740	1.73	0.304
Subject6	30	1765	0.73	0.002	42	2765	1.69	0.305	43	2763	1.71	0.322
Subject7	31	1873	0.78	0.002	41	2780	1.64	0.281	41	2855	1.65	0.283
Subject8	30	1920	0.83	0.002	39	3031	1.77	0.305	39	3049	1.81	0.313
Subject9	37	1862	0.81	0.129	48	2864	1.71	0.377	46	2799	1.62	0.326
Subject10	27	1859	0.83	0.137	30	2720	1.71	0.371	31	2731	1.66	0.33

CPP: coronary perfusion pressure; CO: cardiac output; brainO2: cerebral tissue oxygen volume; $heartO_2$: myocardial tissue oxygen volume.

Tables 8.3 and 8.4 show the model outputs, CPP, CO, $brainO_2$ and $heartO_2$ during spontaneous ventilation, after CA, during CPR following the AHA guidelines (AHA-CPR), during CPR with optimal personalized CPR parameters (PERS-CPR), and during CPR with the new optimized protocol based on the median values of the optimized CPR parameters (OPT-CPR). CPP and CO were partially restored after 5 minutes for both CPR protocols. However, compared to the AHA protocol, all the model outputs were improved with the optimised CPR strategy (Table 8.3). Whilst the CPP was moderately improved, the myocardial tissue oxygen volume ($heartO_2$) was more than 5 times higher during optimized CPR. Similarly, the cerebral tissue oxygen volume ($brainO_2$) was nearly doubled during optimized CPR compared to standard CPR. Considering the reduction in ventilation parameters, this better oxygenation of the vital organs can only be explained by the increased CO.

Table 8.5 Model outputs during spontaneous ventilation (SPV) and cardiac arrest (CA).

Parameters	**Unit**	**SPV**	**CA**
CPP	mmHg	80	0
CO	ml min^{-1}	5000	0
$brainO_2$	ml	1.83	0
$heartO_2$	ml	0.32	0

CPP, coronary perfusion pressure; CO, cardiac output; $brainO_2$, cerebral tissue oxygen volume; $heartO_2$, myocardial tissue oxygen volume.

8.4 Discussion

In this study, I developed and validated a new, highly-integrated model of the cardiopulmonary systems. After the onset of CA, the aortic pressure exponentially decreases and reaches a mean systemic filling pressure (MSFP) of 10 mmHg after 4 minutes of CA in keeping with clinical observations (see Figure 8.6) [225]. Additionally, the MSFP of around 10 mmHg agrees with the observation in Repesse *et al.* [226] that deceased intensive care unit patients who happened to have central venous catheter and arterial lines had a MSFP of around 12 mmHg.

Our model presented no aortic regurgitation and moderate to severe retrograde blood flow from the left ventricle into the left atrium (3-16 ml) as well as antegrade blood flow from the left ventricle into the aorta during the compression phase of CPR, in keeping with the observations of Kim *et al.* [220]. The CO reaches a maximum of 2800 ml min^{-1} which is 56% of the CO during spontaneous circulation. During CPR, CO can vary dramatically depending on CC quality. In Fodden *et al.* [225] the median CO was found to be approximately 2040 ml min^{-1}, which is again in keeping with our results.

During personalised optimal CPR, the CPP is moderately increased from 30 mmHg to 38 mmHg, however, the myocardial tissue oxygen volume ($heartO_2$) is more than 5 times higher than during standard CPR (Table 8.3). The cerebral tissue oxygen volume ($brainO_2$) is nearly doubled during optimized CPR compared to standard CPR. Considering the reduction in minute ventilation and FiO_2 from 7800 ml min^{-1} to 1500 ml min^{-1}, and 100% to 80%, respectively, during the optimized CPR protocols, the improvements in oxygenation of the vital organs can only be explained by the increase in CO of nearly 1000 ml min^{-1}. Interestingly, these potential benefits were preserved when I applied a single CPR protocol (OPT-CPR) to the cohort, based on the median values of the personalized CPR parameters – indeed in some cases this protocol slightly improved on the personalized results, likely due to the optimization algorithm failing to find the exact global optimum.

While the median optimised maximal sternal displacement (6.2 cm) and median compression ratio (52%) agree with the AHA guidelines, the median CC rate (67 compressions min^{-1}) identified in our optimized protocol is considerably lower than the range recommended by the AHA guidelines of 100-120 compressions min^{-1} [30]. The corresponding optimized ventilation strategy (minute ventilation 1500 ml min^{-1}) suggests that a more restrained ventilation strategy could help mitigate the detrimental hemodynamic effects of mechanical ventilation whilst maintaining sufficient arterial oxygenation.

Whilst the total absence of ventilation during CPR has been shown to be associated with poor outcomes [70], a similar negative outcome has been observed when hyperventilation is used [65]. Indeed, a lower minute ventilation at the beginning of CPR could help mitigate the negative hemodynamic effects of ventilation on CO and could avoid hyperoxaemia, which

has been shown to be detrimental to long terms outcomes. However, whilst at the beginning of CPR ensuring blood circulation is key, ventilation becomes crucial as CO_2 clearance becomes necessary during prolonged CPR or after a long period of untreated CA.

Previous studies have used mathematical models of the cardiovascular system to investigate alternative CPR strategies ranging from interposed abdominal compression [143, 144], combined chest and abdominal compression and decompression [145-147], impedance valve [148, 149], and passive leg raise [150, 151]. Jung *et al.* applied optimal control to identify the CC and decompression frequency and compression ratio that maximized the coronary perfusion pressure (CPP) [157] and the blood flow as measured by the pressure difference between the thoracic aorta and the right atrium [158]. In both papers, the authors identified the optimal waveform to include both compression and decompression of the chest to the maximum allowable extent and a compression ratio of 40%. However, one study [157] found the optimal CC rate to be 90 compressions min^{-1} and the other 60 compressions min^{-1}. Whilst our optimal maximal sternal displacement was similarly higher (6.2 cm) than the AHA recommendations and our optimal CC rate lower (67 compressions min^{-1}), our optimal compression ratio was only slightly higher (52%) than the AHA recommendations whereas Jungs *et al.* was lower (40%). These discrepancies may arise from the fact that while Jungs' studies considered decompression and the waveform shape variation, our study included the optimization of ventilatory parameters during CPR. Additionally, their model did not include a pulmonary system or mechanisms of gas exchange.

Similarly, Babbs *et al.* [160] investigated the optimal CC frequency for different sized individuals, from neonates to adults and found that whilst high frequency for neonates (>120 compressions min^{-1}) was advantageous, in adults there may be benefit from lower compression frequencies near 60 compressions min^{-1}. In another study Babbs [25] identified the optimal CPR to be reciprocal compression and decompression of the chest and the abdomen to the maximum allowable extent with a CC rate of 80 compressions min^{-1} and a compression ratio of 50%. Both these studies support our results.

John *et al.* [159] investigated the optimal CC pressure and rate to maximize CO and found them to be respectively 100 mmHg, which is approximately a maximal sternal displacement of 5.7 cm, and 110 compressions min^{-1}, both similar to those recommended in the AHA guidelines. However, similarly to the findings of Jung *et al.*, the study of John *et al.* did not include a model of the pulmonary system or gas exchange. Finally, Turner *et al.* investigated the benefits of continuous CC over the usual 5:1 or 15:2 ratios of compression to ventilation [222] and found that lower ventilation ratios (15:2 and 50:5) produced significantly greater oxygen delivery to the body. These results are in keeping with ours, suggesting that lower ventilatory frequency can effectively oxygenate tissues during CPR.

Compared to previous studies, our model has the unique advantage of using a high-fidelity, computational model of the respiratory and cardiovascular systems that includes extensive cardiopulmonary interactions. Our model is the first to use multiple sources of human data during CPR [220, 223, 224] and fine-tune cardiovascular parameters to create a bank of 10 virtual subjects to study CPR. These parameters were selected based on their expected changes during cardiac arrest and CPR, influenced by cardiovascular control mechanisms like baroreflex and chemoreflex. Through the optimization process, our model successfully replicated hemodynamic and gas exchange outputs in the virtual subjects, aligning closely with the observed data from the literature. This comprehensive approach not only utilized human data for subject creation but also demonstrated the model's ability to accurately simulate and reproduce physiological responses observed in real-world scenarios.

Our model has limitations. The lack of complex biological processes (i.e. high levels of inflammatory cytokines) limits its usefulness for the study of post-CA treatment and management which affects the whole body (multi-organ failure). Our model does not account for the electrophysiology of the heart or the cardiovascular control mechanism (i.e. chemoreflex, effect of vasopressors or inotropes) which can be important when studying CPR. Finally, our model does not account for the role of the precipitating aetiology, which can require a particular CPR strategy.

8.5 Conclusion

In this study, I identified optimal CPR strategies in a cohort of ten virtual subjects using a novel, high-fidelity, computational model of the cardiopulmonary systems. Myocardial tissue oxygen volume was more than 5 times greater, and cerebral tissue oxygen volume was nearly doubled during our optimized CPR protocol. Compared to current AHA guidelines, the identified optimal CPR strategy had the same compression ratio (52%), a slightly greater CC depth (6.2 cm), a lower CC rate (67 compressions min^{-1}), and a less aggressive ventilation strategy (V_T 250 ml, V_f, 6 breaths min^{-1}). The results of this study highlight the potential negative hemodynamic effects of excessive ventilation, which could increase pulmonary vascular resistance, impeding CO. Future clinical trials evaluating modifications in multiple CPR parameters simultaneously could help elucidate optimal CPR strategies with significant benefits to patients. However, it is crucial to acknowledge the inherent limitations of computational models. The absence of intricate factors like anaerobic respiration and lactate production, coupled with the oversimplification and limited portrayal of tissues, might impact the precision of our simulation. Furthermore, this study focused on healthy virtual subjects, and the extrapolation of these findings to real-world scenarios requires careful consideration, especially in the context of patients with comorbidities. The necessity to account for such complexities in future research becomes apparent, ensuring that our understanding of optimal CPR strategies is both comprehensive and applicable to a broader spectrum of individuals

Chapter 9. Simulation of cardiopulmonary resuscitation strategies in myocardial infarction and asphyxia.

This chapter describes the project that has been done as part of the Wellcome Trust Biomedical Vacation Scholarship 2022. I co-supervised the undergraduate student Jordan Stocker-Palmer with Dr. Marianna Laviola.

My contribution to this work is:

- Coding the new protocol simulation
- Running the computational simulations
- Providing guidance in the analysis of the results (understanding the findings and producing the figures and tables)
- Revising the student's report

9.1 Introduction

Myocardial infarction (MI), the ischaemia of the myocardial tissue, remains the leading cause of cardiac arrest (CA). In its severe form pulmonary embolism (PE), i.e., the blockage of the pulmonary artery, inducing hypoxia can cause CA. Reversing the pathology that caused the CA is one of the crucial aspects of successful cardiopulmonary resuscitation (CPR). Therefore, modelling different precipitating pathologies is key to determine successful CPR strategies.

While standard CPR protocols exist, research has suggested that tailoring CPR strategies to the underlying aetiology of cardiac arrest may improve outcomes [227]. Therefore, investigating precipitating aetiology-specific CPR strategies for MI and PE is crucial for improving the outcomes of cardiac arrest. This could lead to the development of tailored CPR protocols that are effective in improving survival rates and reducing morbidity and

mortality associated with these conditions. However, further research is needed to determine the most effective and safe CPR strategies.

In this study, I used the ICSM simulation suite to better understand if CPR strategies should be specific to the precipitating aetiology of CA. This chapter's objectives are to 1) model acute MI and acute PE and their associated compensatory mechanisms in an otherwise healthy individual; 2) CA induced by MI and PE and standard CPR; and 3) identify the optimal CPR strategy in terms of chest compressions and ventilation parameters with a genetic algorithm for both aetiology specific CA.

9.2 Methods

I used the ICSM simulation suite, as previously described in Chapter 4 along with the thoracic model described in great length in Chapter 8.

9.2.1 Modelling acute myocardial infarction (MI)

To model myocardial infarction I used the canine myocardial infarction model from Lekven et al. [215]. These authors investigated the hemodynamic and metabolic compensatory mechanisms during graded myocardial ischaemia in anesthetized and mechanically ventilated dogs. The graded coronary ischaemia was done in two stages: 1) during the first MI phase (MI1), the coronary blood flow (CF) was reduced by 20% compared to baseline and 2) during the second MI phase (MI2) the CF was reduced by 50% compared to baseline (Table 9.1 canine model).

Lekven et al. [215] found that a reduction in coronary blood flow was closely associated with concomitant ventricular dilatation and reduced myocardial contractility, and this finding could explain the maintained cardiac output at a reduced level of myocardial oxygen supply. Decreased myocardial contractility reduced myocardial oxygen demand, whereas ventricular dilatation-maintained stroke volume on a geometric basis [215].

After simulating 5 min of mechanical ventilation in a virtual healthy subject, the baseline model outputs for a virtual human subject were obtained. All these model outputs were in

accordance with the human physiological ranges. Then, I used the Lekven et al. [215] canine data and the virtual healthy subject baseline model outputs to linearly interpolate the expected model outputs in human during MI1 and MI2 (Table 9.1).

Table 9.1. Hemodynamic and metabolic effects of graded reduction in coronary blood flow in a canine model [215] and the expected model outputs in a human, obtained using the ICSM simulation suite, for the same graded reduction in coronary blood flow.

	Canine Model [215]			**Expected model outputs in humans**		
Parameters	**Baseline**	**MI1**	**MI2**	**Baseline**	**MI1**	**MI2**
SV ($ml.beat^{-1}$)	22	22	17	88	88	68
CPP (mmHg)	95	62	49	80	52	41
CF ($ml.min^{-1}$)	93	72	47	274	212	138
LVSP (mmHg)	110	106	91	124	120	103
LVEDP (mmHg)	3	5	11	4	7	14
LV work ($mmHg.ml.s^{-1}$)	4.06	4	2.55	8	8	5
HR ($beats.min^{-1}$)	149	148	149	70	70	70
VO_2h ($ml.min^{-1}$)	9.8	7.8	5.6	29	23	17
O_2 extraction (%)	71	78	81	53	58	60

SV: stroke volume; CPP: coronary pulmonary pressure; CF: coronary flow; LVSP: left ventricle systolic pressure; LVEDP: left ventricle end diastolic pressure; LV work: left ventricle work; HR: heart rate; VO_2h: myocardial oxygen consumption rate; O_2 extraction: oxygen extraction from arterial to venous blood.

To simulate MI, the coronary artery resistance constant (Rsa4c) was modified to achieve the required reduction in coronary blood flow. Additionally, five input parameters were tuned to achieve the expected model outputs inferred from Lekven et al. paper shown in Table 9.1. The five input parameters tuned were: the systemic vascular resistance constant (RSAc), the left ventricular systolic contractility constant (Elvsysc) the left ventricular diastolic pressure constant (Plv0c), the myocardial oxygen consumption rate (VO_2h) and the heart rate (HR).

9.2.2 Modelling acute pulmonary embolism (PE)

To model pulmonary embolism , I used a porcine model of pulmonary embolism from Schultz et al. [228]. Schultz et al. study [228] investigated haemodynamic and metabolic compensatory mechanisms during PE in anesthetized and mechanically ventilated pigs. This study found to mimic accurately pulmonary embolization in humans with signs of right ventricular strain (dilation) with preserved systemic circulation.

To simulate PE, the pulmonary artery resistance was modified to achieve the required increase in mean pulmonary artery pressure. Additionally, three input parameters were tuned to achieve the expected model outputs inferred from Schultz et al. paper (Table 9.2): the anatomical shunt (anatShunt), the systemic venous resistance (SVR), and the heart rate (HR).

Table 9.2. Hemodynamic and metabolic effects of graded pulmonary artery embolization in a porcine model and [228] in a healthy virtual human subject.

	Porcine Model [228]			Human Model		
Parameters	**Baseline**	**PE1**	**PE2**	**Baseline**	**PE1**	**PE2**
HR (bpm)	50	60	80	70	84	112
MPAP (mmHg)	16	27	30	21	36	40
MAP (mmHg)	70	74	72	95	100	98
CO ($L.min^{-1}$)	4.4	4	4.5	6.15	5.59	6.29
RVSV (ml)	90	70	60	88	69	59
RVEDV (ml)	145	155	160	163	174	180
RVESV (ml)	60	80	100	64	86	107
RVEF (%)	60	45	37	60	45	37
$ETCO_2$(kPa)	5.5	4.2	4	5.22	3.99	3.80
$PaCO_2$ (kPa)	5	5.5	6.3	5.38	5.92	6.78
PaO_2 (kPa)	16	12	10	13.23	9.92	8.27
Arterial pH	7.52	7.49	7.43	7.41	7.38	7.32

HR: heart rate; MPAP: mean pulmonary artery pressure; MAP: mean artery pressure; CO: cardiac output; RVSV: right ventricle stroke volume; RVEDV: right ventricle end diastolic volume; RVESV: right ventricle end systolic volume; RVEF: right ventricle ejection fraction; $ETCO_2$: end tidal carbon monoxide; $PaCO_2$: arterial carbon dioxide partial pressure; PaO_2: arterial oxygen partial pressure.

9.2.3 Protocol

A virtual healthy subject was configured as in our previous study [219]. In line with the methodology employed in the animal studies, baseline parameter values for the virtual healthy human subject were obtain after 5minutes of mechanical ventilation. The mechanical ventilation settings were maintained constant, up to induction of cardiac arrest, for both precipitating aetiology (Table 9.3).

Table 9.3. Mechanical ventilation settings.

Mechanical ventilation settings	Values
V_f (breaths.min^{-1})	16
V_T (ml)	480
$Fi0_2$ (%)	21
PEEP (cmH2O)	0

V_f: ventilatory frequency; V_T: tidal volume; FiO_2: fraction of inspired oxygen; PEEP: positive end expiratory pressure.

After obtaining the baseline values, the first phase of the precipitating aetiology (MI1 or PE1) was simulated, followed by the second phase of the precipitating aetiology (MI2 or PE2). Both phases lasted 5 minutes each and were followed by 5 minutes of asystole and then 5 minutes of standard CPR (std-CPR). CA was simulated by setting the heart rate to 0, effectively forcing the heart to be in constant diastole. Additionally, the subject was apnoeic with the upper airway obstructed. During std-CPR, apnoea was maintained, however, the upper airway was no longer obstructed allowing passive ventilation from chest compressions. CC were modelled using the thoracic modelled presented in Chapter 8. Briefly, three parameters were used to modify the CC: the end compression force (F_{max}) a surrogate for the maximal sternal displacement, the CC rate (CC_{rate}) and the compression ratio (i.e., the proportion of time under compression during compression and decompression cycle), (C_R). Standard CPR was simulated following the ERC guidelines, i.e. Maximal end compression force: $F_{max} = 400\ N$, chest compression rate: $CC_{rate} = 120\ cpm$, and compression ratio: $C_R = 0.50$. Figure 9.1 shows the simulation time frame for both precipitating aetiologies.

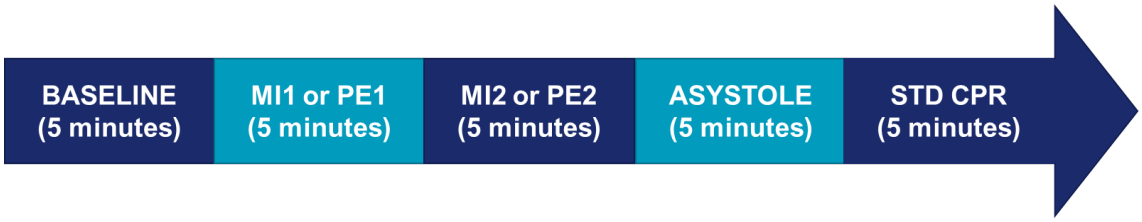

Figure 9.1 Simulation time frame for both precipitating aetiologies.

9.2.4 Identification of aetiology specific optimal CPR

In this study, I used a genetic algorithm (GA) method to solve the optimization problem. Briefly, the algorithm: 1) creates a random initial population from the parameter space, defined by the boundaries of the input parameters; 2) calculates the individual scores of each member of this population, by running the simulation and deriving the cost (8); 3) generates members of the next population through the selecting best individuals of the existing population (elitism), combining the characteristics of two different members (crossover), and making changes to randomly selected individuals (mutation) 4) repeats steps 2)-3) until an optimal solution is found that satisfies a pre-defined criteria, in this case the improvement in cost function between consecutive generations is below 10^{-3} or the number of generations exceed 100 (Figure 9.2).

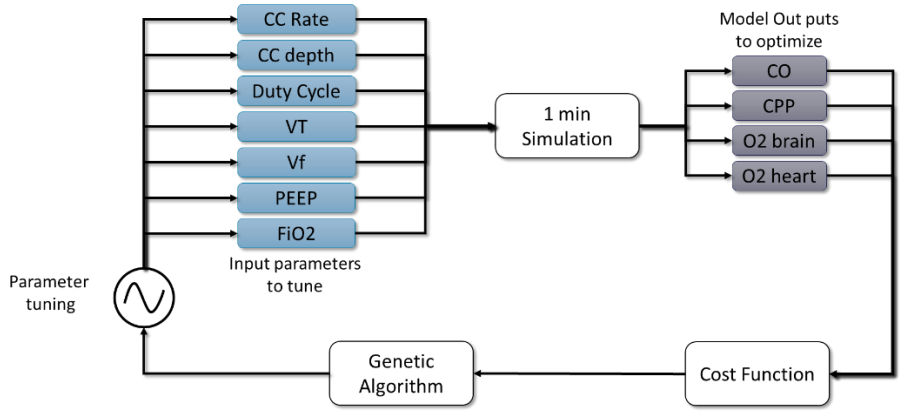

Figure 9.2 Schematic diagram of the genetic algorithm.

The aim in using the GA was to find the sets of CPR parameters that minimize the cost function ($Cost$) defined as:

Equation 9.1

$$Cost = w\left|\frac{CPP_m - CPP_d}{CPP_d}\right| + w\left|\frac{CO_m - CO_d}{CO_d}\right| + w\left|\frac{brainO2_m - brainO2_d}{brainO2_d}\right| + w\left|\frac{heartO2_m - heartO2_d}{heartO2_d}\right|$$

where, CPP is the coronary perfusion pressure, CO is the cardiac output, brainO_2 is the cerebral tissue oxygen volume, heartO_2 is the myocardial tissue oxygen volume, the

subscript ‘m defines the simulation output parameters, the subscript ‘d defines the desired value of these output parameters and $w = \frac{1}{4}$ is the weight assigned to each objective. The desired value of CPP, CO, brainO_2 and heartO_2 during CPR were defined as those during mechanical ventilation (Table 9.6).

These outcome parameters (CPP, CO, brain O_2 and heart O_2) were chosen because of their association with return of spontaneous circulation (ROSC). Additionally, constraints related to the safety and practicality of the CC were added. The end compression force (F_{max}) was ranged between 0 and 500 N, the CC rate (CC_{rate}) between 60 and 150 compressions per minute (cpm), the compression ratio (C_R) between 20% and 80%, tidal volume (V_T) between 100 and 1000 ml, the ventilatory frequency (V_f) between 0 and 20 breaths per minute, the positive end expiratory pressure (PEEP) between 0 and 15 cmH_2O and the fraction of inspired oxygen (FiO_2) between 21% and 100%. Finally, the step increase of each parameter to obtain relevant values was constrained.

Following the modelling of standard CPR after MI and PE, the simulations of optimized CPR were run for 5 minutes during each cycle of the GA.

9.3 Results

9.3.1 Myocardial Infarction (MI) model

Table 9.4 presents the haemodynamic and metabolic model outputs in a virtual subject during graded coronary ischaemia. The first seven parameters on the table are the input parameters tuned to achieve the expected model outputs during graded coronary ischaemia shown in Table 9.1. Overall, the model outputs in Table 9.4 follow closely the expected results presented in Table 9.1. The coronary blood flow reduction during MI1 and MI2 closely followed the expected flow reduction. During MI1 the CF was to 211 ml.min^{-1}compared to the expected 212 ml.min^{-1}and during MI2 the CF was 137 ml.min^{-1}compared to the expected 139 ml.min^{-1}.

Table 9.4 ,Hemodynamic and metabolic effects of graded reduction in coronary blood flow in a healthy virtual subject.

	Baseline	model MI1	model MI2
Model input parameters			
Rsa4c (mmHg s.ml^{-1})	18.0	18.00	25.00
RSAc (mmHg s.ml^{-1})	0.80	0.60	0.70
Elvsysc (mmHg.ml^{-1})	2.50	2.00	1.00
Plv0	1.00	1.50	3.00
Elamin (mmHg.ml^{-1})	0.20	0.10	0.10
VO_2h (ml.min^{-1})	29	23	17
HR (beats.min^{-1})	70	70	70
Haemodynamic model outputs			
CF (ml.min^{-1})	274	211	137
SV (ml.beat^{-1})	88	89	68
MAP (mmHg)	95	84	78
CPP (mmHg)	80	68	65
LVSP (mmHg)	124	115	103
LVEDP (mmHg)	4	6	17
LVEDV (ml)	145	152	176
LVESV (ml)	56	61	107
EF (%)	62	60	39
LV work (mmHg.ml.s^{-1})	8	7	5
Metabolic model outputs			
PaO_2 (kPa)	13.23	13.32	13.22
$PaCO_2$ (kPa)	5.38	5.42	5.28
$VtissO_2$ (ml)	0.29	0.28	0.25
CvO_2h (ml.ml^{-1})	96	93	80
O_2 extraction (%)	53	54	60

Rsa4c: myocardial capillary resistance constant; RSAc: systemic arterial resistance constant; Elvsysc: left ventricle elastance; Plv0: left ventricle end diastolic pressure constant; Elamin: left atria diastolic elastance; VO_2h: myocardial oxygen consumption rate; HR: heart rate; CF: coronary flow; SV: left ventricle stroke volume; MAP: mean arterial pressure; CPP: coronary perfusion pressure; LVSP: left ventricle systolic pressure; LVEDP: left ventricle end diastolic pressure; LVEDV: left ventricle end diastolic volume; LVESV: left ventricle end systolic volume; EF: ejection fraction; LV work: left ventricle work; PaO_2: arterial oxygen partial pressure; $PaCO_2$: arterial carbon dioxide partial pressure;$VtissO_2$: tissue volume of oxygen; CvO_2h: myocardial venous oxygen concentration; O_2 extraction: oxygen extraction percentage from the arterial to the venous blood.

Similarly, the stroke volume closely matched the expected stroke volume with a SV of 89 ml.beat^{-1} compared to 88 ml.beat^{-1} during MI1 and a SV of 68 ml.beat^{-1} compared to 68 ml.beat^{-1} during MI2. The same can be observed with the left ventricle systolic pressure LVSP (MI1: 115 mmHg vs. 120 mmHg and MI2: 103 mmHg vs. 103 mmHg), the left ventricle end diastolic pressure LVEDP (MI1: 6 mmHg vs. 7 mmHg and MI2: 17 mmHg vs. 14 mmHg), the left ventricle work (MI1: 7 mmHg.ml.s^{-1} vs. 8 mmHg.ml.s^{-1} and MI2: 5 mmHg.ml.s^{-1} vs. 5 mmHg.ml.s^{-1}), and the oxygen extraction (MI1: 54 % vs. 58 % and MI2: 60 % vs. 60 %). The coronary perfusion pressure CPP followed a downward trend similarly to the expected results however the absolute values were different with a CPP of 68 mmHg compared to the expected 52 mmHg during MI1 and a CPP of 65 mmHg compared to the expected 41 mmHg during MI2.

9.3.2 Pulmonary Embolism (PE) model

Table 9.5 presents the haemodynamic and gas exchange model outputs in a virtual subject during graded pulmonary embolism. The first five parameters on the table are the input parameters tuned to achieve the expected model outputs during graded pulmonary embolism shown in Table 9.2. Overall, the haemodynamic model outputs in table 9.5 follow closely the expected results presented in Table 9.2. The mean pulmonary arterial pressure (MPAP) increased during PE1 and PE2 closely following the expected outputs. During PE1 the MPAP was 35 mmHg compared to the expected 36 mmHg and during PE2 the MPAP was 46 mmHg compared to the expected 40 mmHg. The same can be observed with the mean arterial pressure MAP (PE1: 96 mmHg vs. 100 mmHg and PE2: 90 mmHg vs. 98 mmHg), the cardiac output CO (PE1: 5.7 L.min^{-1} vs. 5.6 L.min^{-1} and PE2: 6.3 L.min^{-1} vs. 6.3 L.min^{-1}), the right ventricle stroke volume RVSV (PE1: 68 ml.beat^{-1} vs. 68 ml.beat^{-1} and PE2: 56 ml.beat^{-1} vs. 59 ml.beat^{-1}) , the right ventricle end systolic volume RVESV (PE1: 167 ml vs. 174 ml and PE2: 168 ml vs. 180 ml), the right ventricle end diastolic volume RVEDV (PE1: 90 ml vs. 86 ml and PE2: 106 ml vs. 107 ml), and the ejection fraction EF (PE1: 46 % vs. 45 % and PE2: 37 % vs. 37 %).

Table 9.5. Hemodynamic and metabolic effects of graded pulmonary artery embolization.

	Baseline	model PE1	model PE2
Model input parameters			
HR (bpm)	70	84	112
Rpac (mmHg s.ml^{-1})	0.023	0.60	1.30
anatShunt	0.020	0.20	0.50
RSAc (mmHg s.ml^{-1})	0.800	0.90	0.70
Elvsysc (mmHg.ml^{-1})	2.500	2.50	2.70
Haemodynamic model outputs			
MPAP (mmHg)	21	35	46
MAP (mmHg)	95	96	90
CO (L.min^{-1})	6.2	5.7	6.3
RVSV (ml.beat^{-1})	88	68	56
RVEDV (ml)	153	167	168
RVESV (ml)	64	90	106
RVEF (%)	58	46	37
Gas exchange model outputs			
$ETCO_2$ (kPa)	5.35	5.10	4.89
$PaCO_2$ (kPa)	5.51	5.46	5.88
PaO_2 (kPa)	13.25	8.68	5.66
Arterial pH	7.40	7.40	7.38
heartO_2 (ml)	0.29	0.28	0.24
brainO_2 (ml)	1.85	1.62	1.36

HR: heart rate; Rpac: pulmonary arterial resistance constant; anatShunt: anatomical shunt; RSAc: systemic arterial resistance constant; Elvsysc: left ventricle systolic elastance constant; MPAP: mean pulmonary arterial pressure; MAP: mean arterial pressure; CO: cardiac output; RVSV: right ventricle stroke volume; RVEDV: right ventricle end diastolic volume; RVESV: right ventricle end systolic volume; RVEF: right ventricle ejection fraction; $ETCO_2$: end tidal carbon dioxide; $PaCO_2$: arterial carbon dioxide partial pressure; PaO_2: arterial oxygen partial pressure; heartO_2: myocardial tissue volume of oxygen; brainO_2: cerebral tissue volume of oxygen.

Table 9.5 also shows the gas exchange model outputs, which whilst following the same trend as the expected outputs in Table 9.2 do not reach the same amplitude of values. The end tidal CO_2 ($ETCO_2$) steadily decreases from 5.35 kPa to 5.10 kPa during PE1 and to 4.89 kPa during PE2, however the expected model outputs are respectively 3.99 kPa and 3.80 kPa during PE1 and PE2. The same can be observed with the arterial carbon dioxide partial pressure $PaCO_2$ (PE1: 5.46 kPa vs. 5.92 kPa and PE2: 5.88 kPa vs. 6.78 kPa), the arterial oxygen partial pressure PaO_2 (PE1: 8.68 kPa vs. 9.92 kPa and PE2: 5.66 k Pa vs. 8.27 kPa) and the arterial pH (PE1: 7.40 vs. 7.38 and PE2: 7.38 vs. 7.32).

9.3.3 Cardiac arrest, standard CPR and optimal CPR

Table 9.6 presents the haemodynamic and gas exchange model outputs during mechanical ventilation, during standard CPR (Std-CPR) after MI and PE and during optimized CPR (Opt-CPR) after MI and PE. Both optimized CPR have achieved improved model outputs, with the cardiac output increasing from 3.4 $L.min^{-1}$ to 5.1 $L.min^{-1}$ for MI and 3.3 $L.min^{-1}$ to 5.2 $L.min^{-1}$ for PE. A similar improvement can be observed with the coronary perfusion pressure CPP (MI: 67 mmHg vs. 49 mmHg, PE: 69 mmHg vs. 49 mmHg), the myocardial tissue volume of oxygen $heartO_2$ (MI: 0.28 ml vs. 0.14 ml, PE: 0.03 ml vs. 0.00 ml), and the cerebral tissue volume of oxygen $brainO_2$ (MI: 2.11 ml vs. 1.64 ml, PE: 1.64 ml vs. 0.90 ml).

Table 9.7 presents the CC and ventilation parameters during standard CPR and optimized CPR after MI and PE. Both optimized CPR had a significant increase in end compression force (F_{max}) and compression ratio (C_R) whilst they both had a decrease in CC rate, tidal volume (V_T) and fraction of inspired oxygen (FiO_2). The ventilatory frequency is the only parameter that was increased for the optimized CPR following MI and decreased for the optimized CPR following the PE compared to standard CPR.

Table 9.6. Haemodynamic and gas exchange model outputs during mechanical ventilation (MV), standard CPR (Std-CPR) and optimized CPR (Opt-CPR) after myocardial infarction (MI) and pulmonary embolism (PE).

	Baseline MV	**Std-CPR after MI**	**Std-CPR after PE**	**Opt-CPR after MI**	**Opt-CPR after PE**
Haemodynamic					
HR (beats.min^{-1})	70	0	0	0	0
LVSV (ml.beat^{-1})	88	29	27	46	61
CO (L.min^{-1})	6.2	3.4	3.3	5.1	5.2
SASP (mmHg)	122	127	125	149	149
MAP (mmHg)	95	71	69	92	92
MPAP (mmHg)	21	73	77	79	83
CPP (mmHg)	80	49	49	67	69
LVEF (%)	62	32	31	37	37
SVR (mmHg.s.ml^{-1})	0.91	1.31	1.29	1.63	1.61
Gas Exchange					
PaO_2 (kPa)	13.23	81.33	4.91	64.16	6.54
$PaCO_2$ (kPa)	5.38	4.77	5.80	5.55	8.95
$ETCO_2$ (kPa)	5.22	4.65	4.15	5.09	7.71
Arterial pH	7.41	7.44	7.39	7.40	7.26
$brainO_2$ (ml)	1.84	1.64	0.90	2.11	1.64
$heartO_2$ (ml)	0.28	0.14	0.00	0.28	0.03

HR: heart rate; LVSV: left ventricle stroke volume; CO: cardiac output; SASP: systemic artery systolic pressure; MAP: mean arterial pressure; CO: cardiac output; MPAP: mean pulmonary arterial pressure; CPP: coronary perfusion pressure; LVEF: left ventricle ejection fraction; SVR: systemic vascular resistance; PaO_2: arterial oxygen partial pressure; $PaCO_2$: arterial carbon dioxide partial pressure; $heartO_2$: myocardial tissue volume of oxygen; $brainO_2$: cerebral tissue volume of oxygen.

Table 9.7. Standard (Std-CPR) and optimized (Opt-CPR) CPR parameters following myocardial infarction (MI) and pulmonary embolism (PE).

Parameters	Std-CPR	MI Opt-CPR	PE Opt-CPR
CC rate (cpm)	120	112	84
F_{max} (N)	400	494	497
C_R (%)	50	68	69
Vf (breaths.min^{-1})	12	14	6
V_T (ml)	650	500	450
FiO_2 (%)	100	80	90
PEEP (cmH_2O)	0	0	0

CC rate: chest compression rate (compressions min^{-1}); F_{Max}: maximal chest compression force ; C_R: compression ratio; V_f: ventilatory frequency; V_T: tidal volume; FiO_2: fraction of inspired oxygen; PEEP: positive end expiratory pressure.

9.4 Discussion

In this study, standard and optimized CPR following MI and PE were modelled. Both precipitating aetiologies closely matched the expected model outputs presented in Tables 9.1 and 9.2 with the exception of the gas exchange model outputs during graded PE. During graded MI a steady deterioration of the left ventricle during MI1 and MI2 can be observed. Whilst the stroke volume is maintained during MI1, the increase of the left ventricle systolic volume (LVSV) and end diastolic pressure (LVEDP) and volume (LVEDV) and the concomitant decrease of the left ventricle systolic pressure (LVSP), mean arterial pressure (MAP) and ejection fraction (EF) indicate the dilation of the left ventricle as coping mechanism to the graded myocardial infarction a common remodelling immediately after MI [229].

Similarly, during graded PE a steady dilation of the right ventricle can be observed with the increased right ventricle end diastolic and systolic volumes and the reduction in stroke volume and ejection fraction. These findings in addition to the increased mean pulmonary arterial pressure are clear indications of acute PE in human subject [230].

In this pulmonary embolism model, the arterial partial pressure of oxygen (PaO_2) drops significantly lower than the expected model outputs whilst the arterial partial pressure of carbon dioxide ($PaCO_2$) does not increase as much most likely due to the clearance of CO_2 remaining relatively high as shown by the end tidal CO_2 not decreasing as much. These discrepancies might arise from the way pulmonary embolism was modelled by dramatically increasing the anatomical shunt from 20% to 50 % and the pulmonary artery resistance more than doubling from 0.6 mmHg s.ml^{-1} to 1.3 mmHg s.ml^{-1}.

The optimized CPR strategies identified by the genetic algorithm were different to each other and to the standard CPR. Both these strategies outperformed the standard CPR. Indeed, all the model outputs associated with ROSC (CPP, CO, brain O_2 and heart O_2) were considerably improved with optimized CPR. The strategies themselves had a similar increase in end compression force and compression ratio. However, the minute ventilation of both strategies was considerably different with the optimized MI CPR having a minute ventilation of 7 L.min^{-1} and the optimized PE CPR having a minute ventilation of 2.7 L.min^{-1}. The reduction of minute ventilation was counterbalanced with a higher fraction of inspired oxygen from PE compared to MI.

While the optimized CPR strategies demonstrated notable enhancements in all model outputs related to the return of spontaneous circulation (ROSC), it is crucial to acknowledge that the ISCM simulation suite is, at its core, a computational model of the cardiovascular and respiratory systems, carrying inherent limitations. This computational framework, while valuable, falls short of completely replicating the complexities observed in clinical scenarios of MI or PE cardiac arrests. Notably, certain biological processes integral to the ischemic response in MI, such as anaerobic respiration and lactate production, were not incorporated into the model. Furthermore, the impact of drug administration during CPR, particularly the use of antithrombotic agents commonly employed in clinical settings, could significantly deviate expected model outputs.

Recognizing these constraints is paramount for a nuanced interpretation, emphasizing the intricate challenge of translating computational model results to real-world clinical outcomes. The absence of specific biological processes and the potential influence of drug interventions during CPR underscore the need for caution in drawing direct parallels between computational simulations and the multifaceted reality of clinical scenarios.

9.5 Conclusion

In this study, I used a computational model of the cardiopulmonary systems to identify the optimized CPR strategies for subjects experiencing CA caused by MI or PE. The genetic algorithm utilized found distinct CPR strategies for each underlying cause. Both optimized CPR strategies involved an increase in end compression force (F_{MAX}) and compression ratio (C_R), along with a decrease in chest compression rate (CCrate), tidal volume (V_T), and fraction of inspired oxygen (FiO_2). The ventilatory frequency (V_f) was the only parameter increased for the optimized CPR following MI and decreased for the optimized CPR following PE compared to standard CPR. Additionally, all model outputs associated with return of spontaneous circulation were improved with the optimized CPR strategies compared to standard CPR. These findings suggest that tailored CPR strategies specific to the underlying cause are crucial for better patient outcomes.

Chapter 10. Effect of CPR strategies on cardiac output

10.1 Introduction

The need of ventilation during cardiac arrest (CA), to deliver oxygen and remove carbon dioxide from the blood, is generally accepted. Despite positive-pressure ventilation with pure oxygen being the gold standard in advance life support (ALS), its effectiveness, as well as the hemodynamic impact of positive end expiratory pressure (PEEP) and fraction of inspired oxygen (FiO_2) on cardiac output (CO) during cardiopulmonary resuscitation (CPR), are still poorly understood [64].

Furthermore, while numerous clinical trials have attempted to determine the optimal chest compression depth and rate for achieving ROSC and survival to hospital discharge, limited information is available on the impact of chest compression ratio. Moreover, due to the challenges in monitoring cardiac output during CPR, there is little evidence of the clear association between chest compression parameters, ventilation parameters, and CO during CPR.

Thus, the objective of this study is to investigate the effect of various CPR parameters - such as end compression force (F_{max}), chest compression rate (CC_{rate}), compression ratio (C_R), tidal volume (V_T), ventilatory frequency (V_f), FiO_2, and PEEP, on the CO during CPR in ten virtual healthy subjects.

10.2 Methods

The ICSM simulation suite was used, as described in Chapter 4 along with all the newly developed modules presented in Chapter 8. Ten virtual subjects were configured as in Chapter 8. After 5 minutes of SPV, CA was simulated for 5 minutes by setting the heart rate to 0, effectively forcing the heart to be in constant diastole. Additionally, the apnoea module was activated with obstructed upper airway. During CPR, the subjects were no longer

apnoeic, and the airway were no longer obstructed. When a parameter was varied, the remaining six parameters were maintained at their baseline values defined by the American Heart Association (AHA) guidelines: i.e. CC rate 100 compressions.min^{-1}, compression ratio 50%, CC depth 5 cm (associated with a Fmax of 400 N), V_T 650 ml, V_f 12 breaths.min^{-1}, FiO_2 100% and PEEP 0 cmH2O.

10.3 Results

Figure 10.1 shows the effect of chest compression parameters (F_{MAX}, $CC_{rate,}$ C_R) on CO in the ten subjects. The results are presented as the average and the maximum and minimum for the ten subjects. The end compression force has a nearly linear positive impact on the CO up until 400 N. Beyond 400 N, the positive impact of the end compression force persists, but it seems to have a diminishing effect, indicating a slowdown in the rate of increase. The chest compression rate has a nearly linear small negative impact on CO. Finally, the compression ratio peaks at around 50% before steadily decreasing to the initial value.

Figure 10.2 shows the effect of the ventilation parameters (V_T, V_f, PEEP and FiO_2) on CO. The results are presented as the average and the maximum and minimum for the ten subjects. The results indicate that the CO during CPR is the linearly negatively impacted by PEEP. Both the V_f and V_T reach a peak at around 8 breaths.min^{-1} and 450 ml respectively. Finally, the fraction of inspired oxygen does not have any impact on the CO.

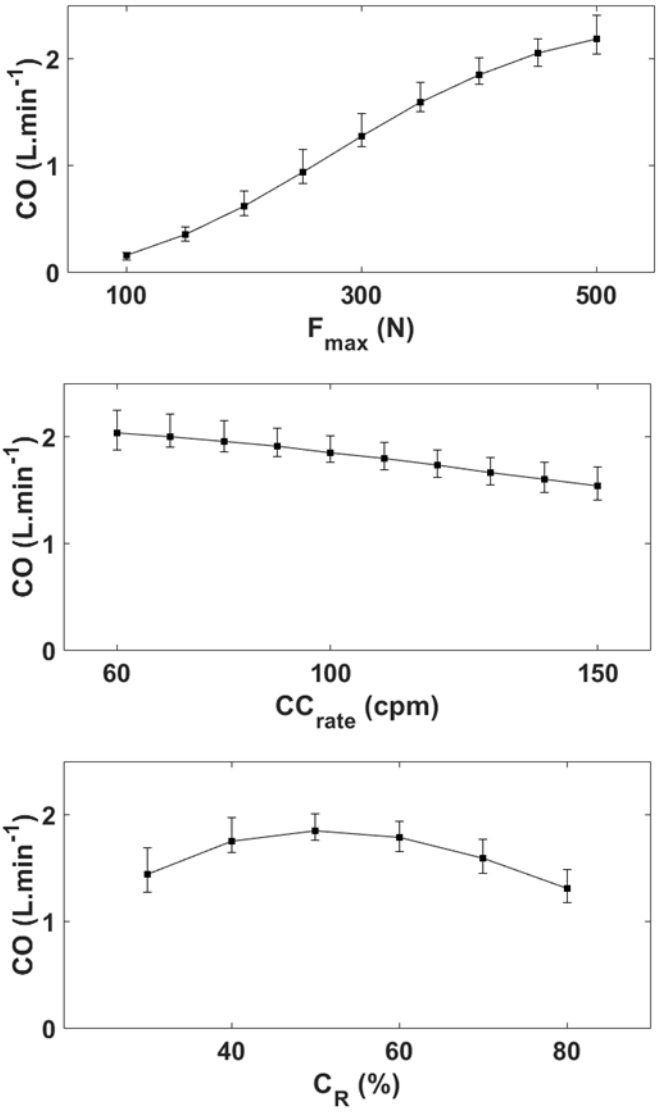

Figure 10.1 Effect of chest compression parameters on cardiac output (CO) during CPR for 10 virtual subjects. F_{max}: end compression force; CC_{rate}: chest compression rate; and C_R: compression ratio.

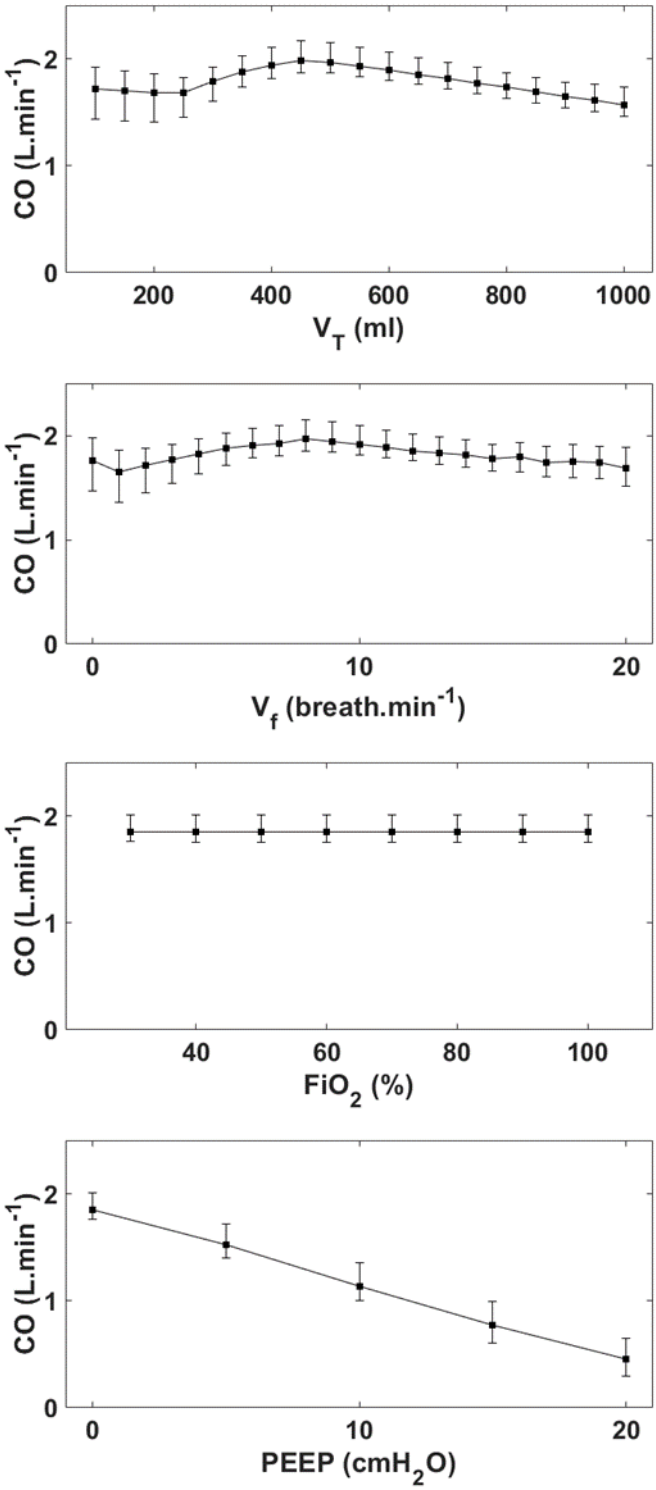

Figure 10.2 Effect of ventilation parameters on cardiac output (CO) during CPR for 10 virtual subjects. V_T: tidal volume; V_f: ventilatory frequency; FiO_2: fraction on inspired oxygen; and PEEP: positive end expiratory pressure.

10.4 Discussion

In this investigation, a quantitative exploration was conducted to discern the impact of CPR parameters on CO in a cohort of ten virtual subjects. The remarkably consistent effects of all parameters across these subjects are evident from the narrow error bars, emphasizing the uniformity in their influence on CO. Notably, the end compression force (F_{max}) emerged as the most influential parameter, eliciting a substantial increase in CO from 0.2 $L.min^{-1}$ to 2.2 $L.min^{-1}$. Following closely, positive end-expiratory pressure (PEEP) proved to be the second most impactful parameter, inducing a decrease in CO from 1.9 $L.min^{-1}$ to 0.4 $L.min^{-1}$. The compression ratio (CC_R) ranked as the third most influential parameter, peaking at around 50%, followed by compression rate (CC_{rate}). Surprisingly, variables such as ventilation frequency (V_f), tidal volume (V_T), and fraction of inspired oxygen (FiO_2) exhibited no significant impact on CO.

The dominance of Fmax and PEEP in affecting CO can be attributed to their profound influence on intrathoracic pressure. The noteworthy negative impact of PEEP on CO suggests that a consistently elevated intrathoracic pressure detrimentally affects venous return, subsequently affecting stroke volume and overall CO.

This study provides valuable insights into the nuanced effects of both CC and ventilation parameters on CO. While optimal tidal volume and ventilation frequency do exist, their impact on CO pales in comparison to the substantial influence exerted by CC depth and the presence of PEEP. Notably, compression ratio (C_R) emerges as the third most critical parameter in terms of its impact on CO—an aspect often overlooked and not previously investigated in animal or clinical studies. This underscores the importance of considering C_R in optimizing CPR strategies, offering a novel perspective on its potential significance in cardiac output modulation.

Chapter 11. Development of a personalised model of CPR

11.1 Introduction

Despite advances in CPR techniques and equipment, survival rates following cardiac arrest remain low. A significant factor contributing to the poor outcomes is the lack of individualized treatment options. Traditional CPR involves a standardized approach with limited ability to tailor treatment to the unique needs of each patient.

Personalized CPR, on the other hand, has emerged as a promising approach to improve outcomes in various medical fields, including CPR. By integrating patient-specific data, personalized medicine allows for a more targeted and effective treatment strategy. In the context of CPR, personalized medicine could help identify the optimal CPR strategy using real time haemodynamic and gas exchange data from patients.

Overall, the application of personalized CPR has the potential to significantly improve outcomes and survival rates. However, there is still much work to be done to develop and implement personalized approaches in the context of CPR. This study aims to validate the ICSM simulation suite newly integrated thoracic model against individual haemodynamic data during CPR. Once the validation successful, the model will be used to identify personalized CPR strategies retrospectively on each patient.

11.2 Methods

I used the ICSM simulation suite, as described in Chapter 4 along with all the module developments presented in Chapter 8. To validate the newly integrated thoracic model, I used the Berve *et al*. [231] intra-arterial blood pressures shown in Figures 11.1 and 11.2. In this study Berve *et al.* [231] recorded haemodynamic measures during 30 minutes of CPR in 126 patients.

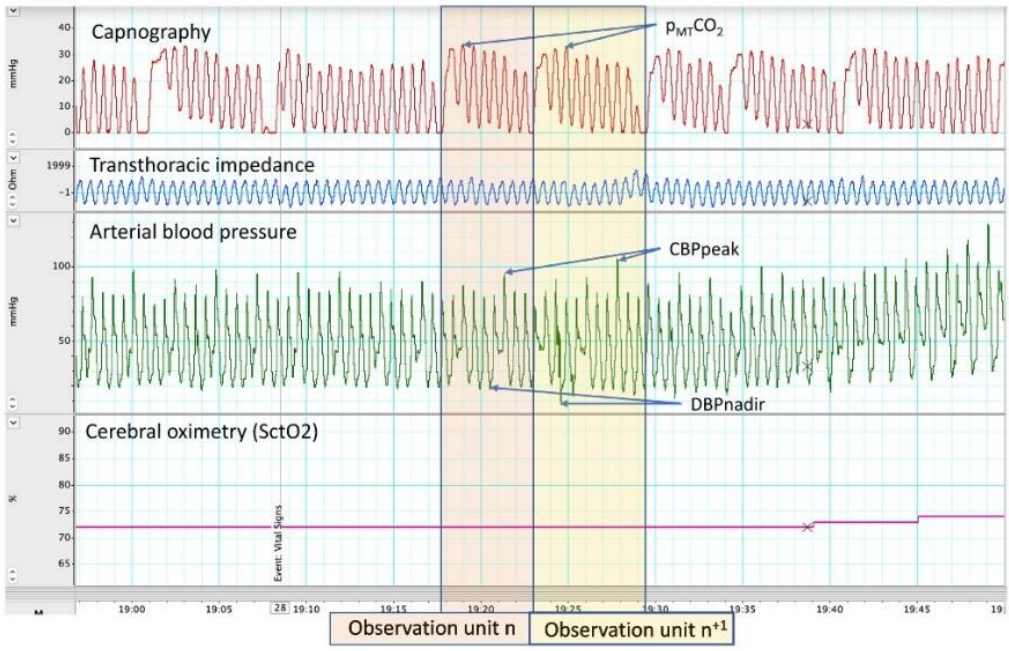

Figure 11.1 Time-aligned haemodynamic data from an Intervention group patient during 1 min of CPR presented in a MATLAB screenshot.

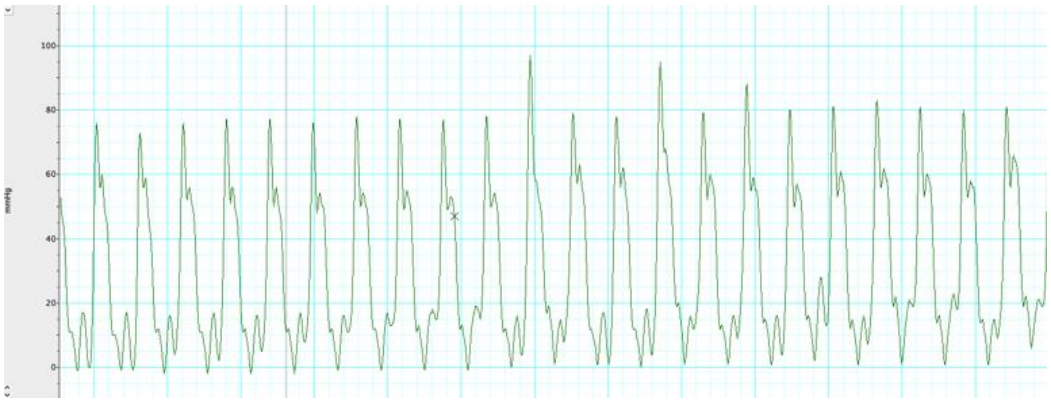

Figure 11.2 Femoral artery pressure during CPR [5]

The simulation of CPR followed as closely as possible the patient's scenario: 5 minutes of spontaneous ventilation, 5 minutes of untreated cardiac arrest, and standard mechanical CPR for one minute using the LUCAS 3 chest compression device. To accurately replicate the chest compressions from LUCAS 3, the chest compression depth followed the ones advertised on the LUCAS 3 website as shown in Figure 11.3.

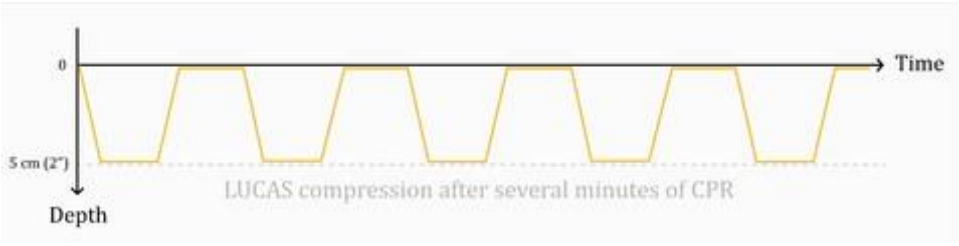

Figure 11.3 LUCAS 3 compression depth waveform

The aim of the optimization algorithm (Figure 11.4) was to find the sets of cardiovascular parameters (i.e., resistances, capacitances, inductances) that minimize the cost function defined as the coefficient of variation of the root mean squared error (RMSE) between model-simulated and literature data. The RMSE is calculated as:

Equation 11.1

$$COST = RMSE = \frac{\sqrt{\frac{\sum_{i=1}^{n}(\hat{y}_i - y_i)^2}{n}}}{\bar{y}}$$

where y represent the literature data variable (i.e., femoral arterial pressure), $\bar{y}$ is its mean value over the entire duration, y_i represents the generic i[th] sample of the literature data waveform, $\hat{y}_i$ is the model counterpart, and n is the number of samples. The literature data sare shown in Figure 10.2; these were obtained from the recording of the femoral artery pressure during CPR [231].

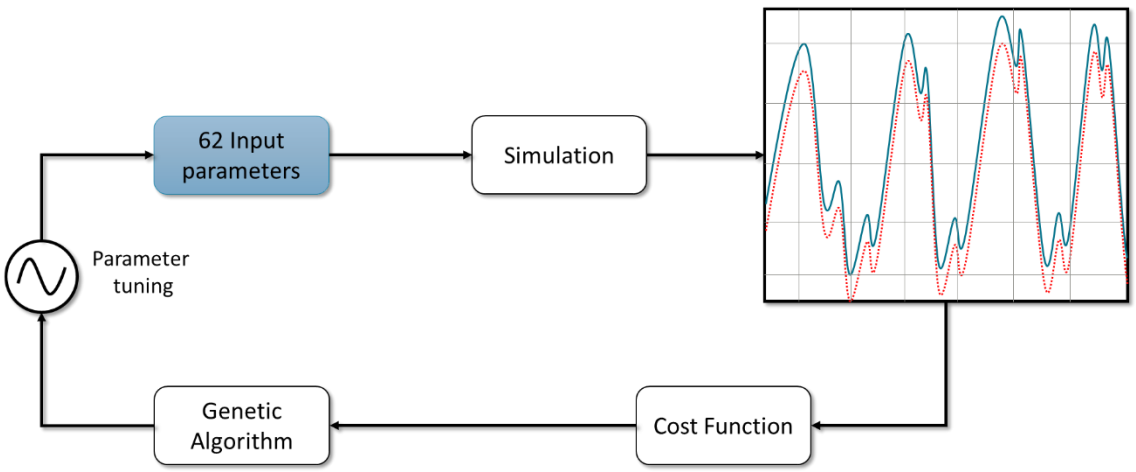

Figure 11.4 Schematic representation of the global optimization algorithm

11.3 Results

After 50 generations, the best cost function obtained was 0.31. The results, shown in Figure 11.5, have been obtained by matching the model output (i.e. pressure in the systemic artery) to the continuous femoral arterial pressure data obtained from Berve *et al*. [231] shown in the Figure 11.2.

The list of input parameters, their baseline values, maximum and minimum values as well as the obtained results after running the global optimization algorithm can be found in Appendix 2.

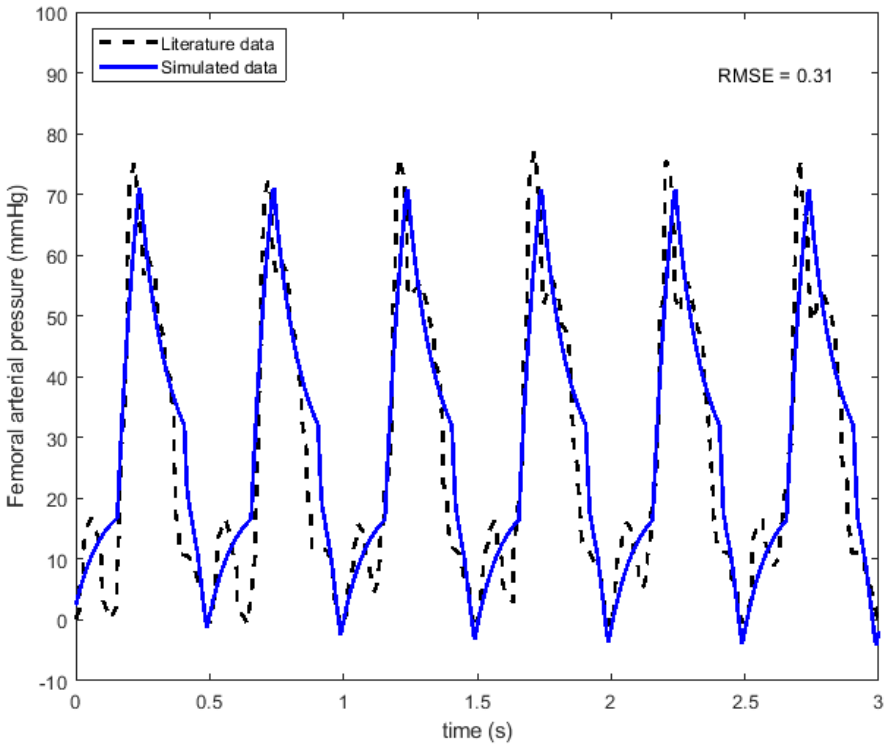

Figure 11.5 Simulated data vs. Literature data after the model was tuned with the GA.

The simulated data closely corresponds to the arterial pressure compression phase recording, apart from the missing "pre-ejection wave" or "dicrotic notch". The pre-ejection wave is associated with the dynamics of blood flow during the compression and decompression phases of CPR mainly due to arterial compliance (the arterial walls rebound), closure of the aortic valve, intrathoracic pressure changes, or CPR artifacts. The root-mean-square error (RMSE) of 0.31 demonstrates the model's accuracy.

11.4 Discussion

There is a significant scarcity in the literature of individual haemodynamic datasets from patients undergoing cardiac arrest and CPR. Consequently, many lumped mathematical models have been developed to simulate CPR in virtual subjects. However, to the best of my knowledge, this is the first instance of a lumped mathematical model being utilized to replicate individual haemodynamic recordings of a patient during CPR. The model's accuracy is demonstrated by its achievement of an RMSE of 0.31.

Validation of the ICSM simulation suite thoracic model against individualized haemodynamic recordings has enabled the creation of a virtual subject. The access to Berve *et al*. [231] clinical trial haemodynamic records would enable me to create a bank of virtual subjects. Similarly to Chapter 8, the optimal personalised CPR strategy could be identified for each subject.

11.5 Conclusion

The ICSM simulation suite thoracic model was validated in this study using individual haemodynamic recordings of a patient undergoing CPR. The model accuracy was demonstrated by a root mean square error of 0.31. With additional access to Berve *et al*. [231] the clinical data, I could test the ICSM simulation suite against multiple patients' recordings and retrospectively identify each subject's optimal CPR strategy.

Chapter 12. Cardiovascular and respiratory control mechanism

12.1 Introduction

Despite significant advances in the field, the survival rate following cardiac arrest remains low. This is partly due to the limited understanding of the underlying mechanisms that control cardiovascular function during cardiac arrest and CPR.

One critical aspect of cardiovascular control is the regulation of blood pressure and blood flow to vital organs. This regulation is achieved through complex mechanisms, including the baroreflex and chemoreflex. The baroreflex is a negative feedback system that regulates blood pressure by adjusting the heart rate and peripheral resistance in response to changes in blood pressure. The chemoreflex, on the other hand, regulates blood pressure and blood flow in response to changes in oxygen and carbon dioxide levels in the body [232].

During cardiac arrest and CPR, these control mechanisms are disrupted, leading to changes in blood pressure, heart rate, and blood flow. The disruption can be exacerbated by the use of vasoactive medications and other interventions used during CPR. The resulting changes in blood pressure and blood flow can have significant effects on the vital organs.

Therefore, understanding the role of cardiovascular control mechanisms such as the baroreflex and chemoreflex during cardiac arrest and CPR is crucial in developing new treatment strategies to improve outcomes. This chapter aims to integrate and adapt the extensive cardiovascular and respiratory control mechanisms developed by Ursino, Magosso, Albanese and Cheng [211, 216, 233-236] to ICSM simulation suite.

12.2 Methods

The ICSM simulation suite was used, as described at length in Chapter 4. Albanese *et al.* [211] model was developed on MATLAB Simulink whilst the ICSM has been developed on

MATLAB. Therefore, to solve the following ordinary differential equations, the 4th order Runge Kutta method is used as:

Equation 12.1

$$\frac{d}{d\mathrm{t}}x = f(t, x)$$

$$k_1 = f(t_n, x_n)$$

$$k_2 = f\left(t_n + \frac{h}{2}, x_t + \frac{h}{2} \cdot k_1\right)$$

$$k_3 = f\left(t_n + \frac{h}{2}, x_t + \frac{h}{2} \cdot k_2\right)$$

$$k_4 = f(t_n + h, x_t + h \cdot k_3)$$

$$x_{t+1} = x_t + \frac{h}{6}(k_1 + 2 \cdot k_2 + 2 \cdot k_3 + k_4)$$

where x is the parameter to solve, and h is the time step, varying from 0.005 s and 1e-04 s. In order to solve the ODE a cardiovascular "while" loop was created to allow a smaller time step (h2 = 1e-04 s). The pressure, flow and volume of the CVS compartments are calculated in the loop along with the CVS control mechanism parameters. All the following equations and input parameters presented in this chapter were directly obtained from Ursino, Magosso, Albanese and Cheng [211, 216, 233-236].

12.2.1 Cardiovascular control mechanisms

The following description of the cardiovascular control mechanism was extracted from Albanese *et al.* [211].

“The cardiovascular control model includes the main short-term regulation mechanisms (time duration <2 min) that act on the cardiovascular function in response to acute hemodynamic and blood gas composition perturbations. The model is based on the previous work of Ursino, Magosso and Cheng [211, 216, 233-236] and a high-level schematic block diagram highlighting its input-output interconnections is shown in Figure 12.1. Briefly, the

model includes the action of carotid sinus baroreceptors, peripheral chemoreceptors, lung stretch receptors, autoregulation mechanisms, and a CNS directly mediated ischemic response. The afferent information coming from baroreceptors, chemoreceptors, and lung stretch receptors is first processed at the level of the autonomic nervous system (ANS), which in turn, modulates sympathetic and parasympathetic activities in the neural efferent pathways. Sympathetic and parasympathetic neural fibres then control the cardiovascular system via modifications of heart period (HP), maximum ventricular contractility ($E_{\mathrm{max,lv}}$ and $E_{\mathrm{max,rv}}$), resistances of the systemic peripheral beds (R_{jp}) and systemic venous unstressed volumes ($V_{\mathrm{u,jp}}$). The HP is assumed to depend on a balance between sympathetic and parasympathetic activities, whereas all other effectors are assumed under the control of sympathetic fibres only. Circulation in the most vital vascular beds, i.e., the coronary and brain compartments, is assumed to be independent of the ANS modulation, only affected by local autoregulation mechanisms. Finally, the effect of a CNS ischemic response is modelled by assuming that PaO_2 and $PaCO_2$ can alter the sensitivity of the efferent sympathetic fibres to the stimuli coming from the afferent receptors (baroreceptors, chemoreceptors, and lung stretch receptors). The mathematical equations governing the model have been taken from Ursino and Magosso [216, 234] where a detailed explanation can be found. However, the equations pertaining to the afferent peripheral chemoreceptor's pathway (see Figure 12.1) have been replaced with a more detailed model proposed in Ursino and Magosso [235] also used in the spontaneous ventilation respiratory control model" [211].

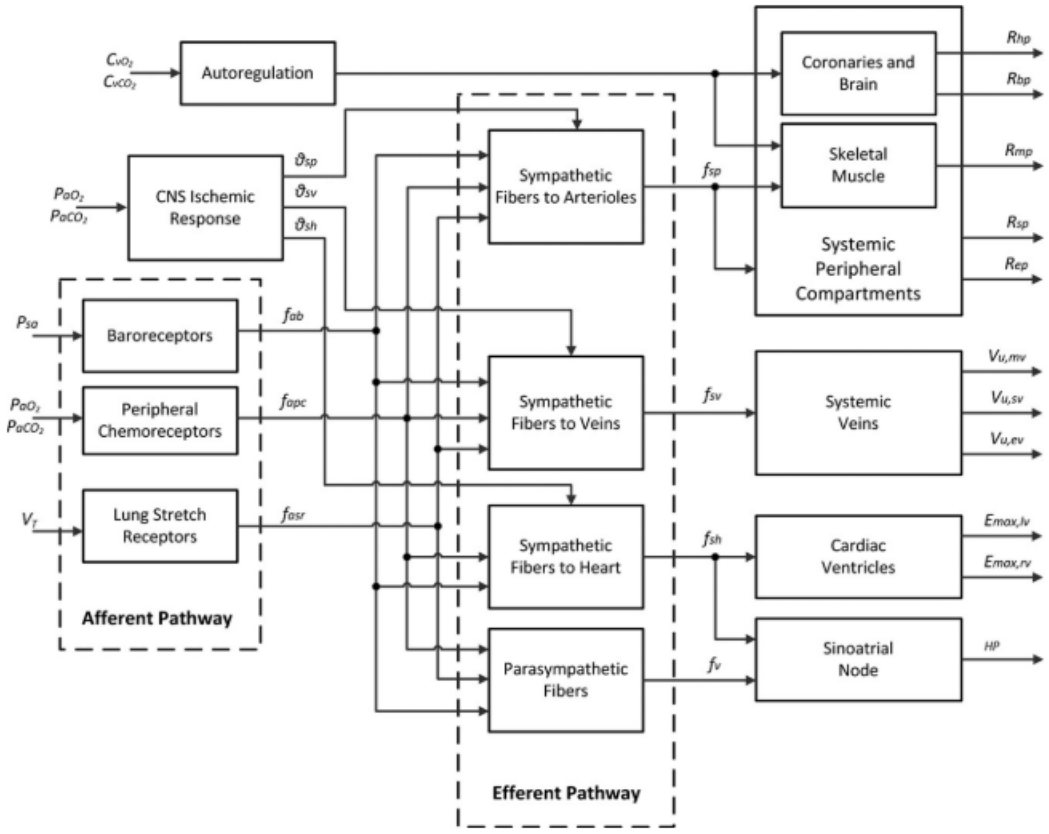

Figure 12.1 Schematic block diagram of the cardiovascular control model. Psa, systemic arterial pressure; VT, tidal volume; fab, $fapc$, and $fasr$, afferent firing frequency of baroreceptors, peripheral chemoreceptors, and lung stretch receptors respectively; θsp, θsv, and θsh, offset terms representing the effect of the CNS ischemic response on the sympathetic fibers directed to peripheral circulation, veins, and heart, respectively; fsp, fsv, and fsh, activity in the efferent sympathetic fibres directed to the peripheral circulation, the veins, and the heart, respectively; f_v, activity in the vagal efferent fibres; Rhp, Rbp, Rmp, Rsp, and Rep, systemic peripheral resistance in coronary, brain, skeletal muscle, splanchnic, and extra splanchnic vascular beds, respectively; Vu,mv,Vu,sv, and Vu,ev, venous unstressed volume in skeletal muscle, splanchnic, and extrasplanchnic vascular bed, respectively; $Emax,lv$ and $Emax,rv$, end-systolic elastance of the left and right ventricle, respectively; HP, heart period.[211]

Afferent neural pathway

The parameters used for the afferent neural pathway are presented in Table 12. 1.

Baroreflex

The baroreflex takes as an input the aortic pressure P_{sa} and calculates the afferent firing rate of the baroreceptor f_{ab}.

Equation 12.2

$$\frac{d\tilde{P}}{dt} = P_{sa} + \tau_{z,b} \cdot \frac{dP_{sa}}{dt} - \frac{\tilde{P}}{\tau_{p,b}}$$

Equation 12.3

$$f_{ab} = \frac{f_{ab,min} + f_{ab,max} \cdot e^{\left(\frac{\tilde{P}-P_n}{k_{ab}}\right)}}{1 + e^{\left(\frac{\tilde{P}-P_n}{k_{ab}}\right)}}$$

Peripheral chemoreflex

The peripheral chemoreceptor takes for input the arterial oxygen saturation Sa_{O_2}, the arterial CO_2 concentration and its time derivative Ca_{CO_2} and $\frac{d}{dt}Ca_{CO_2}$ and calculate the afferent firing rate of the peripheral chemoreceptor.

Equation 12.4

$$x_{O_2} = Ax\left(1 - Sa_{O_2}\right) + Bx$$

Equation 12.5

$$\varphi_{O_2} = K_{O_2}\left[1 - e^{\left(\frac{-x_{O_2}}{K_{O_2}}\right)}\right]$$

Equation 12.6

$$\varphi_{CO_2} = K_{CO_2}\left(Ca_{CO_2} - C_t\right)$$

Equation 12.7

$$\Phi = \varphi_{O_2} \cdot \varphi_{CO_2}$$

Equation 12.8

$$f_{cstat} = \begin{cases} K_{stat}\left[1 - e^{\left(\frac{-\Phi}{K_{stat}}\right)}\right] & Ca_{CO_2} > C_t \\ 0 & Ca_{CO_2} < C_t \end{cases}$$

Equation 12.9

$$\frac{d}{dt}\varphi_{CO_2dyn} = \frac{\tau_{zh}\frac{d}{dt}Ca_{CO_2} - \varphi_{CO_2dyn}}{\tau_{ph}}$$

Equation 12.10

$$\bar{\varphi}_c = K_{stat}\left[1 - e^{\left(\frac{-\Phi}{K_{stat}}\right)}\right] + K_{dyn}\left[1 - e^{\left(\frac{-\varphi_{CO_2dyn}}{K_{dyn}}\right)}\right]$$

Equation 12.11

$$\frac{d}{dt}\varphi_c = \frac{\bar{\varphi}_c - \varphi_c}{\tau_{pl}}$$

Equation 12.12

$$f_{ac} = \begin{cases}\varphi_c & \varphi_c > 0 \\ 0 & \varphi_c < 0\end{cases}$$

Lung stretch receptor

The lung stretch receptor takes for input the tidal volume VT and calculate the afferent firing rate of the lung stretch receptor.

Equation 12.13

$$\varphi_{ap} = G_{ap} \cdot V_T$$

Equation 12.14

$$\frac{df_{ap}}{dt} = \frac{\varphi_{ap} - f_{ap}}{\tau_p}$$

Table 12.1 Basal values of parameters for afferent neural pathway. [211, 233, 235]

	Baroreflex	
$f_{ab,min}$= 2.52 spikes.s^{-1}	τ_{pb} = 2.076 s	P_n=92 mmHg
$f_{ab,max}$= 47.78 spikes.s^{-1}	τ_{zb}=6.37 s	k_{ab}=11.76 mmHg
	Peripheral chemoreceptor	
τ_{ph}=3.5 s	Ax=600	K_{O_2}=200
τ_{zh}=600 s	Bx=10.18	K_{CO_2}=1 s^{-1}
τ_{pl}=3.5 s	C_t=0.36 L.L-1	K_{dyn}=45 s^{-1}
		K_{stat}=20 s^{-1}
	Lung stretch receptor	
G_{ap} = 11.76 l^{-1}.spikes.s^{-1}		τ_p=2 s

See (211, 233, 235) for explanation of symbols.

Central nervous system ischemic response

The parameters used for the CNS ischemic response are presented in Table 12. 2. The central nervous system ischemic response takes for input the arterial partial pressure of O_2 and CO_2 (Pa_{O_2}, Pa_{CO_2}) and calculates θ_{sp}, θ_{sv} and θ_{sh} , the offset terms representing the effect of the CNS ischemic response on the sympathetic fibres directed to peripheral circulation, veins, and heart, respectively.

Equation 12.15

$$\omega_{sj} = \frac{\chi_{sj}}{1 - e^{\left(\frac{Pa_{O_2} - \bar{P}_{O_2 sj}}{k_{isc,sj}}\right)}} \qquad j = p, v, h$$

Equation 12.16

$$\frac{d\Delta\theta_{O2,sj}}{dt} = \frac{\omega_{sj} - \Delta\theta_{O2,sj}}{\tau_{isc}} \qquad j = p, v, h$$

Equation 12.17

$$\frac{d\Delta\theta_{CO2,sj}}{dt} = \frac{g_{ccsj}\left(Pa_{CO2} - Pa_{CO2,n}\right) - \Delta\theta_{CO2,sj}}{\tau_{cc}} \qquad j = p, v, h$$

Equation 12.18

$$\theta_{sj} = \theta_{sjn} - \Delta\theta_{O2,sj} - \Delta\theta_{CO2,sj} \qquad j = p, v, h$$

Table 12.2 Basal values of parameters for central nervous system ischemic response.[236]

CNS ischemic response		
χ_{sp}=6 s^{-1}	$\tilde{P}_{O_2sp}$=30 mmHg	$k_{isc,sp}$=2 mmHg
χ_{sv}=6 s^{-1}	$\tilde{P}_{O_2sv}$=30 mmHg	$k_{isc,sv}$=2 mmHg
χ_{sh}=53 s^{-1}	$\tilde{P}_{O_2sh}$=45 mmHg	$k_{isc,sh}$=6 mmHg
θ_{spn}=13.32 s^{-1}	g_{ccsp}=1.5 $mmHg^{-1}.s^{-1}$	τ_{cc}=20 s
θ_{svn}=13.32 s^{-1}	g_{ccsv}=0 $mmHg^{-1}.s^{-1}$	τ_{isc}=30 s
θ_{shn}=3.6 s^{-1}	g_{ccsh}=1 $mmHg^{-1}.s^{-1}$	Pa_{CO2n}=40 mmHg

See (236) for explanation of symbols.

Efferent pathway

The parameters used for the efferent pathway are presented in Table 12. 3. The efferent neural pathway is defined by the following equation:

Equation 12.19

$$f_{sj} = \begin{cases} f_{es,\infty} + (f_{es,0} - f_{es,\infty}) \cdot e^{\left(k_{es}\left(W_{b,sj}\cdot f_{ab} + W_{c,sj}\cdot f_{ac} + W_{p,sj}\cdot f_{ap} - \theta_{sj}\right)\right)} & f_{sj} < f_{es,max} \\ f_{es,max} & f_{sj} \geq f_{es,max} \end{cases}$$

$$j = p, v, h$$

The efferent vagal pathway is defined as,

Equation 12.20

$$f_v = \frac{f_{ev,0} + f_{ev,\infty} \cdot e^{\left(\frac{f_{ab}-f_{ab,0}}{k_{ev}}\right)}}{1 + e^{\left(\frac{f_{ab}-f_{ab,0}}{k_{ev}}\right)}} + W_{c,v} \cdot f_{ac} - W_{p,v} \cdot f_{ap} - \theta_v$$

Table 12.3 Basal values of parameters for efferent pathway. [216,235]

Efferent sympathetic pathway		
$W_{b,sp}$=-1.1375	$W_{c,sp}$=1.716	$W_{p,sp}$=-0.3997
$W_{b,sv}$=-1.0806	$W_{c,sv}$=1.716	$W_{p,sp}$=-0.2907
$W_{b,sh}$=-1.75	$W_{c,sh}$=1	$W_{p,sh}$=0
$f_{es,\infty}$=2.10 spikes.s^{-1}	$f_{es,min}$=2.66 spikes.s^{-1}	k_{es}=0.0675 s
$f_{es,0}$=16.11 spikes.s^{-1}	$f_{es,max}$=60 spikes.s^{-1}	
Efferent vagal pathway		
$f_{ev,\infty}$=6.3 spikes.s^{-1}	$W_{p,v}$=0.103	θ_v=-0.68 spikes.s^{-1}
$f_{ev,0}$=3.2 spikes.s^{-1}	$W_{c,v}$=0.2	k_{ev}=7.06 spikes.s^{-1}
$f_{ab,0}$=25 spikes.s^{-1}		

See (216, 235) for explanation of symbols.

Reflex regulation

The parameters used for the reflex regulation are presented in Table 12. 4. The effect of the activity in the efferent sympathetic fibres directed to the peripheral circulation (f_{sp}) is calculated below where θ denotes the peripheral resistances (R_{sp}, R_{sv}, R_{sh}):

Equation 12.21

$$\sigma_\theta = \begin{cases} G_\theta \cdot \ln\left(f_{sp}(t - D_\theta) - f_{es,min} + 1\right) & f_{sp} \geq f_{es,min} \\ 0 & f_{sp} < f_{es,min} \end{cases}$$

The effect of the activity in the efferent sympathetic fibres directed to the veins (f_{sv}) is calculated below where θ denotes the venous unstressed volume ($V_{u,mv}$, $V_{u,sv}$, $V_{u,ev}$):

Equation 12.22

$$\sigma_\theta = \begin{cases} G_\theta \cdot \ln\left(f_{sv}(t - D_\theta) - f_{es,min} + 1\right) & f_{sv} \geq f_{es,min} \\ 0 & f_{sv} < f_{es,min} \end{cases}$$

The effect of the activity in the efferent sympathetic fibres directed to the heart (f_{sh}) is calculated below where θ denotes the cardiac elastances ($E_{max,rv}$ and $E_{max,lv}$):

Equation 12.23

$$\sigma_\theta = \begin{cases} G_\theta \cdot \ln\left(f_{sh}(t - D_\theta) - f_{es,min} + 1\right) & f_{sv} \geq f_{es,min} \\ 0 & f_{sv} < f_{es,min} \end{cases}$$

Equation 12.24

$$\Delta\theta = \sigma_\theta - \tau_\theta \cdot \frac{d\Delta\theta}{dt}$$

Equation 12.25

$$\theta = \Delta\theta + \theta_0$$

The heart period T is controlled by the activity in the vagal efferent fibres (f_v) and the activity in the efferent sympathetic fibres directed to the heart (f_{sh}).

Equation 12.26

$$\sigma_{T,s} = \begin{cases} G_{T,s} \cdot \ln\left(f_{sh}\left(t - D_{T,s}\right) - f_{es,min} + 1\right) & f_{sh} \geq f_{es,min} \\ 0 & f_{sh} < f_{es,min} \end{cases}$$

Equation 12.27

$$\Delta T, s = \sigma_{T,s} - \tau_{T,s} \cdot \frac{d\Delta T, s}{dt}$$

Equation 12.28

$$\sigma_{T,v} = G_{T,v} \cdot f_v\left(t - D_{T,v}\right)$$

Equation 12.29

$$\Delta T, v = \sigma_{T,v} - \tau_{T,v} \cdot \frac{d\Delta T, v}{dt}$$

Equation 12.30

$$T = \Delta T, s + \Delta T, v + T_0$$

However, with reference to skeletal muscle does not furnish the true value of peripheral resistance since skeletal muscle is further controlled by local O_2 mechanisms. Hence, for skeletal muscle only, I adopted a different symbol (i.e., $R_{mp,n}$) to remind us that the true value of R_{mp} is obtained in the model only after inclusion of the O_2 effect.

Table 12.4 Basal values of parameters for reflex regulation.[233]

Reflex regulation		
G_{Emaxlv}=0.475 mmHg.ml^{-1}.v^{-1}	τ_{Emaxlv}=8 s	D_{Emaxlv}=2 s
G_{Emaxrv}=0.282 mmHg.ml^{-1}.v^{-1}	τ_{Emaxrv}=8 s	D_{Emaxrv}=2 s
G_{Rsp}=0.695 mmHg.ml^{-1}.v^{-1}	τ_{Rsp}=6 s	D_{Rsp}=2 s
G_{Rep}=1.94 mmHg.ml^{-1}.v^{-1}	τ_{Rep}=6 s	D_{Rep}=2 s
G_{Rmp}=2.47 mmHg.ml^{-1}.v^{-1}	τ_{Rmp}=6 s	D_{Rmp}=2 s
G_{Vusv}=-265.4 ml.v^{-1}	τ_{Vusv}=20 s	D_{Vusv}=5 s
G_{Vuev}=-74.21 ml.v^{-1}	τ_{Vuev}=20 s	D_{Vuev}=5 s
G_{Vumv}=-58.29 ml.v^{-1}	τ_{Vumv}=20 s	D_{Vumv}=5 s
G_{Ts}=-0.13 s.v^{-1}	τ_{Ts}=2 s	D_{Ts}=2 s
G_{Tv}=0.09 s.v^{-1}	τ_{Tv}=1.5 s	D_{Tv}=0.2 s
R_{sp0}=2.49 mmHg.s.ml^{-1}	V_{usv0}=1435.4 ml	E_{maxlv0}=2.5 mmHg.ml^{-1}
R_{ep0}=1.655 mmHg.s.ml^{-1}	V_{uev0}=640.73 ml	E_{maxrv0}=1 mmHg.ml^{-1}
R_{mp0}=2.106 mmHg.s.ml^{-1}	V_{umv0}=503.26 ml	T_0=0.58 s

See (233) for explanation of symbols.

Autoregulation (local blood flow control)

The parameters used for the autoregulation are presented in Table 12. 5. The local metabolic control of cerebral blood (R_{bp}) flow is governed by the following equations:

Equation 12.31

$$\Phi_b = \frac{A + \frac{B}{1 + C \cdot e^{(D \cdot \log(Pa_{CO2}))}}}{A + \frac{B}{1 + C \cdot e^{(D \cdot \log(Pa_{CO2,n}))}}} - 1$$

Equation 12.32

$$x_{b,CO2} = \Phi_b - \tau_{CO2} \cdot \frac{dx_{b,CO2}}{dt}$$

Equation 12.33

$$x_{b,O2} = -\left(g_{b,O2} \cdot \left(C_{vb,O2} - C_{vb,O2n}\right) + \tau_{O2} \cdot \frac{dx_{b,O2}}{dt}\right)$$

Equation 12.34

$$G_{bp} = G_{bpn} \cdot \left(1 + x_{b,CO2}\right)$$

Equation 12.35

$$R_{bp} = \frac{1}{G_{bp}}$$

The local control of coronary (R_{hp}) and muscular (R_{mp}) peripheral resistances is governed by the following equations:

Equation 12.36

$$\Phi_j = \frac{1 - e^{\left(\frac{Pa_{CO2} - Pa_{CO2,n}}{k_{j,CO2}}\right)}}{1 + e^{\left(\frac{Pa_{CO2} - Pa_{CO2,n}}{k_{j,CO2}}\right)}} \qquad j = h, m$$

Equation 12.37

$$x_{j,CO2} = \Phi_j - \tau_{CO2} \cdot \frac{dx_{j,CO2}}{dt} \qquad j = h, m$$

Equation 12.38

$$x_{j,O2} = -\left(g_{j,O2} \cdot \left(C_{vj,O2} - C_{vj,O2n}\right) + \tau_{O2} \cdot \frac{dx_{j,O2}}{dt}\right) \qquad j = h, m$$

Equation 12.39

$$R_{jp} = R_{jpn} \cdot \frac{(1 + x_{j,CO2})}{(1 + x_{j,O2})} \qquad j = h, m$$

Table 12.5 Basal values of parameters for autoregulation. [211,236]

	Local regulation	
A=20.9	g_{bO2}=140	G_{bpn}= 0.15 ml.mmHg^{-1}.s^{-1}
B=92.8	g_{hO2}=490	R_{hpn}=19.71 mmHg.s.ml^{-1}
C=10570	g_{mO2}=420	R_{mpn}=4.48 mmHg.s.ml^{-1}
D=-5.251	$C_{vb,O2n}$=0.14	$k_{h,CO2}$=11.11 mmHg
τ_{O2}=10 s	$C_{vh,O2n}$=0.11	$k_{m,CO2}$=142.8 mmHg
τ_{CO2}=20 s	$C_{vm,O2n}$=0.155	

See (211, 236) for explanation of symbols.

12.2.2 Respiratory control mechanism

The following description of the respiratory control mechanism was extracted from Albanese *et al.* [211].

“The respiratory control model includes both the peripheral and central chemoreceptors. A schematic block diagram of the model is shown in Figure 12.2. The central chemoreceptors are assumed to be sensitive to $PaCO_2$, whereas the peripheral chemoreceptors are assumed to be sensitive to both PaO_2 and $PaCO_2$. The central and peripheral chemoreceptors directly affect the respiratory rate RR and the amplitude of the respiratory muscle pressure generator, $P_{mus,min}$.” [211]. The spontaneous respiratory control model has been added to help the validation of the model.

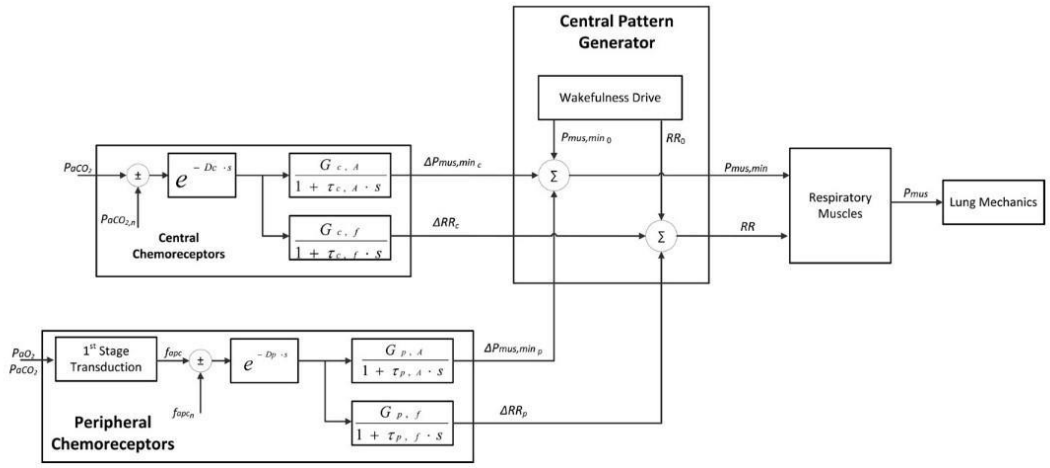

Figure 12.2 Schematic block diagram of the respiratory control model. $P_{mus,min0}$ and RR_0 , basal values of respiratory muscle pressure amplitude and respiratory rate. $\Delta P_{mus,minC}$ and ΔRR_C , variations in respiratory rate and respiratory muscle pressure amplitude induced by the central chemoreceptors; $\Delta P_{mus,minP}$ and ΔRR_P, variations in respiratory rate and respiratory muscle pressure amplitude induced by the peripheral chemoreceptors [211].

New spontaneous ventilation model

The spontaneous ventilation is defined by a square wave, controlled by the $P_{mus,min}$, respiratory muscle pressure amplitude and by RR the respiratory rate. The respiratory muscle pressure is calculated as:

Equation 12.40

$$P_{mus}(t) = \begin{cases} \dfrac{P_{mus,min}\left(T_{resp} - TI\right)}{TE} & 0 \le t < TI \\ 0 & TI \le t \le T_{resp} \end{cases}$$

Where $P_{mus,min}$ is the minimum end-inspiratory pressure value representing the amplitude of the inspiratory efforts, T_{resp} is the respiratory period, TI and TE are the duration of the inspiratory and expiratory phases and are considered fixed fractions of T_{resp}:

Equation 12.41

$$T_{resp} = \frac{60}{RR} = TI + TE$$

Equation 12.42

$$TI = TE \cdot IE_{ratio}$$

Respiratory control model

The respiratory control model affects the respiratory system via modifications in the amplitude ($P_{mus,min}$) and the frequency (RR) of the P_{mus} according to:

Equation 12.43

$$P_{mus,min} = P_{mus,min0} + \Delta P_{mus,minC} + \Delta P_{mus,minP}$$

Equation 12.44

$$RR = RR_0 + \Delta RR_C + \Delta RR_P$$

Where $P_{mus,min0}$ is the basal value of the respiratory muscle pressure amplitude, RR_0 is the basal value of the respiratory muscle pressure frequency, ΔRR_C and $\Delta P_{mus,minC}$ are the variations in respiratory rate and respiratory muscle pressure amplitude induced by the central chemoreceptors, and ΔRR_P and $\Delta P_{mus,minP}$ are the variations in respiratory rate and respiratory muscle pressure amplitude induced by the peripheral chemoreceptors. All the parameters used in the respiratory control model are in Table 12.6. Two parameters were calibrated to achieve stabilisation of the simulations,$G_{p,A}$ was changed from 1310 to 1.310, similarly $G_{c,A}$ was changed from 850 to 0.850.

Table 12.6 Parameters of the respiratory control model [211].

Peripheral Chemoreceptors		
D_p = 7 s	$G_{p,A}$ = 1.310 cmH2O.v^{-1}	$G_{p,f}$ = 0.8735 breaths.min^{-1}.v^{-1}
$\tau_{p,A}$ = 83 s	$\tau_{p,f}$ = 147.78	$f_{apc,n}$ = 3.7 spikes.s^{-1}
Central Chemoreceptors		
D_c = 8 s	$G_{c,A}$ = 0.850 cmH2O.mmHg^{-1}	$G_{c,f}$ = 0.9 breaths.min^{-1}.v^{-1}
$\tau_{c,A}$ = 105 s	$\tau_{c,f}$ = 400 s	PaCO2,n = 40 mmHg

See (211) for explanation of symbols.

The central chemoreceptor mechanism is given by:

Equation 12.45

$$\frac{d\Delta P_{mus,minC}}{dt} = \frac{-\Delta P_{mus,minC} + G_{c,A} \cdot u_c}{\tau_{c,A}}$$

Equation 12.46

$$\frac{d\Delta RR_C}{dt} = \frac{-\Delta RR_C + G_{c,f} \cdot u_c}{\tau_{c,f}}$$

Equation 12.47

$$u_c(t) = Pa_{CO2}(t - D_c) - Pa_{CO2,n}$$

The peripheral chemoreceptor mechanism is given by:

Equation 12.48

$$\frac{d\Delta P_{mus,minP}}{dt} = \frac{-\Delta P_{mus,minP} + G_{p,A} \cdot u_p}{\tau_{p,A}}$$

Equation 12.49

$$\frac{d\Delta RR_p}{dt} = \frac{-\Delta RR_p + G_{p,f} \cdot u_p}{\tau_{p,f}}$$

Equation 12.50

$$u_p(t) = f_{ac}(t - D_p) - f_{ac,n}$$

12.2.3 Protocol

Following integration of the control mechanisms, a virtual healthy subject was configured according to our previous study [219]. To assess the validity of these control mechanisms under normal room air conditions, the virtual subject was spontaneously breathing air containing 21% oxygen and 0.03% carbon dioxide for a period of 5 minutes.

Similarly to Cheng et al. [236] I have used a two relevant studies to validate the control mechanisms [237, 238]. In these studies, groups of healthy volunteers were subjected to hypercapnia and hypoxia by breathing gas mixtures with varying levels of oxygen and carbon dioxide while recording physiological responses in terms of respiratory and

cardiovascular variables. The collected data represent the average responses across multiple subjects to different levels of oxygen and carbon dioxide challenges and were used for comparison with the virtual subject.

To validate the control mechanisms during hypercapnia, I utilized the study conducted by Reynolds et al. [237]. In line with the study, the virtual subject was exposed to a gas mixture composed of 7% carbon dioxide in air for a duration of 25 minutes following 5 minutes of spontaneous ventilation with room air. This was followed by an additional 20-minute period of room air ventilation.

Similarly, to validate the control mechanisms during hypoxia, I used the study by Reynolds et al. [238]. As per the study, the virtual subject was exposed to a gas mixture consisting of 8% oxygen in air for a period of 10 minutes, following 5 minutes of spontaneous ventilation with room air. This was followed by an additional 20-minute period of room air ventilation.

12.3 Results & Findings

12.3.1 Response during spontaneous ventilation

Figure 12.3 illustrates the impact of spontaneous ventilation on stroke volume and arterial blood pressure. Exhalation increases intrathoracic pressure, which raises pleural pressure and results in a corresponding increase in both stroke volume and blood pressure. While all the values displayed fall within physiological ranges, the pleural pressure is slightly elevated beyond expected levels. Additionally, the blood pressure reaches a peak systolic pressure of approximately 115 mmHg, which is lower than the typical level of 120 mmHg.

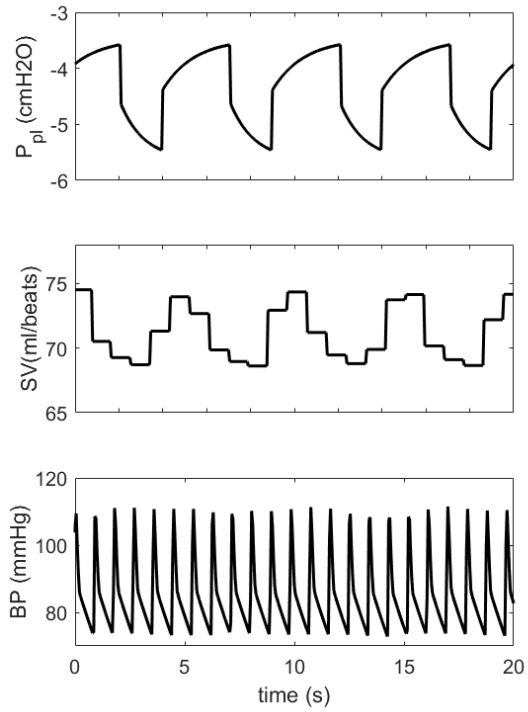

Figure 12.3 Effect of spontaneous ventilation on cardiovascular function. P_{pl}: pleural pressure; SV: stroke volume; BP: blood pressure.

Figure 12.4 illustrates the respiratory profile observed during spontaneous ventilation. Similar to Figure 12.3, all values depicted in this context fall within the physiological range. Alveolar partial pressure of oxygen and carbon dioxide fluctuate between 12.4-13.3 kPa (93-100 mmHg) and 5.1-5.6 kPa (38-42 mmHg), respectively. The tidal volume measures around 400 ml, slightly below the anticipated value. This suggests a need to fine-tune the respiratory control mechanisms parameters associated with tidal volume, as outlined in Table 12.6.

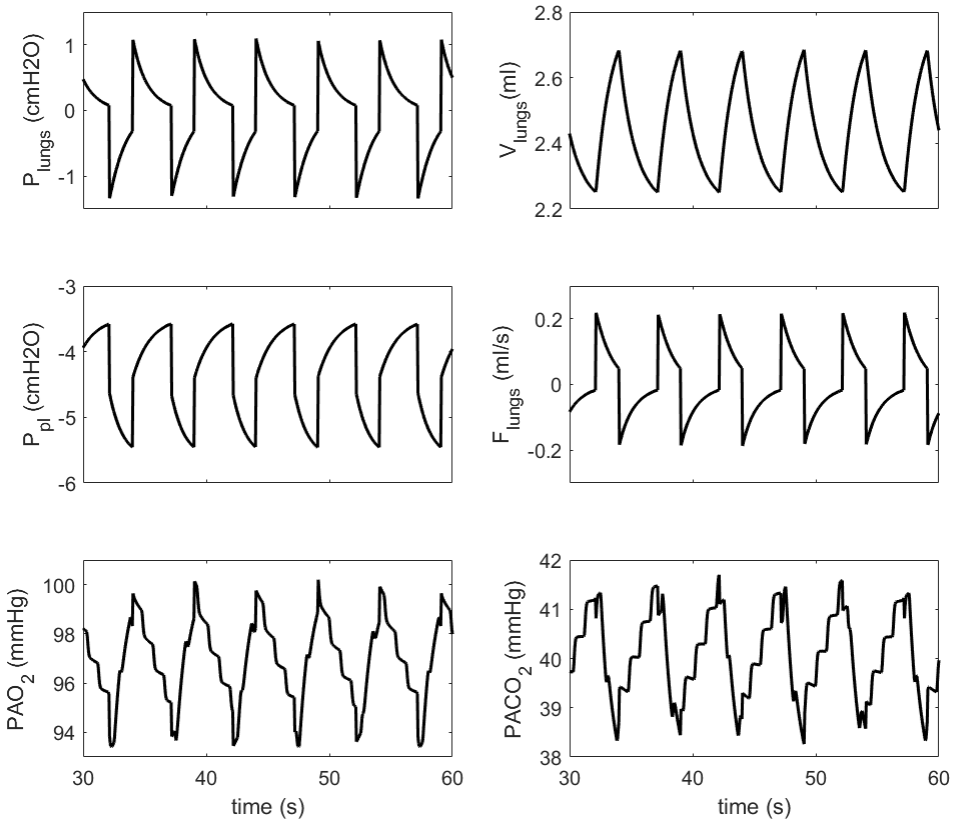

Figure 12.4 Respiratory profile during spontaneous ventilation. P_{lungs}: alveolar pressure; V_{lungs}: lungs volumes; P_{pl}: pleural pressure; F_{lungs}: air flow; PAO_2: alveolar partial pressure of oxygen; $PACO_2$: alveolar partial pressure of carbon dioxide.

12.3.2 Response to hypercapnic stimulus

The respiratory response to a hypercapnic stimulus of 7% CO_2 over 25 minutes is demonstrated in Figure 12.5. In general, the simulated data followed the trends of the experimental data. However, the model output for tidal volume did not match the expected data closely, as it increased from 0.4 $L.breath^{-1}$ to 0.5 $L.breath^{-1}$, rather than the expected increase to 1.6 $L.breath^{-1}$ during the hypercapnic stimulus. This lack of increase in tidal volume caused an overshoot in alveolar partial pressure of carbon dioxide and an undershoot of the alveolar partial pressure of oxygen. The only model output that closely matched the experimental data was the respiratory rate.

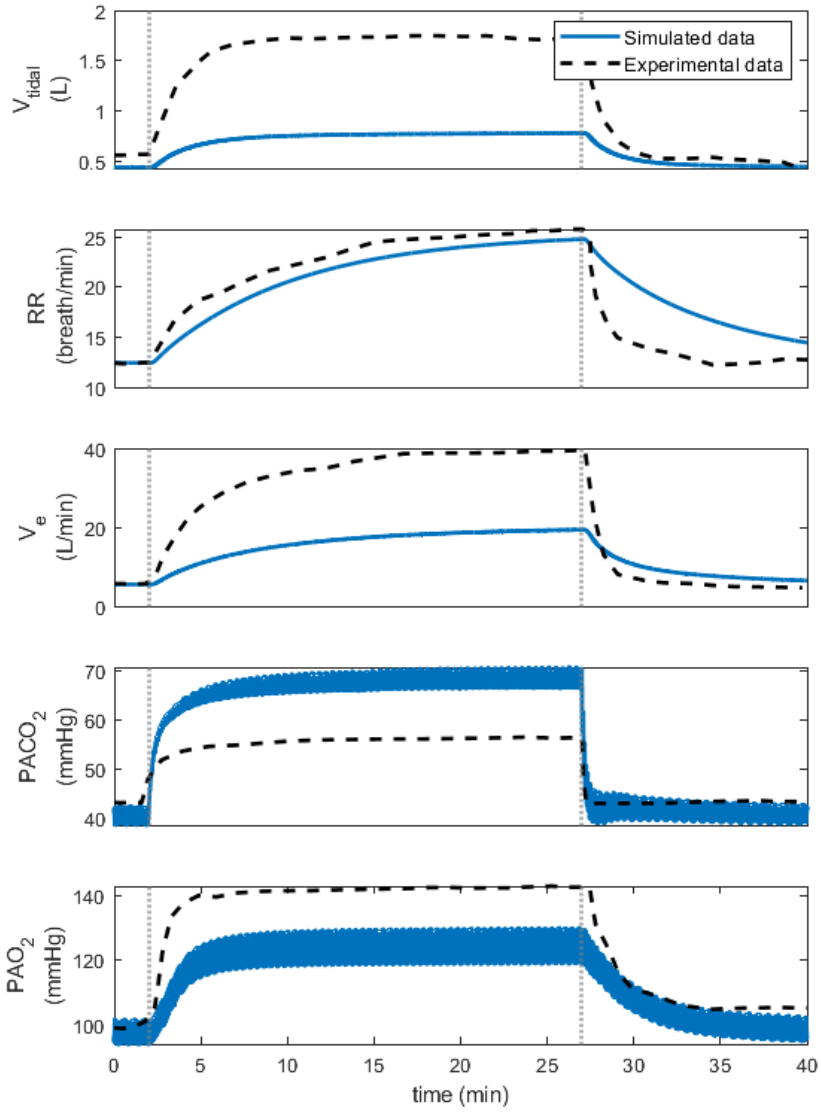

Figure 12.5 Respiratory response to a 25-min 7% CO2 hypercapnic stimulus. VT: tidal volume, RR: respiratory rate; Ve: minute ventilation; PACO2: alveolar partial pressure of carbon dioxide; PAO2: alveolar partial pressure of oxygen.

12.3.3 Response to hypoxic stimulus

Displayed in Figure 12.6 is the respiratory response to a hypoxic stimulus of 8% O_2 over 10 minutes. Although all the simulated data followed the same trend as the experimental data, the overall matching is poor. Similar to Figure 12.5, the respiratory rate increased similarly to the experimental data, but the tidal volume did not increase significantly, resulting in a lower minute ventilation. As a consequence, the reduced minute ventilation led to an undershoot of both the alveolar partial pressure of oxygen and carbon dioxide.

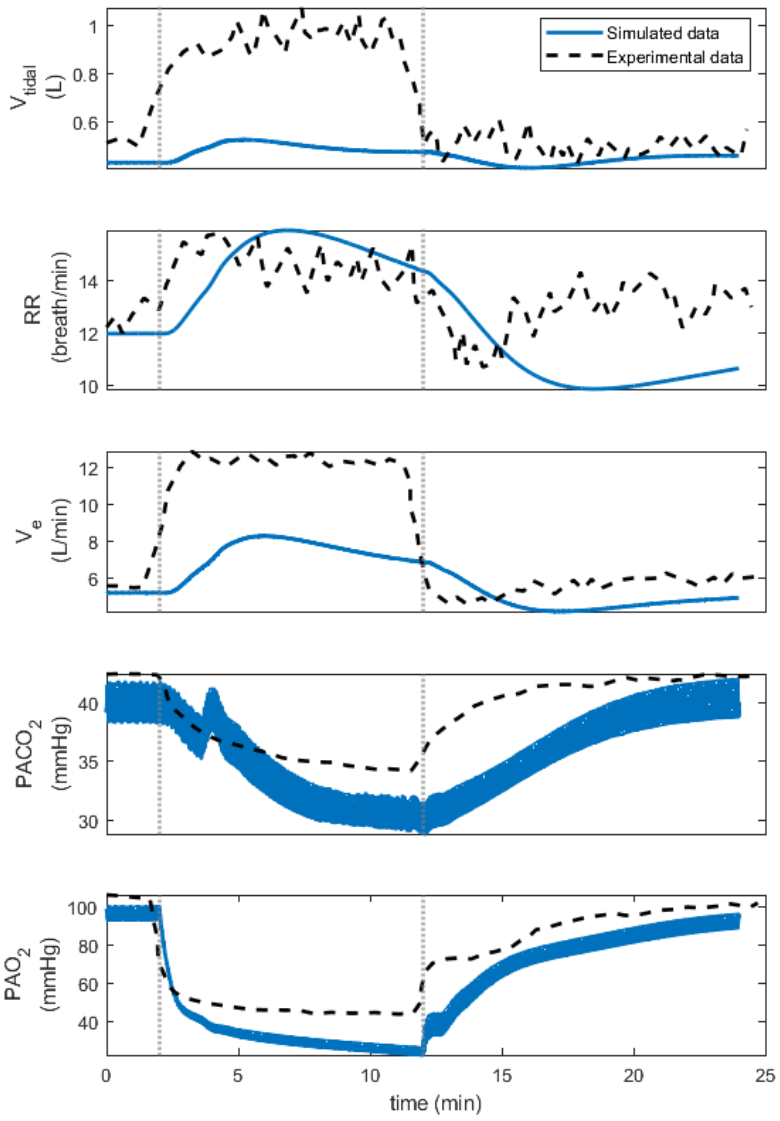

Figure 12.6 Respiratory response to a 10-min 8% O_2 hypoxic stimulus. V_T: tidal volume, RR: respiratory rate; V_e: minute ventilation; $PACO_2$: alveolar partial pressure of carbon dioxide; PAO_2: alveolar partial pressure of oxygen.

12.4 Conclusion

This chapter introduces the incorporation of novel cardiovascular and respiratory control mechanisms, as developed by Cheng et al., into the ICSM simulation suite. The model demonstrates satisfactory performance during spontaneous ventilation with room air. However, to achieve precise model matching under hypercapnic and hypoxic stimuli, further calibration of the parameters governing tidal volume is necessary. Exploring the cardiovascular control mechanisms during hypoxia and hypercapnia holds potential for valuable insights into these processes during cardiac arrest and CPR, paving the way for

further investigation and the development of innovative therapies. This enhanced understanding has the potential to contribute to improved survival rates and better outcomes for individuals experiencing cardiac arrest. It's important to note that due to time constraints, the input parameters were not fine-tuned, and the control mechanisms were not adapted to the ICSM. Given more time, a refinement would involve utilizing arterial pH instead of $PaCO_2$ as the driving force for chemoreceptor control, offering a more accurate representation, especially during metabolic acidosis in the context of cardiac arrest.

Chapter 13. Conclusions

13.1 Scientific contributions to the field

This thesis encompasses a series of studies, summarizing the key scientific findings. In Chapter 8, optimal CPR strategies were identified for ten virtual subjects. The optimized CPR protocol yielded a remarkable five-fold increase in myocardial tissue oxygen volume and nearly double cerebral tissue oxygen volume. Notably, the optimal CPR strategy maintained the same compression ratio as the current AHA guidelines but featured a slightly greater chest compression depth, lower chest compression rate, and a less aggressive ventilation strategy. These findings highlight the potential adverse hemodynamic effects of excessive ventilation, such as increased pulmonary vascular resistance and compromised cardiac output.

Chapter 9 emphasized the significance of tailored CPR strategies based on the underlying cause of cardiac arrest. The employment of a genetic algorithm led to the discovery of distinct CPR strategies for subjects experiencing CA due to myocardial infarction (MI) or pulmonary embolism (PE). Both optimized CPR strategies involved an increase in end compression force and compression ratio, coupled with a decrease in chest compression rate, tidal volume, and fraction of inspired oxygen. Ventilatory frequency was the sole parameter increased for the optimized CPR following MI and decreased for the optimized CPR following PE, compared to standard CPR.

Chapter 10 provided a quantitative analysis of the impact of CPR parameters on cardiac output in ten virtual subjects. End compression force and positive end-expiratory pressure emerged as the most influential factors due to their effect on intrathoracic pressure. Remarkably, the compression ratio ranked as the third most important parameter affecting cardiac output, underscoring the need for further exploration of this underappreciated aspect of chest compression.

Lastly, in Chapter 11, the validation of the ICSM simulation suite's thoracic model using individual haemodynamic recordings from a patient undergoing CPR demonstrated its

potential for simulating individualized patient data to retrospectively identify optimized CPR strategies.

The research significantly advances the field of biomedical engineering by introducing a novel and highly integrated approach to studying cardiac arrest (CA) and cardiopulmonary resuscitation (CPR). The Interdisciplinary Collaboration in Systems Medicine (ICSM) simulation suite, with its unparalleled level of integration, represents a significant advancement. The creation of a bank of CA and CPR subjects marks a crucial milestone, enabling controlled and systematic experimentation within a virtual population, as exemplified by the outcomes in Chapter 8.

Furthermore, the inclusion of multiple organ compartments within the ICSM simulation suite departs from traditional approaches. This emphasis on optimizing organ-specific oxygenation aligns with the clinical goal of ensuring adequate oxygen delivery to vital tissues during resuscitation.

In summary, this research not only advances the field of computational modelling in CA and CPR but also introduces innovative concepts. The ICSM simulation suite's unique integration and the creation of a subject bank offer a new paradigm for studying these critical events. The results in Chapter 8 validate the suite's reliability, while the focus on organ-specific oxygenation aligns with the broader objective of enhancing real-life patient outcomes in resuscitation scenarios. These findings have the potential to shape the future of research in resuscitation medicine, setting a new standard for computational modelling in the field.

13.2 Limitations

Lumped mathematical models of the cardiovascular and respiratory systems offer a simplified representation of complex physiological processes, making them valuable tools for research and analysis. However, they have several limitations:

Lack of Spatial Information: Lumped models typically do not account for spatial variations in organ or tissue properties. They assume uniform behaviour within a compartment, which may not accurately reflect real anatomical structures and variations.

Oversimplification of Geometry: Lumped models may oversimplify the geometry of blood vessels, neglecting the complex branching and tapering of vessels, as well as the impact of vessel geometry on flow dynamics.

Ignoring Fluid Dynamics: Lumped models often neglect important fluid dynamics effects, such as turbulence, which can be significant in large vessels and can affect pressure and flow patterns.

Inability to Model Local Effects: Lumped models are not well-suited for capturing local effects, such as the development of atherosclerotic plaques in specific regions of arteries or localized pulmonary disease.

Limited Representation of Tissues: These models may not account for the interactions between the cardiovascular and respiratory systems and specific tissues, which is crucial for understanding diseases like heart failure, chronic obstructive pulmonary disease (COPD), or pulmonary embolism.

Lack of Realistic Hemodynamic: Lumped models often use simplifications for arterial compliance, resistance, and flow patterns, which may not accurately represent the complex behaviour of arteries and arterioles, especially during pathological conditions.

Despite these limitations, lumped models are valuable for gaining insights into the behaviour of the cardiovascular and respiratory systems, and they serve as useful tools for educational and research purposes. Regarding the ISCM simulation suite for investigating cardiac arrest and CPR strategies, several limitations need acknowledgment:

Complex Biological Processes: One of the major limitations I need to acknowledge is that my ICSM simulation suite doesn't consider complex biological processes, such as the influence of high levels of inflammatory cytokines, electrolyte imbalances, and lactate

concentrations. These processes are critical in understanding post-cardiac arrest treatment and the management of multiple organ failure. Without accounting for these complexities, my model may not fully capture the intricate responses of patients in real-life cardiac arrest (CA) and cardiopulmonary resuscitation (CPR) scenarios.

Electrophysiological Detail for Defibrillation: Another constraint I face is the absence of comprehensive electrophysiological modelling of the heart, which is essential for accurately simulating defibrillation. The intricate electrical activity of the heart during defibrillation plays a pivotal role in determining the effectiveness of defibrillation strategies. Without this level of detail, my model's applicability to real-life defibrillation scenarios could be compromised.

Absence of Models for Vasopressors and Inotropes: It's also worth noting that my ICSM simulation suite does not model the effects of vasopressors and inotropes, crucial factors in CPR studies. These medications are integral to resuscitation efforts, and not having them in my model may limit my exploration of a wide range of CPR strategies and their outcomes. However, these could be implemented in the future.

Scarcity of Human Validation Data: Another significant challenge I've encountered in my research is the scarcity of human data available for validating simulations of CA and CPR. While I could relatively easily validate the new components of my computational model during spontaneous ventilation, validating the model during CA and CPR simulations became notably complex. The lack of reliable human hemodynamic, gas exchange, and ventilation data during these critical events poses a challenge for accurately replicating human responses.

These limitations and constraints underscore the need for ongoing refinement and development of computer models for CA and CPR research. While these models offer valuable insights and controlled experimentation, it's essential to use them in conjunction with clinical studies and real-life data to enhance their applicability to real-world scenarios.

13.3 Future work and studies

For future research and studies, building upon the foundation of this research would hold great promise. Accessing additional data sources, particularly from the NCT02479152 clinical trial, would be paramount. This clinical trial meticulously recorded haemodynamic measures during 30 minutes of CPR in 126 patients, providing invaluable data to broaden the research scope.

One of the primary objectives would be to leverage this data for the creation of a more extensive virtual subject repository. These virtual subjects would undergo simultaneous continuous calibration using continuous recordings of physiological parameters like femoral arterial pressure, end-tidal carbon dioxide (ETCO2), and cerebral oximetry. Such calibration processes would aim to enhance the accuracy and reliability of the virtual subjects within the model.

With a virtual subject bank at hand, the research would extend into ambitious studies dedicated to advancing our knowledge of CPR and resuscitation strategies. These studies would encompass:

- Exploring Chest Compression Waveforms: Investigating the efficacy of different chest compression waveforms, such as square, sine, and semi-square waveforms. This exploration would provide insights into optimizing compression techniques for better outcomes during CPR.
- Compression and Decompression Strategies: Delving into the impact of compression and decompression CPR strategies on the virtual subject bank. This research would help identify the most effective resuscitation techniques and fine-tune their application.
- Airway Management Techniques: Investigating various airway management techniques during CPR, including nasal cannula, bag mask ventilation, tracheal intubation, and endotracheal intubation. This would shed light on the best practices for maintaining adequate oxygenation during resuscitation efforts.

Moreover, completing the calibration of the respiratory and cardiovascular control mechanisms, as presented in Chapter 12, would be done. This fine-tuning of control mechanisms would facilitate a more precise representation of physiological responses during CPR, ultimately contributing to the enhancement of resuscitation strategies.

13.4 Additional work

As part of my doctoral research, I participated in a multidisciplinary project that aimed to investigate tissue oxygenation in critically ill patients during permissive hypercapnia. In this project, I collaborated with Dr. Marianna Laviola to configure and execute all the simulations (Appendix 5). Additionally, I developed a simplified version of the ICSM simulation suite using MATLAB-Simulink (MathWorks, Natick, MA). This simplified version can be used to teach and illustrate the basic concepts of the ICSM simulation suite (Appendix 6).

References

[1] Office for National Statitiscs (ONS), "Deaths registered in England and Wales ONS 2018, Annual data on deaths registered by age, sex and selected underlying cause of death.," Office for National Statitiscs (ONS), 2019.

[2] C. X. Wong, A. Brown, D. H. Lau, S. S. Chugh, C. M. Albert, J. M. Kalman, and P. Sanders, “Epidemiology of Sudden Cardiac Death: Global and Regional Perspectives,” *Heart Lung Circ,* vol. 28, no. 1, pp. 6-14, 2019.

[3] R. Graham, M. A. McCoy, and A. M. Schultz, "Strategies to Improve Cardiac Arrest Survival: A Time to Act, The National Academies Collection: Reports funded by National Institutes of Health," *Strategies to Improve Cardiac Arrest Survival: A Time to Act*, R. Graham, M. A. McCoy and A. M. Schultz, eds., Washington (DC): National Academies Press (US), 2015.

[4] S. P. Abhilash, and N. Namboodiri, “Sudden cardiac death--historical perspectives,” *Indian heart journal,* vol. 66 Suppl 1, no. Suppl 1, pp. S4-S9, 2014.

[5] D. S. Grimes, “An epidemic of coronary heart disease,” *QJM: An International Journal of Medicine,* vol. 105, no. 6, pp. 509-518, 2012.

[6] J. E. Dalen, J. S. Alpert, R. J. Goldberg, and R. S. Weinstein, “The epidemic of the 20(th) century: coronary heart disease,” *Am J Med,* vol. 127, no. 9, pp. 807-12, 2014.

[7] K. Patel, and J. E. Hipskind, "Cardiac Arrest," *StatPearls*, Treasure Island (FL): StatPearls Publishing, 2020.

[8] R. N. Pittman., *Regulation of Tissue Oxygenation*, Virginia Commonwealth University, Richmond, Virginia: Morgan & Claypool Life Sciences., 2011.

[9] T. Standl, T. Annecke, I. Cascorbi, A. R. Heller, A. Sabashnikov, and W. Teske, “The Nomenclature, Definition and Distinction of Types of Shock,” *Deutsches Arzteblatt international,* vol. 115, no. 45, pp. 757-768, 2018.

[10] K. Markstaller, A. Rudolph, J. Karmrodt, H. W. Gervais, R. Goetz, A. Becher, M. David, O. S. Kempski, H. U. Kauczor, W. F. Dick, and B. Eberle, “Effect of chest compressions only during experimental basic life support on alveolar collapse and recruitment,” *Resuscitation,* vol. 79, no. 1, pp. 125-32, 2008.

[11] J. G. Hardman, J. S. Wills, and A. R. Aitkenhead, “Investigating hypoxemia during apnea: validation of a set of physiological models,” *Anesth Analg,* vol. 90, no. 3, pp. 614-8, 2000.

[12] C. Hawkes, S. Booth, C. Ji, S. J. Brace-McDonnell, A. Whittington, J. Mapstone, M. W. Cooke, C. D. Deakin, C. P. Gale, R. Fothergill, J. P. Nolan, N. Rees, J. Soar, A. N. Siriwardena, T. P. Brown, and G. D. Perkins, “Epidemiology and outcomes from out-of-hospital cardiac arrests in England,” *Resuscitation,* vol. 110, pp. 133-140, 2017.

[13] R. E. Klabunde, *Cardiovascular physiology concepts*: Second edition. Philadelphia, PA : Lippincott Williams & Wilkins/Wolters Kluwer, 2012.

[14] T. Kalogeris, C. P. Baines, M. Krenz, and R. J. Korthuis, “Cell biology of ischemia/reperfusion injury,” *International review of cell and molecular biology,* vol. 298, pp. 229-317, 2012.

[15] G. Hagberg, H. Ihle-Hansen, E. C. Sandset, D. Jacobsen, H. Wimmer, and H. Ihle-Hansen, “Long Term Cognitive Function After Cardiac Arrest: A Mini-Review,” *Frontiers in Aging Neuroscience,* vol. 14, 2022-May-26, 2022.

[16] C. Jou, R. Shah, A. Figueroa, and J. K. Patel, “The Role of Inflammatory Cytokines in Cardiac Arrest,” *J Intensive Care Med,* vol. 35, no. 3, pp. 219-224, 2020.

[17] B. W. Bottiger, J. Motsch, H. Bohrer, T. Boker, M. Aulmann, P. P. Nawroth, and E. Martin, “Activation of blood coagulation after cardiac arrest is not balanced adequately by activation of endogenous fibrinolysis,” *Circulation,* vol. 92, no. 9, pp. 2572-8, 1995.

[18] J. M. Dargin, and L. L. Emlet, “Thrombolysis during out-of-hospital cardiac arrest: a lesson in the law of diminishing returns,” *Critical care (London, England),* vol. 14, no. 2, pp. 304-304, 2010.

[19] R. Bellomo, J. Martensson, and G. M. Eastwood, “Metabolic and electrolyte disturbance after cardiac arrest: How to deal with it,” *Best Pract Res Clin Anaesthesiol,* vol. 29, no. 4, pp. 471-84, 2015.

[20] S. Girotra, P. S. Chan, and S. M. Bradley, “Post-resuscitation care following out-of-hospital and in-hospital cardiac arrest,” *Heart,* vol. 101, no. 24, pp. 1943-1949, 2015.

[21] J. P. Nolan, J. Soar, G. B. Smith, C. Gwinnutt, F. Parrott, S. Power, D. A. Harrison, E. Nixon, and K. Rowan, “Incidence and outcome of in-hospital cardiac arrest in the United Kingdom National Cardiac Arrest Audit,” *Resuscitation,* vol. 85, no. 8, pp. 987-92, 2014.

[22] L. W. Andersen, M. J. Holmberg, K. M. Berg, M. W. Donnino, and A. Granfeldt, “In-Hospital Cardiac Arrest A Review,” *Jama-Journal of the American Medical Association,* vol. 321, no. 12, pp. 1200-1210, 2019.

[23] P. A. Meaney, B. J. Bobrow, M. E. Mancini, J. Christenson, A. R. de Caen, F. Bhanji, B. S. Abella, M. E. Kleinman, D. P. Edelson, R. A. Berg, T. P. Aufderheide, V. Menon, and M. Leary, “Cardiopulmonary resuscitation quality: [corrected] improving cardiac resuscitation outcomes both inside and outside the hospital: a consensus statement from the American Heart Association,” *Circulation,* vol. 128, no. 4, pp. 417-35, 2013.

[24] H. L. Tan, N. Dagres, B. W. Böttiger, P. J. Schwartz, and E.-N. Investigators, “European Sudden Cardiac Arrest network: towards Prevention, Education and New Effective Treatments (ESCAPE-NET): A major European Horizon 2020 project focused on cardiac arrest,” *European Heart Journal,* vol. 39, no. 2, pp. 86-88, 2018.

[25] G. Ghasemzadeh, M. Soodmand, and M. T. Moghadamnia, “The Cardiac Risk Factors of Coronary Artery Disease and its relationship with Cardiopulmonary resuscitation: A retrospective study,” *The Egyptian heart journal : (EHJ) : official bulletin of the Egyptian Society of Cardiology,* vol. 70, no. 4, pp. 389-392, 2018.

[26] J. Engdahl, M. Holmberg, B. W. Karlson, R. Luepker, and J. Herlitz, “The epidemiology of out-of-hospital 'sudden' cardiac arrest,” *Resuscitation,* vol. 52, no. 3, pp. 235-245, 2002.

[27] J. P. Nolan, R. A. Berg, L. W. Andersen, F. Bhanji, P. S. Chan, M. W. Donnino, S. H. Lim, M. H. Ma, V. M. Nadkarni, M. A. Starks, G. D. Perkins, P. T. Morley, J. Soar, and C. Utstein, “Cardiac Arrest and Cardiopulmonary Resuscitation Outcome Reports: Update of the Utstein Resuscitation Registry Template for In-Hospital Cardiac Arrest: A Consensus Report From a Task Force of the International Liaison Committee on Resuscitation (American Heart Association, European Resuscitation Council, Australian and New Zealand Council on Resuscitation, Heart and Stroke

Foundation of Canada, InterAmerican Heart Foundation, Resuscitation Council of Southern Africa, Resuscitation Council of Asia)," *Resuscitation*, 2019.

[28] N. Chen, C. W. Callaway, F. X. Guyette, J. C. Rittenberger, A. A. Doshi, C. Dezfulian, and J. Elmer, "Arrest etiology among patients resuscitated from cardiac arrest," *Resuscitation,* vol. 130, pp. 33-40, 2018.

[29] A. Sakhuja, M. Sztajnkrycer, S. Vallabhajosyula, W. Cheungpasitporn, R. Patch, 3rd, and J. Jentzer, "National trends and outcomes of cardiac arrest in opioid overdose," *Resuscitation,* vol. 121, pp. 84-89, 2017.

[30] J. Soar, J. P. Nolan, B. W. Böttiger, G. D. Perkins, C. Lott, P. Carli, T. Pellis, C. Sandroni, M. B. Skrifvars, G. B. Smith, K. Sunde, and C. D. Deakin, "European Resuscitation Council Guidelines for Resuscitation 2015: Section 3. Adult advanced life support," *Resuscitation,* vol. 95, pp. 100-47, 2015.

[31] A. Chalkias, E. Arnaoutoglou, and T. Xanthos, "Personalized physiology-guided resuscitation in highly monitored patients with cardiac arrest-the PERSEUS resuscitation protocol," *Heart Fail Rev,* vol. 24, no. 4, pp. 473-480, 2019.

[32] N. A. Paradis, H. R. Halperin, K. B. Kern, V. Wenzel, and D. A. Chamberlain, *Cardiac Arrest : The Science and Practice of Resuscitation Medicine*, Cambridge, UNITED KINGDOM: Cambridge University Press, 2007.

[33] Y. Azeli, J. V. Lorente Olazabal, M. I. Monge García, and A. Bardají, "Understanding the Adverse Hemodynamic Effects of Serious Thoracic Injuries During Cardiopulmonary Resuscitation: A Review and Approach Based on the Campbell Diagram," *Frontiers in physiology,* vol. 10, pp. 1475-1475, 2019.

[34] S. Cipani, C. Bartolozzi, P. Ballo, and A. Sarti, "Blood flow maintenance by cardiac massage during cardiopulmonary resuscitation: Classical theories, newer hypotheses, and clinical utility of mechanical devices," *Journal of the Intensive Care Society,* vol. 20, no. 1, pp. 2-10, 2019.

[35] J. Considine, R. J. Gazmuri, G. D. Perkins, P. J. Kudenchuk, T. M. Olasveengen, C. Vaillancourt, C. Nishiyama, T. Hatanaka, M. E. Mancini, S. P. Chung, R. Escalante-Kanashiro, and P. Morley, "Chest compression components (rate, depth, chest wall recoil and leaning): A scoping review," *Resuscitation*, 2019.

[36] A. H. Idris, D. Guffey, T. P. Aufderheide, S. Brown, L. J. Morrison, P. Nichols, J. Powell, M. Daya, B. L. Bigham, D. L. Atkins, R. Berg, D. Davis, I. Stiell, G. Sopko, and G. Nichol, "Relationship between chest compression rates and outcomes from cardiac arrest," *Circulation,* vol. 125, no. 24, pp. 3004-3012, 2012.

[37] A. H. Idris, D. Guffey, P. E. Pepe, S. P. Brown, S. C. Brooks, C. W. Callaway, J. Christenson, D. P. Davis, M. R. Daya, R. Gray, P. J. Kudenchuk, J. Larsen, S. Lin, J. J. Menegazzi, K. Sheehan, G. Sopko, I. Stiell, G. Nichol, and T. P. Aufderheide, "Chest compression rates and survival following out-of-hospital cardiac arrest," *Crit Care Med,* vol. 43, no. 4, pp. 840-848, 2015.

[38] H. M. Ashoor, E. Lillie, W. Zarin, B. Pham, P. A. Khan, V. Nincic, F. Yazdi, M. Ghassemi, J. Ivory, R. Cardoso, G. D. Perkins, A. R. de Caen, and A. C. Tricco, "Effectiveness of different compression-to-ventilation methods for cardiopulmonary resuscitation: A systematic review," *Resuscitation,* vol. 118, pp. 112-125, 2017.

[39] T. Vadeboncoeur, U. Stolz, A. Panchal, A. Silver, M. Venuti, J. Tobin, G. Smith, M. Nunez, M. Karamooz, D. Spaite, and B. Bobrow, "Chest compression depth and survival in out-of-hospital cardiac arrest," *Resuscitation,* vol. 85, no. 2, pp. 182-188, 2014.

[40] I. G. Stiell, S. P. Brown, G. Nichol, S. Cheskes, C. Vaillancourt, C. W. Callaway, L. J. Morrison, J. Christenson, T. P. Aufderheide, D. P. Davis, C. Free, D. Hostler, J. A. Stouffer, and A. H. Idris, "What is the optimal chest compression depth during out-of-hospital cardiac arrest resuscitation of adult patients?," *Circulation,* vol. 130, no. 22, pp. 1962-70, 2014.

[41] I. G. Stiell, S. P. Brown, J. Christenson, S. Cheskes, G. Nichol, J. Powell, B. Bigham, L. J. Morrison, J. Larsen, E. Hess, C. Vaillancourt, D. P. Davis, and C. W. Callaway, "What is the role of chest compression depth during out-of-hospital cardiac arrest resuscitation?," *Crit Care Med,* vol. 40, no. 4, pp. 1192-8, 2012.

[42] S. Riyapan, T. Naulnark, O. Ruangsomboon, W. Chaisirin, C. Limsuwat, N. Prapruetkit, T. Chakorn, and A. Monsomboon, "Improving quality of chest compression in thai emergency department by using real-time audio-visual feedback cardio-pulmonary resuscitation monitoring," *Journal of the Medical Association of Thailand,* vol. 102, no. 3, pp. 245-251, 2019.

[43] C. F. Babbs, A. E. Kemeny, W. Quan, and G. Freeman, "A new paradigm for human resuscitation research using intelligent devices," *Resuscitation,* vol. 77, no. 3, pp. 306-315, 2008.

[44] S. Cheskes, M. R. Common, A. P. Byers, C. Zhan, A. Silver, and L. J. Morrison, "The association between chest compression release velocity and outcomes from out-of-hospital cardiac arrest," *Resuscitation,* vol. 86, pp. 38-43, 2015.

[45] A. Kovacs, T. F. Vadeboncoeur, U. Stolz, D. W. Spaite, T. Irisawa, A. Silver, and B. J. Bobrow, "Chest compression release velocity: Association with survival and favorable neurologic outcome after out-of-hospital cardiac arrest," *Resuscitation,* vol. 92, pp. 107-114, 2015.

[46] J. Holmén, J. Herlitz, M. Jimenez-Herrera, T. Karlsson, and C. Axelsson, "Passive leg raising in out-of-hospital cardiac arrest," *Resuscitation,* vol. 137, pp. 94-101, 2019.

[47] A. Movahedi, S. R. Mirhafez, H. Behnam-Voshani, H. Reihani, A. Kavosi, G. A. Ferns, and J. Malekzadeh, "A Comparison of the Effect of Interposed Abdominal Compression Cardiopulmonary Resuscitation and Standard Cardiopulmonary Resuscitation Methods on End-tidal CO2 and the Return of Spontaneous Circulation Following Cardiac Arrest: A Clinical Trial," *Acad Emerg Med,* vol. 23, no. 4, pp. 448-54, 2016.

[48] M. Shanmugasundaram, and K. Lotun, "Refractory Out of Hospital Cardiac Arrest," *Current cardiology reviews,* vol. 14, no. 2, pp. 109-114, 2018.

[49] S. Gates, R. Lall, T. Quinn, C. D. Deakin, M. W. Cooke, J. Horton, S. E. Lamb, A. M. Slowther, M. Woollard, A. Carson, M. Smyth, K. Wilson, G. Parcell, A. Rosser, R. Whitfield, A. Williams, R. Jones, H. Pocock, N. Brock, J. J. Black, J. Wright, K. Han, G. Shaw, L. Blair, J. Marti, C. Hulme, C. McCabe, S. Nikolova, Z. Ferreira, and G. D. Perkins, "Prehospital randomised assessment of a mechanical compression device in out-of-hospital cardiac arrest (PARAMEDIC): a pragmatic, cluster randomised trial and economic evaluation," *Health Technol Assess,* vol. 21, no. 11, pp. 1-176, 2017.

[50] P. L. Wang, and S. C. Brooks, "Mechanical versus manual chest compressions for cardiac arrest," *Cochrane Database Syst Rev,* vol. 8, no. 8, pp. Cd007260, 2018.

[51] K. Hayashida, T. Tagami, T. Fukuda, M. Suzuki, N. Yonemoto, Y. Kondo, T. Ogasawara, A. Sakurai, Y. Tahara, K. Nagao, A. Yaguchi, and N. Morimura, "Mechanical Cardiopulmonary Resuscitation and Hospital Survival Among Adult Patients With Nontraumatic Out-of-Hospital Cardiac Arrest Attending the Emergency Department: A Prospective, Multicenter, Observational Study in Japan (SOS-

KANTO [Survey of Survivors after Out-of-Hospital Cardiac Arrest in Kanto Area] 2012 Study)," *J Am Heart Assoc,* vol. 6, no. 11, 2017.

[52] C. J. Twohig, B. Singer, G. Grier, and S. J. Finney, "A systematic literature review and meta-analysis of the effectiveness of extracorporeal-CPR versus conventional-CPR for adult patients in cardiac arrest," *J Intensive Care Soc,* vol. 20, no. 4, pp. 347-357, 2019.

[53] D. A. Gomes, J. Presume, J. Ferreira, A. F. Oliveira, T. Miranda, C. Brízido, C. Strong, and A. Tralhão, "Extracorporeal cardiopulmonary resuscitation for refractory out-of-hospital cardiac arrest: a systematic review and meta-analysis of randomized clinical trials," *Intern Emerg Med,* vol. 18, no. 7, pp. 2113-2120, Oct, 2023.

[54] C. Lafuente-Lafuente, and M. Melero-Bascones, "Active chest compression-decompression for cardiopulmonary resuscitation," *Cochrane Database Syst Rev,* vol. 2013, no. 9, pp. Cd002751, 2013.

[55] T. P. Aufderheide, G. Nichol, T. D. Rea, S. P. Brown, B. G. Leroux, P. E. Pepe, P. J. Kudenchuk, J. Christenson, M. R. Daya, P. Dorian, C. W. Callaway, A. H. Idris, D. Andrusiek, S. W. Stephens, D. Hostler, D. P. Davis, J. V. Dunford, R. G. Pirrallo, I. G. Stiell, C. M. Clement, A. Craig, L. Van Ottingham, T. A. Schmidt, H. E. Wang, M. L. Weisfeldt, J. P. Ornato, and G. Sopko, "A trial of an impedance threshold device in out-of-hospital cardiac arrest," *N Engl J Med,* vol. 365, no. 9, pp. 798-806, 2011.

[56] A. Sugiyama, S. Duval, Y. Nakamura, K. Yoshihara, and D. Yannopoulos, "Impedance Threshold Device Combined With High-Quality Cardiopulmonary Resuscitation Improves Survival With Favorable Neurological Function After Witnessed Out-of-Hospital Cardiac Arrest," *Circ J,* vol. 80, no. 10, pp. 2124-32, 2016.

[57] P. Niforopoulou, N. Iacovidou, P. Lelovas, G. Karlis, A. Papalois, S. Siakavellas, V. Spapis, G. Kaparos, I. Siafaka, and T. Xanthos, "Correlation of Impedance Threshold Device use during cardiopulmonary resuscitation with post-cardiac arrest Acute Kidney Injury," *Am J Emerg Med,* vol. 35, no. 6, pp. 846-854, 2017.

[58] J. Pritchard, J. Roberge, J. Bacani, M. Welsford, and S. Mondoux, "Implementation of Chest Compression Feedback Technology to Improve the Quality of Cardiopulmonary Resuscitation in the Emergency Department: A Quality Initiative Test-of-change Study," *Cureus,* vol. 11, no. 8, pp. e5523, 2019.

[59] R. M. Sutton, B. French, P. A. Meaney, A. A. Topjian, C. S. Parshuram, D. P. Edelson, S. Schexnayder, B. S. Abella, R. M. Merchant, M. Bembea, R. A. Berg, V. M. Nadkarni, and I. American Heart Association's Get With The Guidelines–Resuscitation, "Physiologic monitoring of CPR quality during adult cardiac arrest: A propensity-matched cohort study," *Resuscitation,* vol. 106, pp. 76-82, 2016.

[60] R. W. Morgan, B. French, T. J. Kilbaugh, M. Y. Naim, H. Wolfe, G. Bratinov, W. Shoap, T.-C. Hsieh, V. M. Nadkarni, R. A. Berg, and R. M. Sutton, "A quantitative comparison of physiologic indicators of cardiopulmonary resuscitation quality: Diastolic blood pressure versus end-tidal carbon dioxide," *Resuscitation,* vol. 104, pp. 6-11, 2016.

[61] M. Y. Naim, R. M. Sutton, S. H. Friess, G. Bratinov, U. Bhalala, T. J. Kilbaugh, J. W. Lampe, V. M. Nadkarni, L. B. Becker, and R. A. Berg, "Blood Pressure- and Coronary Perfusion Pressure-Targeted Cardiopulmonary Resuscitation Improves 24-Hour Survival From Ventricular Fibrillation Cardiac Arrest," *Crit Care Med,* vol. 44, no. 11, pp. e1111-e1117, 2016.

[62] C. Sandroni, S. Parnia, and J. P. Nolan, “Cerebral oximetry in cardiac arrest: a potential role but with limitations,” *Intensive Care Med,* vol. 45, no. 6, pp. 904-906, 2019.

[63] K. G. Monsieurs, J. P. Nolan, L. L. Bossaert, R. Greif, I. K. Maconochie, N. I. Nikolaou, G. D. Perkins, J. Soar, A. Truhlář, J. Wyllie, and D. A. Zideman, “European Resuscitation Council Guidelines for Resuscitation 2015: Section 1. Executive summary,” *Resuscitation,* vol. 95, pp. 1-80, 2015.

[64] C. Kill, W. Dersch, and H. Wulf, “Advanced life support and mechanical ventilation,” *Curr Opin Crit Care,* vol. 18, no. 3, pp. 251-5, 2012.

[65] T. P. Aufderheide, G. Sigurdsson, R. G. Pirrallo, D. Yannopoulos, S. McKnite, C. von Briesen, C. W. Sparks, C. J. Conrad, T. A. Provo, and K. G. Lurie, “Hyperventilation-induced hypotension during cardiopulmonary resuscitation,” *Circulation,* vol. 109, no. 16, pp. 1960-5, 2004.

[66] T. P. Aufderheide, and K. G. Lurie, “Death by hyperventilation: a common and life-threatening problem during cardiopulmonary resuscitation,” *Crit Care Med,* vol. 32, no. 9 Suppl, pp. S345-51, 2004.

[67] R. L. Cordioli, D. L. Grieco, E. Charbonney, J. C. Richard, and D. Savary, “New physiological insights in ventilation during cardiopulmonary resuscitation,” *Curr Opin Crit Care,* vol. 25, no. 1, pp. 37-44, 2019.

[68] R. A. Berg, A. B. Sanders, K. B. Kern, R. W. Hilwig, J. W. Heidenreich, M. E. Porter, and G. A. Ewy, “Adverse hemodynamic effects of interrupting chest compressions for rescue breathing during cardiopulmonary resuscitation for ventricular fibrillation cardiac arrest,” *Circulation,* vol. 104, no. 20, pp. 2465-70, 2001.

[69] R. McDannold, B. J. Bobrow, V. Chikani, A. Silver, D. W. Spaite, and T. Vadeboncoeur, “Quantification of ventilation volumes produced by compressions during emergency department cardiopulmonary resuscitation,” *Am J Emerg Med,* vol. 36, no. 9, pp. 1640-1644, 2018.

[70] D. Yannopoulos, T. Matsuura, S. McKnite, N. Goodman, A. Idris, W. Tang, T. P. Aufderheide, and K. G. Lurie, “No assisted ventilation cardiopulmonary resuscitation and 24-hour neurological outcomes in a porcine model of cardiac arrest,” *Crit Care Med,* vol. 38, no. 1, pp. 254-60, 2010.

[71] H. Schotola, K. Toischer, A. F. Popov, A. Renner, J. D. Schmitto, J. Gummert, M. Quintel, M. Bauer, L. S. Maier, and S. Sossalla, “Mild metabolic acidosis impairs the β-adrenergic response in isolated human failing myocardium,” *Critical care (London, England),* vol. 16, no. 4, pp. R153-R153, 2012.

[72] E. Charbonney, S. Delisle, D. Savary, G. Bronchti, M. Rigollot, A. Drouet, B. Badat, P. Ouellet, P. Gosselin, A. Mercat, L. Brochard, and J. M. Richard, “A new physiological model for studying the effect of chest compression and ventilation during cardiopulmonary resuscitation: The Thiel cadaver,” *Resuscitation,* vol. 125, pp. 135-142, 2018.

[73] D. L. Grieco, J. B. L, A. Drouet, I. Telias, S. Delisle, G. Bronchti, C. Ricard, M. Rigollot, B. Badat, P. Ouellet, E. Charbonney, J. Mancebo, A. Mercat, D. Savary, and J. M. Richard, “Intrathoracic Airway Closure Impacts CO2 Signal and Delivered Ventilation during Cardiopulmonary Resuscitation,” *Am J Respir Crit Care Med,* vol. 199, no. 6, pp. 728-737, 2019.

[74] C. Duchatelet, M. Wolfskeil, M. Vanwulpen, and S.-H. Idrissi, “Effect of positive end-expiratory pressure during cardiopulmonary resuscitation on short-term survival,” *Resuscitation,* vol. 142, pp. e7-e8, 2019.

[75] W. G. Voelckel, K. G. Lurie, T. Zielinski, S. McKnite, P. Plaisance, V. Wenzel, and K. H. Lindner, “The effects of positive end-expiratory pressure during active compression decompression cardiopulmonary resuscitation with the inspiratory threshold valve,” *Anesth Analg,* vol. 92, no. 4, pp. 967-74, 2001.

[76] C. McCaul, A. Kornecki, D. Engelberts, P. McNamara, and B. P. Kavanagh, “Positive end-expiratory pressure improves survival in a rodent model of cardiopulmonary resuscitation using high-dose epinephrine,” *Anesthesia and Analgesia,* vol. 109, no. 4, pp. 1202-1208, 2009.

[77] Z. G. Hevesi, D. N. Thrush, J. B. Downs, and R. A. Smith, “Cardiopulmonary resuscitation: effect of CPAP on gas exchange during chest compressions,” *Anesthesiology,* vol. 90, no. 4, pp. 1078-83, 1999.

[78] J. M. Saïssy, G. Boussignac, E. Cheptel, B. Rouvin, D. Fontaine, L. Bargues, J. P. Levecque, A. Michel, and L. Brochard, “Efficacy of continuous insufflation of oxygen combined with active cardiac compression-decompression during out-of-hospital cardiorespiratory arrest,” *Anesthesiology,* vol. 92, no. 6, pp. 1523-30, 2000.

[79] C. Bertrand, F. Hemery, P. Carli, P. Goldstein, C. Espesson, M. Rüttimann, J. M. Macher, B. Raffy, P. Fuster, F. Dolveck, A. Rozenberg, E. Lecarpentier, P. Duvaldestin, J. M. Saissy, G. Boussignac, and L. Brochard, “Constant flow insufflation of oxygen as the sole mode of ventilation during out-of-hospital cardiac arrest,” *Intensive Care Med,* vol. 32, no. 6, pp. 843-51, 2006.

[80] J. C. Moore, L. Lamhaut, A. Hutin, K. W. Dodd, A. E. Robinson, M. C. Lick, B. J. Salverda, M. B. Hinke, J. Labarere, G. Debaty, and N. Segal, “Evaluation of the Boussignac Cardiac arrest device (B-card) during cardiopulmonary resuscitation in an animal model,” *Resuscitation,* vol. 119, pp. 81-88, 2017.

[81] J. R. Benger, K. Kirby, S. Black, S. J. Brett, M. Clout, M. J. Lazaroo, J. P. Nolan, B. C. Reeves, M. Robinson, L. J. Scott, H. Smartt, A. South, E. A. Stokes, J. Taylor, M. Thomas, S. Voss, S. Wordsworth, and C. A. Rogers, “Effect of a Strategy of a Supraglottic Airway Device vs Tracheal Intubation During Out-of-Hospital Cardiac Arrest on Functional Outcome: The AIRWAYS-2 Randomized Clinical Trial,” *Jama,* vol. 320, no. 8, pp. 779-791, 2018.

[82] L. White, T. Melhuish, R. Holyoak, T. Ryan, H. Kempton, and R. Vlok, “Advanced airway management in out of hospital cardiac arrest: A systematic review and meta-analysis,” *American Journal of Emergency Medicine,* vol. 36, no. 12, pp. 2298-2306, 2018.

[83] H. E. Wang, R. H. Schmicker, M. R. Daya, S. W. Stephens, A. H. Idris, J. N. Carlson, M. R. Colella, H. Herren, M. Hansen, N. J. Richmond, J. C. J. Puyana, T. P. Aufderheide, R. E. Gray, P. C. Gray, M. Verkest, P. C. Owens, A. M. Brienza, K. J. Sternig, S. J. May, G. R. Sopko, M. L. Weisfeldt, and G. Nichol, “Effect of a Strategy of Initial Laryngeal Tube Insertion vs Endotracheal Intubation on 72-Hour Survival in Adults With Out-of-Hospital Cardiac Arrest: A Randomized Clinical Trial,” *Jama,* vol. 320, no. 8, pp. 769-778, 2018.

[84] P. Jabre, A. Penaloza, D. Pinero, F. X. Duchateau, S. W. Borron, F. Javaudin, O. Richard, D. de Longueville, G. Bouilleau, M. L. Devaud, M. Heidet, C. Lejeune, S. Fauroux, J. L. Greingor, A. Manara, J. C. Hubert, B. Guihard, O. Vermylen, P. Lievens, Y. Auffret, C. Maisondieu, S. Huet, B. Claessens, F. Lapostolle, N. Javaud, P. G. Reuter, E. Baker, E. Vicaut, and F. Adnet, “Effect of Bag-Mask Ventilation vs Endotracheal Intubation During Cardiopulmonary Resuscitation on Neurological Outcome After Out-of-Hospital Cardiorespiratory Arrest: A Randomized Clinical Trial,” *Jama,* vol. 319, no. 8, pp. 779-787, 2018.

[85] S. S. Gul, S. A. Cohen, K. L. Avery, M. P. Balakrishnan, R. Balu, M. A. B. Chowdhury, D. Crabb, K. W. Huesgen, C. W. Hwang, C. B. Maciel, T. W. Murphy, F. Han, and T. K. Becker, “Cardiac arrest: An interdisciplinary review of the literature from 2018,” *Resuscitation,* vol. 148, pp. 66-82, 2020.

[86] C. Sandroni, M. B. Skrifvars, and J. Soar, “Vasopressors, antiarrhythmics, oxygen, and intubation in out-of-hospital cardiac arrest: possibly less is more,” *Intensive Care Med,* vol. 45, no. 10, pp. 1454-1458, 2019.

[87] H. Kempton, R. Vlok, C. Thang, T. Melhuish, and L. White, “Standard dose epinephrine versus placebo in out of hospital cardiac arrest: A systematic review and meta-analysis,” *American Journal of Emergency Medicine,* vol. 37, no. 3, pp. 511-517, 2019.

[88] G. D. Perkins, C. Ji, C. D. Deakin, T. Quinn, J. P. Nolan, C. Scomparin, S. Regan, J. Long, A. Slowther, H. Pocock, J. J. M. Black, F. Moore, R. T. Fothergill, N. Rees, L. O'Shea, M. Docherty, I. Gunson, K. Han, K. Charlton, J. Finn, S. Petrou, N. Stallard, S. Gates, and R. Lall, “A Randomized Trial of Epinephrine in Out-of-Hospital Cardiac Arrest,” *N Engl J Med,* vol. 379, no. 8, pp. 711-721, 2018.

[89] M. W. Hubble, and C. Tyson, “Impact of Early Vasopressor Administration on Neurological Outcomes after Prolonged Out-of-Hospital Cardiac Arrest,” *Prehosp Disaster Med,* vol. 32, no. 3, pp. 297-304, 2017.

[90] G. D. Perkins, C. Kenna, C. Ji, C. D. Deakin, J. P. Nolan, T. Quinn, C. Scomparin, R. Fothergill, I. Gunson, H. Pocock, N. Rees, L. O'Shea, J. Finn, S. Gates, and R. Lall, “The influence of time to adrenaline administration in the Paramedic 2 randomised controlled trial,” *Intensive Care Med,* vol. 46, no. 3, pp. 426-436, 2020.

[91] J. P. Nolan, C. D. Deakin, C. Ji, S. Gates, A. Rosser, R. Lall, and G. D. Perkins, “Intraosseous versus intravenous administration of adrenaline in patients with out-of-hospital cardiac arrest: a secondary analysis of the PARAMEDIC2 placebo-controlled trial,” *Intensive Care Med,* vol. 46, no. 5, pp. 954-962, 2020.

[92] R. T. Fothergill, A. C. Emmerson, R. Iyer, J. Lazarus, M. Whitbread, J. P. Nolan, C. D. Deakin, and G. D. Perkins, “Repeated adrenaline doses and survival from an out-of-hospital cardiac arrest,” *Resuscitation,* vol. 138, pp. 316-321, 2019.

[93] W. Yan, W. Dong, X. Song, W. Zhou, and Z. Chen, “Therapeutic effects of vasopressin on cardiac arrest: a systematic review and meta-analysis,” *BMJ Open,* vol. 13, no. 4, pp. e065061, 2023.

[94] P. J. Kudenchuk, S. P. Brown, M. Daya, T. Rea, G. Nichol, L. J. Morrison, B. Leroux, C. Vaillancourt, L. Wittwer, C. W. Callaway, J. Christenson, D. Egan, J. P. Ornato, M. L. Weisfeldt, I. G. Stiell, A. H. Idris, T. P. Aufderheide, J. V. Dunford, M. R. Colella, G. M. Vilke, A. M. Brienza, P. Desvigne-Nickens, P. C. Gray, R. Gray, N. Seals, R. Straight, and P. Dorian, “Amiodarone, Lidocaine, or Placebo in Out-of-Hospital Cardiac Arrest,” *N Engl J Med,* vol. 374, no. 18, pp. 1711-22, 2016.

[95] M. S. Sekhon, P. N. Ainslie, and D. E. Griesdale, “Clinical pathophysiology of hypoxic ischemic brain injury after cardiac arrest: a "two-hit" model,” *Crit Care,* vol. 21, no. 1, pp. 90, 2017.

[96] J. C. Jentzer, M. D. Chonde, and C. Dezfulian, “Myocardial Dysfunction and Shock after Cardiac Arrest,” *Biomed Res Int,* vol. 2015, pp. 314796, 2015.

[97] A. Binks, and J. P. Nolan, “Post-cardiac arrest syndrome,” *Minerva Anestesiol,* vol. 76, no. 5, pp. 362-8, 2010.

[98] A. Mangla, M. R. Daya, and S. Gupta, “Post-resuscitation care for survivors of cardiac arrest,” *Indian heart journal,* vol. 66 Suppl 1, no. Suppl 1, pp. S105-S112, 2014.

[99] R. Khera, S. CarlLee, A. Blevins, M. Schweizer, and S. Girotra, “Early coronary angiography and survival after out-of-hospital cardiac arrest: a systematic review and meta-analysis,” *Open Heart,* vol. 5, no. 2, pp. e000809, 2018.

[100] J. E. Bray, K. Smith, C. Hein, J. Finn, M. Stephenson, P. Cameron, D. Stub, G. D. Perkins, H. Grantham, P. Bailey, D. Brink, N. Dodge, and S. Bernard, “The EXACT protocol: A multi-centre, single-blind, randomised, parallel-group, controlled trial to determine whether early oxygen titration improves survival to hospital discharge in adult OHCA patients,” *Resuscitation,* vol. 139, pp. 208-213, 2019.

[101] J. H. Kilgannon, A. E. Jones, N. I. Shapiro, M. G. Angelos, B. Milcarek, K. Hunter, J. E. Parrillo, and S. Trzeciak, “Association between arterial hyperoxia following resuscitation from cardiac arrest and in-hospital mortality,” *Jama,* vol. 303, no. 21, pp. 2165-71, 2010.

[102] J. Pilcher, M. Weatherall, P. Shirtcliffe, R. Bellomo, P. Young, and R. Beasley, “The effect of hyperoxia following cardiac arrest - A systematic review and meta-analysis of animal trials,” *Resuscitation,* vol. 83, no. 4, pp. 417-22, 2012.

[103] C. H. Wang, W. T. Chang, C. H. Huang, M. S. Tsai, P. H. Yu, A. Y. Wang, N. C. Chen, and W. J. Chen, “The effect of hyperoxia on survival following adult cardiac arrest: a systematic review and meta-analysis of observational studies,” *Resuscitation,* vol. 85, no. 9, pp. 1142-8, 2014.

[104] H. E. Wang, D. K. Prince, I. R. Drennan, B. Grunau, D. J. Carlbom, N. Johnson, M. Hansen, J. Elmer, J. Christenson, P. Kudenchuk, T. Aufderheide, M. Weisfeldt, A. Idris, S. Trzeciak, M. Kurz, J. C. Rittenberger, D. Griffiths, J. Jasti, S. May, and I. Resuscitation Outcomes Consortium, “Post-resuscitation arterial oxygen and carbon dioxide and outcomes after out-of-hospital cardiac arrest,” *Resuscitation,* vol. 120, pp. 113-118, 2017.

[105] P. Jakkula, V. Pettilä, M. B. Skrifvars, J. Hästbacka, P. Loisa, M. Tiainen, E. Wilkman, J. Toppila, T. Koskue, S. Bendel, T. Birkelund, R. Laru-Sompa, M. Valkonen, and M. Reinikainen, “Targeting low-normal or high-normal mean arterial pressure after cardiac arrest and resuscitation: a randomised pilot trial,” *Intensive Care Med,* vol. 44, no. 12, pp. 2091-2101, 2018.

[106] P. Jakkula, M. Reinikainen, J. Hästbacka, P. Loisa, M. Tiainen, V. Pettilä, J. Toppila, M. Lähde, M. Bäcklund, M. Okkonen, S. Bendel, T. Birkelund, A. Pulkkinen, J. Heinonen, T. Tikka, and M. B. Skrifvars, “Targeting two different levels of both arterial carbon dioxide and arterial oxygen after cardiac arrest and resuscitation: a randomised pilot trial,” *Intensive Care Med,* vol. 44, no. 12, pp. 2112-2121, 2018.

[107] K. Ameloot, C. De Deyne, W. Eertmans, B. Ferdinande, M. Dupont, P. J. Palmers, T. Petit, P. Nuyens, J. Maeremans, J. Vundelinckx, M. Vanhaverbeke, A. Belmans, R. Peeters, P. Demaerel, R. Lemmens, J. Dens, and S. Janssens, “Early goal-directed haemodynamic optimization of cerebral oxygenation in comatose survivors after cardiac arrest: the Neuroprotect post-cardiac arrest trial,” *Eur Heart J,* vol. 40, no. 22, pp. 1804-1814, 2019.

[108] M. Abdalla, A. Mohamed, W. Mohamed, K. Khtab, H. Cattoni, and M. Salih, “Targeted temperature management after cardiac arrest: Updated meta-analysis of all-cause mortality and neurological outcomes,” *IJC Heart & Vasculature,* vol. 24, pp. 100400, 2019.

[109] R. Kalra, G. Arora, N. Patel, R. Doshi, L. Berra, P. Arora, and N. S. Bajaj, “Targeted Temperature Management After Cardiac Arrest: Systematic Review and Meta-analyses,” *Anesth Analg,* vol. 126, no. 3, pp. 867-875, 2018.

[110] C. H. V. Duez, A. M. Grejs, A. N. Jeppesen, A. D. Schrøder, E. Søreide, J. F. Nielsen, and H. Kirkegaard, “Neuron-specific enolase and S-100b in prolonged targeted temperature management after cardiac arrest: A randomised study,” *Resuscitation,* vol. 122, pp. 79-86, 2018.

[111] E. Lopez-de-Sa, M. Juarez, E. Armada, J. C. Sanchez-Salado, P. L. Sanchez, P. Loma-Osorio, A. Sionis, M. C. Monedero, M. Martinez-Sellés, J. C. Martín-Benitez, A. Ariza, A. Uribarri, J. M. Garcia-Acuña, P. Villa, P. J. Perez, C. Storm, A. Dee, and J. L. Lopez-Sendon, “A multicentre randomized pilot trial on the effectiveness of different levels of cooling in comatose survivors of out-of-hospital cardiac arrest: the FROST-I trial,” *Intensive Care Med,* vol. 44, no. 11, pp. 1807-1815, 2018.

[112] A. Padkin, “Glucose control after cardiac arrest,” *Resuscitation,* vol. 80, no. 6, pp. 611-612, 2009.

[113] C. Sasson, M. A. M. Rogers, J. Dahl, and A. L. Kellermann, “Predictors of survival from out-of-hospital cardiac arrest a systematic review and meta-analysis,” *Circulation: Cardiovascular Quality and Outcomes,* vol. 3, no. 1, pp. 63-81, 2010.

[114] E. F. Paiva, J. H. Paxton, and B. J. O'Neil, “The use of end-tidal carbon dioxide (ETCO2) measurement to guide management of cardiac arrest: A systematic review,” *Resuscitation,* vol. 123, pp. 1-7, 2018.

[115] S. Schnaubelt, P. Sulzgruber, J. Menger, K. Skhirtladze-Dworschak, F. Sterz, and M. Dworschak, “Regional cerebral oxygen saturation during cardiopulmonary resuscitation as a predictor of return of spontaneous circulation and favourable neurological outcome - A review of the current literature,” *Resuscitation,* vol. 125, pp. 39-47, 2018.

[116] T. Boucek, M. Mlcek, P. Krupickova, M. Huptych, T. Belza, O. Kittnar, A. Linhart, and J. Belohlavek, “Brain perfusion evaluated by regional tissue oxygenation as a possible quality indicator of ongoing cardiopulmonary resuscitation. An experimental porcine cardiac arrest study,” *Perfusion,* vol. 33, no. 1_suppl, pp. 65-70, 2018.

[117] I. Kedan, W. Ciozda, J. A. Palatinus, H. N. Palatinus, and A. Kimchi, “Prognostic value of point-of-care ultrasound during cardiac arrest: a systematic review,” *Cardiovasc Ultrasound,* vol. 18, no. 1, pp. 1, 2020.

[118] K. S. Han, S. J. Kim, E. J. Lee, K. Y. Park, J. Y. Lee, and S. W. Lee, “Impact of rapid lactate clearance as an indicator of hemodynamic optimization on outcome in out-of-hospital cardiac arrest: A retrospective analysis,” *PloS one,* vol. 14, no. 4, pp. e0214547-e0214547, 2019.

[119] S. D'Arrigo, S. Cacciola, M. Dennis, C. Jung, E. Kagawa, M. Antonelli, and C. Sandroni, “Predictors of favourable outcome after in-hospital cardiac arrest treated with extracorporeal cardiopulmonary resuscitation: A systematic review and meta-analysis,” *Resuscitation,* vol. 121, pp. 62-70, 2017.

[120] B.-C. Zhou, Z. Zhang, J.-J. Zhu, L.-J. Liu, and C.-F. Liu, “Blood Lactate or Lactate Clearance: Which Is Robust to Predict the Neurological Outcomes after Cardiac Arrest? A Systematic Review and Meta-Analysis,” *BioMed research international,* vol. 2018, pp. 8014213-8014213, 2018.

[121] J. During, J. Dankiewicz, T. Cronberg, C. Hassager, J. Hovdenes, J. Kjaergaard, M. Kuiper, N. Nielsen, T. Pellis, P. Stammet, J. Vulto, M. Wanscher, M. Wise, A. Aneman, and H. Friberg, “Lactate, lactate clearance and outcome after cardiac

arrest: A post-hoc analysis of the TTM-Trial," *Acta Anaesthesiol Scand,* vol. 62, no. 10, pp. 1436-1442, 2018.

[122] A. J. Lautz, R. W. Morgan, M. Karlsson, C. D. Mavroudis, T. S. Ko, D. J. Licht, V. M. Nadkarni, R. A. Berg, R. M. Sutton, and T. J. Kilbaugh, "Hemodynamic-Directed Cardiopulmonary Resuscitation Improves Neurologic Outcomes and Mitochondrial Function in the Heart and Brain," *Crit Care Med,* vol. 47, no. 3, pp. e241-e249, 2019.

[123] J. Soar, I. Maconochie, M. H. Wyckoff, T. M. Olasveengen, E. M. Singletary, R. Greif, R. Aickin, F. Bhanji, M. W. Donnino, M. E. Mancini, J. P. Wyllie, D. Zideman, L. W. Andersen, D. L. Atkins, K. Aziz, J. Bendall, K. M. Berg, D. C. Berry, B. L. Bigham, R. Bingham, T. B. Couto, B. W. Böttiger, V. Borra, J. E. Bray, J. Breckwoldt, S. C. Brooks, J. Buick, C. W. Callaway, J. N. Carlson, P. Cassan, M. Castrén, W. T. Chang, N. P. Charlton, A. Cheng, S. P. Chung, J. Considine, K. Couper, K. N. Dainty, J. A. Dawson, M. F. de Almeida, A. R. de Caen, C. D. Deakin, I. R. Drennan, J. P. Duff, J. L. Epstein, R. Escalante, R. J. Gazmuri, E. Gilfoyle, A. Granfeldt, A. M. Guerguerian, R. Guinsburg, T. Hatanaka, M. J. Holmberg, N. Hood, S. Hosono, M. J. Hsieh, T. Isayama, T. Iwami, J. L. Jensen, V. Kapadia, H. S. Kim, M. E. Kleinman, P. J. Kudenchuk, E. Lang, E. Lavonas, H. Liley, S. H. Lim, A. Lockey, B. Lofgren, M. H. Ma, D. Markenson, P. A. Meaney, D. Meyran, L. Mildenhall, K. G. Monsieurs, W. Montgomery, P. T. Morley, L. J. Morrison, V. M. Nadkarni, K. Nation, R. W. Neumar, K. C. Ng, T. Nicholson, N. Nikolaou, C. Nishiyama, G. Nuthall, S. Ohshimo, D. Okamoto, B. O'Neil, G. Yong-Kwang Ong, E. F. Paiva, M. Parr, J. L. Pellegrino, G. D. Perkins, J. Perlman, Y. Rabi, A. Reis, J. C. Reynolds, G. Ristagno, C. C. Roehr, T. Sakamoto, C. Sandroni, S. M. Schexnayder, B. R. Scholefield, N. Shimizu, M. B. Skrifvars, M. A. Smyth, D. Stanton, J. Swain, E. Szyld, J. Tijssen, A. Travers, D. Trevisanuto, C. Vaillancourt, P. Van de Voorde, S. Velaphi, T. L. Wang, G. Weiner, M. Welsford, J. A. Woodin, J. Yeung, J. P. Nolan, and M. Fran Hazinski, "2019 International Consensus on Cardiopulmonary Resuscitation and Emergency Cardiovascular Care Science With Treatment Recommendations: Summary From the Basic Life Support; Advanced Life Support; Pediatric Life Support; Neonatal Life Support; Education, Implementation, and Teams; and First Aid Task Forces," *Circulation,* vol. 140, no. 24, pp. e826-e880, 2019.

[124] F. Kramer, S. Just, and T. Zeller, "New perspectives: systems medicine in cardiovascular disease," *BMC Systems Biology,* vol. 12, no. 1, pp. 57, 2018.

[125] C. R. Hooijmans, A. Tillema, M. Leenaars, and M. Ritskes-Hoitinga, "Enhancing search efficiency by means of a search filter for finding all studies on animal experimentation in PubMed," *Laboratory animals,* vol. 44, no. 3, pp. 170-175, 2010.

[126] P. Camacho, H. Fan, Z. Liu, and J.-Q. He, "Large Mammalian Animal Models of Heart Disease," *Journal of cardiovascular development and disease,* vol. 3, no. 4, pp. 30, 2016.

[127] M. Vognsen, B. K. Fabian-Jessing, N. Secher, B. Lofgren, C. Dezfulian, L. W. Andersen, and A. Granfeldt, "Contemporary animal models of cardiac arrest: A systematic review," *Resuscitation,* vol. 113, pp. 115-123, 2017.

[128] C. Gu, and J. C. Jun, "Does Hypoxia Decrease the Metabolic Rate?," *Frontiers in endocrinology,* vol. 9, pp. 668-668, 2018.

[129] E. P. Judge, J. M. Hughes, J. J. Egan, M. Maguire, E. L. Molloy, and S. O'Dea, "Anatomy and bronchoscopy of the porcine lung. A model for translational respiratory medicine," *Am J Respir Cell Mol Biol,* vol. 51, no. 3, pp. 334-43, 2014.

[130] A. Islam, S. E. Kim, J. C. Yoon, A. Jawad, W. Tian, Y. J. Yoo, I. S. Kim, D. Ahn, B. Y. Park, Y. Hwang, J. H. Lee, H. J. Tae, J. H. Cho, and K. Kim, "Protective effects of

therapeutic hypothermia on renal injury in an asphyxial cardiac arrest rat model," *J Therm Biol,* vol. 94, pp. 102761, 2020.

[131] S. Cheruku, S. Dave, K. Goff, C. Park, C. Ebeling, L. Cohen, K. Styrvoky, C. Choi, V. Anand, and C. Kershaw, "Cardiopulmonary Resuscitation in Intensive Care Unit Patients With Coronavirus Disease 2019," *Journal of cardiothoracic and vascular anesthesia,* vol. 34, no. 10, pp. 2595-2603, 2020.

[132] E. Boissady, M. Kohlhauer, F. Lidouren, H. Hocini, C. Lefebvre, S. Chateau-Jouber, N. Mongardon, N. Deye, A. Cariou, P. Micheau, B. Ghaleh, and R. Tissier, "Ultrafast Hypothermia Selectively Mitigates the Early Humoral Response After Cardiac Arrest," *J Am Heart Assoc,* vol. 9, no. 23, pp. e017413, 2020.

[133] M. Y. Diao, J. Zheng, Y. Shan, S. Xi, Y. Zhu, W. Hu, and Z. Lin, "Hypothermia prevents hippocampal oxidative stress and apoptosis via the GSK-3β/Nrf2/HO-1 signaling pathway in a rat model of cardiac arrest-induced brain damage," *Neurol Res,* vol. 42, no. 9, pp. 773-782, 2020.

[134] Y. Hu, D. Sun, Y. Li, X. Wang, W. Jiang, H. Shi, and D. Cui, "Increased PINK1/Parkin-mediated mitophagy explains the improved brain protective effects of slow rewarming following hypothermia after cardiac arrest in rats," *Exp Neurol,* vol. 330, pp. 113326, 2020.

[135] B. Zhang, Q. Gu, X. Chen, Y. You, M. Chen, Y. Qian, Y. Chen, and W. Yu, "Temperature Variability Does Not Attenuate the Beneficial Effects of Therapeutic Hypothermia on Cellular Apoptosis and Endoplasmic Reticulum Stress in the Cerebral Cortex of a Swine Cardiac Arrest Model," *Neurocrit Care,* vol. 34, no. 3, pp. 769-780, 2021.

[136] K. Skok, M. Duh, A. Stožer, A. Markota, and M. Gosak, "Thermoregulation: A journey from physiology to computational models and the intensive care unit," *Wiley Interdiscip Rev Syst Biol Med*, pp. e1513, 2020.

[137] B. K. Fabian-Jessing, M. F. Vallentin, N. Secher, F. B. Hansen, C. Dezfulian, A. Granfeldt, and L. W. Andersen, "Animal models of cardiac arrest: A systematic review of bias and reporting," *Resuscitation,* vol. 125, pp. 16-21, 2018.

[138] L. P. Freedman, I. M. Cockburn, and T. S. Simcoe, "The Economics of Reproducibility in Preclinical Research," *PLoS biology,* vol. 13, no. 6, pp. e1002165-e1002165, 2015.

[139] A. Santiago, J. Aguado-Sierra, M. Zavala-Ake, R. Doste-Beltran, S. Gomez, R. Aris, J. C. Cajas, E. Casoni, and M. Vazquez, "Fully coupled fluid-electro-mechanical model of the human heart for supercomputers," *Int J Numer Method Biomed Eng,* vol. 34, no. 12, pp. e3140, 2018.

[140] K. Sagawa, R. K. Lie, and J. Schaefer, "Translation of Otto Frank's paper "Die Grundform des Arteriellen Pulses" Zeitschrift für Biologie 37: 483-526 (1899)," *J Mol Cell Cardiol,* vol. 22, no. 3, pp. 253-4, 1990.

[141] A. C. Guyton, T. G. Coleman, and H. J. Granger, "Circulation: overall regulation," *Annu Rev Physiol,* vol. 34, pp. 13-46, 1972.

[142] C. F. Babbs, J. C. Weaver, S. H. Ralston, and L. A. Geddes, "Cardiac, thoracic, and abdominal pump mechanisms in cardiopulmonary resuscitation: studies in an electrical model of the circulation," *Am J Emerg Med,* vol. 2, no. 4, pp. 299-308, 1984.

[143] C. F. Babbs, “Relative effectiveness of interposed abdominal compression CPR: sensitivity analysis and recommended compression rates,” *Resuscitation,* vol. 66, no. 3, pp. 347-55, 2005.

[144] Y. Zhang, and J. M. Karemaker, “Abdominal counter pressure in CPR: what about the lungs? An in silico study,” *Resuscitation,* vol. 83, no. 10, pp. 1271-6, 2012.

[145] C. F. Babbs, “CPR techniques that combine chest and abdominal compression and decompression: hemodynamic insights from a spreadsheet model,” *Circulation,* vol. 100, no. 21, pp. 2146-52, 1999.

[146] C. F. Babbs, “Efficacy of interposed abdominal compression-cardiopulmonary resuscitation (CPR), active compression and decompression-CPR and Lifestick CPR: basic physiology in a spreadsheet model,” *Crit Care Med,* vol. 28, no. 11 Suppl, pp. N199-202, 2000.

[147] C. F. Babbs, “Design of near-optimal waveforms for chest and abdominal compression and decompression in CPR using computer-simulated evolution,” *Resuscitation,* vol. 68, no. 2, pp. 277-93, 2006.

[148] C. F. Babbs, “Effects of an impedance threshold valve upon hemodynamics in Standard CPR: studies in a refined computational model,” *Resuscitation,* vol. 66, no. 3, pp. 335-45, 2005.

[149] C. F. Babbs, and D. Yannopoulos, “A dose-response curve for the negative bias pressure of an intrathoracic pressure regulator during CPR,” *Resuscitation,* vol. 71, no. 3, pp. 365-8, 2006.

[150] D. A. Shin, J. Park, J. C. Lee, S. D. Shin, and H. C. Kim, “Computational simulation of passive leg-raising effects on hemodynamics during cardiopulmonary resuscitation,” *Comput Methods Programs Biomed,* vol. 140, pp. 195-200, 2017.

[151] Y. Zhang, M. Jiménez-Herrera, C. Axelsson, and Y. Cheng, “Not Bad: Passive Leg Raising in Cardiopulmonary Resuscitation-A New Modeling Study,” *Front Physiol,* vol. 7, pp. 665, 2016.

[152] C. F. Babbs, “Biophysics of cardiopulmonary resuscitation with periodic z-axis acceleration or abdominal compression at aortic resonant frequencies,” *Resuscitation,* vol. 69, no. 3, pp. 455-69, 2006.

[153] C. F. Babbs, and K. B. Kern, “Optimum compression to ventilation ratios in CPR under realistic, practical conditions: a physiological and mathematical analysis,” *Resuscitation,* vol. 54, no. 2, pp. 147-57, 2002.

[154] C. F. Babbs, and V. Nadkarni, “Optimizing chest compression to rescue ventilation ratios during one-rescuer CPR by professionals and lay persons: children are not just little adults,” *Resuscitation,* vol. 61, no. 2, pp. 173-81, 2004.

[155] J. R. Fitz-Clarke, “Effect of tidal volume on gas exchange during rescue ventilation,” *Respir Physiol Neurobiol,* vol. 273, pp. 103335, 2020.

[156] J. M. Boe, and C. F. Babbs, “Mechanics of cardiopulmonary resuscitation performed with the patient on a soft bed vs a hard surface,” *Acad Emerg Med,* vol. 6, no. 7, pp. 754-7, 1999.

[157] E. Jung, C. F. Babbs, S. Lenhart, and V. A. Protopopescu, “Optimal strategy for cardiopulmonary resuscitation with continuous chest compression,” *Acad Emerg Med,* vol. 13, no. 7, pp. 715-21, 2006.

[158] E. Jung, S. Lenhart, V. Protopopescu, and C. Babbs, “Optimal control applied to a thoraco-abdominal CPR model,” *Math Med Biol,* vol. 25, no. 2, pp. 157-70, 2008.

[159] A. R. John, M. Manivannan, and T. V. Ramakrishnan, “Computer-Based CPR Simulation Towards Validation of AHA/ERC Guidelines,” *Cardiovasc Eng Technol,* vol. 8, no. 2, pp. 229-235, 2017.

[160] C. F. Babbs, A. Meyer, and V. Nadkarni, “Neonatal CPR: room at the top--a mathematical study of optimal chest compression frequency versus body size,” *Resuscitation,* vol. 80, no. 11, pp. 1280-4, 2009.

[161] G. J. Noordergraaf, T. J. Dijkema, W. J. P. M. Kortsmit, W. H. A. Schilders, G. J. Scheffer, and A. Noordergraaf, “Modeling in Cardiopulmonary Resuscitation: Pumping the Heart,” *Cardiovascular Engineering,* vol. 5, no. 3, pp. 105-118, 2005.

[162] D. A. Shin, and J. C. Lee, “Mathematical model of modified hybrid pump mechanism for cardiopulmonary resuscitation,” *Comput Methods Programs Biomed,* vol. 206, pp. 106106, Apr 18, 2021.

[163] N. Biller-Andorno, A. Ferrario, S. Joebges, T. Krones, F. Massini, P. Barth, G. Arampatzis, and M. Krauthammer, “AI support for ethical decision-making around resuscitation: proceed with care,” *J Med Ethics*, 2021.

[164] S. N. Bose, A. Verigan, J. Hanson, L. M. Ahumada, S. R. Ghazarian, N. A. Goldenberg, A. Stock, and J. P. Jacobs, “Early identification of impending cardiac arrest in neonates and infants in the cardiovascular ICU: a statistical modelling approach using physiologic monitoring data,” *Cardiol Young,* vol. 29, no. 11, pp. 1340-1348, 2019.

[165] C. E. Kennedy, N. Aoki, M. Mariscalco, and J. P. Turley, “Using Time Series Analysis to Predict Cardiac Arrest in a PICU,” *Pediatr Crit Care Med,* vol. 16, no. 9, pp. e332-9, 2015.

[166] J. Kim, M. Chae, H. J. Chang, Y. A. Kim, and E. Park, “Predicting Cardiac Arrest and Respiratory Failure Using Feasible Artificial Intelligence with Simple Trajectories of Patient Data,” *J Clin Med,* vol. 8, no. 9, 2019.

[167] F. Meng, Z. Zhang, X. Hou, Z. Qian, Y. Wang, Y. Chen, Y. Wang, Y. Zhou, Z. Chen, X. Zhang, J. Yang, J. Zhang, J. Guo, K. Li, L. Chen, R. Zhuang, H. Jiang, W. Zhou, S. Tang, Y. Wei, and J. Zou, “Machine learning for prediction of sudden cardiac death in heart failure patients with low left ventricular ejection fraction: study protocol for a retroprospective multicentre registry in China,” *BMJ Open,* vol. 9, no. 5, pp. e023724, 2019.

[168] R. Ueno, L. Xu, W. Uegami, H. Matsui, J. Okui, H. Hayashi, T. Miyajima, Y. Hayashi, D. Pilcher, and D. Jones, “Value of laboratory results in addition to vital signs in a machine learning algorithm to predict in-hospital cardiac arrest: A single-center retrospective cohort study,” *PLoS One,* vol. 15, no. 7, pp. e0235835, 2020.

[169] D. H. Jang, J. Kim, Y. H. Jo, J. H. Lee, J. E. Hwang, S. M. Park, D. K. Lee, I. Park, D. Kim, and H. Chang, “Developing neural network models for early detection of cardiac arrest in emergency department,” *Am J Emerg Med,* vol. 38, no. 1, pp. 43-49, 2020.

[170] A. Elola, E. Aramendi, E. Rueda, U. Irusta, H. Wang, and A. Idris, “Towards the Prediction of Rearrest during Out-of-Hospital Cardiac Arrest,” *Entropy (Basel),* vol. 22, no. 7, 2020.

[171] L. H. van Dongen, P. P. Harms, M. Hoogendoorn, D. S. Zimmerman, E. M. Lodder, L. M. t Hart, R. Herings, H. van Weert, G. Nijpels, K. M. A. Swart, A. A. van der

Heijden, M. T. Blom, P. J. Elders, and H. L. Tan, “Discovery of predictors of sudden cardiac arrest in diabetes: rationale and outline of the RESCUED (REcognition of Sudden Cardiac arrest vUlnErability in Diabetes) project,” *Open Heart,* vol. 8, no. 1, 2021.

[172] M. M. Churpek, T. C. Yuen, C. Winslow, D. O. Meltzer, M. W. Kattan, and D. P. Edelson, “Multicenter Comparison of Machine Learning Methods and Conventional Regression for Predicting Clinical Deterioration on the Wards,” *Crit Care Med,* vol. 44, no. 2, pp. 368-74, 2016.

[173] T. Tsuji, T. Nobukawa, A. Mito, H. Hirano, Z. Soh, R. Inokuchi, E. Fujita, Y. Ogura, S. Kaneko, R. Nakamura, N. Saeki, M. Kawamoto, and M. Yoshizumi, “Recurrent probabilistic neural network-based short-term prediction for acute hypotension and ventricular fibrillation,” *Sci Rep,* vol. 10, no. 1, pp. 11970, 2020.

[174] S. K, S. V, A. G. E, and P. S. K, “Explainable artificial intelligence for heart rate variability in ECG signal,” *Healthc Technol Lett,* vol. 7, no. 6, pp. 146-154, 2020.

[175] K. Kido, N. Ono, M. D. Altaf-Ul-Amin, S. Kanaya, and M. Huang, “The Feasibility of Arrhythmias Detection from A Capacitive ECG Measurement Using Convolutional Neural Network,” *Annu Int Conf IEEE Eng Med Biol Soc,* vol. 2019, pp. 3494-3497, 2019.

[176] Q. Y. Lin, Y. L. Zhang, J. Bai, J. Q. Liu, and H. H. Li, “VEGF-C/VEGFR-3 axis protects against pressure-overload induced cardiac dysfunction through regulation of lymphangiogenesis,” *Clin Transl Med,* vol. 11, no. 3, pp. e374, 2021.

[177] S. Sabut, O. Pandey, B. S. P. Mishra, and M. Mohanty, “Detection of ventricular arrhythmia using hybrid time-frequency-based features and deep neural network,” *Phys Eng Sci Med,* vol. 44, no. 1, pp. 135-145, 2021.

[178] I. Isasi, U. Irusta, E. Aramendi, T. Eftestøl, J. Kramer-Johansen, and L. Wik, “Rhythm Analysis during Cardiopulmonary Resuscitation Using Convolutional Neural Networks,” *Entropy (Basel),* vol. 22, no. 6, 2020.

[179] L. Zhao, Y. Bao, Y. Zhang, R. Ye, and A. Zhang, “Recognition of Abnormal Chest Compression Depth Using One-Dimensional Convolutional Neural Networks,” *Sensors (Basel),* vol. 21, no. 3, 2021.

[180] M. D. Ivanović, J. Hannink, M. Ring, F. Baronio, V. Vukčević, L. Hadžievski, and B. Eskofier, “Predicting defibrillation success in out-of-hospital cardiac arrested patients: Moving beyond feature design,” *Artif Intell Med,* vol. 110, pp. 101963, 2020.

[181] V. Krasteva, S. Ménétré, J. P. Didon, and I. Jekova, “Fully Convolutional Deep Neural Networks with Optimized Hyperparameters for Detection of Shockable and Non-Shockable Rhythms,” *Sensors (Basel),* vol. 20, no. 10, 2020.

[182] S. Jonas, A. O. Rossetti, M. Oddo, S. Jenni, P. Favaro, and F. Zubler, “EEG-based outcome prediction after cardiac arrest with convolutional neural networks: Performance and visualization of discriminative features,” *Hum Brain Mapp,* vol. 40, no. 16, pp. 4606-4617, 2019.

[183] J. Johnsson, O. Björnsson, P. Andersson, A. Jakobsson, T. Cronberg, G. Lilja, H. Friberg, C. Hassager, J. Kjaergard, M. Wise, N. Nielsen, and A. Frigyesi, “Artificial neural networks improve early outcome prediction and risk classification in out-of-hospital cardiac arrest patients admitted to intensive care,” *Crit Care,* vol. 24, no. 1, pp. 474, 2020.

[184] N. Pareek, C. Frohmaier, M. Smith, P. Kordis, A. Cannata, J. Nevett, R. Fothergill, R. C. Nichol, M. Sullivan, N. Sunderland, T. W. Johnson, M. Noc, J. Byrne, P. MacCarthy, and A. M. Shah, “A machine learning algorithm to predict a culprit lesion after out of hospital cardiac arrest,” *Catheter Cardiovasc Interv,* vol. 102, no. 1, pp. 80-90, Jul, 2023.

[185] T. B. Tanner, and S. Gitlow, “A computer simulation of cardiac emergencies,” *Proc Annu Symp Comput Appl Med Care*, pp. 894-6, 1991.

[186] F. J. García Fierros, J. J. Moreno Escobar, G. Sepúlveda Cervantes, O. Morales Matamoros, and R. Tejeida Padilla, “Virtual(CPR): Virtual Reality Mobile Application for Training in Cardiopulmonary Resuscitation Techniques,” *Sensors (Basel),* vol. 21, no. 7, 2021.

[187] P. L. Ingrassia, G. Mormando, E. Giudici, F. Strada, F. Carfagna, F. Lamberti, and A. Bottino, “Augmented Reality Learning Environment for Basic Life Support and Defibrillation Training: Usability Study,” *J Med Internet Res,* vol. 22, no. 5, pp. e14910, 2020.

[188] F. Jaskiewicz, D. Kowalewski, K. Starosta, M. Cierniak, and D. Timler, “Chest compressions quality during sudden cardiac arrest scenario performed in virtual reality: A crossover study in a training environment,” *Medicine (Baltimore),* vol. 99, no. 48, pp. e23374, 2020.

[189] M. A. Rushton, I. A. Drumm, S. P. Campion, and J. J. O'Hare, “The Use of Immersive and Virtual Reality Technologies to Enable Nursing Students to Experience Scenario-Based, Basic Life Support Training-Exploring the Impact on Confidence and Skills,” *Comput Inform Nurs,* vol. 38, no. 6, pp. 281-293, 2020.

[190] B. Amuzescu, R. Airini, F. B. Epureanu, S. A. Mann, T. Knott, and B. M. Radu, “Evolution of mathematical models of cardiomyocyte electrophysiology,” *Math Biosci,* vol. 334, pp. 108567, 2021.

[191] F. O. Campos, J. Whitaker, R. Neji, S. Roujol, M. O’Neill, G. Plank, and M. J. Bishop, “Factors Promoting Conduction Slowing as Substrates for Block and Reentry in Infarcted Hearts,” *Biophysical Journal,* vol. 117, no. 12, pp. 2361-2374, 2019.

[192] G. Balaban, C. M. Costa, B. Porter, B. Halliday, C. A. Rinaldi, S. Prasad, G. Plank, T. F. Ismail, and M. J. Bishop, “3D Electrophysiological Modeling of Interstitial Fibrosis Networks and Their Role in Ventricular Arrhythmias in Non-Ischemic Cardiomyopathy,” *IEEE Transactions on Biomedical Engineering,* vol. 67, no. 11, pp. 3125-3133, 2020.

[193] H. Ashikaga, H. Arevalo, F. Vadakkumpadan, R. C. Blake, 3rd, J. D. Bayer, S. Nazarian, M. Muz Zviman, H. Tandri, R. D. Berger, H. Calkins, D. A. Herzka, N. A. Trayanova, and H. R. Halperin, “Feasibility of image-based simulation to estimate ablation target in human ventricular arrhythmia,” *Heart Rhythm,* vol. 10, no. 8, pp. 1109-16, 2013.

[194] Z. Chen, R. Cabrera-Lozoya, J. Relan, M. Sohal, A. Shetty, R. Karim, H. Delingette, J. Gill, K. Rhode, N. Ayache, P. Taggart, C. A. Rinaldi, M. Sermesant, and R. Razavi, “Biophysical Modeling Predicts Ventricular Tachycardia Inducibility and Circuit Morphology: A Combined Clinical Validation and Computer Modeling Approach,” *J Cardiovasc Electrophysiol,* vol. 27, no. 7, pp. 851-60, 2016.

[195] M. Hwang, C.-H. Lim, C. H. Leem, and E. B. Shim, “In silico models for evaluating proarrhythmic risk of drugs,” *APL Bioengineering,* vol. 4, no. 2, pp. 021502, 2020.

[196] S. M. Kamali Shahri, C. Contarino, F. Chifari, M. Mahmoudi, and S. Gelman, “Function of arteries and veins in conditions of simulated cardiac arrest,” *Bioimpacts,* vol. 11, no. 2, pp. 157-164, 2021.

[197] S. F. Bifulco, N. Akoum, and P. M. Boyle, “Translational applications of computational modelling for patients with cardiac arrhythmias,” *Heart*, 2020.

[198] J. G. Hardman, N. M. Bedforth, A. B. Ahmed, R. P. Mahajan, and A. R. Aitkenhead, “A physiology simulator: validation of its respiratory components and its ability to predict the patient's response to changes in mechanical ventilation,” *Br J Anaesth,* vol. 81, no. 3, pp. 327-332, 1998.

[199] J. G. Hardman, and N. M. Bedforth, “Estimating venous admixture using a physiological simulator,” *Br J Anaesth,* vol. 82, no. 3, pp. 346-9, 1999.

[200] J. G. Hardman, and A. R. Aitkenhead, “Estimation of alveolar deadspace fraction using arterial and end-tidal CO2: a factor analysis using a physiological simulation,” *Anaesth Intensive Care,* vol. 27, no. 5, pp. 452-8, 1999.

[201] J. G. Hardman, and A. R. Aitkenhead, “Validation of an original mathematical model of CO(2) elimination and dead space ventilation,” *Anesth Analg,* vol. 97, no. 6, pp. 1840-5, 2003.

[202] A. Das, Z. Gao, P. P. Menon, J. G. Hardman, and D. G. Bates, “A systems engineering approach to validation of a pulmonary physiology simulator for clinical applications,” *J R Soc Interface,* vol. 8, no. 54, pp. 44-55, 2011.

[203] J. G. Hardman, and J. S. Wills, “The development of hypoxaemia during apnoea in children: a computational modelling investigation,” *Br J Anaesth,* vol. 97, no. 4, pp. 564-70, 2006.

[204] R. A. McCahon, M. O. Columb, R. P. Mahajan, and J. G. Hardman, “Validation and application of a high-fidelity, computational model of acute respiratory distress syndrome to the examination of the indices of oxygenation at constant lung-state,” *Br J Anaesth,* vol. 101, no. 3, pp. 358-65, 2008.

[205] H. M. Al-Otaibi, and J. G. Hardman, “Prediction of Fraction of Inspired Oxygen to Achieve a Desired Arterial Partial Pressure of Oxygen Reply,” *American Journal of Respiratory and Critical Care Medicine,* vol. 185, no. 6, pp. 686-686, 2012.

[206] A. Das, M. Haque, M. Chikhani, W. F. Wang, T. Ali, O. Cole, J. G. Hardman, and D. G. Bates, “Development of an Integrated Model of Cardiovascular and Pulmonary Physiology for the Evaluation of Mechanical Ventilation Strategies,” *Annu Int Conf IEEE Eng Med Biol Soc*, pp. 5319-5322, 2015.

[207] M. Chikhani, A. Das, M. Haque, W. Wang, D. G. Bates, and J. G. Hardman, “High PEEP in acute respiratory distress syndrome: quantitative evaluation between improved arterial oxygenation and decreased oxygen delivery,” *British Journal of Anaesthesia,* vol. 117, no. 5, pp. 650-658, 2016.

[208] A. M. Marquez, R. W. Morgan, T. Ko, W. P. Landis, M. M. Hefti, C. D. Mavroudis, M. J. McManus, M. Karlsson, J. Starr, A. L. Roberts, Y. Lin, V. Nadkarni, D. J. Licht, R. A. Berg, R. M. Sutton, and T. J. Kilbaugh, “Oxygen Exposure During Cardiopulmonary Resuscitation Is Associated With Cerebral Oxidative Injury in a Randomized, Blinded, Controlled, Preclinical Trial,” *Journal of the American Heart Association,* vol. 9, no. 9, pp. e015032, 2020.

[209] M. Laviola, C. Niklas, A. Das, D. G. Bates, and J. G. Hardman, “Effect of oxygen fraction on airway rescue: a computational modelling study,” *Br J Anaesth*, 2020.

[210] C. Gilhooley, G. Burnhill, D. Gardiner, H. Vyas, and P. Davies, “Oxygen saturation and haemodynamic changes prior to circulatory arrest: Implications for transplantation and resuscitation,” *J Intensive Care Soc,* vol. 20, no. 1, pp. 27-33, Feb, 2019.

[211] A. Albanese, L. Cheng, M. Ursino, and N. W. Chbat, “An integrated mathematical model of the human cardiopulmonary system: model development,” *Am J Physiol Heart Circ Physiol,* vol. 310, no. 7, pp. H899-921, 2016.

[212] S. Bozkurt, “Mathematical modeling of cardiac function to evaluate clinical cases in adults and children,” *PloS one,* vol. 14, no. 10, pp. e0224663-e0224663, 2019.

[213] N. Westerhof, J.-W. Lankhaar, and B. E. Westerhof, “The arterial Windkessel,” *Medical & Biological Engineering & Computing,* vol. 47, no. 2, pp. 131-141, 2009.

[214] R. E. Redgrave, S. Tual-Chalot, B. J. Davison, E. Greally, M. Santibanez-Koref, J. E. Schneider, A. M. Blamire, and H. M. Arthur, “Using MRI to predict future adverse cardiac remodelling in a male mouse model of myocardial infarction,” *Int J Cardiol Heart Vasc,* vol. 11, pp. 29-34, 2016.

[215] J. Lekven, O. D. Mjos, and J. K. Kjekshus, “Compensatory mechanisms during graded myocardial ischemia,” *Am J Cardiol,* vol. 31, no. 4, pp. 467-73, 1973.

[216] M. Ursino, and E. Magosso, “Acute cardiovascular response to isocapnic hypoxia. I. A mathematical model,” *Am J Physiol Heart Circ Physiol,* vol. 279, no. 1, pp. H149-65, 2000.

[217] S. Watts, J. E. Smith, R. Gwyther, and E. Kirkman, “Closed chest compressions reduce survival in an animal model of haemorrhage-induced traumatic cardiac arrest,” *Resuscitation,* vol. 140, pp. 37-42, 2019.

[218] B. V. Johnson, J. Coult, C. Fahrenbruch, J. Blackwood, L. Sherman, P. Kudenchuk, M. Sayre, and T. Rea, “Cardiopulmonary resuscitation duty cycle in out-of-hospital cardiac arrest,” *Resuscitation,* vol. 87, pp. 86-90, 2015.

[219] C. Daudre-Vignier, M. Laviola, A. Das, D. G. Bates, and J. G. Hardman, “Identification of an optimal CPR chest compression protocol,” *Annu Int Conf IEEE Eng Med Biol Soc,* vol. 2021, pp. 5459-5462, 2021.

[220] H. Kim, S. O. Hwang, C. C. Lee, K. H. Lee, J. Y. Kim, B. S. Yoo, S. H. Lee, J. H. Yoon, K. H. Choe, and A. J. Singer, “Direction of blood flow from the left ventricle during cardiopulmonary resuscitation in humans: its implications for mechanism of blood flow,” *American Heart Journal,* vol. 156, no. 6, pp. 1222.e1-7, 2008.

[221] K. B. Kern, R. W. Hilwig, R. A. Berg, and G. A. Ewy, “Efficacy of chest compression-only BLS CPR in the presence of an occluded airway,” *Resuscitation,* vol. 39, no. 3, pp. 179-88, 1998.

[222] I. Turner, S. Turner, and V. Armstrong, “Does the compression to ventilation ratio affect the quality of CPR: a simulation study,” *Resuscitation,* vol. 52, no. 1, pp. 55-62, 2002.

[223] R. F. Redberg, K. J. Tucker, T. J. Cohen, J. P. Dutton, M. L. Callaham, and N. B. Schiller, “Physiology of blood flow during cardiopulmonary resuscitation. A transesophageal echocardiographic study,” *Circulation,* vol. 88, no. 2, pp. 534-542, 1993.

[224] K. R. Sheak, D. J. Wiebe, M. Leary, S. Babaeizadeh, T. C. Yuen, D. Zive, P. C. Owens, D. P. Edelson, M. R. Daya, A. H. Idris, and B. S. Abella, “Quantitative relationship between end-tidal carbon dioxide and CPR quality during both in-

hospital and out-of-hospital cardiac arrest," *Resuscitation,* vol. 89, pp. 149-154, 2015.

[225] D. I. Fodden, A. C. Crosby, and K. S. Channer, "Doppler measurement of cardiac output during cardiopulmonary resuscitation," *J Accid Emerg Med,* vol. 13, no. 6, pp. 379-82, 1996.

[226] X. Repessé, C. Charron, J. Fink, A. Beauchet, F. Deleu, M. Slama, G. Belliard, and A. Vieillard-Baron, "Value and determinants of the mean systemic filling pressure in critically ill patients," *Am J Physiol Heart Circ Physiol,* vol. 309, no. 5, pp. H1003-H1007, 2015.

[227] A. R. Panchal, K. M. Berg, K. G. Hirsch, P. J. Kudenchuk, M. D. Rios, J. G. Cabañas, M. S. Link, M. C. Kurz, P. S. Chan, P. T. Morley, M. F. Hazinski, and M. W. Donnino, "2019 American Heart Association Focused Update on Advanced Cardiovascular Life Support: Use of Advanced Airways, Vasopressors, and Extracorporeal Cardiopulmonary Resuscitation During Cardiac Arrest: An Update to the American Heart Association Guidelines for Cardiopulmonary Resuscitation and Emergency Cardiovascular Care," *Circulation,* vol. 140, no. 24, pp. e881-e894, 2019.

[228] J. Schultz, A. Andersen, I. L. Gade, S. Ringgaard, B. Kjaergaard, and J. E. Nielsen-Kudsk, "A porcine in-vivo model of acute pulmonary embolism," *Pulm Circ,* vol. 8, no. 1, pp. 2045893217738217, 2018.

[229] R. L. Anthonio, D. J. van Veldhuisen, and W. H. van Gilst, "Left Ventricular Dilatation After Myocardial Infarction: ACE Inhibitors, β-Blockers, or Both?," *Journal of Cardiovascular Pharmacology,* vol. 32, pp. S1-S8, 1998.

[230] R. Sukhija, W. S. Aronow, K. Yalamanchili, J. Lee, J. A. McClung, J. A. Levy, and R. N. Belkin, "Association of right ventricular dilatation with bilateral pulmonary embolism, pulmonary embolism in a main pulmonary artery and lobar, segmental and subsegmental pulmonary embolism in 190 patients with acute pulmonary embolism," *Cardiology,* vol. 103, no. 3, pp. 156-7, 2005.

[231] P. O. Berve, B. M. Hardig, T. Skålhegg, H. Kongsgaard, J. Kramer-Johansen, and L. Wik, "Mechanical active compression-decompression versus standard mechanical cardiopulmonary resuscitation: A randomised haemodynamic out-of-hospital cardiac arrest study," *Resuscitation,* vol. 170, pp. 1-10, 2022.

[232] J. A. Hill, "Cardiovascular physiology by Robert M. Berne and Matthew N. Levy Mosby-Year Book, Inc., St. Louis (1997) 323 pages, illustrated, $35.95 ISBN: 0-8151-0901-6," *Clinical Cardiology,* vol. 21, no. 4, pp. 310-311, 1998.

[233] M. Ursino, "Interaction between carotid baroregulation and the pulsating heart: a mathematical model," *Am J Physiol,* vol. 275, no. 5, pp. H1733-47, 1998.

[234] E. Magosso, and M. Ursino, "A mathematical model of CO2 effect on cardiovascular regulation," *Am J Physiol Heart Circ Physiol,* vol. 281, no. 5, pp. H2036-52, 2001.

[235] M. Ursino, and E. Magosso, "A theoretical analysis of the carotid body chemoreceptor response to O2 and CO2 pressure changes," *Respiratory Physiology & Neurobiology,* vol. 130, no. 1, pp. 99-110, 2002.

[236] L. Cheng, A. Albanese, M. Ursino, and N. W. Chbat, "An integrated mathematical model of the human cardiopulmonary system: model validation under hypercapnia and hypoxia," *Am J Physiol Heart Circ Physiol,* vol. 310, no. 7, pp. H922-37, 2016.

[237] W. J. Reynolds, J. H T Milhorn, and J. G H Holloman, “Transient ventilatory response to graded hypercapnia in man,” *Journal of Applied Physiology,* vol. 33, no. 1, pp. 47-54, 1972.

[238] W. J. Reynolds, and J. H T Milhorn, “Transient ventilatory response to hypoxia with and without controlled alveolar PCO2,” *Journal of Applied Physiology,* vol. 35, no. 2, pp. 187-196, 1973.

Replacement of animal models of cardiac arrest and resuscitation strategies using a computer simulation

Appendix

Clara Daudré-Vignier, Meng 20205015

Supervisors:

Dr. Marianna Laviola

Prof. Jonathan G. Hardman

Anaesthesia & Critical Care, Academic Unit 3 (Injury, Inflammation and Recovery Sciences), School of Medicine, University of Nottingham

This work leading to submission of this thesis was funded by the National Centre for the Replacement, Reduction and Refinement of Animals in Research (NC3Rs, NC/S001328/1)

Table of Contents

Appendix 1. Thoracic model validation (Chapter 8)

In order to validate the thoracic model, 58 parameters of the cardiovascular model have been tuned for the cohort of ten virtual subjects (Table S1)

Table S1. Cardiovascular parameters tuned for the thoracic model validation.

Parameters	Unit	baseline value	Subject 1	Subject 2	Subject 3	Subject 4	Subject 5	Subject 6	Subject 7	Subject 8	Subject 9	Subject 10
Rlvc	mmHg.s/ml	0.002	0.007	0.007	0.008	0.006	0.006	0.004	0.006	0.005	0.009	0.006
Rrvc	mmHg.s/ml	0.001	0.006	0.006	0.007	0.009	0.007	0.009	0.006	0.008	0.006	0.006
Rlac	mmHg.s/ml	0.002	0.012	0.015	0.008	0.015	0.016	0.015	0.017	0.018	0.009	0.017
Rrac	mmHg.s/ml	0.001	0.007	0.007	0.008	0.004	0.007	0.006	0.007	0.006	0.007	0.005
Rpac	mmHg.s/ml	0.023	0.124	0.131	0.126	0.125	0.113	0.116	0.129	0.111	0.087	0.139
Rpvc	mmHg.s/ml	0.0056	0.029	0.031	0.025	0.028	0.024	0.040	0.037	0.017	0.042	0.023
Rsac	mmHg.s/ml	0.06	0.186	0.118	0.252	0.154	0.130	0.178	0.150	0.149	0.120	0.264
RSAc	mmHg.s/ml	0.91	1.655	1.738	1.048	0.868	0.539	1.191	1.573	1.198	0.599	0.689
Rtv_0	mmHg.s/ml	0.025	0.115	0.091	0.092	0.095	0.110	0.131	0.154	0.150	0.131	0.121
Rsv_0	mmHg.s/ml	0.025	0.089	0.082	0.083	0.082	0.083	0.087	0.060	0.047	0.078	0.055
Lsac	$mmHg.s^2/ml$	2.20E-04	0.002	0.002	0.002	0.002	0.002	0.002	0.002	0.002	0.001	0.002
Lpac	$mmHg.s^2/ml$	1.80E-04	0.000	0.000	0.000	0.000	0.000	0.001	0.000	0.001	0.001	0.000
Elamin	mmHg/ml	0.2	1.021	0.992	1.042	0.999	1.626	1.604	1.820	0.653	1.244	1.582
Eramin	mmHg/ml	0.2	1.592	1.620	1.571	1.627	1.634	1.740	1.606	1.620	1.543	1.845
Elvdiasc	mmHg/ml	-	0.900	0.936	0.794	0.920	0.904	0.928	0.900	0.837	0.767	0.715
Vlv_0	Ml	-	52.150	50.500	49.900	49.450	55.000	47.350	51.700	49.150	50.650	44.800
Ervdiasc	mmHg/ml	-	0.263	0.290	0.280	0.294	0.332	0.157	0.320	0.343	0.259	0.340
Vrv_0	Ml	-	47.050	42.550	43.000	68.350	49.300	52.300	45.550	41.200	53.050	62.350
Cpa	ml/mmHg	0.76	5.204	2.964	2.164	5.410	1.981	4.130	4.587	4.862	5.959	2.004
Clungs1	ml/mmHg	5.8	44.107	30.917	29.862	34.786	26.872	30.917	31.972	34.083	31.445	37.248

Cpv	ml/mmHg	25.37	133.301	153.629	148.156	105.938	129.392	137.211	145.810	147.374	133.301	138.774
Csa	ml/mmHg	0.28	0.442	0.446	0.382	0.335	0.502	0.472	0.442	0.621	0.421	0.438
Csa1	ml/mmHg	1.1532	8.376	4.970	5.635	8.749	7.213	9.455	5.136	4.223	3.973	8.666
Csa2	ml/mmHg	1.0788	6.258	6.513	6.586	6.550	5.383	6.550	6.258	4.873	6.805	7.315
Csa3	ml/mmHg	0.8184	5.291	5.214	4.981	5.214	5.291	3.019	5.472	5.885	4.801	7.538
Csa4	ml/mmHg	0.1488	0.892	0.688	0.706	0.681	0.663	0.754	0.641	0.553	0.564	0.655
Csa5	ml/mmHg	0.5208	0.835	1.348	1.378	0.744	1.710	1.733	1.265	1.823	1.635	1.536
Csv1	ml/mmHg	42.777	273.944	389.313	330.427	361.673	319.611	257.119	330.427	213.856	251.110	290.769
Csv2	ml/mmHg	14	97.375	56.382	112.477	72.348	88.313	58.971	93.060	53.362	44.732	48.184
Csv3	ml/mmHg	10.997	16.169	8.381	9.668	10.956	7.032	10.220	9.607	9.055	12.060	8.810
Csv4	ml/mmHg	2.499	9.823	7.966	7.158	11.276	9.500	10.145	6.916	7.239	9.419	5.786
Csv5	ml/mmHg	7.497	34.814	61.387	25.109	24.416	44.750	34.583	49.602	41.053	41.515	37.125
CC_alpha	-	0	3.757	3.958	3.673	3.725	3.651	3.747	3.757	3.852	3.863	3.303
ftp_tv	-	0	0.851	0.834	0.875	0.851	0.840	0.875	0.968	0.956	0.814	0.991
ftp_ra	-	0	0.344	0.399	0.312	0.399	0.359	0.446	0.406	0.312	0.392	0.421
ftp_rv	-	0	0.453	0.527	0.459	0.472	0.543	0.558	0.543	0.566	0.495	0.553
ftp_pa	-	0	0.238	0.356	0.213	0.366	0.376	0.436	0.366	0.507	0.366	0.371
ftp_lungs1	-	0	0.235	0.267	0.151	0.192	0.234	0.253	0.145	0.088	0.242	0.239
ftp_pv	-	0	0.904	0.843	0.803	0.828	0.820	0.848	0.862	0.660	0.660	0.795
ftp_la	-	0	0.398	0.380	0.370	0.370	0.517	0.618	0.434	0.550	0.546	0.510
ftp_lv	-	0	0.940	0.940	0.935	0.935	0.950	0.924	0.888	0.976	0.961	0.937
ftp_sa	-	0	0.364	0.250	0.325	0.227	0.449	0.459	0.439	0.403	0.420	0.377
Retro_lungs	-	0	0.424	0.414	0.346	0.422	0.501	0.322	0.396	0.582	0.406	0.564

Retro_pv	-	0	0.320	0.510	0.170	0.583	0.178	0.453	0.225	0.307	0.477	0.391
Retro_sa1	-	0	0.591	0.280	0.456	0.384	0.425	0.356	0.371	0.282	0.320	0.366
Retro_sa2	-	0	0.841	0.810	0.528	0.760	0.697	0.771	0.320	0.306	0.774	0.693
Retro_sa3	-	0	0.942	0.993	0.753	0.936	0.431	0.505	0.336	0.472	0.356	0.488
Retro_sa4	-	0	0.329	0.313	0.301	0.316	0.354	0.236	0.323	0.799	0.603	0.472
Retro_sa5	-	0	0.705	0.640	0.879	0.668	0.712	0.446	0.801	0.326	0.678	0.531
Retro_sv1	-	0	0.281	0.118	0.304	0.186	0.156	0.150	0.170	0.152	0.109	0.161
Retro_sv2	-	0	0.373	0.255	0.216	0.395	0.463	0.208	0.222	0.300	0.480	0.352
Retro_sv3	-	0	0.919	0.962	0.733	0.812	0.759	0.864	0.762	0.829	0.722	0.812
Retro_sv4	-	0	0.537	0.667	0.553	0.458	0.569	0.354	0.690	0.964	0.641	0.602
Retro_sv5	-	0	0.771	0.666	0.997	0.672	0.714	0.696	0.759	0.690	0.648	0.810
Retro_sv	-	0	0.101	0.133	0.130	0.172	0.226	0.107	0.313	0.284	0.226	0.094
Retro_tv	-	0	0.166	0.223	0.159	0.228	0.187	0.188	0.241	0.156	0.099	0.198
Retro_ra	-	0	0.365	0.212	0.290	0.382	0.247	0.389	0.283	0.403	0.321	0.495
Retro_la	-	0	0.608	0.675	0.519	0.738	0.346	0.675	0.774	0.359	0.483	0.397

The parameters starting with the letter R are the resistances, with a C are the capacitances, with a L are the inductances, with a E are the elastances, with a V are the volumes, with ft are the thoracic pump factor and with Retro are the retrograded blood flow factor. The cardiovascular abbreviations are SV, systemic vein; TV, thoracic vein; RA, right atria; RV, right ventricle; PA, pulmonary artery; PP, pulmonary perfusion; PV, pulmonary vein; LA, left atrium; LV, left ventricle; SA, aorta; SA1/SV1, splanchnic systemic artery/vein; SA2/SV2, extra-splanchnic systemic artery/vein; SA3/SV3, muscle systemic artery/vein; SA4/SV4, myocardial systemic artery/vein; and SA5/SV5, cerebral systemic artery/vein. Finally, CC_alpha is a factor applied to the chest compression force.

Appendix 2. Individual haemodynamic recording matching (Chapter 11)

In order to match the individual blood pressure recording and the arterial blood pressure model output, 67 parameters of the cardiovascular model have been tuned for the virtual subject (Table S2)

Table S2. Cardiovascular parameters tuned for the matching of continuous data.

Parameter	Unit	Value
Rlvc	mmHg.s/ml	0.001261
Rrvc	mmHg.s/ml	0.008528
Rlac	mmHg.s/ml	0.011727
Rrac	mmHg.s/ml	0.008659
Rpac	mmHg.s/ml	0.121222
Rpvc	mmHg.s/ml	0.02087
Rsac	mmHg.s/ml	0.27748
Rsa1c	mmHg.s/ml	19.89995
Rsa2c	mmHg.s/ml	5.917304
Rsa3c	mmHg.s/ml	28.42812
Rsa4c	mmHg.s/ml	46.60615
Rsa5c	mmHg.s/ml	28.67037
Rsv1c	mmHg.s/ml	0.191026
Rsv2c	mmHg.s/ml	0.008312
Rsv3c	mmHg.s/ml	0.370666
Rsv4c	mmHg.s/ml	1.971033
Rsv5c	mmHg.s/ml	0.686894
Rsv_0	mmHg.s/ml	0.088282
Rsvv_0	mmHg.s/ml	0.187368
Lsac	$mmHg.s^2/ml$	0.001266
Lpac	$mmHg.s^2/ml$	0.001034
Elamin	mmHg/ml	1.40767
Eramin	mmHg/ml	1.430366
Elvdiasc	mmHg/ml	3.959549
Vlv_0	ml	98.20545
Ervdiasc	mmHg/ml	0.980998
Vrv_0	ml	43.8965
Cpac	ml/mmHg	3.801321

Clungs1c	ml/mmHg	23.26671
Cpvc	ml/mmHg	97.74237
Csac	ml/mmHg	0.12096
Csa1c	ml/mmHg	7.468513
Csa2c	ml/mmHg	2.574432
Csa3c	ml/mmHg	3.205336
Csa4c	ml/mmHg	0.367228
Csa5c	ml/mmHg	4.35984
Csv1c	ml/mmHg	166.0541
Csv2c	ml/mmHg	122.1512
Csv3c	ml/mmHg	90.92789
Csv4c	ml/mmHg	23.97513
Csv5c	ml/mmHg	56.19453
CC_alpha	-	1.94484
ftp_sv	-	0.179172
ftp_ra	-	0.269852
ftp_rv	-	0.539788
ftp_pa	-	0.569295
ftp_lungs1	-	0.011528
ftp_pv	-	0.331722
ftp_la	-	0.39794
ftp_lv	-	0.150556
ftp_sa	-	0.881051
Retro_lungs1	-	0.806948
Retro_pv	-	0.335208
Retro_sa1	-	0.35082
Retro_sa2	-	0.533838
Retro_sa3	-	0.060267
Retro_sa4	-	0.999724
Retro_sa5	-	0.080208

Retro_sv1	-	0.8551
Retro_sv2	-	0.481352
Retro_sv3	-	0.533475
Retro_sv4	-	0.053838
Retro_sv5	-	0.241728
Retro_svv	-	0.35894
Retro_sv	-	0.669994
Retro_ra	-	0.965851
Retro_la	-	0.840343

The parameters starting with the letter R are the resistances, with a C are the capacitances, with a L are the inductances, with a E are the elastances, with a V are the volumes, with ft are the thoracic pump factor and with Retro are the retrograded blood flow factor. The cardiovascular abbreviations are SV, systemic vein; TV, thoracic vein; RA, right atria; RV, right ventricle; PA, pulmonary artery; PP, pulmonary perfusion; PV, pulmonary vein; LA, left atrium; LV, left ventricle; SA, aorta; SA1/SV1, splanchnic systemic artery/vein; SA2/SV2, extra-splanchnic systemic artery/vein; SA3/SV3, muscle systemic artery/vein; SA4/SV4, myocardial systemic artery/vein; and SA5/SV5, cerebral systemic artery/vein. Finally, CC_alpha is a factor applied to the chest compression force.

Appendix 3. Identification of an optimal CPR chest compression protocol

This paper was published in IEEE Engineering in Medicine and Biology Society conference proceeding 2021:

C. Daudre-Vignier, M. Laviola, A. Das, D.G. Bates and J.G. Hardman, "Identification of an optimal CPR chest compression protocol", in proceedings of the 43rd Annual International Conference of the IEEE Engineering in Medicine and Biology Society, 2021. [1]

My contribution to the work is:

- Conception and design of the study
- Running simulations
- Analysis and interpretation of data
- Drafting the article and revising it critically for important intellectual content
- Final approval for all aspects of the work
- Final approval of the version to be submitted and agreement to be accountable for all aspects of the work.

Identification of an optimal CPR chest compression protocol.

C. Daudre-Vignier[1], M. Laviola[1], A. Das[2], D.G. Bates[2] and J.G. Hardman[1,3]

***Abstract*— In this study, we used a high-fidelity integrated computational model of the respiratory and cardiovascular systems to investigate cardiopulmonary resuscitation (CPR) after cardiac arrest in a virtual healthy subject. For the purpose of this work, a newly developed thoracic model has been integrated to the current model, to study the influence of external chest compressions upon the arrested circulation during CPR. We evaluated the chest compression (CC) parameters, namely, end compression force, compression rate, and duty cycle to optimize the coronary perfusion pressure and the systolic blood pressure, using a genetic algorithm. While the sternal displacement associated with the CC force agreed with the ERC guidelines, the CC rate and duty cycle were respectively higher and lower than the ones recommended by the ERC guidelines. The effect of these CC parameters on cardiac output (CO) were also assessed. The end compression force was the parameter with the largest impact on CO, while the compression rate and duty cycle scarcely influence it.**

***Relevance*— Our results may aid in understanding the underlying pathophysiology of cardiac arrest and help guide research into the refinement of CPR strategies, without sacrificing animals or conducting clinical trials, which are difficult to undertake in crisis scenarios.**

I. Introduction

Cardiac arrest remains a leading cause of death in many countries. Despite the many years of research on CPR and attempts to improve outcomes, survival to hospital discharge remains consistently low. When performing chest compression three main components are considered: depth, rate, and duty cycle. While the European Resuscitation Council (ERC) advance life support guideline [1] advises compression depth of 5-6 cm, a rate of 100-120 compression per minute and a duty cycle of 50% in compression, a majority of studies fail to find an association between these parameters and CPR outcomes [2]. The question therefore arises as to what are the optimal chest compression depth, rate, and duty cycle.

Many human trials have attempted to identify the optimal CPR strategy, however, the ethical constraints, time scale, the presence of confounding variables, the heterogeneity of the population and sample size present major obstacle. Similarly, many animal models fail to summarize the severity of human cardiac arrest due to interspecies physiological discrepancies and lack of methodical rigor [3]. Computer simulation is a new alternative to the animal and clinical trials because it allows replacing animals and not putting at risk patients in crisis scenarios, plus it allows complete reproducibility of the methods, configuration of individualized patients and mechanistic results.

The present paper describes: i) the relevant components of the current recently updated computational model and cardiopulmonary interactions; ii) the new integrated thoracic model; iii) the comparison between cardiovascular model outputs and literature data and iv) the use of a genetic algorithm (GA) to optimize the chest compression parameters.

II. Method

A. Description of the cardiopulmonary model

The Interdisciplinary Collaboration in Systems Medicine (ICSM) simulation suite, used for this study, is a high-fidelity integrated computational model of the respiratory and cardiovascular systems. The core model has been extensively validated in multiple previous investigations [4, 5]. The respiratory model includes a series deadspace volume, 100 independently configurable alveolar compartments and apneic state. The cardiovascular model consists of 19 compartments (Figure 1).

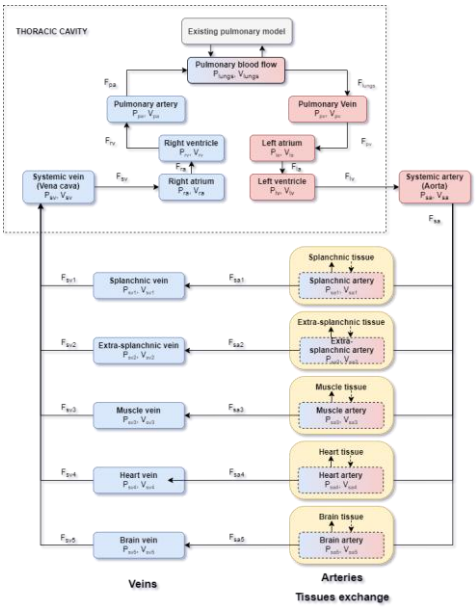

Figure 1. Schematic of updated cardiovascular model.

The equations describing each vascular compartment i have been recently updated by enforcing conservation of mass and balance of forces. The main equations were obtained from Albanese and colleagues' work [6]. Briefly, all the vascular compartments are modelled as a two elements windkessel system with a resistance (R_i), and capacitance (C_i) and in the systemic artery and the pulmonary artery an additional impedance (L_i) was added. The thoracic vein (sv) was also

[1] Academic Unit 3 - Injury, Inflammation and Recovery Science, School of Medicine, University of Nottingham, UK; [2]School of Engineering, University of Warwick, UK; [3]Nottingham University Hospitals NHS Trust, UK. Corresponding author: Clara.Daudre-Vignier@nottingham.ac.uk.

updated to enable its collapse. The thoracic vein and the aortic artery resistances were modified to account for the compartments volume. Additionally, a similar partitioning of the tissues was made splanchnic, extra-splanchnic, muscle, brain, and heart (Figure 1). The organ tissues were defined by their oxygen consumption per minute ($V\dot{O}_2$), volume ($Vtiss$), and perfusion ($\dot{Q}$). In addition, the model of ventricular and atrial contractions was recently updated based on Bozkurt work [7].

B. Cardiopulmonary interactions

The model includes the effect of the pulmonary vasoconstriction which results in a 'U' shape change pulmonary vascular resistance (PVR) at around the functional residual capacitance (FRC). The effect of hypoxic vasoconstriction is also modelled by increasing the PVR in response to hypoxia caused by the alveoli collapse.

Additionally, the effect of the pleural pressure has been integrated to the current model [6] and is defined by the following equation:

$$Ppl = P_{alv} - \frac{V_{alv} - V_{u,alv}}{C_{alv}} \tag{1}$$

where V_{alv} is the alveolar volume, P_{alv} is the alveolar pressure, C_{alv} is the alveolar compliance, and $V_{u,alv}$ is the alveolar unstressed volume.

C. Description of the new thoracic model

For the purposes of this study, a new thoracic model has been added to the current computational model and is adapted from Babbs chest wall model [8]. The external chest compression force $F(t)$, applied at the sternum, is expressed as a function of the end compression force (F_{max}), compression rate (CC_{rate}) and the duty cycle ($Duty_{cycle}$) such as:

$$F(t) = \begin{cases} F_{max}\dfrac{1-\cos\left(\pi(t-T1)\right)}{2} & 0 \le t < T1 \\ F_{max}\dfrac{1-\cos\left(\pi\dfrac{(t-T1)}{(T-T1)}\right)}{2} & T1 \le t < T \end{cases} \tag{2}$$

where T is the period of compression and decompression and $T1$ is the compression period ($T1 = T \cdot Duty_{cycle}$).

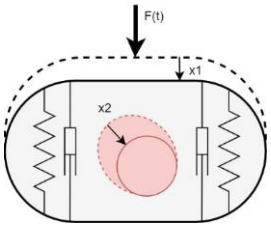

Figure 2. Schematic of the thoracic model. The paired spring and damper represent the elastic behavior of the chest wall under the compression force $F(t)$, including hysteresis. x_1 and x_2 represent the displacements of the sternum and the cardiac chambers under the compression force $F(t)$, respectively. The red and grey area represents the mediastinal tissue.

To relate the external chest compression force $F(t)$ and the sternum displacement (x_1), the thorax is modelled as a simple mechanical spring-damper system (Figure 2). The displacement of the sternum in response to the compression force is given by the following equation:

$$F(t) - kx_1 - \mu\dot{x}_1 = 0 \tag{3}$$

where x_1 is sternal displacement, $\dot{x}_1$ is the velocity of sternal displacement, k is the spring constant, and μ is the damping constant. To relate the sternal displacement (x_1) to the intrathoracic tissue (mediastinum) pressure (P_M), the mediastinum is modelled as an elastic material of Young's modulus of elasticity E.

The rate of change of the cardiac chambers diameters ($\dot{x}_2$) due to the changes in internal blood volume are considered and defined as follows:

$$\dot{x}_2 = \frac{F_{in} - F_{out}}{A_c} \tag{4}$$

where F_{in} and F_{out} are respectively the flows entering and leaving the cardiac chambers, and A_c is the cross-sectional area of cardiac chambers. However, the changes in diameters in the intrathoracic vascular compartments are negligeable ($\dot{x}_2 = 0$). Therefore, the relationship between the mediastinum pressure (P_M), the velocity of sternal displacement ($\dot{x}_1$) and rate of change of the compartment diameters ($\dot{x}_2$) is given by:

$$\frac{P_M}{dt} = \alpha\frac{E(\dot{x}_1 + \dot{x}_2)}{d_0} \tag{5}$$

Where α is a scalar, and d_0 is the combined mediastinal tissues width. The effect of chest compression on the alveolar pressure is also modelled. The resulting pressure on the alveoli (P_{CC}) is related to the sternal displacement (x_1) by the following equation:

$$P_{CC} = \frac{x_1 A_{lungs}}{C_{lungs}} \tag{6}$$

where, A_{lungs} is the cross-section of lung squeezed by sternal compression and C_{lungs} is the combined lung-chest wall compliance. The pressure in each alveolus (pi) is then updated as:

$$pi = \begin{cases} \dfrac{Si(10\cdot vi - 300)^3}{6600} - P_{ext,i} - P_{CC} \ , vi > 0 \\ 0 \ , otherwise \end{cases} \tag{7}$$

$$for\ i = 1, \dots, Ncomp$$

where Si is a scalar that determines the intra-alveolar pressure for a given volume, vi is the volume of the ith alveolar compartment, and $P_{ext,i}$ is the effective net pressure generated by the sum of the effects of factors outside each alveolus that act to distend that alveolus.

The updated alveolar pressure affects the pleural pressure (Ppl) (Equation 1).

In this model, all the cardiovascular compartments enclosed in the thoracic cavity (Figure 1) experience a combination of pleural (Ppl) and mediastinal pressure (P_M), such that:

$$\frac{dP_i}{dt} = \frac{F_{in} - F_{out}}{C_i} + \frac{dPpl}{dt} + f_{tp} \cdot \frac{dP_M}{dt} \quad (8)$$

where, $f_{tp} = 0.75$ is the thoracic pump factor which determines the degree to which the ''thoracic pump'' mechanism of CPR is working.

D. Genetic algorithm

In this paper, we used a genetic algorithm method to solve the optimization problem. Briefly, the algorithm: 1) creates a random initial population from the parameter space defined by the boundaries of the input parameters; 2) calculates the individual scores of each member of this population by running the simulation and deriving the cost (8); 3) generates members of the next population through the selecting best individuals of the existing population (elitism), combining the characteristics of two different members (crossover), and making changes to randomly selected individuals (mutation) 4) repeat steps 2)-3) until an optimal solution is found that satisfies a pre-defined criteria, in this case the improvement in cost function between consecutive generations is below 10^{-3} or the number of generations exceed 100.

The aim of the genetic algorithm was to find the sets of chest compression parameters that minimize the cost function defined as:

$$\begin{aligned} &Cost \\ &= w_1 \left| \frac{CPP_{model} - CPP_{desired}}{CPP_{desired}} \right| \\ &+ w_2 \left| \frac{SBP_{model} - SBP_{desired}}{SBP_{desired}} \right| \end{aligned} \quad (8)$$

where, CPP is the coronary perfusion pressure, SBP is the systolic blood pressure, the subscript 'model' defines the simulation output parameters, the subscript 'desired' defines the desired value of these output parameters and $w_1 = w_2 = \frac{1}{2}$ are the weights assigned to each objective. The desired value of CPP and SBP during CPR were defined as those during spontaneous ventilation (Table II).

We selected these outcome parameters (CPP and SBP) because of their association with return of spontaneous circulation. Indeed, CPP is defined as the difference between the aortic diastolic pressure minus the right atria diastolic pressure and gives an indication of the myocardial blood flow during CPR. In an animal study by Maryam et al. [9], targeting a systolic blood pressure of 100 mmHg and CPP>20 mmHg improved survival compared to the guidelines.

Additionally, we added constraints related to the safety and practicality of the chest compressions. The end compression force (F_{max}) was ranged between 0 and 400 N, the chest compression rate (CC_{rate}) between 60 and 150 compressions per minute (cpm), and the duty cycle ($Duty_{cycle}$) between 0.2 and 0.8. Finally, we constrained the genetic algorithm to only give integer values for F_{max} and CC_{rate}, as a results with decimal place would not be relevant.

E. Protocol

A virtual healthy subject was configured as in our previous study [3]. After 10 minutes of spontaneous ventilation (SPV), cardiac arrest (CA) was simulated for 5 minutes by setting the heart rate to 0, effectively forcing the heart to be in constant diastole. Additionally, we activated the apnoea module with obstructed upper airway. During CPR, apnoea was maintained however, the upper airway was no longer obstructed allowing passive ventilation from chest compressions. CPR was simulated for 1 minute following the ERC guidelines ($i.e. F_{max} = 400\ (N)$, $CC_{rate} = 120\ (cpm)$, and $Duty_{cycle} = 0.50$) as well as following the results of the genetic algorithm, i.e. optimized protocol. For comparison of the results, we selected Hyun's work [10] because it is one the most recent work on humans with detailed methodology and cardiovascular data.

The genetic algorithm and model simulations used Matlab version R2019b.v9 (MathWorks Inc., Natick, MA, USA).

III. Results

A. Cardiovascular model outputs

Table I compares the simulated cardiovascular model outputs when CPR is performed following the ERC guidelines *versus* Hyun *et al.*[10] work.

TABLE I. MODEL OUTPUTS VS. LITERATURE HUMAN DATA FROM HYUN *ET AL.* [10] DURING CPR.

Outputs	**Unit**	***Hyun et al.* data**	**CPR (ERC)**
Peak LV pressure	mmHg	112 ± 37	76.9
Peak aorta pressure	mmHg	105 ± 41	76.9
Peak RA pressure	mmHg	89 ± 27	83.2
End CC LV pressure	mmHg	8 ± 11	-2.6
End CC aorta pressure	mmHg	33 ± 10	38.7
End CC RA pressure	mmHg	8 ± 6	2
CPP	mmHg	25 ± 9	36.7
Stroke volume	ml	25 ± 8	11.6
Ejection fraction	%	34 ± 16	9

LV: left ventricle; RA: right atrium; CC: chest compression.

The model outputs are overall similar to the ones observed in humans [10]. Moreover, when CPR is performed according to the ERC guidelines, CPR only provides 17-27% of the normal cardiac output [10]. Similarly, only 10-30% of the blood flow to the heart and 30%-40% of the normal blood flow to the brain is achieved [11]. Our model provides a maximum cardiac output of 1.39 L/min which is 28% of the normal blood flow. Additionally, 17.7% and 17.7% of the normal blood flow goes to the heart and the brain, respectively.

B. Genetic algorithm

After 17 generations, the genetic algorithm identified the optimal CC parameters to be: $F_{max} = 400\ (N)$, $CC_{rate} = 137\ (cpm)$, and $Duty_{cycle} = 0.28$; the associated maximal sternal displacement was 5 cm. While the sternal displacement agrees with the ERC guidelines, the CC rate and

duty cycle are respectively higher and lower than the ones recommended by the ERC guidelines [1].

Table II. shows the model outputs, CPP, SBP and CO at the end of the three different stages: SPV, CA, CPR following the ERC guidelines (ERC) and CPR with the optimised protocol (OPT). CPP, SBP and CO are partially restored after 1 minute for both CPR protocols.

TABLE II. MODEL OUTPUTS DURING SPONTANEOUS VENTILATION (SPV), CARDIAC ARREST (CA) AND CARDIOPULMONARY RESUSCITATION (CPR).

Parameters	Unit	SPV	CA	CPR (ERC)	CPR (OPT)
CPP	mmHg	75	0	36.7	41
SBP	mmHg	114	7.7	76.9	73
CO	L/min	4.98	0	1.39	1.45

CPP: coronary perfusion pressure; SPB: systolic blood pressure; CO: cardiac output; ERC: European Resuscitation Council; OPT: optimised.

Compared to the ERC protocol, the optimised protocol produces values of CPP and CO that are closer to the values produced during normal breathing (Table II).

C. Effect of external compression force, rate, and duty cycle on cardiac output

Figure 3 shows the effect of the compression force, compression rate and duty cycle on CO. When a parameter was evaluated, the other two remained constant ($F_{max} = 400\ (N)$, $CC_{rate} = 138\ (cpm)$, and $Duty_{cycle} = 0.28$).

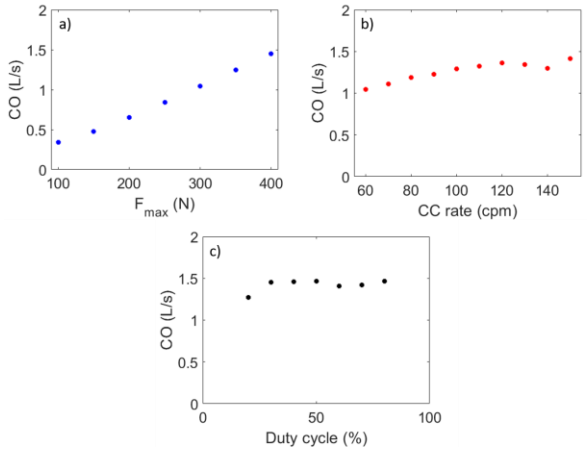

Figure 3. a) cardiac output vs. F_{max} b) cardiac output vs. CC_{rate} c) cardiac output vs. $Duty_{cycle}$.

The model indicates that the CO during CPR is linearly correlated (r^2 =0.99) to the compression force F_{max} and remains fairly constant when the CC_{rate} and $Duty_{cycle}$ change.

IV. CONCLUSION

Integration of a new detailed thoracic model to the current highly integrated cardiopulmonary model has produced a powerful tool to study CPR. The model outputs obtained following the ERC guidelines were similar to the ones observed in the literature data [10, 11], although the stroke volume and the blood flow to the brain achieved were lower.

In this study, the genetic algorithm identified the optimal CC parameters to be: $F_{max} = 400\ (N)$, $CC_{rate} = 137\ (cpm)$, and $Duty_{cycle} = 0.28$ resulting in a sternal displacement of 5 cm. The end compression force (F_{max}) is the parameter with the greatest impact on CO, while the compression rate (CC_{rate}) and duty cycle ($Duty_{cycle}$) scarcely influence CO.

Our simulations did not account for modifications of the tissue's vascular resistances nor the ventilation. Future work will investigate the modelling of the tissue's vascular resistance and ventilation, improving the accuracy of the CPR simulations.

ACKNOWLEDGMENT

This work is supported by National Centre of 3Rs (NC/S001328/1).

REFERENCES

[1] J. Soar, J. P. Nolan, B. W. Böttiger, G. D. Perkins, C. Lott, P. Carli, T. Pellis, C. Sandroni, M. B. Skrifvars, G. B. Smith, K. Sunde, and C. D. Deakin, "European Resuscitation Council Guidelines for Resuscitation 2015: Section 3. Adult advanced life support," *Resuscitation*, vol. 95, pp. 100-47, Oct, 2015.

[2] J. Considine, R. J. Gazmuri, G. D. Perkins, P. J. Kudenchuk, T. M. Olasveengen, C. Vaillancourt, C. Nishiyama, T. Hatanaka, M. E. Mancini, S. P. Chung, R. Escalante-Kanashiro, and P. Morley, "Chest compression components (rate, depth, chest wall recoil and leaning): A scoping review," *Resuscitation*, Sep 16, 2019.

[3] B. K. Fabian-Jessing, M. F. Vallentin, N. Secher, F. B. Hansen, C. Dezfulian, A. Granfeldt, and L. W. Andersen, "Animal models of cardiac arrest: A systematic review of bias and reporting," *Resuscitation*, vol. 125, pp. 16-21, Apr, 2018.

[4] A. Das, M. Haque, M. Chikhani, W. F. Wang, T. Ali, O. Cole, J. G. Hardman, and D. G. Bates, "Development of an Integrated Model of Cardiovascular and Pulmonary Physiology for the Evaluation of Mechanical Ventilation Strategies," *2015 37th Annual International Conference IEEE Engineering in Medicine and Biology Society (EMBC)*, pp. 5319-5322, 2015.

[5] M. Laviola, A. Das, M. Chikhani, D. G. Bates, and J. G. Hardman, "Computer simulation clarifies mechanisms of carbon dioxide clearance during apnoea," *British Journal of Anaesthesia*, vol. 122, no. 3, pp. 395-401, Mar, 2019.

[6] A. Albanese, L. Cheng, M. Ursino, and N. W. Chbat, "An integrated mathematical model of the human cardiopulmonary system: model development," *Am J Physiol Heart Circ Physiol*, vol. 310, no. 7, pp. H899-921, Apr 1, 2016.

[7] S. Bozkurt, "Mathematical modeling of cardiac function to evaluate clinical cases in adults and children," *PloS one*, vol. 14, no. 10, pp. e0224663-e0224663, 2019.

[8] C. F. Babbs, "Design of near-optimal waveforms for chest and abdominal compression and decompression in CPR using computer-simulated evolution," *Resuscitation*, vol. 68, no. 2, pp. 277-93, Feb, 2006.

[9] M. Y. Naim, R. M. Sutton, S. H. Friess, G. Bratinov, U. Bhalala, T. J. Kilbaugh, J. W. Lampe, V. M. Nadkarni, L. B. Becker, and R. A. Berg, "Blood Pressure- and Coronary Perfusion Pressure-Targeted Cardiopulmonary Resuscitation Improves 24-Hour Survival From Ventricular Fibrillation Cardiac Arrest," *Critical care medicine*, vol. 44, no. 11, pp. e1111-e1117, 2016.

[10] H. Kim, S. O. Hwang, C. C. Lee, K. H. Lee, J. Y. Kim, B. S. Yoo, S. H. Lee, J. H. Yoon, K. H. Choe, and A. J. Singer, "Direction of blood flow from the left ventricle during cardiopulmonary resuscitation in humans: its implications for mechanism of blood flow," *Am Heart J*, vol. 156, no. 6, pp. 1222.e1-7, Dec, 2008.

[11] A. R. John, M. Manivannan, and T. V. Ramakrishnan, "Computer-Based CPR Simulation Towards Validation of AHA/ERC Guidelines," *Cardiovasc Eng Technol*, vol. 8, no. 2, pp. 229-235, Jun, 2017.

Appendix 4. Evaluating Current Guidelines for Cardiopulmonary Resuscitation using an Integrated Computational Model of the Cardiopulmonary System

This paper was be published in the Resuscitation journal as original article:

Clara Daudre-Vignier, Declan G. Bates, Timothy E. Scott, Jonathan G Hardman, Marianna Laviola, “Evaluating Current Guidelines for Cardiopulmonary Resuscitation using an Integrated Computational Model of the Cardiopulmonary System” [2]

My contribution to the work is:

- Conception and design of the study
- Running simulations
- Analysis and interpretation of data
- Drafting the article and revising it critically for important intellectual content
- Final approval for all aspects of the work
- Final approval of the version to be submitted and agreement to be accountable for all aspects of the work.

Available online at ScienceDirect

Resuscitation

journal homepage: www.elsevier.com/locate/resuscitation

Experimental paper

Evaluating current guidelines for cardiopulmonary resuscitation using an integrated computational model of the cardiopulmonary system

Clara Daudre-Vignier[a], *Declan G. Bates*[b], *Timothy E. Scott*[c], *Jonathan G. Hardman*[a,d], *Marianna Laviola*[a,*]

Abstract

Objective: We aimed to use a high-fidelity computational model that captures key interactions between the cardiovascular and pulmonary systems to investigate whether current CPR protocols could potentially be improved.

Methods: We developed and validated the computational model against available human data. We used a global optimisation algorithm to find CPR protocol parameters that optimise the outputs associated with return of spontaneous circulation in a cohort of 10 virtual subjects.

Results: Compared with current protocols, myocardial tissue oxygen volume was more than 5 times higher, and cerebral tissue oxygen volume was nearly doubled, during optimised CPR. While the optimal maximal sternal displacement (5.5 cm) and compression ratio (51%) found using our model agreed with the current American Heart Association guidelines, the optimal chest compression rate was lower (67 compressions min^{-1}). Similarly, the optimal ventilation strategy was more conservative than current guidelines, with an optimal minute ventilation of 1500 ml min^{-1} and inspired fraction of oxygen of 80%. The end compression force was the parameter with the largest impact on CO, followed by PEEP, the compression ratio and the CC rate.

Conclusions: Our results indicate that current CPR protocols could potentially be improved. Excessive ventilation could be detrimental to organ oxygenation during CPR, due to the negative haemodynamic effect of increased pulmonary vascular resistance. Particular attention should be given to the chest compression force to achieve satisfactory CO. Future clinical trials aimed at developing improved CPR protocols should explicitly consider interactions between chest compression and ventilation parameters.

Keywords: Cardiac arrest, Cardiopulmonary resuscitation, Chest compressions, Computational simulation, Modelling

Introduction

Cardiac arrest (CA) is a leading cause of death in many countries – despite years of research, survival rates remain consistently low.[1] Cardiopulmonary resuscitation (CPR) is an emergency procedure consisting of chest compressions combined with positive pressure ventilation, intended to restore flow of oxygenated blood to the brain and heart. Some clinical trials in humans have attempted to identify optimal CPR strategies.[2–5] However, ethical and practical constraints, short time scales, the presence of confounding variables, and heterogeneity of the patient population present major obstacles to performing clinical research in this area. Animal models often fail to represent the severity of human CA accurately, due to interspecies physiological differences and lack of methodical rigor.[6–7] Computer simulation is a novel and promising alternative to animal and clinical trials that is free of most ethical and practical constraints, allows complete reproducibility of methods and results, and offers mechanistic insight into the effectiveness of treatment strategies.

When performing chest compression (CC), three main components are typically considered: depth, rate, and compression ratio. While the European Resuscitation Council (ERC) advanced life support guideline[8] advises a compression depth of 5–6 cm, a rate of 100–120 compressions min^{-1}, and a compression ratio (i.e. the proportion of compression time during the compression / decompression cycle) of 50%, the majority of studies have failed to find an

* Corresponding author.
E-mail address: marianna.laviola@nottingham.ac.uk (M. Laviola).

https://doi.org/10.1016/j.resuscitation.2023.109758
Received 4 January 2023; Received in Revised form 24 February 2023; Accepted 27 February 2023

association between these parameters and outcomes. A recent systematic review and meta-analysis by Considine *et al.*,[9] which included more than 15,000 subjects, reported outcomes associated with CC rate. Overall, the majority of the studies did not find any associations between the CC rate and outcomes (survival with good neurological outcome, survival to hospital discharge and return of spontaneous circulation [ROSC]) in out-of-hospital cardiac arrest). Only two studies found otherwise; Idris *et al.*[2] found an association between CC rate and ROSC with the rate of ROSC peaking at 125 compressions min^{-1}, and Idris *et al.*[3] found that CC rates between 100 and 120 compressions min^{-1} were associated with greatest survival to hospital discharge.

The evidence regarding the effect of CC depth on ROSC and survival is more consistent. In the study of Babbs *et al.*,[10] for shocks delivered after 5 min of CA, a CC depth >5 cm compared with CC depth <5 cm was associated with a greater chance of transient ROSC. Similarly, Stiell *et al.*[11] found a strong association between survival outcomes and increased compression depth, and that maximal survival was in the depth interval of 4.03–5.53 cm,[12] suggesting that the target depth in the AHA guidelines may be too great. The effect of the CC compression ratio on ROSC and long-term outcome has not been investigated in any clinical studies. However, in a study by Johnson *et al.*[13] the median compression ratio was 38.8% and a relatively shorter compression phase (lower compression ratio) was associated with a greater chance of survival.

The haemodynamic effects of pulmonary ventilation during CPR also remain unclear. Some researchers[14] have argued that whilst modest PEEP could help mitigate alveolar collapse, high intrathoracic pressure during decompression could prevent venous return and thus reduce stroke volume and organ perfusion, while others[15] have speculated that high intrathoracic pressure could enhance CC-generated CO by further ejecting blood out of the left ventricle. There is therefore an urgent need for further research into the combined impact of different airway strategies, ventilation techniques, positive end expiratory pressures (PEEP) and inhaled oxygen (FiO_2) on CPR effectiveness.[16]

This study presents a highly integrated computational model of the cardiopulmonary systems that can be used to investigate these variables in detail. Preliminary results from this study were presented in.[17]

Methods

Cardiopulmonary computational model

The model used in this study is a high-fidelity, integrated, computational model of the respiratory and cardiovascular systems which has been extensively validated in multiple previous investigations.[18–22] The respiratory model includes a series deadspace volume and 100 independently configurable alveolar compartments (each with distinct gas and blood flow models). The cardiovascular model comprises 20 compartments with 4 cardiac chambers, 3 compartments representing the pulmonary circulation and the remainder representing the systemic vasculature. Extensive, novel modelling was undertaken to adapt the model for the specific purposes of this study; this is described in detail in the Supplementary online materials.

Cohort of virtual subjects

We used human haemodynamic and gas exchange data from three sources to validate our model; the end-compression and end-decompression pressures from Kim *et al.*,[23] which describes the mechanisms of forward blood flow generation during CPR in ten patients with non-traumatic CA; the end-compression and end-decompression left ventricular volume from Redberg *et al.*[24] which used transoesophageal echocardiography in 18 subjects; and the end tidal CO_2 ($ETCO_2$) ranges from Sheak *et al.*[25] which examined CPR in 583 in- and out-of-hospital CAs.

To match these data, we used a Genetic Algorithm (GA) to find combinations of the 58 cardiovascular parameters in the model that produce the closest matching between the model outputs and the haemodynamic and gas exchange data on CPR[23–25] (Table 1). Details of the GA and the 58 cardiovascular parameters tuned for the thoracic model validation are presented in the Supplementary Material. The cost function ($Cost_{Val}$) to be minimised is:

$$\begin{aligned} Cost_{Val} = {} & w\,|PeakLV_m - PeakLV_d| + w\,|EDLVP_m - EDLVP_d| \\ & + w\,|PeakSA_m - PeakSA_d| \\ & + w\,|EDSAP_m - EDSAP_d| + w\,|PeakRA_m - PeakRA_d| \\ & + w\,|EDRAP_m - EDRAP_d| \\ & + w\,|CPP_m - CPP_d| + w\,|SV_m - SV_d| + w\,|EF_m - EF_d| \\ & + w\,|EDVLV_m - EDVLV_d| \\ & + w\,|ESVLV_m - ESVLV_d| + w\,|ETCO2_m - ETCO2_d| \end{aligned} \quad (14)$$

where, $PeakLV$ is the peak left ventricular pressure, $EDLVP$ is the left ventricular end-compression pressure, $PeakSA$ is the peak aortic pressure, $EDSAP$ is the aortic end-compression pressure, $PeakRA$ is the peak right atrial pressure, $EDRAP$ is the right atrial end-compression pressure, CPP is the coronary perfusion pressure, SV is the stroke volume, EF is the ejection fraction, $EDVLV$ is the end diastolic left ventricular volume, $ESVLV$ is the end systolic left ventricular volume and $ETCO2$ is the end tidal CO_2 partial pressure. The subscript 'm' defines the model simulation output parameters, the subscript 'd' defines the desired value of these output parameters, and $w = \frac{1}{12}$ is the weight assigned to each objective, which has been assigned equal in order to avoid favouring or disfavouring the matching of one model output over another. The desired value for each of the parameters was defined based on the haemodynamic and gas exchange data in Table 1.

Based on the optimisation results, we chose ten sets of model parameters that produced adequate levels of variability within the physiological bounds for the model outputs, to create a cohort of ten virtual subjects (Table 1).

Optimisation of the CPR parameters

To identify optimal personalised CPR parameters, we employed a GA to simultaneously vary all CPR parameters and find those that minimise the cost function ($Cost_{Opt}$) defined as:

$$\begin{aligned} Cost_{Opt} = {} & w\left|\frac{CPP_m - CPP_d}{CPP_d}\right| + w\left|\frac{CO_m - CO_d}{CO_d}\right| \\ & + w\left|\frac{brainO2_m - brainO2_d}{brainO2_d}\right| \\ & + w\left|\frac{heartO2_m - heartO2_d}{heartO2_d}\right| \end{aligned} \quad (15)$$

where CPP is the coronary perfusion pressure, CO is the cardiac output, $brainO_2$ is the cerebral tissue oxygen volume, $heartO_2$ is the myocardial tissue oxygen volume, the subscript 'm' defines the simulation output parameters, the subscript 'd' defines the desired

Table 1 – Literature human data[26,29–30] versus model outputs during CPR.

Variable	Unit	Literature human data	Model outputs
EC LV pressure	mmHg	112 ± 37 [1]	111 ± 13
EC aorta pressure	mmHg	105 ± 41 [1]	110 ± 13
EC RA pressure	mmHg	89 ± 27 [1]	88 ± 9
ED LV pressure	mmHg	8 ± 11 [1]	11 ± 7
ED aorta pressure	mmHg	33 ± 10 [1]	36 ± 4
ED RA pressure	mmHg	8 ± 6 [1]	6 ± 3
CPP	mmHg	25 ± 9 [1]	30 ± 7
Stroke volume	ml	19 ± 6 [2]	19 ± 1
EC LV volume	ml	50 ± 7 [2]	72 ± 6
ED LV Volume	ml	70 ± 10 [2]	70 ± 7
Ejection fraction	%	34 ± 16 [1]	50 ± 8
$ETCO_2$	mmHg	30 ± 5 [3]	26 ± 1

EC, end compression; ED, end diastolic; LV, left ventricle; RA, right atria; CPP, coronary perfusion pressure; $ETCO_2$, end tidal CO_2; 1: Kim *et al.*[26], 2:Redberg *et al.*[30], 3:Sheak *et al.*[31].

value of these output parameters, and $w = \frac{1}{4}$ is the weight assigned to each objective, which has been assigned equal in order to avoid favouring or disfavouring the matching of one model output over another. The desired value of CPP, CO, $brainO_2$ and $heartO_2$ during CPR were defined as those observed during baseline (i.e. spontaneous ventilation) since the primary objective of CPR is to restore spontaneous circulation and return to baseline values (Table 3).

We selected these outcome parameters (CPP, CO, $brainO_2$ and $heartO_2$) because of their association with return of spontaneous circulation; in an animal study by Naim *et al.*,[26] targeting a systolic blood pressure of 100 mmHg and CPP >20 mmHg improved survival compared to the AHA guidelines. The CO is the amount of blood flow restored during CPR and is therefore crucial to achieve return of spontaneous circulation.

We added constraints to the optimisation problem related to the safety and practicality of the CC. The end compression force (F_{max}) was allowed to vary between 0 and 500 N, the CC rate (CC_{rate}) between 60 and 150 compressions min^{-1}, the compression ratio ($Duty_{cycle}$) between 20% and 80%, tidal volume (V_T) between 100 and 1000 ml, the ventilatory frequency (V_f) between 0 and 20 breaths min^{-1}, the positive end expiratory pressure (PEEP) between 0 and 15 cmH_2O, and the fraction of inspired oxygen (FiO_2) between 21% and 100%.

We then simulated CPR using the median values of the optimised compression depths, rates, duty cycles, and ventilation found for the entire cohort, to determine whether a modified CPR protocol could offer advantages over current guidelines.

CPR simulation protocol

While the ten virtual subjects were identical during spontaneous ventilation, during CA and CPR their cardiovascular input parameters were different to allow a variation in model outputs during CPR. The 58 cardiovascular parameters that define each subject can be found in the online supplementary material (Table S1).

After 5 minutes of spontaneous ventilation, CA was simulated for 5 minutes by setting the heart rate to 0, effectively forcing the heart to be in constant diastole. Additionally, the apnoea module was activated with the upper airway obstructed. During CPR, the subjects were no longer apnoeic, and the airway was no longer obstructed. The baseline CPR strategy followed as closely as possible the one used in Kim's work[23] which in turn followed the American Heart Association (AHA) guidelines: CC rate 100 compressions min^{-1}, compression ratio 50%, CC depth 5 cm, tidal volume 650 ml, ventilation rate 12 breaths min^{-1} and fraction of inspired oxygen 100%. However, the effect of repeated epinephrine administration was not modelled.

Ethical statement

Approval from a research ethics committee was not sought, since the data were obtained from previously published literature (whose studies had already received ethical approval).

Results

Model validation

Table 1 compares the simulated cardiovascular model outputs when CPR was performed following the AHA guidelines *versus* the haemodynamic and gas exchange data during CPR from the literature described above.[23–25] All the model outputs are within the physiological ranges observed during standard CPR in humans (see also the online supplementary material).

Optimal CPR parameters

Table 2 shows the optimal personalized CPR parameters for each subject identified by the GA, as well as the median optimised values over the cohort. The CC rate and compression ratio are the two parameters with the largest ranges over the cohort, from 62-104 compressions min^{-1} and 41–58%, respectively. The PEEP, CC force and its associated maximal sternal displacement are the two parameters that remain relatively constant at 0 cmH_2O and 495 N (5–6 cm of displacement), respectively. Similarly, all the ventilatory parameters varied with a mean tidal volume of 250 ml, ventilatory frequency of 6 breaths min^{-1} and a fraction of inspired oxygen of 80%. Overall, the median optimal minute ventilation was 1500 ml min^{-1}.

Tables 3 and 4 show the model outputs, CPP, CO, $brainO_2$ and $heartO_2$ during spontaneous ventilation, after CA, during CPR following the AHA guidelines (AHA-CPR), during CPR with optimal personalized CPR parameters (PERS-CPR), and during CPR with the new optimised protocol based on the median values of the optimised CPR parameters (OPT-CPR). CPP and CO were partially restored after 5 minutes for all CPR protocols. However, compared to the AHA pro-

Table 2 – Optimal CPR parameters for the cohort of 10 subjects.

Subjects #	CC rate	Max Force	CC depth	Compression ratio	V_T	V_f	PEEP	FiO_2
AHA	100–120	400–500	5–6	50	650	12	0	100
Median ± SD	67 ± 15	498 ± 3	6.2 ± 0.1	52 ± 5	250 ± 103	6 ± 2	0 ± 0	85 ± 16
Subject 1	66	495	6.1056	41	550	2	0	70
Subject 2	62	500	6.3431	50	200	9	0	70
Subject 3	80	494	6.0817	49	250	8	0	50
Subject 4	104	494	6.0023	58	250	6	0	70
Subject 5	65	498	6.2379	46	300	5	0	100
Subject 6	60	493	6.2813	51	200	8	0	90
Subject 7	67	500	6.3807	58	300	2	0	90
Subject 8	65	499	6.3365	53	300	5	0	100
Subject 9	87	497	6.0989	52	200	6	0	90
Subject 10	93	499	6.0654	52	250	6	0	80

CC rate, chest compression rate (compressions min^{-1}); Max Force, maximal chest compression force (N); CC depth, maximal sternal displacement (cm); Compression ratio (%); V_T, tidal volume (ml); V_f, ventilatory frequency (breaths min^{-1}); PEEP, positive end expiratory pressure (cmH2O); FiO_2, fraction of inspired oxygen (%).

Table 3 – Model outputs during spontaneous ventilation (SPV) and cardiac arrest (CA).

Parameters	Unit	SPV	CA
CPP	mmHg	80	0
CO	ml min^{-1}	5000	0
$brainO_2$	ml	1.83	0
$heartO_2$	ml	0.32	0

CPP, coronary perfusion pressure; CO, cardiac output; $brainO_2$, cerebral tissue oxygen volume; $heartO_2$, myocardial tissue oxygen volume.

Table 4 – Model outputs using the standard CPR protocol (AHA-CPR), the optimised CPR protocol (OPT-CPR) and personalised CPR (PERS-CPR).

	AHA-CPR				OPT-CPR				PERS-CPR			
	CPP	CO	$brainO_2$	$heartO_2$	CPP	CO	$brainO_2$	$heartO_2$	CPP	CO	$brainO_2$	$heartO_2$
	mmHg	ml min^{-1}	ml	ml	mmHg	ml min^{-1}	ml	Ml	mmHg	ml min^{-1}	ml	ml
Median ± SD	**30 ± 7**	**1853 ± 100**	**0.80 ± 0.7**	**0.061 ± 0.05**	**39 ± 7**	**2822 ± 143**	**1.73 ± 0.06**	**0.326 ± 0.05**	**38 ± 8**	**2830 ± 300**	**1.68 ± 0.1**	**0.320 ± 0.02**
subject1	30	1806	0.75	0.002	38	2946	1.74	0.327	35	2891	1.71	0.331
subject2	34	2014	0.88	0.048	45	3105	1.80	0.324	46	3151	1.78	0.325
subject3	32	1912	0.89	0.121	39	3001	1.82	0.379	38	2920	1.68	0.339
subject4	20	1759	0.79	0.166	25	2778	1.77	0.450	22	2404	1.5	0.323
subject5	27	1761	0.74	0.002	34	2700	1.68	0.291	35	2740	1.73	0.304
subject6	30	1765	0.73	0.002	42	2765	1.69	0.305	43	2763	1.71	0.322
subject7	31	1873	0.78	0.002	41	2780	1.64	0.281	41	2855	1.65	0.283
subject8	30	1920	0.83	0.002	39	3031	1.77	0.305	39	3049	1.81	0.313
subject9	37	1862	0.81	0.129	48	2864	1.71	0.377	46	2799	1.62	0.326
subject10	27	1859	0.83	0.137	30	2720	1.71	0.371	31	2731	1.66	0.33

CPP, coronary perfusion pressure; CO, cardiac output; $brainO_2$, cerebral tissue oxygen volume; $heartO_2$, myocardial tissue oxygen volume; AHA, American Heart Association.

tocol, all the model outputs were improved with the optimised CPR strategy (Table 4). Whilst the CPP was moderately improved, the myocardial tissue oxygen volume ($heartO_2$) was more than 5 times higher during optimised CPR. Similarly, the cerebral tissue oxygen volume ($brainO_2$) was nearly doubled during optimised CPR compared to standard CPR. Considering the reduction in ventilation parameters, this better oxygenation of the vital organs can only be explained by the increased CO.

Discussion

In this study, we developed and validated a new, highly-integrated model of the cardiopulmonary systems. After the onset of CA, the aortic pressure exponentially decreases and reaches a mean systemic filling pressure (MSFP) of 10 mmHg after 4 minutes of CA in keeping with clinical observations (see Fig. S3 in the SM).[27] Additionally, the MSFP of around 10 mmHg agrees with the observation in

Repesse *et al.*[28] that deceased intensive care unit patients who happened to have central venous catheter and arterial lines had a MSFP of around 12 mmHg.

Our model presented no aortic regurgitation and moderate to severe retrograde blood flow from the left ventricle into the left atrium (3–16 ml) as well as antegrade blood flow from the left ventricle into the aorta during the compression phase of CPR, in keeping with the observations of Kim *et al.*[23] The CO reaches a maximum of 2800 ml min^{-1} which is 56% of the CO during spontaneous circulation. During CPR, CO can vary dramatically depending on CC quality. In Fodden *et al.*[27] the median CO was found to be approximately 2040 ml min^{-1}, which is again in keeping with our results.

During personalized CPR, the CPP is moderately increased from 30 mmHg to 38 mmHg, however, the myocardial tissue oxygen volume ($heartO_2$) is more than 5 times higher than during standard CPR (Table 2). The cerebral tissue oxygen volume ($brainO_2$) is nearly doubled during optimised CPR compared to standard CPR. Considering the reduction in minute ventilation and FiO_2 from 7800 ml min^{-1} to 1500 ml min^{-1}, and 100% to 80%, respectively, during the optimised CPR protocols, the improvements in oxygenation of the vital organs can only be explained by the increase in CO of nearly 1000 ml min^{-1}. Interestingly, these potential benefits were preserved when we applied a single CPR protocol (OPT-CPR) to the cohort, based on the median values of the personalized CPR parameters – indeed in some cases this protocol slightly improved on the personalized results, likely due to the optimisation algorithm failing to find the exact global optimum.

While the median optimised maximal sternal displacement (6.2 cm) and median compression ratio (52%) agree with the AHA guidelines, the median CC rate (67 compressions min^{-1}) identified in our optimised protocol is considerably lower than the range recommended by the AHA guidelines of 100–120 compressions min^{-1}.[29] The corresponding optimised ventilation strategy (minute ventilation 1500 ml min^{-1}) suggests that a more restrained ventilation strategy could help mitigate the detrimental hemodynamic effects of mechanical ventilation whilst maintaining sufficient arterial oxygenation.

Whilst the total absence of ventilation during CPR has been shown to be associated with poor outcomes,[15] a similar negative outcome has been observed when hyperventilation is used.[30] Indeed, a lower minute ventilation at the beginning of CPR could help mitigate the negative hemodynamic effects of ventilation on CO and could avoid hyperoxaemia, which has been shown to be detrimental to long terms outcomes. However, whilst at the beginning of CPR ensuring blood circulation is key, ventilation becomes crucial as CO_2 clearance becomes necessary during prolonged CPR or after a long period of untreated CA.

Previous studies have used mathematical models of the cardiovascular system to investigate alternative CPR strategies ranging from interposed abdominal compression,[31–32] combined chest and abdominal compression and decompression,[33–35] impedance valve,[36–37] and passive leg raise.[38–39] Jung *et al.* applied optimal control to identify the CC and decompression frequency and compression ratio that maximized the coronary perfusion pressure (CPP)[40] and the blood flow as measured by the pressure difference between the thoracic aorta and the right atrium.[41] In both papers, the authors identified the optimal waveform to include both compression and decompression of the chest to the maximum allowable extent and a compression ratio of 40%. However, one study[40] found the optimal CC rate to be 90 compressions min^{-1} and the other 60 compressions min^{-1}. Whilst our optimal maximal sternal displacement was similarly higher (6.2 cm) than the AHA recommendations and our optimal CC rate lower (67 compressions min^{-1}), our optimal compression ratio was only slightly higher (52%) than the AHA recommendations whereas Jungs *et al.* was lower (40%). These discrepancies may arise from the fact that while Jungs' studies considered decompression and the waveform shape variation, our study included the optimisation of ventilatory parameters during CPR. Additionally, their model did not include a pulmonary system or mechanisms of gas exchange.

Similarly, Babbs *et al.*[42] investigated the optimal CC frequency for different sized individuals, from neonates to adults and found that whilst high frequency for neonates (>120 compressions min^{-1}) was advantageous, in adults there may be benefit from lower compression frequencies near 60 compressions min^{-1}. In another study Babbs[25] identified the optimal CPR to be reciprocal compression and decompression of the chest and the abdomen to the maximum allowable extent with a CC rate of 80 compressions min^{-1} and a compression ratio of 50%. Both these studies support our results.

John *et al.*[43] investigated the optimal CC pressure and rate to maximize CO and found them to be respectively 100 mmHg, which is approximately a maximal sternal displacement of 5.7 cm, and 110 compressions min^{-1}, both similar to those recommended in the AHA guidelines. However, similarly to the findings of Jung *et al.*, the study of John *et al.* did not include a model of the pulmonary system or gas exchange. Finally, Turner *et al.* investigated the benefits of continuous CC over the usual 5:1 or 15:2 ratios of compression to ventilation[44] and found that lower ventilation ratios (15:2 and 50:5) produced significantly greater oxygen delivery to the body. These results are in keeping with ours, suggesting that lower ventilatory frequency can effectively oxygenate tissues during CPR.

Compared to previous studies, our model has the unique advantage of using a high-fidelity, computational model of the respiratory and cardiovascular systems that includes extensive cardiopulmonary interactions. Our model is the first to be comprehensively validated against multiple sources of human data during CPR,[23–25] and our study is the first to use a cohort of ten virtual subjects to study CPR. Finally, the optimal CPR was identified with a genetic algorithm, enabling for the first time optimisation of multiple CPR parameters simultaneously.

Our model has limitations. The lack of complex biological processes (i.e. high levels of inflammatory cytokines) limits its usefulness for the study of post-CA treatment and management which affects the whole body (multi-organ failure). Our model does not account for the electrophysiology of the heart or the cardiovascular control mechanism (i.e. chemoreflex, effect of vasopressors or inotropes) which can be important when studying CPR. Finally, our model does not account for the role of the precipitating aetiology, which can require a particular CPR strategy.

Conclusions

In this study, we identified optimal CPR strategies in a cohort of virtual subjects using a novel, high-fidelity, computational model of the cardiopulmonary systems. Myocardial tissue oxygen volume was more than 5 times greater, and cerebral tissue oxygen volume was nearly doubled during our optimised CPR protocol. Compared to current AHA guidelines, the identified optimal CPR strategy had the same compression ratio (52%), a slightly greater

CC depth (6.2 cm), a lower CC rate (67 compressions min^{-1}), and a less aggressive ventilation strategy (V_T 250 ml, V_f, 6 breaths min^{-1}). Our results highlight the potential negative hemodynamic effects of excessive ventilation, which could increase pulmonary vascular resistance, impeding CO. Future clinical trials evaluating modifications in multiple CPR parameters simultaneously could help elucidate optimal CPR strategies with significant benefits to patients.

Conflicts of interest

The authors declare that they have no competing interests.

Availability of data and materials

All data and code used in the study are available upon request from the corresponding author.

Authors' contributions

Conception and design of the study: CDV, DGB, JGH, ML.

Running simulations: CDV.

Analysis and interpretation of data: CDV, DGB, TES, JGH, ML.

Drafting the article and revising it critically for important intellectual content: CDV, DGB, TES, JGH, ML.

Final approval for all aspects of the work: CDV, DGB, TES, JGH, ML.

Final approval of the version to be submitted and agreement to be accountable for all aspects of the work: CDV, DGB, TES, JGH, ML.

Funding

This work is funded by the National Centre of 3Rs PhD studentship "Replacement of animal models of CA and CPR using computer simulation" (NC/S001328/1).

Acknowledgements

This work is funded by the National Centre of 3Rs PhD studentship "Replacement of animal models of CA and CPR using computer simulation" (NC/S001328/1).

Appendix A. Supplementary material

Supplementary data to this article can be found online at https://doi.org/10.1016/j.resuscitation.2023.109758.

Author details

[a]*Anaesthesia & Critical Care, Injury, Inflammation and Recovery Science Academic Unit, School of Medicine, University of Nottingham, Nottingham NG7 2UH, UK* [b]*School of Engineering, University of Warwick, Coventry CV4 7AL, UK* [c]*Academic Department of Military Anaesthesia and Critical Care, Royal Centre for Defence Medicine, ICT Centre, Birmingham B15 2SQ, UK* [d]*Nottingham University Hospitals NHS Trust, Nottingham NG7 2UH, UK*

REFERENCES

1. Gräsner JT, Wnent J, Herlitz J, et al. Survival after out-of-hospital cardiac arrest in Europe - Results of the EuReCa TWO study. Resuscitation 2020;148:218–26.
2. Idris AH, Guffey D, Aufderheide TP, et al. Relationship between chest compression rates and outcomes from cardiac arrest. Circulation 2012;125:3004–12.
3. Idris AH, Guffey D, Pepe PE, et al. Chest compression rates and survival following out-of-hospital cardiac arrest. Crit Care Med 2015;43:840–8.
4. Vadeboncoeur T, Stolz U, Panchal A, et al. Chest compression depth and survival in out-of-hospital cardiac arrest. Resuscitation 2014;85:182–8.
5. Kovacs A, Vadeboncoeur TF, Stolz U, et al. Chest compression release velocity: Association with survival and favorable neurologic outcome after out-of-hospital cardiac arrest. Resuscitation 2015;92:107–14.
6. Fabian-Jessing BK, Vallentin MF, Secher N, et al. Animal models of cardiac arrest: A systematic review of bias and reporting. Resuscitation 2018;125:16–21.
7. Vognsen M, Fabian-Jessing BK, Secher N, et al. Contemporary animal models of cardiac arrest: A systematic review. Resuscitation 2017;113:115–23.
8. Monsieurs KG, Nolan JP, Bossaert LL, et al. European Resuscitation Council Guidelines for Resuscitation 2015: Section 1. Executive summary. Resuscitation 2015;95:1–80.
9. Considine J, Gazmuri RJ, Perkins GD, et al. Chest compression components (rate, depth, chest wall recoil and leaning): A scoping review. Resuscitation 2019.
10. Babbs CF, Kemeny AE, Quan W, Freeman G. A new paradigm for human resuscitation research using intelligent devices. Resuscitation 2008;77:306–15.
11. Stiell IG, Brown SP, Christenson J, et al. What is the role of chest compression depth during out-of-hospital cardiac arrest resuscitation? Crit Care Med 2012;40:1192–8.
12. Stiell IG, Brown SP, Nichol G, et al. What is the optimal chest compression depth during out-of-hospital cardiac arrest resuscitation of adult patients? Circulation 2014;130:1962–70.
13. Johnson BV, Coult J, Fahrenbruch C, et al. Cardiopulmonary resuscitation duty cycle in out-of-hospital cardiac arrest. Resuscitation 2015;87:86–90.
14. Cordioli RL, Grieco DL, Charbonney E, Richard JC, Savary D. New physiological insights in ventilation during cardiopulmonary resuscitation. Curr Opin Crit Care 2019;25:37–44.
15. Yannopoulos D, Matsuura T, McKnite S, et al. No assisted ventilation cardiopulmonary resuscitation and 24-hour neurological outcomes in a porcine model of cardiac arrest. Crit Care Med 2010;38:254–60.
16. Soar J, Maconochie I, Wyckoff MH, et al. 2019 International Consensus on Cardiopulmonary Resuscitation and Emergency Cardiovascular Care Science With Treatment Recommendations: Summary From the Basic Life Support; Advanced Life Support; Pediatric Life Support; Neonatal Life Support; Education, Implementation, and Teams; and First Aid Task Forces. Circulation 2019;140:e826–30.
17. Daudre-Vignier C, Laviola M, Das A, Bates DG, Hardman JG. Identification of an optimal CPR chest compression protocol. Annu Int Conf IEEE Eng Med Biol Soc 2021;2021:5459–62.
18. Hardman JG, Bedforth NM, Ahmed AB, Mahajan RP, Aitkenhead AR. A physiology simulator: validation of its respiratory components and its ability to predict the patient's response to changes in mechanical ventilation. Br J Anaesth 1998;81:327–32.

19. Das A, Haque M, Chikhani M, et al. Development of an Integrated Model of Cardiovascular and Pulmonary Physiology for the Evaluation of Mechanical Ventilation Strategies. Annu Int Conf IEEE Eng Med Biol Soc 2015:5319–22.
20. Laviola M, Das A, Chikhani M, Bates DG, Hardman JG. Computer simulation clarifies mechanisms of carbon dioxide clearance during apnoea. Br J Anaesth 2019;122:395–401.
21. Stolady D, Laviola M, Pillai A, Hardman JG. Effect of variable pre-oxygenation endpoints on safe apnoea time using high flow nasal oxygen for women in labour: a modelling investigation. Br J Anaesth 2021;126:889–95.
22. Saffaran S, Das A, Hardman JG, Yehya N, Bates DG. High-fidelity computational simulation to refine strategies for lung-protective ventilation in paediatric acute respiratory distress syndrome. Intens Care Med 2019;45:1055–7.
23. Kim H, Hwang SO, Lee CC, et al. Direction of blood flow from the left ventricle during cardiopulmonary resuscitation in humans: its implications for mechanism of blood flow. Am Heart J 2008;156 (1222):e1–7.
24. Redberg RF, Tucker KJ, Cohen TJ, Dutton JP, Callaham ML, Schiller NB. Physiology of blood flow during cardiopulmonary resuscitation. A transesophageal echocardiographic study. Circulation 1993;88:534–42.
25. Sheak KR, Wiebe DJ, Leary M, et al. Quantitative relationship between end-tidal carbon dioxide and CPR quality during both in-hospital and out-of-hospital cardiac arrest. Resuscitation 2015;89:149–54.
26. Naim MY, Sutton RM, Friess SH, et al. Blood Pressure- and Coronary Perfusion Pressure-Targeted Cardiopulmonary Resuscitation Improves 24-Hour Survival From Ventricular Fibrillation Cardiac Arrest. Crit Care Med 2016;44:e1111–7.
27. Fodden DI, Crosby AC, Channer KS. Doppler measurement of cardiac output during cardiopulmonary resuscitation. J Accid Emerg Med 1996;13:379–82.
28. Repessé X, Charron C, Fink J, et al. Value and determinants of the mean systemic filling pressure in critically ill patients. Am J Physiol Heart Circ Physiol 2015;309:H1003–7.
29. Soar J, Nolan JP, Böttiger BW, et al. European Resuscitation Council Guidelines for Resuscitation 2015: Section 3. Adult advanced life support. Resuscitation 2015;95:100–47.
30. Aufderheide TP, Sigurdsson G, Pirrallo RG, et al. Hyperventilation-induced hypotension during cardiopulmonary resuscitation. Circulation 2004;109:1960–5.
31. Babbs CF. Relative effectiveness of interposed abdominal compression CPR: sensitivity analysis and recommended compression rates. Resuscitation 2005;66:347–55.
32. Zhang Y, Karemaker JM. Abdominal counter pressure in CPR: what about the lungs? An in silico study. Resuscitation 2012;83:1271–6.
33. Babbs CF. CPR techniques that combine chest and abdominal compression and decompression: hemodynamic insights from a spreadsheet model. Circulation 1999;100:2146–52.
34. Babbs CF. Efficacy of interposed abdominal compression-cardiopulmonary resuscitation (CPR), active compression and decompression-CPR and Lifestick CPR: basic physiology in a spreadsheet model. Crit Care Med 2000;28:N199–202.
35. Babbs CF. Design of near-optimal waveforms for chest and abdominal compression and decompression in CPR using computer-simulated evolution. Resuscitation 2006;68:277–93.
36. Babbs CF. Effects of an impedance threshold valve upon hemodynamics in Standard CPR: studies in a refined computational model. Resuscitation 2005;66:335–45.
37. Babbs CF, Yannopoulos D. A dose-response curve for the negative bias pressure of an intrathoracic pressure regulator during CPR. Resuscitation 2006;71:365–8.
38. Shin DA, Park J, Lee JC, Shin SD, Kim HC. Computational simulation of passive leg-raising effects on hemodynamics during cardiopulmonary resuscitation. Comput Methods Programs Biomed 2017;140:195–200.
39. Zhang Y, Jiménez-Herrera M, Axelsson C, Cheng Y. Not Bad: Passive Leg Raising in Cardiopulmonary Resuscitation-A New Modeling Study. Front Physiol 2016;7:665.
40. Jung E, Babbs CF, Lenhart S, Protopopescu VA. Optimal strategy for cardiopulmonary resuscitation with continuous chest compression. Acad Emerg Med: Official J Soc Acad Emerg Med 2006;13:715–21.
41. Jung E, Lenhart S, Protopopescu V, Babbs C. Optimal control applied to a thoraco-abdominal CPR model. Math Med Biol 2008;25:157–70.
42. Babbs CF, Meyer A, Nadkarni V. Neonatal CPR: room at the top–a mathematical study of optimal chest compression frequency versus body size. Resuscitation 2009;80:1280–4.
43. John AR, Manivannan M, Ramakrishnan TV. Computer-Based CPR Simulation Towards Validation of AHA/ERC Guidelines. Cardiovasc Eng Technol 2017;8:229–35.
44. Turner I, Turner S, Armstrong V. Does the compression to ventilation ratio affect the quality of CPR: a simulation study. Resuscitation 2002;52:55–62.

Appendix 5. Tissue oxygenation during permissive hypercapnia in patients with critical illness.

This study was an interdisciplinary collaboration between the School of Medicine of University of Nottingham and the School of Engineering of the University of Warwick.

Clara Daudre-Vignier, Marianna Laviola, Chiara Galli Gorgoni, David W Hewson, Declan G. Bates, Jonathan G Hardman, “Tissue oxygenation during permissive hypercapnia in patients with critical illness”.

My contribution to the work is:

- Conception and design of the study
- Running simulations
- Analysis and interpretation of data
- Drafting the article and revising it critically for important intellectual content

Tissue oxygenation during permissive hypercapnia in mechanically ventilated patients with acute respiratory failure: a computational modelling study

Clara Daudre-Vignier[1]*, Marianna Laviola[1]*, Chiara Galli Gorgoni[2], David W Hewson[1,2], Declan G. Bates[3], Jonathan G Hardman[1,2]

1. Anaesthesia and Critical Care, Academic Unit of Injury, Inflammation and Recovery Science, School of Medicine, University of Nottingham, Nottingham NG7 2UH, UK

2. Department of Anaesthesia, Nottingham University Hospitals NHS Trust, Nottingham NG7 2UH, UK

3. School of Engineering, University of Warwick, Coventry CV4 7AL

* These authors contributed equally to the study.

Corresponding author

Dr David Hewson david.hewson@nottingham.ac.uk

Department of Anaesthesia

C Floor, East Block

Queen's Medical Centre

Nottingham University Hospitals NHS Trust

Nottingham

NG7 2UH

UK

Abbreviated Title: Tissue oxygenation in permissive hypercapnia

ABSTRACT

Background. Lung protective ventilation (LPV) in patients with acute respiratory failure commonly results in reduced carbon dioxide clearance and hypercapnia. The physiological effects of hypercapnia remain incompletely understood. The aim of this study is to elucidate the effects of hypercapnia on tissue oxygenation in the context of acute respiratory failure managed with positive pressure ventilation.

Methods. Four hundred and five simulations were conducted using a high-fidelity computational model of the cardiovascular and pulmonary systems. We examined the effect of arterial carbon dioxide partial pressure on tissue oxygen delivery in the context of varying haemoglobin concentration (Hb), cardiac output (CO) and inspired oxygen fraction (FiO_2) under varying degrees of ventilation-perfusion (VQ) mismatch.

Results. Physiologically relevant hypercapnia ($PaCO_2$ 5.9–13.2 kPa) resulted in improved tissue oxygen partial pressure (PtO_2) (PtO_2 4.5 – 5.7) across the range of VQ mismatch configurations and across the range of controlled physiological variables, i.e. Hb, CO, and FiO_2. Reducing minute ventilation improved PtO_2 across the range of other controlled physiological variables, i.e., Hb, CO, and FiO_2, and across the different VQ mismatches.

Keywords: hypercapnia, respiratory failure, tissue oxygenation, computational simulation.

INTRODUCTION

Acute lung injury (ALI) is characterised by alveolar-capillary inflammation, heterogenous alveolar dysfunction and damage, atelectasis and non-cardiogenic high permeability pulmonary oedema. The resulting profound derangements of gas exchange result in hypoxaemia and hypercapnia. In addition to treatment of the underlying causative illness, the main preventative and therapeutic intervention to support gas exchange in patients with ALI is the use of mechanical ventilation.[4]

Ventilator-associated lung injury (VALI) is caused or aggravated by mechanical ventilation and consequent volutrauma, barotrauma, atelectotrauma and biotrauma.[1–3] By limiting airway pressures and tidal volumes, lung protective ventilation (LPV) strategies have been shown to reduce iatrogenic lung stress and decrease injury to the alveolar wall, leading to improved 28-day mortality [REFs]. Reduced minute ventilation according to LPV principles (together with the deranged gas exchange associated with the fundamental causative pathology) commonly results in arterial hypercapnia in patients with ALI; this is commonly tolerated in the belief that the hypercapnia will have fewer adverse effects than greater energy application to the injured lung. Such "permissive" hypercapnia has been an accepted part of critical care medical practice for over 30 years,[5] although the precise impact of hypercapnia on various body systems during critical illness remains controversial.[6] While increased carbon dioxide partial pressure has been proposed as protective to a range of injured organ systems,[7] recent studies have demonstrated the deleterious effects of carbon dioxide on the respiratory[8 9] and cardiovascular[10 11] systems. In animal models[12] and non-critically ill humans,[13–15] mild-to-moderate hypercapnia is known to cause a right-shift in the oxyhaemoglobin dissociation curve, increased cardiac index, decreased systemic vascular resistance and improved tissue perfusion; however, the effect of hypercapnia on tissue oxygen partial pressure (PtO_2) during acute respiratory failure is unknown. Tissue oxygen partial pressure is considered here to be the partial pressure of oxygen in the tissue interstitium; it provides an indication of regional perfusion and oxygen flux (i.e. the balance between cardiorespiratory oxygen delivery and mitochondrial oxygen consumption). Measurement and control of PtO_2 in the setting of adult and paediatric critical illness is an ongoing area of research interest,[16–18] given the fundamental importance of maintaining tissue oxygenation, promoting wound healing and avoiding tissue infection.

Furthermore, safe levels of hypercapnia and acidaemia in individual patients with ALI remain undefined and it is unclear whether hypercapnic acidaemia carries an outcome benefit independent of low tidal volume ventilation.[19] Invasive strategies such as extracorporeal carbon dioxide removal can effectively limit hypercapnic acidaemia, but it is uncertain which patients should be selected for such treatment, with expertise limited to small studies conducted by specialist centres.[20]

The complex physiological alterations caused by ALI, affecting cardiac output, pulmonary function as well as heart-lung interactions and their effect on tissue oxygenation, are difficult to quantify and challenging to investigate in the clinical environment. Given these

challenges, high fidelity computer simulation of the pathophysiology of ALI is a useful tool with which to elucidate physiological processes in critically ill patients. Animal models have been used to elucidate the role of permissive hypercapnia on tissue oxygenation [REF], but these studies are usually carried out in rodents, which exhibit oxyconformism, a downregulation of metabolic rate and body temperature during hypoxia that does not exist in humans.

The aim of this study was to use computational modelling to quantify the impact of hypercapnia on tissue oxygenation across a clinically relevant range of cardiorespiratory variables, including haemoglobin concentration, cardiac output, tidal volume and inspired oxygen fraction.

METHODS

Computational model

This study used the Interdisciplinary Collaboration in Systems Medicine (ICSM) simulation suite, which is based upon the Nottingham Physiology Simulator, described previously.[21–23] The ICSM computer simulation is a highly integrated, high fidelity computational model of a number of organ systems. The model has been extensively validated, including in the simulation of hypoxaemia in adults.[24 25] The model incorporates 100 alveolar and 19 cardiovascular compartments, which are individually and independently configured. Hypoxic pulmonary vasoconstriction is implemented in the model based on a previously described stimulus-response curve.[26] Arterial partial pressures of oxygen (PaO_2) and carbon dioxide ($PaCO_2$) are determined via iterative resolution of mass conserving equations at the capillary/alveolus interface. In this study, a single tissue block was modelled, with a pre-set O_2 consumption and CO_2 production, receiving the entire cardiac output. The tissue oxygen partial pressure (PtO_2) is determined by iterative resolution of equations at the capillary/tissue interface and is affected by the rates of metabolic consumption and arterial delivery of oxygen. Other aspects of the model related to pulmonary pathophysiology have been validated previously against patient data in the context of ARDS and COPD.[27–34] A detailed description of the ICSM simulation suite is provided in the online Supplementary Material.

Experimental protocol

To represent the spectrum of physiology observed in ALI, the computational model was configured as follows: ideal body weight 70 kg, anatomical deadspace 105 mL, anatomic pulmonary shunt 2%, functional residual capacity 2.2 litres, respiratory quotient 0.8. Oxygen consumption was set to 373 mL min^{-1} simulating an increase of 50% with respect to normal resting physiological values (replicating the increase in oxygen consumption observed in many pathophysiological scenarios in critical illness, including, for example, surgery, trauma and sepsis).

Subject lungs were configured to create three ventilation-perfusion (VQ) mismatches, i.e. mild, moderate and severe. Each pattern of mismatch was created by varying the compartmental bronchiolar inlet resistances and compartmental arteriolar resistances in opposite directions, generating asynchronous alveolar ventilation and a realistic scatter of VQ ratios[35] as follows:

- VQ1 (mild mismatch): vascular resistance (R_v) 0.5–2 times normal, bronchial resistance (R_b) 2–0.5 times normal,
- VQ2 (moderate mismatch): R_v 0.25–4 times normal, R_b 4–0.25 times normal,
- VQ3 (severe mismatch): R_v 0.1–10 times normal, R_b 10–0.1.

The mean (standard deviation) of the three VQ mismatches, i.e. VQ1 (mild), VQ2 (moderate) and VQ3 (severe) and, the arterial blood gases observed during baseline conditions, i.e. 10 minutes of mechanical ventilation with tidal volume (V_T) of 450 ml, ventilatory frequency of 16 breaths min^{-1} and FiO_2 0.21, are shown in Table 1. The parameters affecting the delivery of oxygen, haemoglobin concentration (Hb) and cardiac output (CO) were varied across clinically relevant ranges (6, 8, 10, 12 and 14 g dL^{-1} and 3, 6 and 9 L min^{-1}, respectively) to determine their effect on tissue oxygenation. In all subsequent simulations, the lungs were ventilated for 10 minutes with volume-controlled ventilation at FiO_2 0.5, 0.8 and 1.0, with a ventilatory frequency of 16 breaths min^{-1} and V_T of 250, 350 and 450 ml.

In summary, we configured three virtual subjects defined by their VQ mismatch (mild, moderate, and severe ALI), and varied the parameters affecting the delivery of oxygen, i.e. Hb, CO, and FiO_2, achieving 135 simulations for each subjects and 405 in total.

~~In total, 405 individual simulation runs were conducted in order to examine the above-described scenarios (i.e. 3 levels of VQ mismatches ⇒ 5 values of Hb and 3 values of CO ⇒ 3 levels of FiO_2 ⇒ 3 levels of V_t).~~

Data collection

Each simulation was conducted until stabilisation of blood and tissue gas partial pressures was observed. During each simulation, PaO_2, $PaCO_2$ and PtO_2 were recorded every 100 ms. Since there was beat-to-beat and breath-to-breath variation in these values, outcome data were calculated as the average of the last 100 samples collected once stabilisation was considered to have occurred. Model simulations were performed using a 64-bit Intel Core i7 3.7 GHz Windows 10 personal computer, running Matlab version R2019a.v7 (MathWorks Inc., Natick, MA, USA).

RESULTS

Clinically relevant hypercapnia was observed ($PaCO_2$ 5.9–13.5 kPa) at all values of minute ventilation (4–7.2 L min^{-1}). Increases in $PaCO_2$ were observed after reduction in minute

ventilation (V_E) across the range of FiO_2 and VQ configurations when the values of Hb and CO were fixed at 8 g dL-1 and 6 L min-1 respectively (Figure 1). Similar $PaCO_2$ increase was observed after reduction in minute ventilation across all the range of Hb, CO, FiO_2 and VQ configurations.

The hypercapnia was associated with increased PtO_2 and decreased PaO_2 across the range of VQ configurations and FiO_2 values (Figure 2 and Table 2) when the values of Hb and CO were fixed at 8 g dL-1 and 6 L min-1 respectively. These values Hb and CO were selected as representative of acute pathophysiology observed in critically ill patients. The levels/ranges of pH observed in table 2 (7.15-7.38) correspond to range of acidaemia observed during permissive hypercapnia. The positive effect of hypercapnia on tissue oxygenation were less marked when the partial pressure of oxygen was low and the VQ mismatch more severe, i.e. VQ3 and FiO_2 50%.

Similar results were observed in Figure 3 across all the ranges of the parameters evaluated i.e., Hb, CO, Vt, FiO2 and the VQ mismatch. The reduction in tidal volume (VT) and the correlated hypercapnia, was associated with in increase in tissue oxygenation across all the parameters evaluated except when the delivery of oxygen was low, (i.e., Hb = 6-8, CO = 3, FiO2 = 50%) across all the VQ mismatches.

DISCUSSION

In this computational modelling investigation, we conducted 405 simulations of LPV in the context of critical illness with a variety of VQ mismatch configurations. We showed that allowing increased $PaCO_2$ (as a result of protective ventilation) was consistently associated with increased tissue oxygen tension across clinically relevant ranges of cardiac output, haemoglobin concentration and inspired oxygen concentration. Although this finding is in keeping with previous *in vivo* animal and human physiological research,[13 14 36] our modelling provides new data to quantify this effect in critical illness and demonstrates the effect of hypercapnia on oxygenation, independent of the known effect of carbon dioxide in raising cardiac output and thereby augmenting tissue oxygenation.[37] The close relationship between tissue metabolism and blood flow, partly mediated by vasodilation due to carbon dioxide production from oxidative metabolism is observed in our results. Our results are in keeping with experiments using bicarbonate-buffered solutions which showed greater increases in PtO_2 in the presence of vasodilation induced by larger carbon dioxide concentrations, compared to the application of other vasodilators.[38]

At a cellular level, the improved PtO_2 observed in conditions of arterial hypercapnia can be explained by the promotion of oxygen release from haemoglobin in conditions of low pH and high CO_2. The evolutionary modulation of oxygen delivery according to metabolic demand, the Bohr effect,[39] is a well described phenomenon in healthy[40] and extreme environmental[41–43] conditions. The influence of CO_2 on tissue oxygen tension in circumstances of critical illness is less clear. Circulatory factors known to influence tissue

oxygen tension include inspired oxygen fraction,[44] temperature,[45] haemoglobin concentration[46] and tissue perfusion.[47] We were able to control these factors within the model, and our results suggest that clinically relevant levels of hypercapnia can substantially affect tissue oxygenation, independent of the above factors. The challenge of elucidating physiological relationships in critically ill humans with confounding factors arising from co-existing disease has been previously acknowledged.[13] We believe that our results provide a useful insight into the relationship between arterial CO_2 and tissue oxygenation during critical illness while controlling for these confounding factors.

These results are also in agreement with human studies measuring tissue oxygenation with subcutaneous tonometry during controlled mechanical ventilation of patients without lung injury. Akça and colleagues[13] demonstrated a linear increase in PtO_2 from approximately 6.9–11 kPa when $PaCO_2$ was adjusted in the range of 3–8 kPa in 10 healthy volunteers. The average PaO_2 of the participants was approximately 24 kPa. The same authors described similar findings in 20 surgical patients subjected to hypercapnia in the range $PaCO_2$ 4.0–6.0 kPa; subcutaneous PtO_2 increased from 8.4 kPa in normocapnic conditions to 11.8 kPa during hypercapnia. [48]

There are limitations to our study. Our current computational model provides only a single theoretical tissue interstitium from which a global PtO_2 can be described. Although a useful indicator of overall oxygen balance, a single compartment model does not replicate known inter- or intra-organ variations in oxygen flux observed in animal and human tissue beds.[49–53] It should also be acknowledged that, although there are sound theoretical reasons why tissue oxygen tension is a physiological variable of importance in critical illness,[49] measurement of PtO_2 and integration into clinical decision-making remains unusual. Polarographic,[54] spectroscopic[55] and dynamic fluorescence[56] techniques of PtO_2 measurement remain the subject of research to determine validation and clinical utility,[57–59] but are not in routine clinical usage outside specialist centres and patient groups (most noticeably neuroscience centres caring for severely brain injured adults).[60] Our model usefully overcomes many of the limitations of PtO_2 monitors, including calibration, expense and non-continuous data acquisition, however these issues remain barriers to *in vivo* data acquisition.

Further research is needed to describe the oxygen tension characteristics of specific organ systems under the varying cardiorespiratory conditions of critical illness. The interplay of hypercapnia and tissue oxygen tension with local perfusion pressure, blood flow, oxygen carriage, oxygen extraction and metabolic demand in cerebral, coronary, renal, hepatic and splanchnic tissues remains incompletely understood. Given the aforementioned challenges to physiological research in critical illness, we believe robust computational modelling to be an excellent method to provide such data because such modelling can recreate complex systems of interest while allowing exclusion of unpredictable, irrelevant or random data.

In summary, this study aimed to describe the effect of hypercapnia on tissue oxygenation in the context of acute respiratory failure managed with positive pressure ventilation. Our

results indicate that arterial hypercapnia induced by manipulation of minute ventilation resulted in improved tissue oxygen partial pressure (PtO_2) across the range of VQ mismatch configurations and FiO_2 considered.

AUTHOR'S CONTRIBUTIONS

Design of study: ML, JGH

Design of model: JGH

Simulation runs: CD-V, ML

Interpretation of data: All authors

Writing and final approval of manuscript: All authors

DECLARATION OF INTERESTS

JGH is associate editor-in-chief of the British Journal of Anaesthesia. JGH accepts fees for the provision of advice to the police, crown prosecution service, coroners and solicitors. The other authors have no relevant conflicts to declare.

FUNDING STATEMENT

This work was supported by PhD studentship funding from National Centre of 3Rs (NC/S001328/1).

SUPPLEMENTARY MATERIAL

Supplementary material is available online.

REFERENCES

1. Gattinoni L, Protti A, Caironi P, Carlesso E. Ventilator-induced lung injury: the anatomical and physiological framework. *Crit Care Med* Crit Care Med; 2010; **38**
2. RG B, MA M, A M, D S, BT T, A W. Ventilation with lower tidal volumes as compared with traditional tidal volumes for acute lung injury and the acute respiratory distress syndrome. *N Engl J Med* N Engl J Med; 2000; **342**: 1301–8
3. Hong SB, Huang Y, Moreno-Vinasco L, et al. Essential Role of Pre–B-Cell Colony Enhancing Factor in Ventilator-induced Lung Injury. *Am J Respir Crit Care Med* American Thoracic Society; 2008; **178**: 605
4. Griffiths MJD, McAuley DF, Perkins GD, et al. Guidelines on the management of acute respiratory distress syndrome. *BMJ Open Respir Res* Archives of Disease in childhood; 2019; **6**: e000420
5. Hickling KG. Low volume ventilation with permissive hypercapnia in the Adult Respiratory Distress Syndrome. *Clin Intensive Care* 1992; **3**: 67–78
6. Repessé X, Vieillard-Baron A. Hypercapnia during acute respiratory distress syndrome: the tree that hides the forest! *J Thorac Dis* AME Publications; 2017; **9**: 1420
7. Laffey JG, Kavanagh BP. Carbon dioxide and the critically ill--too little of a good thing? *Lancet (London, England)* Lancet; 1999; **354**: 1283–6
8. Doerr CH, Gajic O, Berrios JC, et al. Hypercapnic Acidosis Impairs Plasma Membrane Wound Resealing in Ventilator-injured Lungs. *Am J Respir Crit Care Med* American Thoracic Society; 2005; **171**: 1371
9. Jaitovich A, Angulo M, Lecuona E, et al. High CO2 levels cause skeletal muscle atrophy via AMP-activated kinase (AMPK), FoxO3a protein, and muscle-specific Ring finger protein 1 (MuRF1). *J Biol Chem* J Biol Chem; 2015; **290**: 9183–94
10. Boissier F, Katsahian S, Razazi K, et al. Prevalence and prognosis of cor pulmonale during protective ventilation for acute respiratory distress syndrome. *Intensive Care Med* Intensive Care Med; 2013; **39**: 1725–33
11. Dessap AM, Charron C, Devaquet J, et al. Impact of acute hypercapnia and augmented positive end-expiratory pressure on right ventricle function in severe acute respiratory distress syndrome. *Intensive Care Med* Intensive Care Med; 2009; **35**: 1850–8
12. Schwartges I, Schwarte LA, Fournell A, Scheeren TWL, Picker O. Hypercapnia induces a concentration-dependent increase in gastric mucosal oxygenation in dogs. *Intensive Care Med* Intensive Care Med; 2008; **34**: 1898–906
13. Akça O, Doufas AG, Morioka N, Iscoe S, Fisher J, Sessler DI. Hypercapnia improves tissue oxygenation. *Anesthesiology* Anesthesiology; 2002; **97**: 801–6
14. Hager H, Reddy D, Mandadi G, et al. Hypercapnia improves tissue oxygenation in morbidly obese surgical patients. *Anesth Analg* Anesth Analg; 2006; **103**: 677–81
15. Fleischmann E, Herbst F, Kugener A, et al. Mild Hypercapnia Increases Subcutaneous and Colonic Oxygen Tension in Patients Given 80% Inspired Oxygen during Abdominal Surgery. *Anesthesiology* American Society of Anesthesiologists; 2006;

104: 944–9

16. Arnež ZM, Ramella V, Papa G, et al. Is the LICOX® PtO 2 system reliable for monitoring of free flaps? Comparison between two cohorts of patients. *Microsurgery* Microsurgery; 2019; **39**: 423–7
17. Okonkwo DO, Shutter LA, Moore C, et al. Brain Oxygen Optimization in Severe Traumatic Brain Injury Phase-II: A Phase II Randomized Trial. *Crit Care Med* Crit Care Med; 2017; **45**: 1907–14
18. Figaji AA, Zwane E, Thompson C, et al. Brain tissue oxygen tension monitoring in pediatric severe traumatic brain injury Part 2: Relationship with clinical, physiological, and treatment factors.
19. Morales-Quinteros L, Camprubí-Rimblas M, Bringué J, Bos LD, Schultz MJ, Artigas A. The role of hypercapnia in acute respiratory failure. *Intensive care Med Exp* Intensive Care Med Exp; 2019; **7**
20. Morelli A, Del Sorbo L, Pesenti A, Ranieri VM, Fan E. Extracorporeal carbon dioxide removal (ECCO 2 R) in patients with acute respiratory failure. *Intensive Care Med* Intensive Care Med; 2017; **43**: 519–30
21. Hardman JG, Bedforth NM, Ahmed AB, Mahajan RP, Aitkenhead AR. A physiology simulator: validation of its respiratory components and its ability to predict the patient's response to changes in mechanical ventilation. *Br J Anaesth* Br J Anaesth; 1998; **81**: 327–32
22. Hardman JG, Bedforth NM. Estimating venous admixture using a physiological simulator. *Br J Anaesth* Br J Anaesth; 1999; **82**: 346–9
23. Bedforth NM, Hardman JG. Predicting patients' responses to changes in mechanical ventilation: a comparison between physicians and a physiological simulator. *Intensive Care Med* Intensive Care Med; 1999; **25**: 839–42
24. Hardman J, Wills J, Analgesia AA-A&, 2000 undefined. Investigating hypoxemia during apnea: validation of a set of physiological models. *journals.lww.com*
25. Stolady D, Laviola M, Pillai A, Anaesthesia JH-BJ of, 2021 undefined. Effect of variable pre-oxygenation endpoints on safe apnoea time using high flow nasal oxygen for women in labour: a modelling investigation. *Elsevier*
26. Marshall BE, Clarke WR, Costarino AT, Chen L, Miller F, Marshall C. The dose-response relationship for hypoxic pulmonary vasoconstriction. *Respir Physiol* Respir Physiol; 1994; **96**: 231–47
27. McCahon RA, Columb MO, Mahajan RP, Hardman JG. Validation and application of a high-fidelity, computational model of acute respiratory distress syndrome to the examination of the indices of oxygenation at constant lung-state. *Br J Anaesth* Br J Anaesth; 2008; **101**: 358–65
28. Das A, Cole O, Chikhani M, et al. Evaluation of lung recruitment maneuvers in acute respiratory distress syndrome using computer simulation. *Crit Care* Crit Care; 2015; **19**
29. Chikhani M, Das A, Haque M, Wang W, Bates DG, Hardman JG. High PEEP in acute respiratory distress syndrome: quantitative evaluation between improved arterial oxygenation and decreased oxygen delivery. *Br J Anaesth* Br J Anaesth; 2016; **117**: 650–8

30. Das A, Haque M, Chikhani M, et al. Hemodynamic effects of lung recruitment maneuvers in acute respiratory distress syndrome. *BMC Pulm Med* BioMed Central Ltd.; 2017; **17**: 1–13

31. Das A, Camporota L, Hardman JG, Bates DG. What links ventilator driving pressure with survival in the acute respiratory distress syndrome? A computational study. *Respir Res* BioMed Central Ltd.; 2019; **20**: 1–10

32. Saffaran S, Das A, Hardman JG, Yehya N, Bates DG. High-fidelity computational simulation to refine strategies for lung-protective ventilation in paediatric acute respiratory distress syndrome. *Intensive Care Med* Intensive Care Med; 2019; **45**: 1055–7

33. Saffaran S, Das A, Laffey JG, Hardman JG, Yehya N, Bates DG. Utility of Driving Pressure and Mechanical Power to Guide Protective Ventilator Settings in Two Cohorts of Adult and Pediatric Patients With Acute Respiratory Distress Syndrome: A Computational Investigation. *Crit Care Med* Crit Care Med; 2020; **48**: 1001–8

34. Wang W, Das A, Ali T, et al. Can computer simulators accurately represent the pathophysiology of individual COPD patients? *Intensive Care Med Exp 2014 21* SpringerOpen; 2014; **2**: 1–14

35. Hardman JG, Aitkenhead AR. Estimating Alveolar Dead Space from the Arterial to End-Tidal CO2 Gradient: A Modeling Analysis. *Anesth Analg* Lippincott Williams and Wilkins; 2003; **97**: 1846–51

36. Wang Z, Su F, Bruhn A, Yang X, Vincent JL. Acute hypercapnia improves indices of tissue oxygenation more than dobutamine in septic shock. *Am J Respir Crit Care Med* Am J Respir Crit Care Med; 2008; **177**: 178–83

37. Mas A, Saura P, Joseph D, … LB-C care, 2000 undefined. Effect of acute moderate changes in PaCO2 on global hemodynamics and gastric perfusion. *journals.lww.com*

38. Duling BR. Changes in microvascular diameter and oxygen tension induced by carbon dioxide. *Circ Res* 1973; **32**: 370–6

39. Bohr C, Haseelbalch K, Krogh A. About a biologically important influence that the carbonic acid tension of the blood has on its oxygen binding 1. *Scand Arch* . 1904;

40. Riggs AF. THE BOHR EFFECT. *Ann Rev Physiol* 1988; **50**: 181–204

41. Jendroszek A, Malte H, Overgaard CB, et al. Allosteric mechanisms underlying the adaptive increase in hemoglobin-oxygen affinity of the bar-headed goose. *J Exp Biol* J Exp Biol; 2018; **221**

42. Samaja M, Crespi T, Guazzi M, Vandegriff KD. Oxygen transport in blood at high altitude: Role of the hemoglobin-oxygen affinity and impact of the phenomena related to hemoglobin allosterism and red cell function. *Eur J Appl Physiol* Springer; 2003; **90**: 351–9

43. Weber RE. High-altitude adaptations in vertebrate hemoglobins. *Respir Physiol Neurobiol* Elsevier; 2007; **158**: 132–42

44. Gottrup F, Firmin R, Rabkin J, … BH-C care, 1987 undefined. Directly measured tissue oxygen tension and arterial oxygen tension assess tissue perfusion. *europepmc.org*

45. Sheffield CW, Sessler DI, Hopf HW, et al. Centrally and locally mediated thermoregulatory responses alter subcutaneous oxygen tension. *Wound Repair Regen*

John Wiley & Sons, Ltd; 1996; **4**: 339–45

46. Gosain A, Rabkin J, Reymond J, Jensen J, Surgery TH-, 1991 undefined. Tissue oxygen tension and other indicators of blood loss or organ perfusion during graded hemorrhage. *europepmc.org*

47. Arkiliç CF, Taguchi A, Sharma N, et al. Supplemental perioperative fluid administration increases tissue oxygen pressure. *Surgery* Mosby; 2003; **133**: 49–55

48. Akça O, Liem E, Suleman M-I, Doufas AG, Galandiuk S, Sessler DI. Effect of intra-operative end-tidal carbon dioxide partial pressure on tissue oxygenation.

49. De Santis V, Singer M. Tissue oxygen tension monitoring of organ perfusion: rationale, methodologies, and literature review. *BJA Br J Anaesth* Oxford Academic; 2015; **115**: 357–65

50. Narotam PK, Morrison JF, Nathoo N. Brain tissue oxygen monitoring in traumatic brain injury and major trauma: outcome analysis of a brain tissue oxygen-directed therapy. *J Neurosurg* J Neurosurg; 2009; **111**: 672–82

51. Brooks AJ, Eastwood J, Beckingham IJ, Girling KJ. Liver tissue partial pressure of oxygen and carbon dioxide during partial hepatectomy. *Br J Anaesth* Br J Anaesth; 2004; **92**: 735–7

52. Boekstegers P, Weidenhöfer S, Pilz G, Werdan K. Peripheral oxygen availability within skeletal muscle in sepsis and septic shock: comparison to limited infection and cardiogenic shock. *Infection* Infection; 1991; **19**: 317–23

53. Leary TS, Klinck JR, Hayman G, Friend P, Jamieson N V., Gupta AK. Measurement of liver tissue oxygenation after orthotopic liver transplantation using a multiparameter sensor. A pilot study. *Anaesthesia* Anaesthesia; 2002; **57**: 1128–33

54. Stewart C, Haitsma I, Zador Z, et al. THE NEW LICOX COMBINED BRAIN TISSUE OXYGEN AND BRAIN TEMPERATURE MONITORASSESSMENT OF IN VITRO ACCURACY AND CLINICAL EXPERIENCE IN SEVERE TRAUMATIC BRAIN INJURY. *Neurosurgery* Oxford Academic; 2008; **63**: 1159–65

55. Wood MD, Jacobson JA, Maslove DM, Muscedere JG, Boyd JG. The physiological determinants of near-infrared spectroscopy-derived regional cerebral oxygenation in critically ill adults. *Intensive Care Med Exp 2019 71* SpringerOpen; 2019; **7**: 1–15

56. Knopp JA, Longmuir IS. Intracellular measurement of oxygen by quenching of fluorescence of pyrenebutyric acid. *Biochim Biophys Acta - Gen Subj* Elsevier; 1972; **279**: 393–7

57. Pascual JL, Georgoff P, Maloney-Wilensky E, et al. Reduced brain tissue oxygen in traumatic brain injury: Are most commonly used interventions successful? *J Trauma - Inj Infect Crit Care* 2011; **70**: 535–46

58. Nangunoori R, Maloney-Wilensky E, Stiefel M, et al. Brain Tissue Oxygen-Based Therapy and Outcome After Severe Traumatic Brain Injury: A Systematic Literature Review.

59. Davies DJ, Clancy M, Dehghani H, et al. Cerebral Oxygenation in Traumatic Brain Injury: Can a Non-Invasive Frequency Domain Near-Infrared Spectroscopy Device Detect Changes in Brain Tissue Oxygen Tension as Well as the Established Invasive Monitor?

60. Le Roux P, Menon DK, Citerio G, et al. Consensus Summary Statement of the

International Multidisciplinary Consensus Conference on Multimodality Monitoring in Neurocritical Care: A statement for healthcare professionals from the Neurocritical Care Society and the European Society of Intensive Care Medicine. *Neurocrit Care* Humana Press Inc.; 2014; **21**: 1–26

Table 1

Baseline characteristics. Mean (SD) and arterial blood gases of the three VQ mismatches, i.e. VQ1 (mild), VQ2 (moderate) and VQ3 (severe) during mechanical ventilation with tidal volume of 450 ml, ventilatory frequency of 16 breaths min^{-1} and FiO_2 0.21. For these baseline characteristics haemoglobin was fixed to 14 g dL^{-1}. CO 3: cardiac output 3 L min^{-1}; CO 6: cardiac output 6 L min^{-1}; CO 9: cardiac output 9 L min^{-1}; PaO_2: arterial partial pressure of oxygen; $PaCO_2$: arterial partial pressure of carbon dioxide; pHa: arterial pH.

	VQ1			**VQ2**			**VQ3**		
	CO 3	**CO 6**	**CO 9**	**CO 3**	**CO 6**	**CO 9**	**CO 3**	**CO 6**	**CO 9**
VQ mean (SD)	2.6 (0.8)	1.4 (0.5)	0.9 (0.4)	3.0 (1.5)	1.6 (0.9)	1.1 (0.7)	3.9 (2.5)	2.1 (1.6)	1.5 (1.1)
pHa	7.4	7.4	7.4	7.4	7.4	7.4	7.3	7.3	7.3
PaO_2 (kPa)	11.5	11.9	12.0	9.8	10.2	10.4	6.0	7.3	7.8
$PaCO_2$ (kPa)	5.8	6.0	6.0	6.1	6.2	6.3	6.8	6.8	6.7
Temperature (C)	37	37	37	37	37	37	37	37	37

Table 2

Partial pressure of carbon dioxide ($PaCO_2$), tissue partial pressure of oxygen (PtO_2), partial pressure of oxygen (PaO_2) and arterial pH (pHa) arising from manipulation of minute ventilation (V_T 250, 350, 450 ml and ventilatory frequency of 16 breaths min^{-1}) for FiO_2 0.5, 0.8 and 1.0, and mild (VQ1), moderate (VQ2), or severe (VQ3) mismatched. Values of haemoglobin and cardiac output are fixed at 8 g dL^{-1} and 6 L min^{-1}, respectively.

		VQ1				VQ2				VQ3			
	V_T ml	$PaCO_2$ kPa	PtO_2 kPa	PaO_2 kPa	pHa	$PaCO_2$ kPa	PtO_2 kPa	PaO_2 kPa	pHa	$PaCO_2$ kPa	PtO_2 kPa	PaO_2 kPa	pHa
FIO_2 0.5	250	11.1	4.7	28.1	7.17	11.8	4.6	20.8	7.15	12.6	4.2	28.1	7.17
	350	7.7	4.2	33.5	7.29	8.4	4.3	29.1	7.26	9.6	4.1	33.5	7.29
	450	5.9	3.9	35.9	7.38	6.6	4.0	32.8	7.35	7.7	3.9	35.9	7.38
FIO_2 0.8	250	11.0	5.2	57.8	7.18	11.7	5.3	54.8	7.15	13.4	5.3	57.8	7.18
	350	7.6	4.6	62.7	7.29	8.4	4.7	60.7	7.26	10.2	4.9	62.7	7.29
	450	5.9	4.2	65.0	7.38	6.5	4.4	63.4	7.35	8.3	4.6	65.0	7.38
FIO_2 1.0	250	10.9	5.5	77.7	7.17	11.6	5.6	75.8	7.15	13.2	5.7	77.7	7.17
	350	7.6	4.9	82.3	7.30	8.3	5.1	81.2	7.26	10.1	5.3	82.3	7.30
	450	5.9	4.5	84.5	7.38	6.5	4.7	83.6	7.35	8.2	5.0	84.5	7.38

LEGEND TO FIGURES

Figure 1. Arterial partial pressure of carbon dioxide ($PaCO_2$) arising from manipulation of minute ventilation (V_E; calculated as the product between tidal volumes [V_t = 250, 350 and 450 mL] and ventilatory frequency of 16 breaths min^{-1}), for FiO_2 0.5, 0.8 and 1.0 and mild, moderate or severe VQ mismatch. Values of Hb and CO are fixed at 8 g dL^{-1} and 6 L min^{-1} respectively.

Figure 2. Tissue partial pressure of oxygen (PtO_2) and arterial partial pressure of oxygen (PaO_2) arising from manipulation of $PaCO_2$ for FiO_2 0.5, 0.8 and 1.0, and mild, moderate, or severe VQ mismatch. Values of Hb and CO are fixed at 8 g dL^{-1} and 6 L min^{-1} respectively.

Figure 3. Tissue oxygen partial pressure (PtO_2) obtained for the different values of haemoglobin concentration (Hb), cardiac output (CO), tidal volumes (V_t), inspired fraction of oxygen (FiO_2) and ventilation-perfusion (VQ) ratios studied.

Figure 1

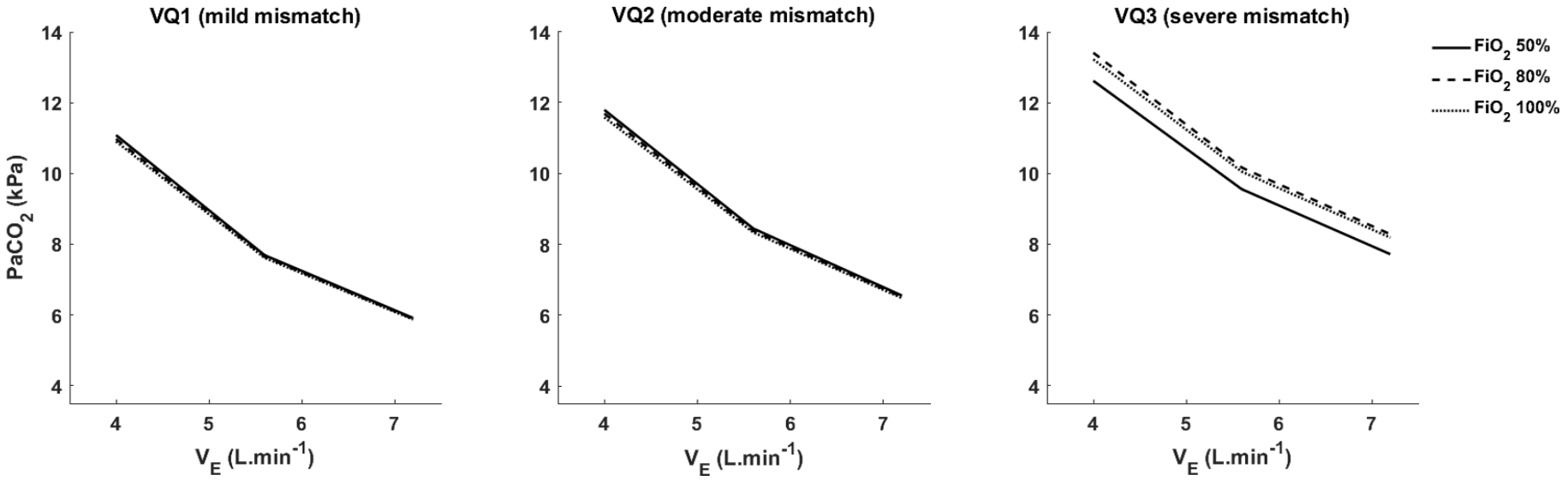
VQ1 (mild mismatch)
VQ2 (moderate mismatch)
VQ3 (severe mismatch)
PaCO2 (kPa)
VE (L.min-1)
FiO2 50%
FiO2 80%
FiO2 100%

Figure 2

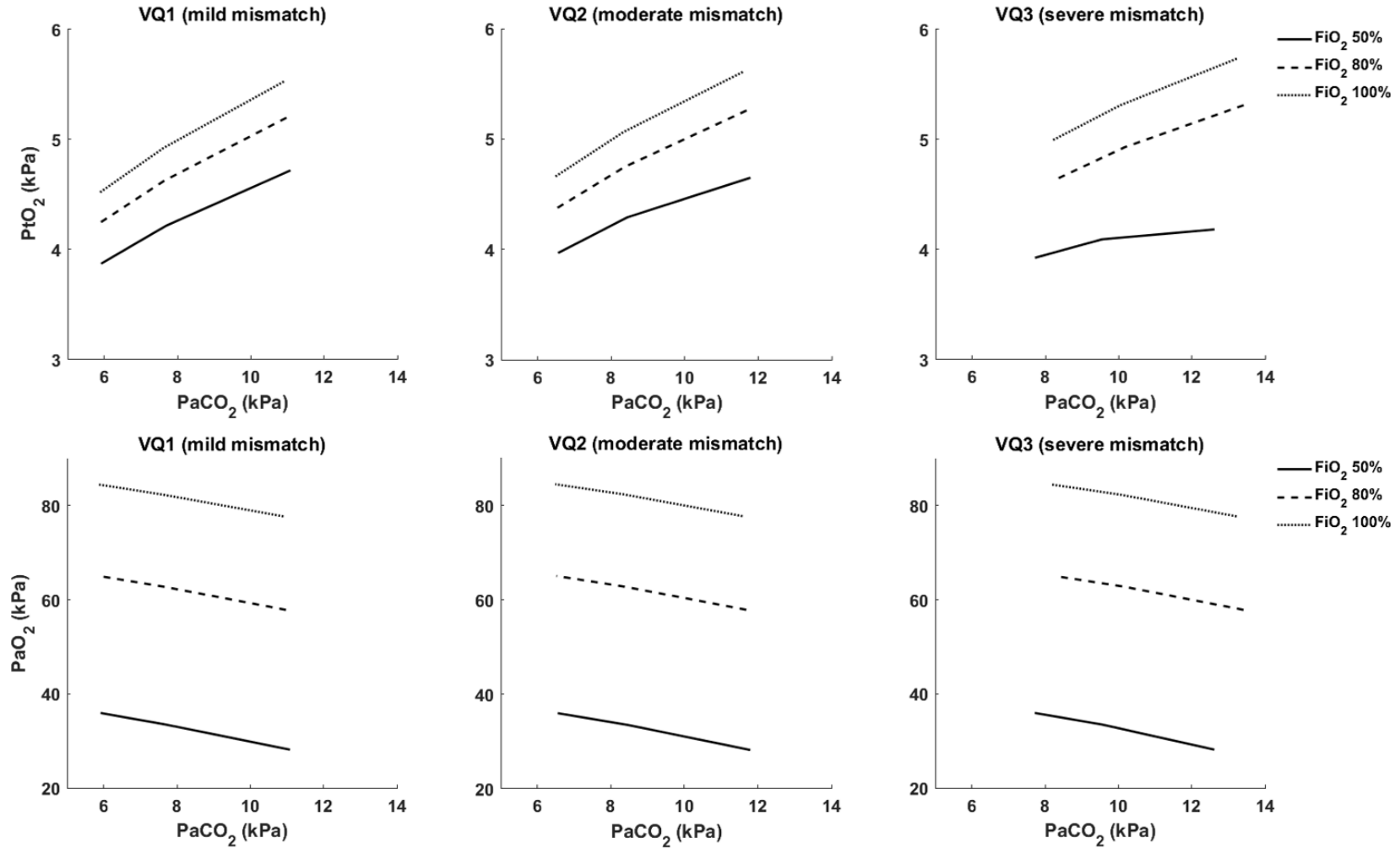
VQ1 (mild mismatch)
VQ2 (moderate mismatch)
VQ3 (severe mismatch)
PtO2 (kPa)
PaO2 (kPa)
PaCO2 (kPa)
FiO2 50%
FiO2 80%
FiO2 100%

Figure 3

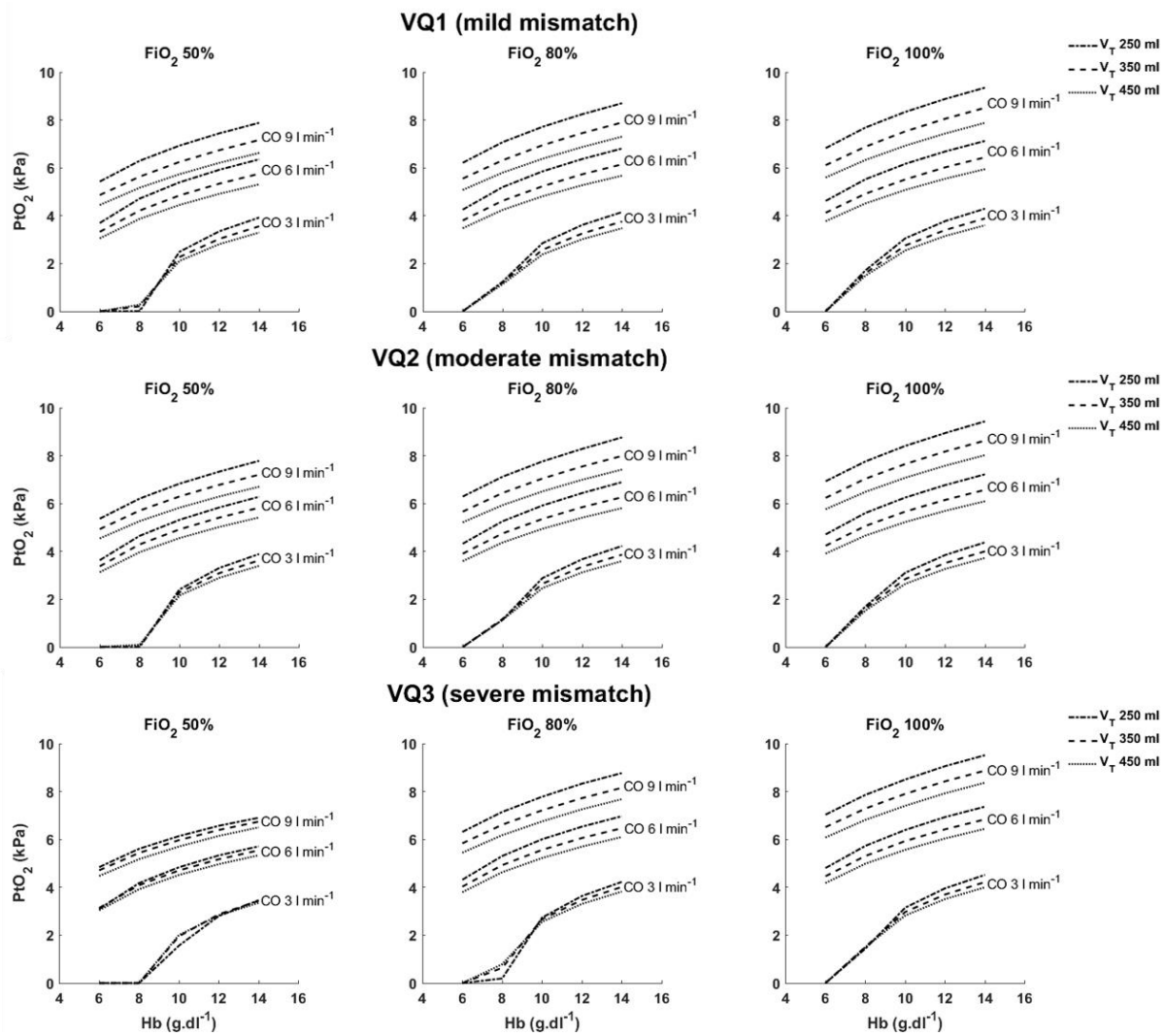
VQ1 (mild mismatch)
VQ2 (moderate mismatch)
VQ3 (severe mismatch)
FiO2 50%
FiO2 80%
FiO2 100%
PtO2 (kPa)
Hb (g.dl-1)
CO 9 l min-1
CO 6 l min-1
CO 3 l min-1
VT 250 ml
VT 350 ml
VT 450 ml

Appendix 6. User-friendly interface development in Simulink

6.1 Introduction

Fully integrated cardiovascular models can result useful for many applications. As described in Section 1.5, animal models of cardiac arrest present many limitations. With the advent of technology and computational power, *in silico* models of human physiology have risen as an attractive alternative to in vivo models. Many laboratories using animal models to study cardiac arrest could be very interested in a computational model to initially test a hypothesis before testing on animals or completely replace their animal models.

6.2 Aim

The aim of this chapter is to develop a Matlab-Simulink (MathWorks, Natick, MA) version of the updated ICSM model along with a graphical user interface (GUI) to make the cardio-pulmonary model user friendly and accessible to scientists without computational skills.
The aim of developing the ICSM model onto Matlab-Simulink is to provide a graphical programming environment which organised into hierarchically smaller subsystems. This will allow users to better understand how the model works and adventure to modify it in accordance to his/her simulations needs.
The aim of the GUI is to provide a control panel where parameters can be adjusted, and external conditions and interventions can be set.

6.3 Methods

In the current version of this chapter, the Simulink simulator is heavily based on Albanese *et al.* work [3], for training purposes. The PNEUMA Release 3.0 software [4, 5] also provides training material for the design of GUI and the development of Matlab-Simulink model. Once I have completed the training, the Simulink simulator will be adapted to match the ICSM model.

6.4 Simulink simulator

The model of the Simulink simulator is mainly based on Albanese *et al.* [3] cardiopulmonary model, apart from the cardiac chambers pressure equations which are based upon Bozkurt [6] work.

The Simulink simulator will be composed of two files, “Simulink_simulator.xls” the main file and “Simulink_initiation.m” which loads the initial parameters. When opening the “Simulink_simulator.xls” file, the user sees Figure 6.1. The three model blocks are labelled with a legend and an image. On the right-hand side, a block of results can be opened (by double clicking the icon) to visualise the results while the simulation is running, and the simulation time is also displayed.

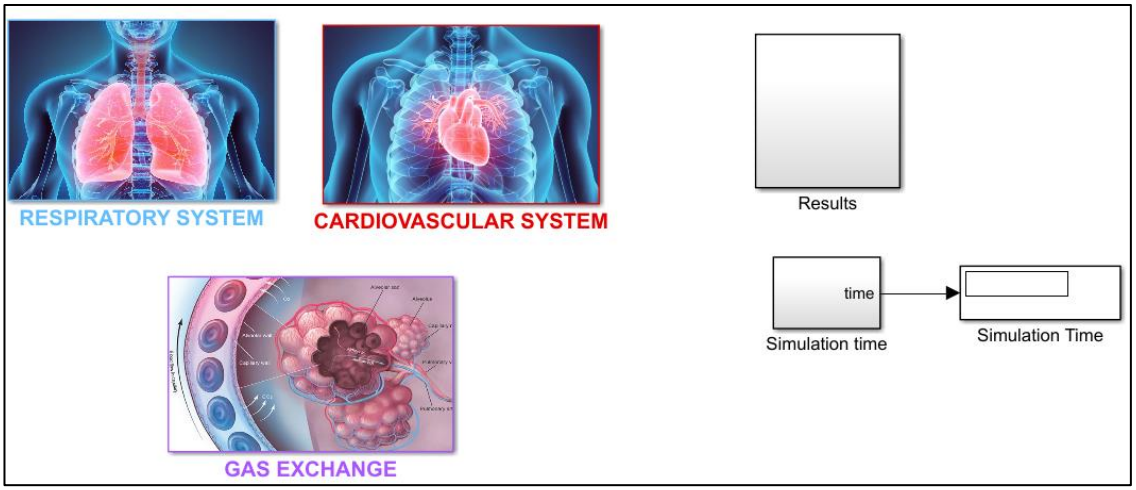

Figure 6.1 Simulink simulator model interface.

When opening the “RESPIRATORY SYSTEM” compartment in Figure 6.1 the pulmonary mechanics model is shown (as displayed in Figure 6.2). The current pulmonary system is based on Albanese *et al.* [3] work but will be modified to match the ICSM simulator. The deadspace (DS) including the larynx, trachea, and bronchi, will be partitioned into 50 compartments while the alveoli, currently composed of a single compartment, will be split into 100 compartments.

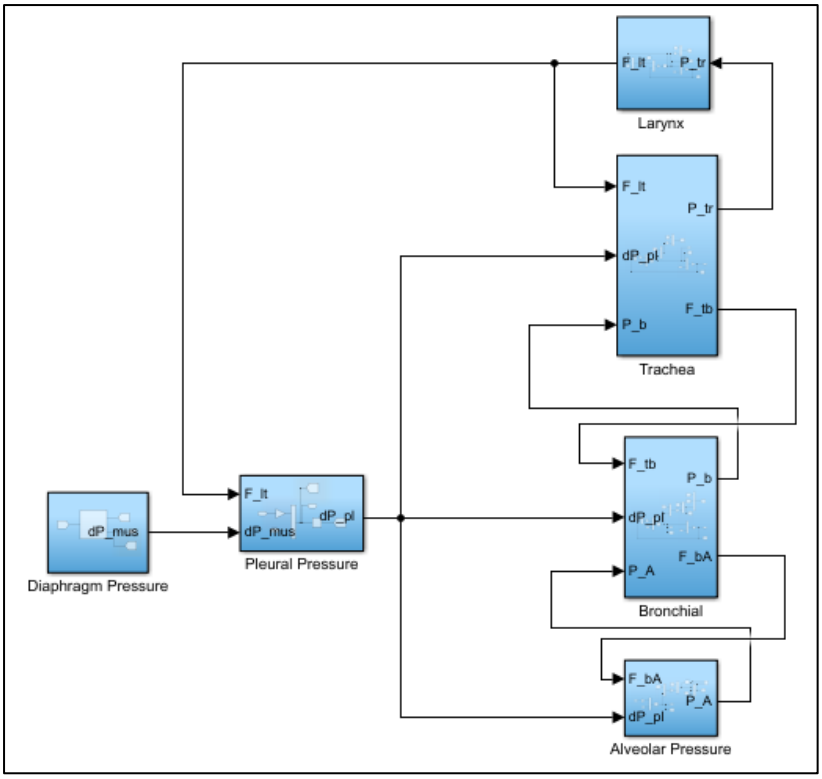

Figure 6.2 Simulink pulmonary block diagram.

When double clicking on the “CARDIOVASCULAR SYSTEM” compartment the cardiovascular mechanics model is displayed as shown in Figure 6.3. The current cardiovascular system is similar to the updated ICSM model and only some parameters need to be modified.

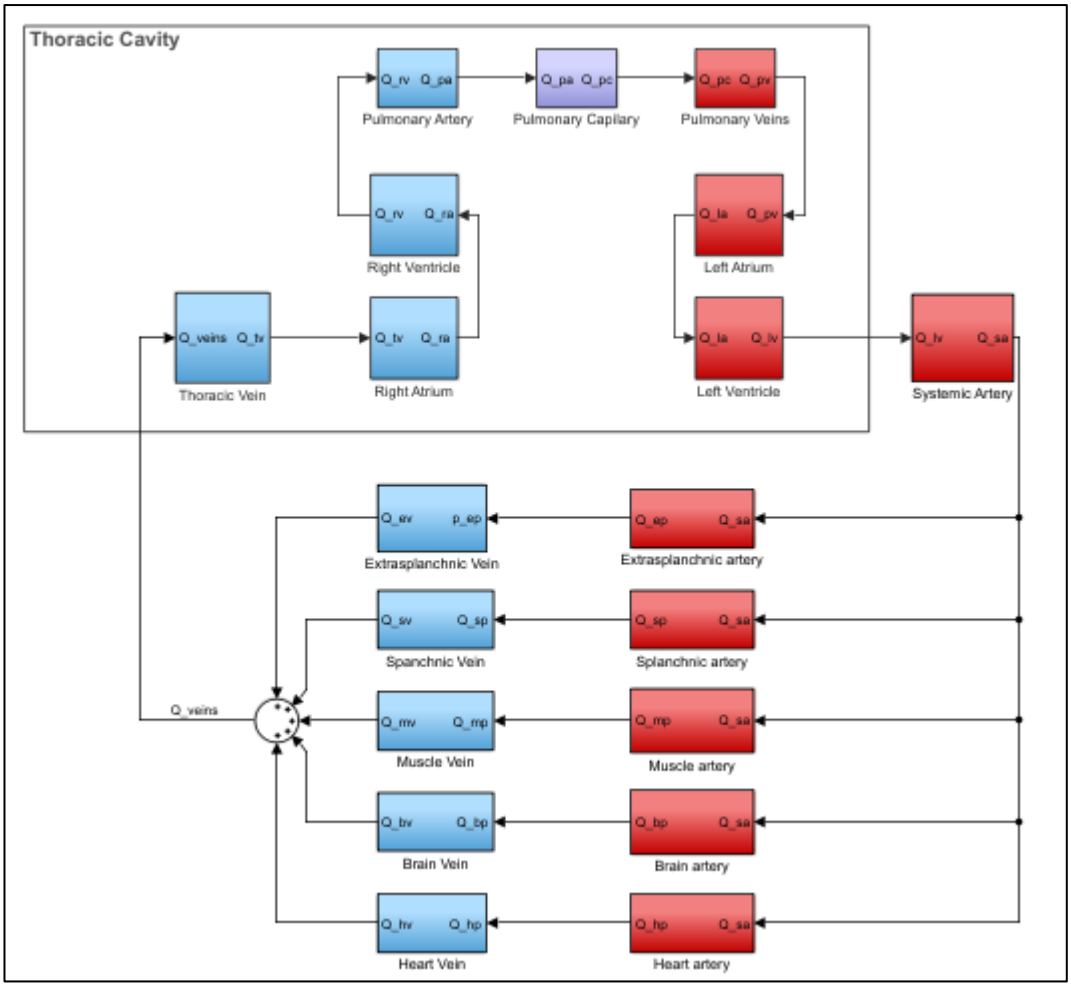

Figure 6.3 Simulink cardiovascular block diagram.

Finally, when double clicking on the “GAS EXCHANGE” compartment Figure 6.4 is shown. The current gas exchange system is based on Albanese *et al.* work [3] but will be modified to match the ICSM simulator. The model will be modified to account for temperature, base excess and pH levels.

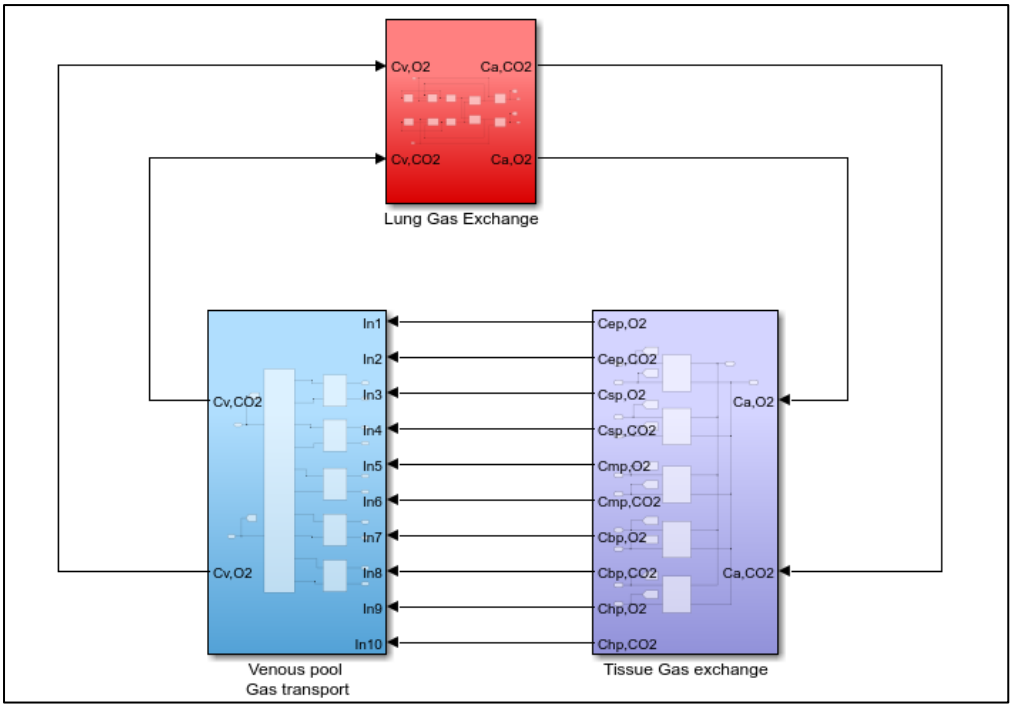

Figure 6.4 Simulink gas exchange block diagram.

Preliminary results

The model was programmed in Matlab-Simulink (MathWorks, Natick, MA), and the numerical integration of the differential equations was performed using the fourth order Runge-Kutta (RK4) method with fixed-step size of 0.5 ms. The following results were obtaining with the current version of the Simulink simulator.

Figures 6.5 and 6.6 presents the respiratory systems results. All the parameter values are within a healthy subject physiological range. In Figure 6.5 the deadspace tidal volume is 40 mL, the alveolar tidal volume is 500 mL and the lung tidal volume is 540 mL. Figure 6.6 shows the alveolar oxygen and carbon dioxide partial pressure which are respectively close to 110 mmHg and 40 mmHg.

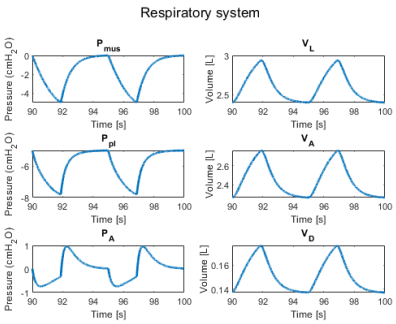

Figure 6.5 Pressure and volume wave-forms generated by the pulmonary model.

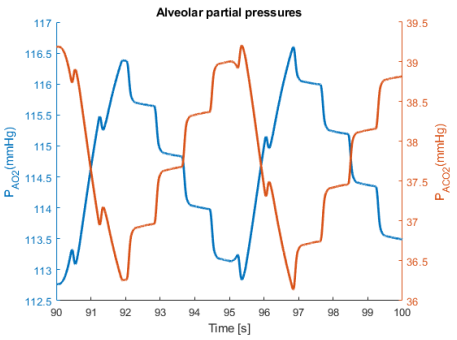

Figure 6.6 Time profile of O2 and CO2 partial pressures in the alveoli during two respiration cycles.

Figures 6.7 presents the cardiovascular results. All the parameter values are within a healthy subject physiological range. However, some parameters adjustment is required to obtain a stroke volume closer to 70 mL.

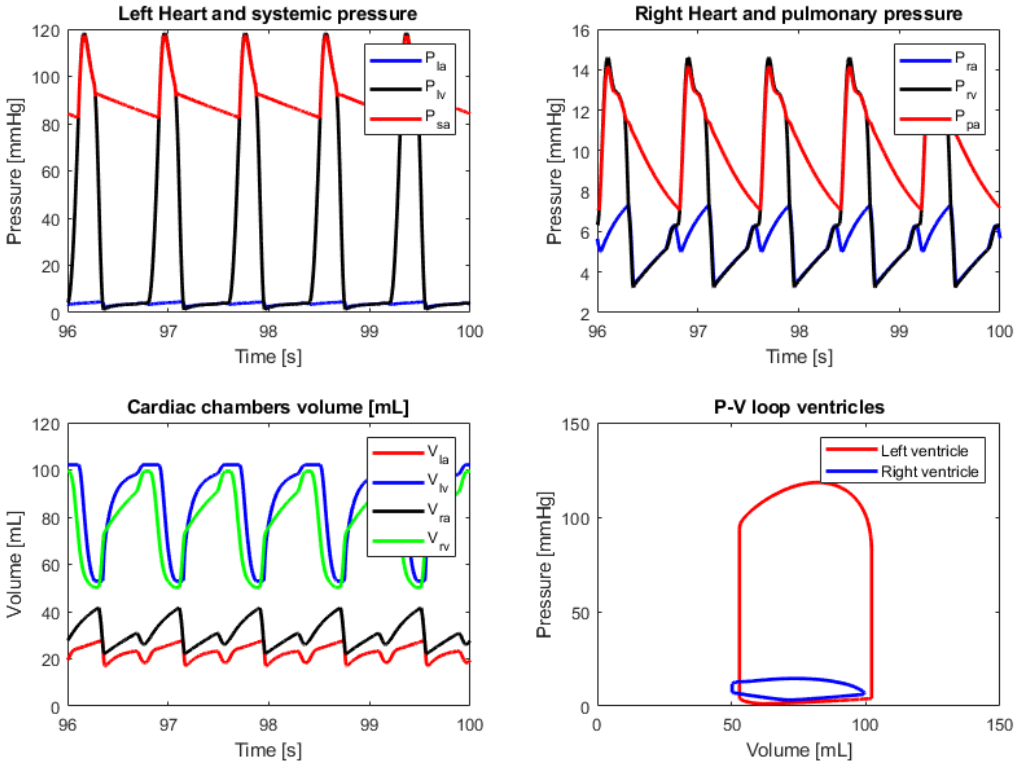

Figure 6.7 a) Pressure in the left ventricle, aorta and left atrium; b) pressure in the right ventricle, pulmonary artery and right atrium; c) volume in the left and right ventricles and atria; d) pressure-volume loop in the left and right ventricles.

Appendix 7. Scoping review search strategy

The scoping review in Pubmed, conducted from March 1st, 2020, to March 1st, 2021, employed the following search approach. The initial segment of the strategy incorporated terms pertinent to cardiac arrest and CPR, while the subsequent part encompassed all pertinent animal types, adhering to the search methodology proposed by Hooijmans *et al*. [7].

((((((((((((((((heart arrest) OR (cardiac arrest)) OR (return of spontaneous circulation)) OR (ROSC)) OR (cardiovascular arrest)) OR (asystole)) OR (pulseless electrical activity)) OR (ventricular fibrillation)) OR (pulseless ventricular tachycardia)) OR (cardiopulmonary arrest)) OR (advanced cardiac life support)) OR (ACLS)) OR (cardiopulmonary resuscitation)) OR (CPR)) OR (heart massage)) OR (cardiac massage)) OR (chest compression)) AND (("animal experimentation"[MeSH Terms] OR "models, animal"[MeSH Terms] OR "invertebrates"[MeSH Terms] OR "Animals"[Mesh:noexp] OR "animal population groups"[MeSH Terms] OR "chordata"[MeSH Terms:noexp] OR "chordata, nonvertebrate"[MeSH Terms] OR "vertebrates"[MeSH Terms:noexp] OR "amphibians"[MeSH Terms] OR "birds"[MeSH Terms] OR "fishes"[MeSH Terms] OR "reptiles"[MeSH Terms] OR "mammals"[MeSH Terms:noexp] OR "primates"[MeSH Terms:noexp] OR "artiodactyla"[MeSH Terms] OR "carnivora"[MeSH Terms] OR "cetacea"[MeSH Terms] OR "chiroptera"[MeSH Terms] OR "elephants"[MeSH Terms] OR "hyraxes"[MeSH Terms] OR "insectivora"[MeSH Terms] OR "lagomorpha"[MeSH Terms] OR "marsupialia"[MeSH Terms] OR "monotremata"[MeSH Terms] OR "perissodactyla"[MeSH Terms] OR "rodentia"[MeSH Terms] OR "scandentia"[MeSH Terms] OR "sirenia"[MeSH Terms] OR "xenarthra"[MeSH Terms] OR "haplorhini"[MeSH Terms:noexp] OR "strepsirhini"[MeSH Terms] OR "platyrrhini"[MeSH Terms] OR "tarsii"[MeSH Terms] OR "catarrhini"[MeSH Terms:noexp] OR "cercopithecidae"[MeSH Terms] OR "hylobatidae"[MeSH Terms] OR "hominidae"[MeSH Terms:noexp] OR "gorilla gorilla"[MeSH Terms] OR "pan paniscus"[MeSH Terms] OR "pan troglodytes"[MeSH Terms] OR "pongo pygmaeus"[MeSH Terms])OR ((animals[tiab] OR animal[tiab] OR mice[Tiab] OR mus[Tiab] OR mouse[Tiab] OR murine[Tiab] OR woodmouse[tiab] OR rats[Tiab] OR rat[Tiab] OR murinae[Tiab] OR muridae[Tiab] OR cottonrat[tiab] OR cottonrats[tiab] OR hamster[tiab] OR hamsters[tiab] OR cricetinae[tiab] OR rodentia[Tiab] OR rodent[Tiab] OR rodents[Tiab] OR pigs[Tiab] OR pig[Tiab] OR swine[tiab] OR swines[tiab] OR piglets[tiab] OR piglet[tiab] OR boar[tiab] OR boars[tiab] OR "sus scrofa"[tiab] OR ferrets[tiab] OR ferret[tiab] OR polecat[tiab] OR polecats[tiab] OR "mustela putorius"[tiab] OR "guinea pigs"[Tiab] OR "guinea pig"[Tiab] OR cavia[Tiab] OR callithrix[Tiab] OR marmoset[Tiab] OR marmosets[Tiab] OR cebuella[Tiab] OR hapale[Tiab] OR octodon[Tiab] OR chinchilla[Tiab] OR chinchillas[Tiab] OR gerbillinae[Tiab] OR gerbil[Tiab] OR gerbils[Tiab] OR jird[Tiab] OR jirds[Tiab] OR merione[Tiab] OR meriones[Tiab] OR rabbits[Tiab] OR rabbit[Tiab] OR hares[Tiab] OR hare[Tiab] OR diptera[Tiab] OR flies[Tiab] OR fly[Tiab] OR dipteral[Tiab] OR drosphila[Tiab] OR drosophilidae[Tiab] OR cats[Tiab] OR cat[Tiab] OR carus[Tiab] OR felis[Tiab] OR nematoda[Tiab] OR nematode[Tiab] OR nematoda[Tiab] OR nematode[Tiab] OR nematodes[Tiab] OR sipunculida[Tiab] OR dogs[Tiab] OR dog[Tiab] OR canine[Tiab] OR canines[Tiab] OR canis[Tiab] OR sheep[Tiab] OR sheeps[Tiab] OR mouflon[Tiab] OR mouflons[Tiab] OR ovis[Tiab] OR goats[Tiab] OR goat[Tiab] OR capra[Tiab] OR capras[Tiab] OR rupicapra[Tiab] OR chamois[Tiab] OR haplorhini[Tiab] OR monkey[Tiab] OR

monkeys[Tiab] OR anthropoidea[Tiab] OR anthropoids[Tiab] OR saguinus[Tiab] OR tamarin[Tiab] OR tamarins[Tiab] OR leontopithecus[Tiab] OR hominidae[Tiab] OR ape[Tiab] OR apes[Tiab] OR pan[Tiab] OR paniscus[Tiab] OR "pan paniscus"[Tiab] OR bonobo[Tiab] OR bonobos[Tiab] OR troglodytes[Tiab] OR "pan troglodytes"[Tiab] OR gibbon[Tiab] OR gibbons[Tiab] OR siamang[Tiab] OR siamangs[Tiab] OR nomascus[Tiab] OR symphalangus[Tiab] OR chimpanzee[Tiab] OR chimpanzees[Tiab] OR prosimians[Tiab] OR "bush baby"[Tiab] OR prosimian[Tiab] OR bush babies[Tiab] OR galagos[Tiab] OR galago[Tiab] OR pongidae[Tiab] OR gorilla[Tiab] OR gorillas[Tiab] OR pongo[Tiab] OR pygmaeus[Tiab] OR "pongo pygmaeus"[Tiab] OR orangutans[Tiab] OR pygmaeus[Tiab] OR lemur[Tiab] OR lemurs[Tiab] OR lemuridae[Tiab] OR horse[Tiab] OR horses[Tiab] OR pongo[Tiab] OR equus[Tiab] OR cow[Tiab] OR calf[Tiab] OR bull[Tiab] OR chicken[Tiab] OR chickens[Tiab] OR gallus[Tiab] OR quail[Tiab] OR bird[Tiab] OR birds[Tiab] OR quails[Tiab] OR poultry[Tiab] OR poultries[Tiab] OR fowl[Tiab] OR fowls[Tiab] OR reptile[Tiab] OR reptilia[Tiab] OR reptiles[Tiab] OR snakes[Tiab] OR snake[Tiab] OR lizard[Tiab] OR lizards[Tiab] OR alligator[Tiab] OR alligators[Tiab] OR crocodile[Tiab] OR crocodiles[Tiab] OR turtle[Tiab] OR turtles[Tiab] OR amphibian[Tiab] OR amphibians[Tiab] OR amphibia[Tiab] OR frog[Tiab] OR frogs[Tiab] OR bombina[Tiab] OR salientia[Tiab] OR toad[Tiab] OR toads[Tiab] OR "epidalea calamita"[Tiab] OR salamander[Tiab] OR salamanders[Tiab] OR eel[Tiab] OR eels[Tiab] OR fish[Tiab] OR fishes[Tiab] OR pisces[Tiab] OR catfish[Tiab] OR catfishes[Tiab] OR siluriformes[Tiab] OR arius[Tiab] OR heteropneustes[Tiab] OR sheatfish[Tiab] OR perch[Tiab] OR perches[Tiab] OR percidae[Tiab] OR perca[Tiab] OR trout[Tiab] OR trouts[Tiab] OR char[Tiab] OR chars[Tiab] OR salvelinus[Tiab] OR "fathead minnow"[Tiab] OR minnow[Tiab] OR cyprinidae[Tiab] OR carps[Tiab] OR carp[Tiab] OR zebrafish[Tiab] OR zebrafishes[Tiab] OR goldfish[Tiab] OR goldfishes[Tiab] OR guppy[Tiab] OR guppies[Tiab] OR chub[Tiab] OR chubs[Tiab] OR tinca[Tiab] OR barbels[Tiab] OR barbus[Tiab] OR pimephales[Tiab] OR promelas[Tiab] OR "poecilia reticulata"[Tiab] OR mullet[Tiab] OR mullets[Tiab] OR seahorse[Tiab] OR seahorses[Tiab] OR mugil curema[Tiab] OR atlantic cod[Tiab] OR shark[Tiab] OR sharks[Tiab] OR catshark[Tiab] OR anguilla[Tiab] OR salmonid[Tiab] OR salmonids[Tiab] OR whitefish[Tiab] OR whitefishes[Tiab] OR salmon[Tiab] OR salmons[Tiab] OR sole[Tiab] OR solea[Tiab] OR "sea lamprey"[Tiab] OR lamprey[Tiab] OR lampreys[Tiab] OR pumpkinseed[Tiab] OR sunfish[Tiab] OR sunfishes[Tiab] OR tilapia[Tiab] OR tilapias[Tiab] OR turbot[Tiab] OR turbots[Tiab] OR flatfish[Tiab] OR flatfishes[Tiab] OR sciuridae[Tiab] OR squirrel[Tiab] OR squirrels[Tiab] OR chipmunk[Tiab] OR chipmunks[Tiab] OR suslik[Tiab] OR susliks[Tiab] OR vole[Tiab] OR voles[Tiab] OR lemming[Tiab] OR lemmings[Tiab] OR muskrat[Tiab] OR muskrats[Tiab] OR lemmus[Tiab] OR otter[Tiab] OR otters[Tiab] OR marten[Tiab] OR martens[Tiab] OR martes[Tiab] OR weasel[Tiab] OR badger[Tiab] OR badgers[Tiab] OR ermine[Tiab] OR mink[Tiab] OR minks[Tiab] OR sable[Tiab] OR sables[Tiab] OR gulo[Tiab] OR gulos[Tiab] OR wolverine[Tiab] OR wolverines[Tiab] OR minks[Tiab] OR mustela[Tiab] OR llama[Tiab] OR llamas[Tiab] OR alpaca[Tiab] OR alpacas[Tiab] OR camelid[Tiab] OR camelids[Tiab] OR guanaco[Tiab] OR guanacos[Tiab] OR chiroptera[Tiab] OR chiropteras[Tiab] OR bat[Tiab] OR bats[Tiab] OR fox[Tiab] OR foxes[Tiab] OR iguana[Tiab] OR iguanas[Tiab] OR xenopus laevis[Tiab] OR parakeet[Tiab] OR parakeets[Tiab] OR parrot[Tiab] OR parrots[Tiab] OR donkey[Tiab] OR donkeys[Tiab] OR mule[Tiab] OR mules[Tiab] OR zebra[Tiab] OR zebras[Tiab] OR shrew[Tiab] OR shrews[Tiab] OR bison[Tiab] OR bisons[Tiab] OR buffalo[Tiab] OR buffaloes[Tiab] OR deer[Tiab] OR deers[Tiab] OR bear[Tiab] OR bears[Tiab] OR panda[Tiab] OR pandas[Tiab] OR "wild hog"[Tiab] OR "wild boar"[Tiab] OR fitchew[Tiab] OR fitch[Tiab] OR beaver[Tiab] OR beavers[Tiab] OR jerboa[Tiab] OR jerboas[Tiab] OR capybara[Tiab] OR capybaras[Tiab]) NOT medline[subset]))

References

[1] C. Daudre-Vignier, M. Laviola, A. Das, D. G. Bates, and J. G. Hardman, “Identification of an optimal CPR chest compression protocol,” *Annu Int Conf IEEE Eng Med Biol Soc,* vol. 2021, pp. 5459-5462, 2021.

[2] C. Daudre-Vignier, D. G. Bates, T. E. Scott, J. G. Hardman, and M. Laviola, “Evaluating current guidelines for cardiopulmonary resuscitation using an integrated computational model of the cardiopulmonary system,” *Resuscitation,* vol. 186, pp. 109758, May, 2023.

[3] A. Albanese, L. Cheng, M. Ursino, and N. W. Chbat, “An integrated mathematical model of the human cardiopulmonary system: model development,” *Am J Physiol Heart Circ Physiol,* vol. 310, no. 7, pp. H899-921, 2016.

[4] O. I. P. Limei Cheng PhD, Hsing-Hua Fan PhD, Michael C.K. Khoo PhD "Simulation of State-CardioRespiratory Interactions PNEUMA " U. o. S. California, ed., Biomedical Simulations Resource (BMSR), 2013.

[5] L. Cheng, and M. C. Khoo, “Modeling the autonomic and metabolic effects of obstructive sleep apnea: a simulation study,” *Front Physiol,* vol. 2, pp. 111, 2011.

[6] S. Bozkurt, “Mathematical modeling of cardiac function to evaluate clinical cases in adults and children,” *PloS one,* vol. 14, no. 10, pp. e0224663-e0224663, 2019.

[7] C. R. Hooijmans, A. Tillema, M. Leenaars, and M. Ritskes-Hoitinga, “Enhancing search efficiency by means of a search filter for finding all studies on animal experimentation in PubMed,” *Laboratory animals,* vol. 44, no. 3, pp. 170-175, 2010.